Cardiff University

School of Earth and Ocean Sciences

Palaeoclimate and palaeoenvironment of the middle Eocene southern Pacific; insights from New Zealand

Catherine E. Burgess

Thesis submitted for the degree of
Doctor of Philosophy

June 2008

ProQuest LLC
789 East Eisenhower Parkway
P.O. Box 1346
Ann Arbor, MI 48106-1346

Delcaration

This work has not previously been accepted in substance for any degree and is not concurrently submitted in candidature for any degree.

Signed ..... (candidate) Date 26/09/08....

This thesis is being submitted in partial fulfillment of the requirements for the degree of PhD.

Signed ..... (candidate) Date 26/09/08

This thesis is the result of my own independent work/investigation, except where otherwise stated.

Other sources are acknowledged by explicit references.

Signed ..... (candidate) Date 26/09/08...

I hereby give consent for my thesis, if accepted, to be available for photocopying and for inter-library loan, and for the title and summary to be made available to outside organisations.

Signed ..... (candidate) Date 26/09/08....

For my family, who have always believed in me.
Thank you.

Abstract

The Hampden Section of South Island, New Zealand, is used to generate a multiproxy record of middle Eocene palaeoclimate. The Hampden Formation is a calcareous clay-rich siltstone deposited in a shelf edge environment, containing exceptionally well-preserved micro- and nannofossils. A range of sedimentary, geochemical and fossil assemblage records from this formation are combined to provide new insights into middle Eocene climate in the southern Pacific Ocean.

A palaeoclimate record generated through the formation spans the period from ~42.1 to ~39.3 Ma and shows clear cooling in ocean mixed-layer temperatures from ~18 °C to ~14 °C, with long period cyclicity (likely ~405 k.y.) superimposed. This cooling trend is punctuated by a transient warm excursion of ~ 2.5 °C lasting ~450 k.y. that may represent the Middle Eocene Climatic Optimum. There is a brief influx of the tropical planktonic foraminifer *Hantkenina australis* during this time and the excursion is also marked by a substantial drop in the sand fraction of the sediment, indicating that the warm interval had a significant impact on the terrestrial realm.

The water temperatures produced from this record are warmer than those previously estimated for similar latitudes, likely due to the excellent preservation of the microfossils reducing the effect of diagenesis on their geochemistry. These temperatures suggest that during the middle Eocene, the site lay in the path of a warm southward flowing current rather than a cold Antarctic gyre. They also support the hypothesis that the global latitudinal temperature gradient was reduced during the middle Eocene.

A shorter high-resolution record of climate was also obtained. This shows ~18 k.y. cyclicity in a range of palaeoclimatic and palaeonvironmental proxies that is considered to have been orbitally forced. The Mg/Ca derived bottom water temperatures range from ~11 to 13 °C and the TEX_{86} derived surface water temperatures from ~22.5 to 24 °C through these cycles. The combination of $\delta^{18}O$ and Mg/Ca in foraminiferal carbonates indicates that there was little or no ice present globally. Despite the lack of ice available to amplify the cycles they had a major and complex effect on both the marine and terrestrial environments.

Acknowledgements

I would like to begin by thanking my primary supervisor, Paul Pearson, who has directed and encouraged this project throughout. His office door has always been open and our discussions have been invaluable in increasing my understanding of my work and sparking new ideas. Carrie Lear has provided invaluable support as my co-supervisor, from teaching me lab and analytical techniques to discussing the fine detail of my results and interpretation. I thank her and wish her and her husband, Trevor, all the best with their new baby, Rowan.

I would also like to thank my supervisor at GNS Science in New Zealand, Hugh Morgans, and his family. Hugh provided help and support in all aspects of New Zealand palaeontology and without his support in the field this work would never have been possible. He and his family welcomed me into their home and made my time in New Zealand a wonderful experience, I am very fortunate to have met them and I am looking forward to visiting again. Also in New Zealand, I would like to thank Chris Hollis who has provided further support, commented on numerous draft documents and kept me in touch with current southern ocean palaeoclimate research. My thanks also go to all those at GNS Science who provided conversation and ideas over coffee or beer and introduced me to New Zealand life.

I would then like to extend my thanks to all those people not directly involved in my PhD who have contributed to my research. Paul Bown at UCL not only taught me nannofossil morphology and taxonomy but carried out a biostratigraphic assessment of samples from Hampden Beach and was always willing to help with my species identifications. Henk Brinkhuis and Appy Sluijs at Utrecht University provided a boundless enthusiasm for dinoflagellates that proved infectious. Henk taught me dinoflagellate taxonomy, environmental interpretation and to appreciate expresso and our discussions helped to clarify my ideas. Rich Pancost and Luke Handley at the University of Bristol carried out organic carbon analyses on the Hampden Beach samples and shared their results and interpretation, significantly enhancing the value of the Hampden Beach section as a palaeoclimatic record and our conversations advanced my ideas and interpretation. Heiko Pälike at Southampton helped in carrying out spectral analysis of my cyclic records and assessing their significance. Ian McMillan and Helen Coxall at Cardiff University helped with benthic and planktonic foraminiferal identification respectively. Ian also helped with benthic foraminiferal environmental

interpretation and was endlessly patient. Mutt Huber at Perdue University has provided discussion regarding Eocene climate modelling and data model mismatch that has proved very interesting and Jenny Pike at Cardiff University has provided general PhD help and advice.

I would also like to thank those people who have provided technical support for my PhD. At Cardiff University, Julia Becker analysed my stable isotope samples, Pete Fisher taught me to use the SEM, Ian McDonald helped in using the ICP-MS, Tony Oldroyd taught me to use the XRD facilities, Lindsey Axe helped with the light microscope facilities and Alice Joy Neidhardt and Alun Rodgers assisted with graphics and printing. At Utrecht University Natasja Welters processed my palynological samples.

Beyond the academic sphere my thanks must first and foremost go to my family, it was my parents encouragement always to ask questions and strive to understand that lead me along the path towards a PhD. My parents and my sister have provided endless support throughout the last three and half years especially the final months of writing up. I would also like to thank my friends in Cardiff, in Suffolk and scattered around the country who have provided life outside my PhD and made my time at Cardiff so enjoyable. Special mentions must go to a few people. Sarah Dare who taught me the joy of girly nights out dancing and was always willing to listen to my latest PhD crisis. Hugh Venables who has always been there for me with advice and encouragement and frequently provided a much-needed dose of common sense! Tracey Scoffin and Sarah Cleaver, my longest standing friends and who never give up on me however infrequently I visit. Anna Hey and Helen Medley with whom I share an office and Jenny Morris, my flatmate all of whom have been endlessly patient and supportive. Also more people than I have space to list among the postgrads in the School of Earth Sciences at Cardiff University and the Cardiff City Triathlon Club.

This project was funded by Natural Environment Research Council studentship number NER/S/A/2004/12723 with additional financial support from GNS Science, New Zealand.

List of Contents

List of Figures

List of Tables

Chapter 3.

List of Plates

Chapter 4.

Chapter 5.

1. Introduction

Current concern regarding anthropogenic input of carbon dioxide to the atmosphere and its impact on future climate has highlighted the importance of understanding global climate and its variability, in a greenhouse world with warmer temperatures and higher partial pressure of atmospheric carbon dioxide (pCO_2) than today. Studying the changing global climate through time allows us to attempt to understand the numerous interlinked processes, forcing mechanisms and feedbacks that occur within the climate system and better predict how it may behave in the future. Furthermore, an important way to test the ability of numerical models to accurately predict changes in climate through time is to compare their predictions for the past to the geological record. Of particular interest is understanding rapid cyclic or transient climatic changes, particularly in relation to temperature and ice-sheet size and stability as ice directly affects global sea level, and the high albedo of ice may provide a positive feedback on high latitude temperature change.

This study focuses on creating a palaeoclimatic record of the middle Eocene southern Pacific Ocean from the Hampden Section on the east coast of South Island, New Zealand. The Hampden Section primarily exposes the middle Eocene Hampden Formation along a shallow dipping cliff section. This formation consists of a calcareous silt to very fine sandstone that contains excellently well preserved foraminifera (Finlay, 1939b; Cameron and Waghorn, 1985; Pearson and Burgess, 2008) and was deposited at approximately 55°S palaeolatitude in a shelf edge environment (see chapter 3). The sediment at this site appears to display cyclic bedding (first observed by P. Pearson and H. Morgans, 2005, pers. comm.), which it is hypothesised reflects orbitally driven climate cycles affecting sedimentation.

The Hampden Formation provides a high latitude shallow marine record from the middle Eocene in which combined records of both the marine and terrestrial environment are preserved. Furthermore, it is considered that the excellent preservation of the foraminifera means that they record an original isotopic and trace metal signature and have not been significantly affected by diagenesis (Pearson et al., 2001) (see Chapter 5). The Hampden Formation therefore, provides an excellent opportunity to better understand the nature of climate cyclicity in a warm world. The ability to apply the range of proxies discussed in Section 1.1 below, will significantly improve

understanding of the climate and ecology of the middle Eocene southern Pacific Ocean and it's temporal variability.

1.1. Palaeoclimatic proxies

Prior to recorded human history there are no directly measured records of climate, so our knowledge of global palaeoclimate is derived from understanding the way that climatic and environmental variables affect the geochemistry and biology of the Earth and so leave a trace in the geological record. Climate proxies are chemical, biological and physical observables that indicate climate directly or the physics of ocean-atmosphere circulation and the chemistry of the carbon cycle, which control climate (Henderson, 2002). The proxy records that are applicable to a shallow marine setting during the Eocene and that this study applies to the Hampden Section are set out briefly below.

1.1.1. Geochemical proxies

1.1.1.1. Biogenic carbonate isotopic composition

The calcium carbonate microfossils at Hampden Beach are exceptionally well-preserved (see Chapter 5) and consequently they provide an excellent archive of biogenic carbonate for geochemical analysis. The most widely used stable isotope proxies in biogenic carbonate are $\delta^{18}O$ (the ratio of ^{18}O to ^{16}O relative to a standard) and $\delta^{13}C$ (the ratio of ^{13}C to ^{12}C relative to a standard). The $\delta^{18}O$ of foraminiferal carbonate is commonly used to obtain water temperature and global ice volume (e.g. Emiliani, 1954; Erez and Luz, 1983) and $\delta^{13}C$ is affected by oceanic productivity, ocean circulation and global carbon cycling (e.g. Shackleton and Boersma, 1981; Zachos et al., 2001).

The use of oxygen isotope ratios in biogenic carbonate to determine marine temperatures in the geological record was first suggested by Urey (1947). The idea was developed by Epstein et al. (1951) who produced the first palaeotemperature equation relating biogenic carbonate $\delta^{18}O$ to water temperature, based on experiments using molluscan carbonate grown at known temperatures. This was then applied to planktonic foraminifera in deep sea cores (Emiliani, 1954) and it was found that foraminifera deposit their skeleton in isotopic equilibrium with sea water and therefore can be used

for palaeoclimatic studies, as long as the isotopic composition of the seawater ($\delta^{18}O_{sw}$) is known. Essentially, the ratio of ^{18}O to ^{16}O ($\delta^{18}O$) secreted into the tests of foraminifera depends quantifiably on two principle factors, the temperature and the $\delta^{18}O$ of the water in which the foraminifera lived and secreted the calcite test, although other factors such as alkalinity may have a minor effect (Spero et al., 1997). The $\delta^{18}O$ of the water ($\delta^{18}O_{sw}$) depends in turn on the local salinity and the global seawater isotopic composition. The salinity of seawater results from the balance between precipitation and evaporation, meaning that with sufficient knowledge of the palaeoceanography of a site, palaeosalinity can be estimated and constrained to a reasonable set of values. The $\delta^{18}O_{sw}$ depends largely on the global ice volume because ^{16}O is preferentially taken up by evaporation and when this is deposited as snow and locked up in terrestrial ice sheets, it leaves the oceans enriched in ^{18}O. The greenhouse world of parts of the Cretaceous and early Eocene is widely assumed to have been effectively ice free, enabling $\delta^{18}O$ to give quantitative temperature records. However, since the early Eocene when temperatures began to cool and it is hypothesised that ice sheets may have begun to develop, the effects of ice volume and temperature on the $\delta^{18}O$ signal of biogenic calcite can not be decoupled without the use of a second proxy for either temperature or ice volume (e.g. Lear et al., 2000).

The original palaeotemperature equation of Epstein et al. (1951) was revised by Erez and Luz (1983) to refer it experimentally to planktonic foraminifera rather than mollusca. Since then, this proxy has been refined numerous times and calibrations have been carried out using multiple species (Katz et al., 2003) and inorganic carbonate (Kim and O'Neil, 1997) to attempt to reduce the impact on the calibration of the difficult to quantify 'vital effect' on isotopic fractionation that varies between species. A good review of the available calibrations is given in Bemis et al. (1998).

The interpretation of foraminiferal carbonate carbon isotopes is more complex than that of oxygen isotopes. Carbon isotopes provide information about the global carbon cycle, which in turn is linked to climate through weathering, productivity and oceanic and atmospheric CO_2 concentrations (Ruddiman, 2001). The $\delta^{13}C$ of foraminiferal calcite reflects the $\delta^{13}C$ of the water in which the organism calcified. In seawater, ^{12}C is preferentially taken up by primary producers, leaving the surface water enriched in ^{13}C where productivity is high (positive $\delta^{13}C$). When organisms die, they sink and return their carbon to deep ocean waters or it is buried and contained in the sedimentary record. This means that the $\delta^{13}C$ difference between the surface and deep

waters recorded by biogenic calcite can provide indicator of primary productivity in the ocean, which in turn depends on temperature, nutrient availability and carbon dioxide concentration (Kroopnick, 1985). However, low values of $\delta^{13}C$ in surface waters may also reflect upwelling of deep water rich in isotopically light organic carbon and nutrients rather than low productivity (Ruddiman, 2001).

The geographical variation in $\delta^{13}C$ can be used to find the relative ages of different water masses and trace changes in global water circulation patterns, as older deep water masses have had longer to accumulate more ^{12}C and become $\delta^{13}C$ depleted (e.g. Curry and Lohmann, 1983). Furthermore, the burial of organic carbon removes ^{12}C from the system, causing an overall rise in oceanic ^{13}C, so the global oceanic $\delta^{13}C$ record provides information about the global carbon cycle and the amount of carbon sequestered in organic rich sediments through time (Zachos et al., 2001). Finally, rapid and short-lived excursions in $\delta^{13}C$ can be used to interpret climatic events such as the Paleocene-Eocene Thermal Maximum (PETM) where a strong negative $\delta^{13}C$ excursion has been used to imply a large release of isotopically light carbon, the most likely source of which is methane hydrate (Dickens et al., 1995; Bice and Marotzke, 2002). The complexity of the carbon cycle and the consequent spatial and temporal variability in $\delta^{13}C$ make it very difficult to interpret this proxy over long time periods or where the oceanography is not well constrained. Despite this, it frequently shows strong trends and cyclic variability in phase with other geochemical and sedimentological climate proxy records (e.g. Zachos et al., 2001; Pälike et al., 2006).

1.1.1.2. Foraminiferal carbonate trace metal composition

A number of palaeoclimate proxies based on the trace metal composition of foraminiferal calcite are currently under development. The most established of these proxies is the ratio of magnesium (Mg) to calcium (Ca) in biogenic calcite, which is used to estimate water temperature (Nürnberg et al., 1996; Lear, 2007). Laboratory cultures and core top studies demonstrate that the Mg/Ca ratio in foraminiferal calcite depends on the water temperature in which the foraminifera calcify and these studies have been used to calibrate several foraminiferal species' Mg/Ca ratios to seawater temperature (Nürnberg et al., 1996; Lea et al., 1999; Mashiotta et al., 1999; Elderfield and Ganssen, 2000). The Mg/Ca ratio of foraminiferal carbonate, like the oxygen isotopic composition, depends on the seawater temperature and seawater composition at the time of calcification. However the Mg/Ca ratio of seawater is more stable through

time than that of $\delta^{18}O_{sw}$ and can be modelled (Wilkinson and Algeo, 1989). This means that foraminiferal Mg/Ca can not only provide a seawater temperature record but then allow the effects of temperature and ice volume on $\delta^{18}O$ to be decoupled enabling the creation of an ice volume record (e.g. Elderfield and Ganssen, 2000; Lear et al., 2000).

In this thesis the combined use of the Mg/Ca and $\delta^{18}O$ proxies at Hampden Beach allows calculation of global ice volume for a snapshot of time during the crucial 'doubthouse' interval between the acknowledged greenhouse world of the early Eocene and the icehouse world of the Early Oligocene 1.2.2.

1.1.1.3. Organic carbon geochemistry

The Hampden Formation contains moderately high levels of organic carbon in the sediment making it suitable for analysis of organic carbon. This enables the use of a suite of geochemical climate proxies that are unrelated to foraminiferal calcite and generated by entirely different ecological groups. Climatic proxies based on organic carbon are a relatively recent development and span a wide range of environmental variables from sea surface temperature (SST) and mean annual air temperature (MAT) to the ratio of marine to terrestrial organic carbon and terrestrial soil pH.

The most extensively used of these organic carbon proxies is TEX_{86}, a SST proxy. It was established by Schouten et al. (2002) that a significant linear correlation occurs between the number of cyclopentane rings in sedimentary membrane lipids derived from marine crenarchaeota and annual mean SSTs. From this correlation, Schouten et al. (2002) developed the TEX_{86} index (TetraEther indeX of tetraethers consisting of 86 carbon atoms) and determined a calibration to SST. This proxy has been applied to several sites at different times through the Cenozoic (e.g. Pearson et al., 2007; Sangiorgi et al., 2008a) and good agreement has been seen with seawater temperatures from well-preserved foraminiferal calcite (Schouten et al., 2003; Pearson et al., 2007). The calibration has recently been refined by Kim et al. (2008).

Less commonly applied than the TEX_{86} proxy but also potentially of interest at Hampden Beach is the ratio of marine to terrestrial organic carbon in the sediment. It has been established that branched tetraether lipids are predominant in terrestrial environments, in contrast to crenarchaeol, the characteristic membrane lipid of non-thermophilic crenarchaeota, which is abundant in marine and lacustrine environments. Based on these findings, an index was developed by Hopmans et al. (2004), the Branched and Isoprenoid Tetraether (BIT) index, based on the relative abundance of

terrestrially derived tetraether lipids versus crenarchaeol. A survey of globally distributed marine and lacustrine surface sediments shows that the BIT index in these environments correlates with the relative fluvial input of terrestrial organic material (Hopmans et al., 2004; Kim et al., 2006) so variations in the BIT index through time at a single site may reflect changing fluvial input. However, it should be noted that since this index is the ratio between terrestrial and marine derived organic carbon, changes in marine productivity may also influence it.

Finally, new proxies still becoming established have been recently developed from membrane lipids found in soils. It has been shown that the Cyclisation ratio of Branched Tetraethers (CBT) is primarily related to the pH of the soil and not temperature, whereas the relative amount of methyl branches, expressed in the Methylation index of Branched Tetraethers (MBT), is positively correlated with the annual Mean Air Temperature (MAT) and, to a lesser extent, negatively correlated with the pH of the soil (Weijers et al., 2007b). This can be used to generate a record of past soil pH and continental temperature (Weijers et al., 2007a; Schouten et al., 2008).

1.1.2. Biological proxies

1.1.2.1. Faunal assemblages

Qualitative estimates of palaeoenvironment and palaeoclimate have long been made by studying fossil remains and inferring the environmental preferences of those creatures from those of their modern day counterparts. For example, the presence of dinosaur and other reptile remains at high latitude was one of the first indicators of Cretaceous and early Eocene warmth and fossil floras are also presented as evidence for warmth during 'greenhouse' periods (Upchurch and Wolfe, 1987).

Oceanic microfossils have been used extensively to produce qualitative and quantitative estimates of environmental conditions including water temperature, salinity, productivity and oxygenation level. The fossil remains of marine plankton are dominantly composed of micro- and nannofossils with hard parts, calcareous foraminifera and coccolithophores, and siliceous diatoms and radiolaria. Dinoflagellates also occur; these are not shell forming but have a tough organic cuticle during the encysted phase of their life cycle, which means that they are frequently preserved in the fossil record. All of these groups are useful in indicating palaeoclimate, they tend to be both abundant and widespread and at least one of them is present in most deep sea

sediments (Ruddiman, 2001). The microfossil groups studied as palaeoenvironmental proxies at Hampden Beach are introduced briefly below and discussed in more detail in Chapter 4.

Benthic foraminifera are commonly used to indicate bottom-water palaeoenvironmental conditions, which in turn may reflect climatic and oceanographic conditions. They have been used in studies of the changes in the Southern Ocean through the Cenozoic (Schröder-Adams, 1991; Hayward et al., 2004). However, most benthic foraminifera can tolerate a wide range of environmental conditions so it is useful to consider assemblages as a whole rather than look for specific indicator species (Van der Zwaan et al., 1999). In particular benthic foraminifera can be used to indicate water depth (Murray, 1973) and bottom water oxygenation (Kaiho, 1994).

Planktonic foraminifera can indicate the temperature of mixed-layer and sub-thermocline seawater. As with benthic foraminifera the use of whole assemblages is more reliable than single species and for the Pleistocene and Holocene "transfer functions" have been developed to quantitatively estimate temperature (e.g. Waelbroeck et al., 1998; Malmgren et al., 2001). However, further back in the Cenozoic the temperature preferences of different species are not sufficiently well constrained and only qualitative temperature estimates are currently made. Nevertheless, the restricted latitudinal distribution of some species can make them good indicators of seawater surface temperature. Furthermore, the ability to carry out geochemical analysis on foraminiferal carbonate enables constraints to be placed on their depth preference within the water column (e.g. Pearson et al., 1993). This allows assemblages to be divided into 'mixed-layer' and 'sub-thermocline' species and their relative abundances may indicate changes in the water column stucture.

Dinoflagellates are influenced by a range of parameters, in particular water temperature, salinity and nutrient availability, so again it is preferable to look at assemblages rather than single species. Within an assemblage specimens can be grouped into species with a temperature preference, for example transantarctic species (Warnaar, 2006) or with an association to different water depths (Brinkhuis, 1994). There is significant overlap between the groups of species that indicate temperature with those that indicate water depth so they should be considered in relation to other available information in order to establish which parameter is providing the major control on assemblage composition. A good review of the use of dinoflagellates as palaeoclimatic proxies is given in Sluijs et al. (2004).

1.1.2.2. Foraminiferal test weight

The thickness of foraminiferal tests has been related to the carbonate saturation state of the seawater in which the organisms calcify, and this in turn to the carbon dioxide concentration ($[CO_2]$) in the seawater (Barker, 2002; Barker and Elderfield, 2002). Seawater surface $[CO_2]$ is generally well equilibrated with atmospheric pCO_2 and thus foraminiferal test weight provides a proxy for pCO_2. However, some studies have also suggested that test thickness may be a result of a more complex interplay of environmental factors than carbonate ion concentration alone (Broecker and Clark, 2004; de Villiers, 2004). This may be of particular significance if a number of aspects of the marine environment are changing over a period of time and the effects cannot be separated. This technique has been used outside of areas of major upwelling or downwelling to reconstruct glacial – interglacial pCO_2 (Barker and Elderfield, 2002) but has not been applied further back into the Cenozoic as exceptionally well preserved foraminiferal tests are required to be confident that test weight is not affected by diagenesis. It is thought that the Hampden Formation contains microfossils of sufficient quality (Chapter 5).

1.1.3. Sedimentary proxies

1.1.3.1. Sediment composition

Changes in sediment type may result from direct or indirect effects of the climate and water column environment on the sediment. For example, oxic or anoxic conditions control the presence or absence of a number of minerals and acidic water will cause increased carbonate dissolution. Furthermore biogenic sediments can reflect local marine ecology, for example an increase in opal accumulation rate is a crude indicator of an increase in biological productivity (De La Rocha et al., 1998). Finally, changes in sediment type can be due to alteration in sediment generation and transport caused by the effect of climate on weathering. The different types of clay minerals in particular, result from different degrees of weathering and the ratios of clay minerals in soil can be a useful proxy for the looking at changes in the extent of chemical versus physical weathering occurring in the sediment source region (Zachos et al., 1992; Robert and Kennett, 1997).

1.1.3.2. Sediment grain size

Sediment grain size depends among other factors on sediment transport energy, frequently bottom water current flow at the site, which provides palaeoceanographic information about the locality. The mean grain size of the sortable silt fraction (10-63μm) of deep ocean sediment has been developed as a quantitative flow speed proxy (McCave et al., 1995; Bianchi et al., 1999) and was first used successfully to track changing high latitude circulation during the Holocene (Bianchi and McCave, 1999). More recently, this proxy has been applied to the Southern Ocean region during the Miocene (Hall et al., 2003) and Oligocene (Pfhul and McCave, 2005) to study the development of the Antarctic Circumpolar Current. Unfortunately the Hampden Foramation is a shelf edge, rather than deepwater site and the palaeoceanography of the region around the Hampden Beach is not sufficiently well constrained to know whether it would be appropriate to use sortable silt to make a quantitative estimate of flow speed. However, the grain size can still give a qualitative indication of transport energy and flow speed both in the marine environment and in the terrestrial fluvial system from which it was sourced.

1.2. Eocene climate

1.2.1. Temperature record

The Paleogene is time of particular interest as it spans a period of transitional climate from the warm greenhouse climate of the Early Eocene to the cooler icehouse world of the Early Oligocene (Zachos et al., 2001). This transition is not smooth but stepwise and with a number of brief reversals that can provide important information about rapid climate change (Figure 1.1).

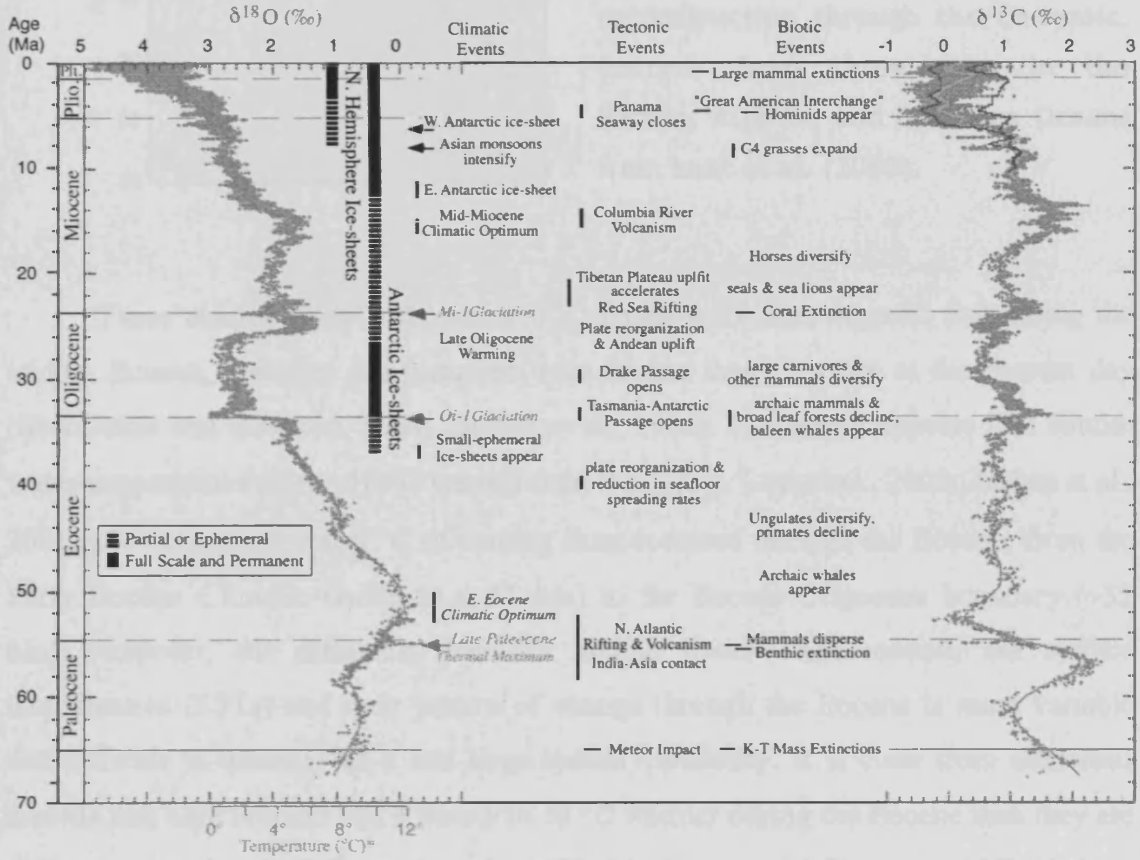

Figure 1.1. Global deep-sea oxygen and carbon isotope records for the past 65 m.y. based on data compiled from more than 40 DSDP and ODP sites with major climatic, tectonic and biotic events also indicated. From Zachos et al. 2001.

Studies combining the use of foraminiferal carbonate Mg/Ca and $\delta^{18}O$ have allowed the separation of temperature and ice volume effects and significantly increased the understanding of climate through this time period (Lear et al., 2000). Mg/Ca based temperature reconstructions indicate that the increase in benthic foraminiferal $\delta^{18}O$ observed through the early and middle Eocene (Figure 1.1) results primarily from

cooling with little or no ice volume effect (Figure 1.2, Lear et al., 2000; Billups and Schrag, 2003).

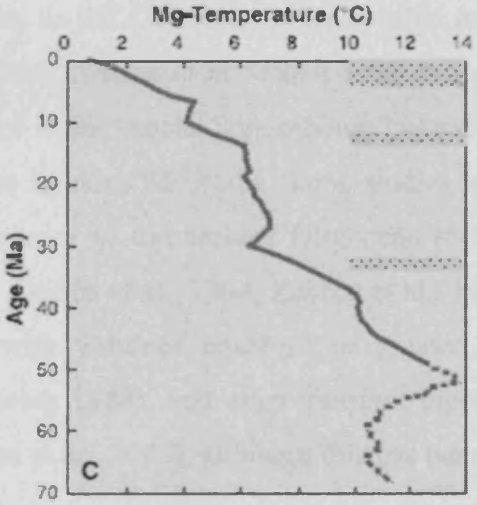

Figure 1.2. Benthic foraminiferal Mg/Ca based, deep-water temperature reconstruction through the Cenozoic. Records from three sites in the Pacific, Atlantic and Southern Oceans from Lear et al. (2000).

These studies agree with earlier $\delta^{18}O$ based work that suggests that during the middle Eocene, seawater temperatures were higher than they are at the present day (Shackleton and Boersma, 1981; Zachos et al., 1994). Globally it appears that bottom water temperatures were ~10 °C warmer than today (e.g. Lear et al., 2000; Zachos et al., 2001) and between 6 and 8 °C of cooling then occurred through the Eocene, from the Early Eocene Climatic Optimum (~51 Ma) to the Eocene-Oligocene boundary (~32 Ma). However, the difference between middle Eocene and modern sea surface temperatures (SSTs) and their pattern of change through the Eocene is more variable and difficult to quantify as it has large spatial variability. It is clear from numerous records that high latitude SSTs were 5 to 10 °C warmer during the Eocene than they are in the present day (e.g. Kennett et al., 1975; Mackensen and Ehrmann, 1992; Bohaty and Zachos, 2003), however low latitude temperatures appear from many records not to have been equivalently higher (e.g. Shackleton and Boersma, 1981). This has lead to a situation termed the 'cool tropics paradox' (D'Hondt and Arthur, 1996) in which the global latitudinal temperature gradient appears to have been significantly flattened during periods of warm, greenhouse climate (Zachos et al., 1994). This paradox is now thought to result partly from the diagenesis of planktonic foraminifera in deepwater sediments (Schrag et al., 1995; Norris and Wilson, 1998; Schrag, 1999; Pearson et al., 2001; Wilson and Norris, 2001) and is addressed and discussed more fully in Chapter 6.

1.2.2. Ice sheet development

As discussed in Section 1.2.1 above, combined Mg/Ca and $\delta^{18}O$ studies indicate that there was a long-term cooling trend, from the greenhouse climate of the early Eocene, to the Oligocene when a large ice cap was more permanently established on Antarctica (Miller et al., 1987; Lear et al., 2000). However the extent and stability of land ice in the crucial "doubthouse" world (Prothero et al., 2003) of the middle and late Eocene remains uncertain. Some studies have suggested there was little or no build-up of ice prior to the earliest Oligocene (Miller et al., 1991; Ehrmann and Mackensen, 1992; Zachos et al., 1994; Zachos et al., 1996), while others have postulated Eocene ice caps with volumes equal to or greater than those of the Holocene (Prentice and Matthews, 1988), and even transient bipolar glaciation as early as the middle Eocene (Tripati et al., 2005), although this has been contested (Edgar et al., 2007).

Sedimentological indicators from around Antarctica in the form of Ice Rafted Debris (IRD), or hiatuses further afield, have been presented as evidence for ice sheets from ca. 42 Ma in the middle Eocene (Ehrmann and Mackensen, 1992; Browning et al., 1996). Eldrett et al. (2007) used similar evidence from the North Atlantic to suggest that ice was present in the Northern Hemisphere during the middle Eocene. Modeling of Antarctica under Eocene conditions of moderately high *p*CO2 has indicated that small ice caps could have been present in upland areas, waxing and waning with the orbital insolation cycles, while larger ice caps could have formed under less extreme greenhouse conditions (DeConto and Pollard, 2003). A number of Eocene model simulations suggest that the buildup of small ephemeral ice sheets may have occurred throughout the Eocene with a critical threshold being crossed in the earliest Oligocene enabling the formation of large permanent ice sheets (Crowley and North, 1991; Barrera and Huber, 1993; Crowley, 1998; DeConto and Pollard, 2003; Lear et al., 2008).

1.2.3. Atmospheric carbon dioxide record

The Eocene provides the most recent period during which the partial pressure of carbon dioxide in the atmosphere (pCO_2) is likely to have been similar to that predicted for the end of this century (Royer et al., 2001; Bernstein et al., 2007; Zachos et al., 2008). The atmospheric pCO_2 is thought to be intimately linked to climate through the greenhouse effect, where high levels of CO_2 trap incoming solar radiation warming the earth (Arrhenius, 1896). Consequently, it is important to establish a record of pCO_2

through the geological past to test this link between CO_2 and climate. A direct link can be observed between temperatures and pCO_2 back to ~800 ka in the ice core record (e.g. Petit et al., 1999; Lüthi et al., 2008). However, further back no direct measurement of CO_2 is available so a number of proxies have been developed including stomatal indices of fossil plant leaves (McElwain, 1998; Beerling and Royer, 2002), boron isotopic composition ($\delta^{11}B$) of foraminiferal carbonate (Hemming and Hanson, 1992; Spivack et al., 1993; Pearson and Palmer, 1999; 2000), the mineralogy of primary ocean carbonates (Demicco et al., 2003; Lowenstein and Demicco, 2006) and alkenones within marine sediments (Pagani et al., 2005). All these proxies have been applied to the Cenozoic and they provide significantly different quantitative estimates of Eocene pCO_2, ranging from ~100 to 3500 ppmv. However, they largely agree on a broad pattern of high CO_2 during the late Cretaceous and Paleocene, declining steeply through the Early Eocene and continuing to decrease, but more gradually, through the Late Eocene and Oligocene (Figure 1.3) (Royer, 2006; Zachos et al., 2008).

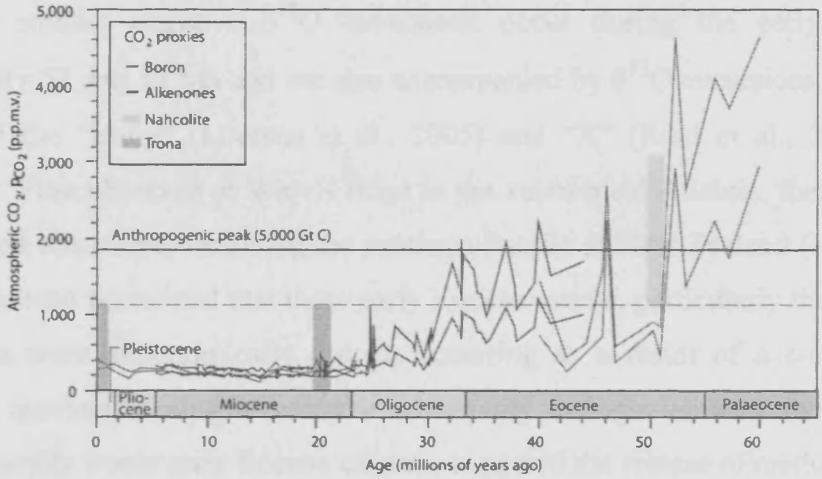

Figure 1.3. Evolution of atmospheric CO_2 levels over the past 65 million years. Data are a compilation of marine and lacustrine proxy records. From Zachos et al. (2008) with original data from Royer (2006).

This broad trend observed in pCO_2 agrees in general terms with the expectation that high temperatures would coincide with high atmospheric pCO_2. To study this link more closely, higher resolution records of pCO_2 and temperature are required; these have been pioneered in the Pleistocene by Barker and Elderfield (2002) using foraminiferal shell weight as a proxy for CO_2 through glacial – interglacial climatic changes as discussed in Section 1.1.2.2 above.

1.3. Eocene transient climate excursions

As noted in Section 1.2, the history of inferred Eocene temperature is not smooth instead the broad trends are punctuated by brief temperature excursions. These indicate that under some conditions, climatic response to forcing may be highly non-linear. The best known and most widely observed of these events is the Paleocene – Eocene Thermal Maximum (PETM) at ~55 Ma. This is a transient (~200 k.y.) negative excursion in $\delta^{18}O$ of between ~1 and 2 ‰ that equates to a temperature rise of 5 to 9 °C, accompanied by a negative excursion in $\delta^{13}C$ of >2.5 ‰, which is observed globally from southern high latitudes (e.g. Kennett and Stott, 1991) through low latitudes (e.g. Thomas et al., 1999) to the Arctic (Sluijs et al., 2006) and also impacts the terrestrial realm (e.g. Bowen et al., 2004). This transient warm event is thought to be related to perturbations in the global carbon cycle, likely including a massive release of methane hydrate, causing the dramatic shift in $\delta^{13}C$ and resulting in a global warming (Dickens et al., 1995; Bice and Marotzke, 2002; Zeebe and Zachos, 2007).

Two smaller negative $\delta^{18}O$ excursions occur during the early Eocene at approximately 53 and 52 Ma and are also accompanied by $\delta^{13}C$ excursions. These have been named the "Elmo" (Lourens et al., 2005) and "X" (Röhl et al., 2005) events respectively. First observed at Walvis ridge in the subtropical Atlantic, they have since been recorded elsewhere, including the southern Pacific at New Zealand (Nicolo et al., 2007). It has been postulated that these early Eocene events, particularly the PETM and Elmo events were astronomically forced, occurring as a result of a coincidence of eccentricity maxima leading to extreme seasonality in high latitudes that, combined with the generally warm early Eocene climate, triggered the release of methane hydrates (Lourens et al., 2005).

A further transient warm event, named the Middle Eocene Climatic Optimum (MECO) has been recorded later in the Eocene, initially dated at approximately 41.5 Ma (Bohaty and Zachos, 2003) but with recalibrated dates varying between 42.7 Ma (Falkowski et al., 2005; Sexton et al., 2006a) and ~40 Ma (Spofforth et al., 2008). This event also shows a transient negative excursion in $\delta^{18}O$, this time of ~1‰, equating to ~4 °C temperature increase occurring over ~600 k.y. However, this event does not show the dramatic shift in $\delta^{13}C$ that accompanies the earlier transient warm intervals, suggesting that it was triggered by a different mechanism, possibly increased pCO_2 (Bohaty and Zachos, 2003). The MECO also differs from the PETM and other early

Eocene events in that it occurs not in a period of general climate warming, but of cooling, also suggesting that the underlying mechanisms may differ. Since the MECO was first named in the Southern Ocean (Bohaty and Zachos, 2003), a number of other middle Eocene transient warm events have been observed in marine carbonate records at lower latitudes (Sexton et al., 2006a; Edgar et al., 2007) and in the northern hemisphere (Spofforth et al., 2008). Foraminiferal assemblages from the Southern Ocean (Galeotti et al., 2002) and southwestern Pacific (Jenkins, 1993) also appear to show a transient warm event in the middle Eocene. However, until their ages are better constrained it is not possible to establish whether these all represent a single MECO event or whether they are perhaps a series of similar events occurring due to an underlying orbital forcing, as has been hypothesised for the early Eocene transient warm events (Lourens et al., 2005). Furthermore, the MECO has so far been observed exclusively in marine materials and it is hoped that the terrestrial material from the site at Hampden Beach may provide the first evidence of its effect on the terrestrial realm (see Chapter 6).

1.4. Milankovitch cyclicity

Cyclic variations in Earth's orbit around the sun cause variations in the total solar radiation reaching the earths surface and in its latitudinal and seasonal distribution. This is turn has an effect on global climate that can be observed in the geological record (Milankovitch, 1941; Hays et al., 1976). These orbital cycles are known as Milankovitch cycles after the astronomer Milutin Milankovitch who first calculated their effect and hypothesized their link to global climate change (Milankovitch, 1941). These cycles occur on periods of approximately 19-23 ka, 41-54 ka and 97-123 ka at the present day although their frequencies have varied slightly through geological time (Laskar et al., 2004).

The 19-23 ka cycles are due to precession, the migration of the earth's spin axis relative to the plane of its orbit; the 41-54 ka cycles are due to obliquity, the degree of tilt of the earth's spin axis relative to the plane of its orbit; and the 97-123 ka cycles are in the eccentricity of the earths orbit, i.e. how elliptical the orbit is (Figure 1.4). The eccentricity cycles also have a longer term 405 ka component, which is calculated to be the most stable of all the Milankovitch cycles through the Cenozoic (Laskar et al., 2004). Furthermore, additional cyclicities occur at longer periods of 1.2 and 2.4 M.y. related to the amplitude modulation of obliquity and eccentricity cycles respectively

(Pälike et al., 2006). The greatest variation in solar insolation at high latitudes is generated by the obliquity cycles, so when ice sheets are present to provide a positive feedback on high latitude climate change, obliquity forced cyclicity is strengthened in the climate record (Pälike et al., 2006).

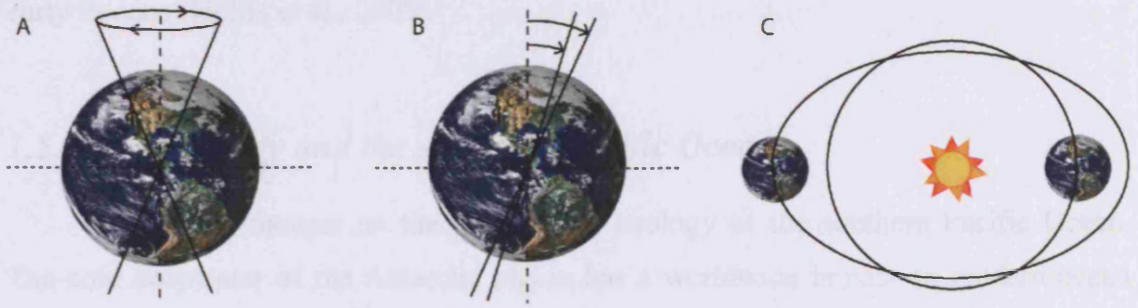

Figure 1.4. Diagrams illustrating the orbital variability that gives rise to Milankovitch cycles. A, precession; B, obliquity; C, eccentricity. In diagrams A and B, the dotted line represents the plane of the earth's orbit and the dashed line, a perpendicular to this plane, the solid lines indicate the spin axis of the earth. In diagram C the two black ellipses represent extremes of eccentricity in the earth's orbit, the degree of ellipticity is highly exaggerated.

Milankovitch cyclicity was first linked to the periodic changes in climate through the Pleistocene (Hays et al., 1976) and proposed as a possible driving force behind the ice ages. Further work has extended the observed record of Milankovitch cycles back in time with records throughout the Cenozoic (e.g. Naish et al., 2001; Wade et al., 2001; Pälike et al., 2006; Kroon and Zachos, 2007) and into the Cretaceous (e.g. Park et al., 1993; Herbert, 1997), Jurassic (Weedon, 1986) and many other studies going back to the Paleozoic. However, records of Milankovitch cyclicity become scarcer further back in time as sediment archives of sufficient quality and resolution become rarer.

The majority of records of Milankovitch scale cyclicity during the Eocene are from Deep Sea Drilling Project (DSDP), Ocean Drilling Program (ODP) or Integrated Ocean Drilling Program (IODP) cores although some shallow marine and terrestrial records are known. These records are widely spatially distributed, for example; the Southern Ocean Tasman Gateway, Leg 189 (Roehl et al., 2002); western North Atlantic Blake Nose, Leg 171B (Wade et al., 2001); eastern South Atlantic Walvis Ridge, Leg 208; southern Atlantic Agulhas Ridge, Leg 177 (Hodell et al., 2002) and the Arctic (ACEX expedition) Leg 302 (Pälike et al., 2008; Sangiorgi et al., 2008b). These records

all show Eocene cycles with a precessional period in foraminiferal or bulk carbonate isotopic composition or sediment composition, with some also showing short and / or long period eccentricity and occasionally obliquity. These records indicate that during the Eocene, precessional and eccentricity forcing dominated over obliquity although some high latitude shallow marine records may also exhibit obliquity cycles during the early Eocene (Hollis et al., 2005).

1.5. Field locality and the southern Pacific Ocean

This study focuses on the climate and ecology of the southern Pacific Ocean. The cold deepwater of the Antarctic region has a worldwide impact on modern ocean circulation and the Eocene "Southern Ocean" must also have played a crucial role in global climate and heat distribution (Bice et al., 1998; Carter et al., 1999; Gersonde et al., 1999; Hodell et al., 2002). It is therefore important to understand the evolution of Southern Ocean palaeoceanography and hydrology to understand not only the climatic evolution of the southern high latitudes but of the whole planet.

Antarctica is currently "thermally isolated" by an eastward flowing Antarctic Circumpolar Current (ACC) that encircles the continent. However, the oceanography of the middle Eocene southern Pacific Ocean was very different to the present day, as there was no deep water flow through the Tasman gateway (between Australia and Antarctica) (Bice et al., 1998; Exon et al., 2004) and hence, no ACC. This means that there was no true Southern Ocean as in the present day, so the term "Southern Ocean" is used to refer collectively to the high southern latitudes of oceans adjacent to Antarctica, before the opening of the Tasman gateway. The southern Pacific was the largest and probably the most important part of this high latitude ocean system (Lyle et al., 2008).

Oceanographic reconstructions based on both proxy evidence and modelling suggest alternative Eocene ocean circulation patterns in the "Southern Ocean". Some reconstructions suggest a warm saline East Australian Current (EAC) that transported heat southwards towards Antarctica, possibly accounting for it's warmth during the Eocene (Murphy and Kennett, 1985; Nelson and Cooke, 2001). This is supported by a number of studies of foraminiferal assemblages, oxygen and carbon isotopic records (Murphy and Kennett, 1985; Pak and Miller, 1992; Gersonde et al., 1999) and sediment deposition (Exon et al., 2004). The model has been refined by a number of studies (Mountain and Miller, 1992; Pak and Miller, 1992; Ramsey and al, 1994; Exon et al., 2004) to incorporate a Southern Ocean deepwater source (proto-Antarctic Bottom

Water) developing by at least the middle Eocene. An alternative scenario has recently been proposed by Huber et al. (2004) who combined studies of biogeographical microfossil distribution and coupled climate models of the Eocene to reconstruct ocean circulation. They suggest that a northward flowing Tasman Current (TC) prevented the penetration of an EAC to high southern latitudes and therefore that heat transport to Antarctica by this current was lower than previously suggested. This circulation appears to fit well with not only with biogeographical data presented by Huber et al. (2004) but earlier palaeoecological data for the region (Huber et al., 2004). This alternative scenario is lent further support by modeling studies that find it difficult to generate low latitude sinking of warm saline deep water (WSDW) and conclude that high latitude deep-water formation is sufficient to generate the high latitude warmth seem during the Eocene if elevated low latitude temperatures are also accepted (e.g. Bice and Marotzke, 2001). These alternative scenarios are discussed further in Section 6.2.5 and illustrated in Figure 1.6 below.

The area of Hampden Beach, on the East Coast of South Island, New Zealand currently lies at approximately 45° south which is well to the north of the Subantarctic Front (SAF) and the influence of the ACC (Figure 1.5). However, this locality is of interest as during the Eocene New Zealand was located approximately 10° further south. This means that Hampden Beach was situated within the critical region of the southern Pacific where it is unclear whether the dominant current was cold water flowing north (e.g. Nelson and Cooke, 2001) (Figure 1.6A) or warmer water flowing south (e.g. Huber et al., 2004) (Figure 1.6B). Records of the ocean temperature from Hampden Beach may therefore be crucial in resolving this uncertainty about Eocene high latitude palaeoceanography and the results are discussed in Sections 6.2.5 and 6.2.7.

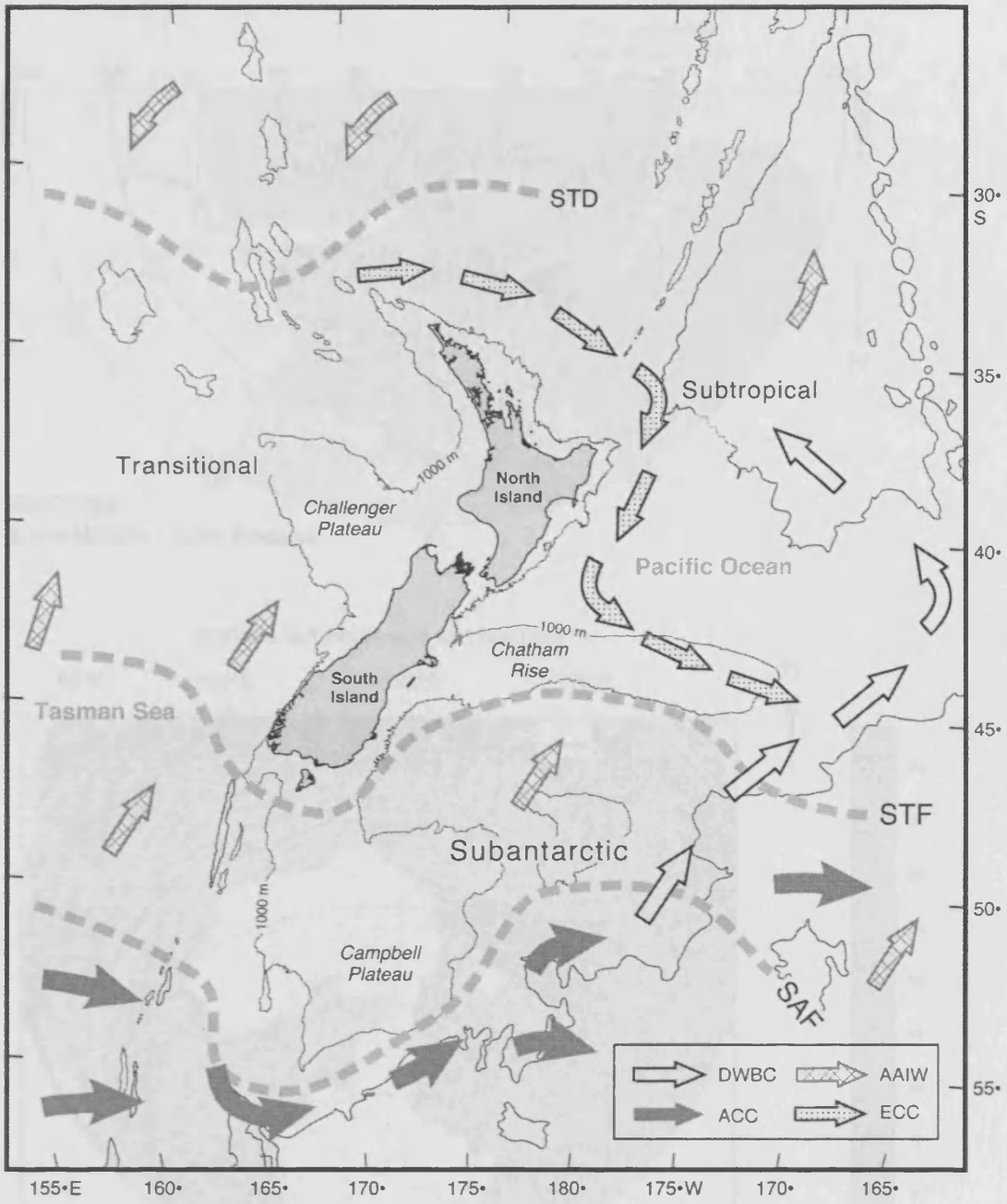

Figure 1.5. Oceanographic setting of present day New Zealand showing the position of ocean major water masses, fronts and current systems. SAF = Subantarctic Front, STF = Subtropical Front, STD = Subtropical Divergence, DWBC = Deep Western Boundary Current, ACC = Antarctic Circumpolar Current, AAIW = Antarctic Intermediate Water, EEC = Equatorial Counter Current, Adapted from (Carter et al., 2004)

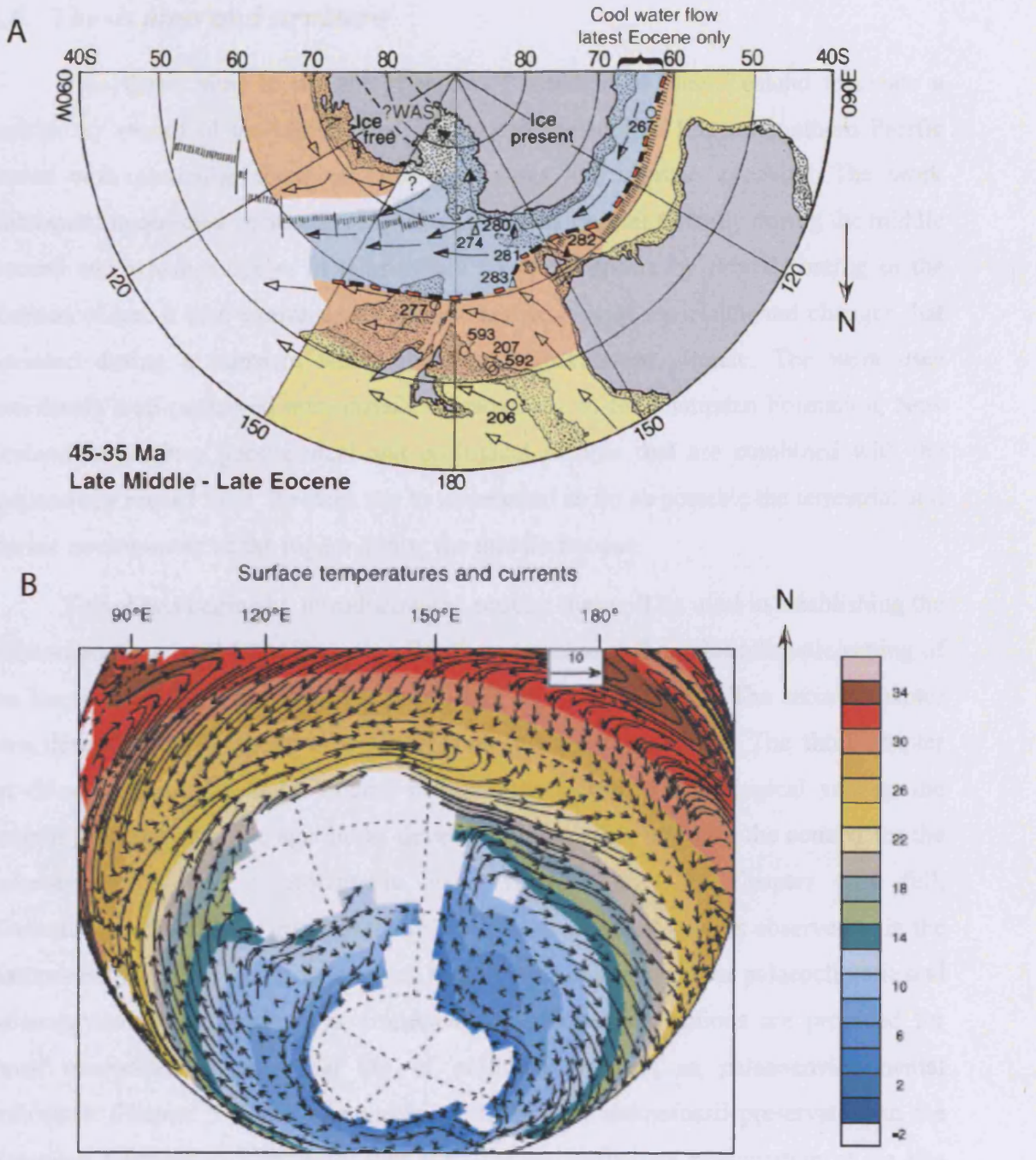

Figure 1.6A. Palaeoceanographic reconstruction of the New Zealand sector of the "Southern Ocean" during the middle Eocene taken from Nelson & Cooke, 2001; B. Modelled middle Eocene ocean circulation taken from Huber et al., 2004.

1.6. Thesis aims and structure

This thesis aims to use the Hampden Formation of New Zealand to create a multiproxy record of the climate and ecology of the middle Eocene southern Pacific Ocean with particular focus on transient events and climate cyclicity. The work addresses the question of whether significant ice was present globally during the middle Eocene and whether cycles in temperature could be driven by orbital forcing in the absence of ice. It also examines the marine and terrestrial environmental changes that occurred during a transient warm event in a greenhouse climate. The work uses excellently well-preserved microfossils characteristic of the Hampden Formation, New Zealand to produce geochemical and ecological records that are combined with the sedimentary record from the same site to understand as far as possible the terrestrial and marine environment of the region during the middle Eocene.

This thesis begins by introducing the proxies that will be used in establishing the palaeoclimatic record from Hampden Beach and outlining the palaeoclimatic setting of the Eocene and the issues that it is hoped this study will address. The second chapter then describes the methods used to generate these proxy records. The third chapter provides study of the field section at Hampden Beach, it's geological setting, the sampling strategy and the age model developed for it. This provides the context for the palaeoecological and palaeoclimatic work which follows. In Chapter 4, a full, illustrated, taxomic list is given of the micro- and nannofossil species observed at in the Hampden Formation. The way in which these fossils can be used for palaeoclimatic and palaeoenvironmental analysis is discussed and species descriptions are provided for those microfossil groups that are of particular interest as palaeoenvironmental indicators. Chapter 5 studies the carbonate micro- and nannofossil preservation in the Hampden Formation. This establishes the excellent carbonate preservation at the site and thus the suitability of foraminifera from this formation for use in geochemical proxy analyses. The final two chapters present the proxy records from Hampden Beach and discuss their palaeoclimatic and palaeoecological implications. Chapter 6 presents the long, low-resolution record through the whole Hampden Formation and establishes an approximately 3 million year record of southern Pacific palaeoclimate including a transient warm event, possibly corresponding to the MECO. Chapter 7 focuses on a high-resolution record in the lower part of the Hampden Formation and provides a detailed record of cyclic marine and terrestrial climatic changes that occur with an ~18 k.y. period.

2. Methods

2.1. Sample collection and preparation

Fieldwork was carried out on the Hampden Section at Hampden Beach between 5th and 23rd February 2005. Trenches were dug back into the cliffside at four sites to remove weathered surface material. Samples spanning 5 cm vertically were then collected from within the trenches, each sample weighing approximately 1kg. Single samples were also dug out of the cliffside every 50 m horizontally, approximately 1m above the base of the cliff (see Section 3.2.1).

At the Institute of Geological and Nuclear Sciences (IGNS) laboratory in Lower Hutt the samples were dried in an oven at 40 °C for approximately 48 hours. They were then lightly crushed using a flat plate into gravel-sized lumps and returned to the oven until their weight stopped decreasing due to water loss (around 24 hours). Approximately 50 g of dried sample was retained to process for organic carbon, nannofossils, diatoms and dinoflagellates. A further 500 g was then weighed out for processing for foraminifera.

The 500 g samples were soaked in 18 MΩ de-ionised (DI) water for approximately one hour and stirred occasionally to encourage disaggregation, before washing through a 63 μm sieve, again using 18 MΩ DI water. The coarse fraction was retained and dried in an oven at 40 °C for approximately 24 hours.

Once dried, the coarse fraction was split into eighths and 7/8ths dry-sieved to obtain fractions > 355 μm, 250-355 μm, 212-250 μm and 63-212 μm to pick for foraminifera.

2.2. Foraminifer oxygen and carbon isotopic analysis

2.2.1. Sample cleaning

As many specimens as possible of the planktonic foraminifera *Globigerinatheka index* were picked from the fraction 212-250 μm and 10 to 20 specimens of the benthic foraminifera *Cibicidoides sp.* were picked from the fraction 250-355 μm.

These specimens were broken open by gently crushing between glass plates and infilling removed as far as possible with a needle and paintbrush. All specimens of *G.*

index were processed as described below for isotopic analysis, the equivalent of approximately 3 specimens of *Cibicidoides* were used for isotopic analysis whilst the remaining fragments were retained for processing for trace metal analysis (see 2.3).

The test fragments were placed in a sample tube, a few drops of 3 % H_2O_2 were added and left for 30 minutes to oxidise any remaining organic carbon. A few drops of methanol were then added and the samples were placed in an ultrasonic bath for 5 seconds to agitate any fine particles and suspend them in the liquid. The liquid was absorbed off the top of the samples and the samples left for approximately one hour to dry completely.

2.2.2. Sample analysis

The samples were then transferred to glass vials and dissolved in phosphoric acid. The carbon dioxide (CO_2) gas produced was analysed to determine the relative abundances of ^{18}O to ^{16}O and ^{13}C to ^{12}C. These isotopic analyses were carried out on a ThermoFinnigan MAT252 mass spectrometer with automated KIEL III carbonate preparation unit at Cardiff University. Stable isotope results were calibrated to the PDB scale by international standard NBS19 and analytical precision derived from repeated runs of the standard was ± 0.08 ‰ for $\delta^{18}O$ and ± 0.05 ‰ for $\delta^{13}C$.

2.3. Foraminifer trace metal analysis

2.3.1. Sample cleaning

The fragments of *Cibicidoides* underwent a modified version of the trace metal cleaning procedure described by Boyle and Keigwin (1985/86). This included clay removal by ultrasonic cleaning in both 18 MΩ DI water and methanol, oxidation of remaining organic carbon and minor acid leaching to remove trace metals adsorbed onto the test surface.

The modified method also included a step to manually remove remaining pyrite and other particulates by placing the samples onto a glass plate under a microscope and identifying and removing particles directly (Barker et al., 2003). This took place after the initial clay removal step and was followed by an additional clay removal step to remove any contaminants introduced whilst the sample was exposed on the glass slide.

The reductive step described in Boyle and Keigwin (1985/86) was omitted as no metal oxide coatings were visible and the reductive process is corrosive to the calcium carbonate (Barker et al., 2003; Rosenthal et al., 2004; Yu et al., 2007). Since the sample size was already limited by the small number of specimens available, the problem of dissolution outweighed the potential benefit of removing very small amounts of metal oxides.

2.3.2. Sample analysis

The samples were dissolved in 120 µl of 0.065 M HNO_3 and centrifuged before removing a 10 µm aliquot and a 100 µl sample from each one. The aliquots were increased in volume by adding a further 290 µl of 0.5 M HNO_3. These aliquots were then analysed on a ThermoElemental X-series Inductively Coupled Plasma Mass Spectrometer (ICP-MS) at Cardiff University. The trace metal standard CFSGS-04 was analysed at calcium concentrations ([Ca]) from 0.1 to 2 mM at the start and end of the run of aliquots and a 0.5 mM standard was analysed every 5^{th} sample. The [Ca] of each of the aliquots was then determined after correcting for instrumental drift through the run.

Standards were created with [Ca] to match each sample to the nearest 0.1 mM using dilutions of the standard CFSGS-04. This enabled each sample to be measured against a standard with a similar [Ca]. Matching a standard to every sample allows the elimination of problems caused by the 'matrix effect', in which the Mg/Ca ratio measured by the mass spectrometer is dependent on the [Ca] of the sample (de Villiers et al., 2002; Lear et al., 2002). This dependency is known to be highly non-linear in the quadrupole ICP-MS used here (see Figure 2.1). The alternative is to dilute all of the samples to a common [Ca], however since some samples were very small it was important to maximise the [Ca] of each sample.

Immediately prior to analysis 300 µl of 0.5 M HNO_3 was added to each sample. This acid was added shortly before analysis to avoid possible leaching from the sample tubes.

The samples were then analysed on the same instrument as used to analyse the aliquots. Consistency standards (CFCS1-04 and CFCS2-04) and the analytical standard (CFSGS-04) at [Ca] of 4 mM were analysed at the start and end of each run, acid blanks (0.5M HNO_3) were analysed every 5 samples. The samples, each immediately followed

by a [Ca] matched standard, were analysed in order of increasing [Ca] to reduce memory effects.

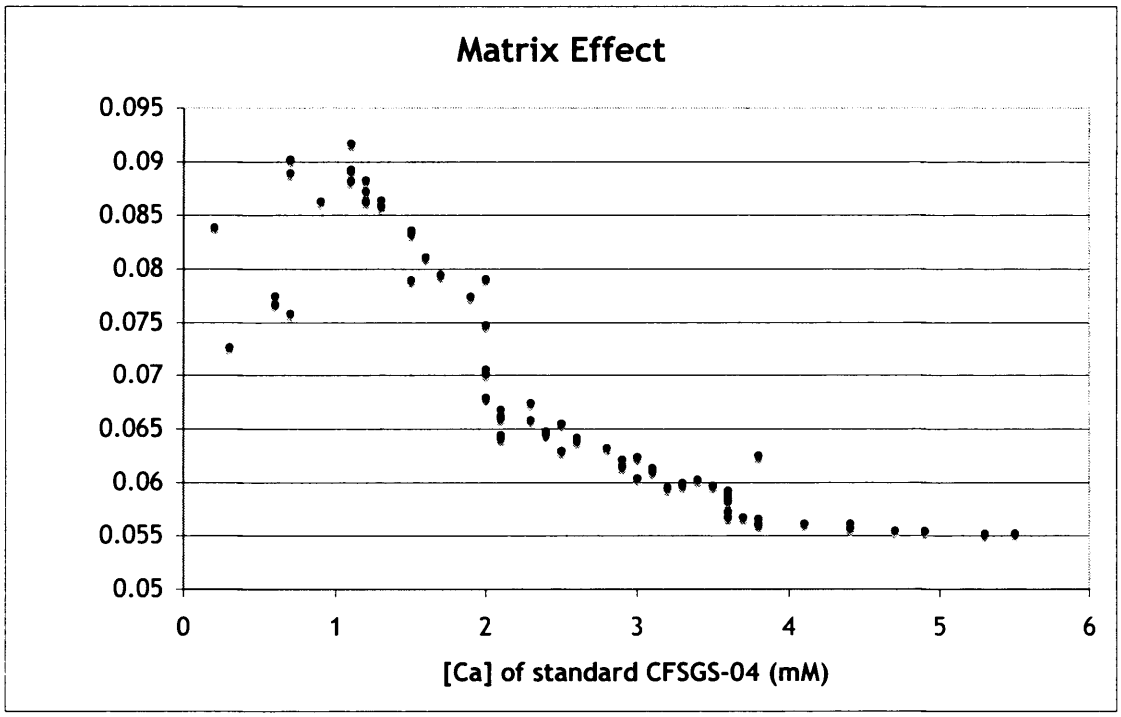

Figure 2.1. The matrix effect produced by the ICP-MS at Cardiff University when analysing standard CFSGS-04 with a true Mg/Ca ratio of 2.49 mmol/mol.

Count data were recorded for aluminium (Al), magnesium (Mg), strontium (Sr), manganese (Mn), cadmium (Cd), uranium (U) and calcium (Ca) and each sample was analysed 4 times. It was found that the first run from each sample often contained a 'bubble' due to the slow uptake of the sample by the low flow nebuliser, giving a low count rate, so all first run data were excluded from subsequent analysis. Samples with anomalously high levels of Al or Sr ($^{27}Al/^{43}Ca$ > 0.1 mmol/mol or $^{88}Sr/^{43}Ca$ >0.0015 mmol/mol) were also excluded from the results as Al and Sr are abundant in clay minerals and are likely to indicate contamination of those samples with clays. The counts of each element in the previous blank were subtracted from the counts of each sample to produce 'blank corrected counts'. Intensity ratios were then calculated between ^{43}Ca and ^{25}Mg, ^{27}Al, ^{55}Mn, ^{88}Sr, ^{111}Cd and ^{238}U based on the mean blank corrected count data from the 3 runs, mean analytical precision for all samples was found to be <1.1% (rsd). The single sample with standard error >4% over 3 runs was excluded from further analysis. The blank corrected intensity ratios for each sample were corrected using their matched standard to give a true abundance ratio.

2.4. Foraminifer test weight analysis

2.4.1. Weighing foraminifera

The planktonic species *Acarinina primitiva* was used for all test weight analysis as sufficient *G. index* were not available following isotopic analysis. All specimens were picked from the 212-250 μm fraction to minimise shell weight variability due to size difference.

Individual foraminifera were placed in a drop of water using a paintbrush, any that appeared opaque when wet were rejected as this indicates infilling of the test. Up to 10 specimens were selected to comprise each sample.

A Sartorius SC2 microbalance was used to weigh two small foil cups, the 'measuring' cup and the 'reference' cup, each of which was weighed 10 times and a mean calculated. Samples were transferred to the measuring cup under a microscope using a dry paintbrush. The cup and the contents were weighed 3 times and a mean and standard error calculated, in all cases the standard error on the mean weight of the measuring cup plus contents was <0.0005%, reflecting the high precision of the balance. The mean weight of the measuring cup was subtracted from the mean total weight to obtain the weight of the foraminifera, which was divided by the number of foraminifera in the sample to find a mean foraminifera weight for each sample. The reference cup was weighed between each sample to check for drift in the balance and the balance was recalibrated if necessary. Every 5 samples the measuring cup was weighed again to check it had not been damaged or collected any debris.

To obtain an estimate of the intra-sample variability in foraminiferal weight a single sample (CB05HB030) was selected and each individual foraminifera within this sample was weighed according to the method above. Again, the analytical error on the mean weight of the measuring cup with foraminifera was found to be below 0.0005% for each foraminifera and frequently lower. The weights of the 10 foraminifera were then added and the mean calculated to be 8.4 ± 0.3 mg, a percentage error of 4%. This illustrates that whilst the % error resulting from intra-sample variability remains reasonably low, it is nearly 4 orders of magnitude greater than the analytical error from the balance and consequently for this data it is misleading to present data showing error bars that reflect only the analytical precision. Unfortunately weighing each foraminifera individually is very time consuming and it is not practical to determine the intra-sample variability for each sample.

2.4.2. Imaging and size correction

Two specimens of *A. primitiva* were selected from sample CB05HB098 and fixed in a well slide in the standard orientation, aperture side facing up. These were the reference specimens and all other specimens were measured in comparison to them.

For each sample the 10 specimens that had been weighed were placed on the well slide beneath the two reference specimens and correctly orientated but not fixed. An image was taken of all 12 specimens with a Lecia DFC 480 camera on a Lecia MZ16 microscope using Earth Basic software for image capture at 4x magnification. One typical specimen from each sample was chosen for further analysis under the scanning electron microscope (SEM) and that specimen was also photographed at 10x magnification. Lighting conditions were kept constant for all images but exposure times were varied to take account of changing ambient light in the room.

The images were then analysed using Image-Pro Plus software (Media Cybermetrics Ltd) allowing the area, major and minor axis length, maximum and minimum diameter, length and width of each specimen on the photograph to be measured. These were normalised for each image to the measurements for the reference foraminifera to account for the effect of difference in ambient light on the images. The mean and standard error of the test area and diameter was then calculated for each sample. This allowed the weight of the specimens to be corrected for their size according to equations 2.1 and 2.2 as outlined in Barker (2002). The mean of the length and area corrected weights was then used as the size normalised weight.

Equation 2.1 $Wt_{A\ norm} = Wt_{meas} * (A_{avr}/A_{meas})^{3/2}$

Equation 2.2 $Wt_{L\ norm} = Wt_{meas} * (L_{avr}/L_{meas})^{3}$

$Wt_{A\ norm}$ is the mean test weight of a sample normalised to area
Wt_{meas} is the measured mean test weight of the sample
A_{avr} is the mean test area of all weighed foraminifera
A_{meas} is the measured mean test area of the sample
L_{avr} is the mean maximum diameter of all weighed foraminifera
L_{meas} is the mean maximum diameter of the sample

Those specimens selected for SEM imaging were mounted on an SEM stub, gold coated and photographed (see 2.5 below). The specimens were then cracked open between glass plates, re-coated and photographed at high magnification to illustrate their internal structure.

2.5. *Scanning Electron Microscopy (SEM)*

All scanning electron microscope photographs were taken using a Veeco FEI (Philips) XL30 ESEM (Environmental Scanning Electron Microscope) FEG (Field Emission Gun), fitted with a secondary electron detector (SE). Specimens were gold coated and photographs were taken in high vacuum mode using SE, this has a resolution of 2 nm at 30 KV and magnification of x10 to x 500,000, scales are indicated on images.

2.6. *Smear slides*

Smear slides were produced to study nannofossils and check for the presence of diatoms. A few mm^3 of complete sample was placed on a glass slide and a small drop of 15 MΩ DI water added using a pipette. A toothpick was used to smear the wet sample fairly evenly across the slide and the slide was then dried on a hotplate. Ultraviolet (UV) resin was then dropped onto the slide and a cover slip placed carefully on top to minimise air bubbles, the resin was cured by placing under a UV lamp for a minimum of 20 minutes.

The slides were then studied under a high power microscope with a 100x oil objective at Cardiff University and also loaned to Paul Bown of University College London for further nannofossil assemblage analysis.

2.7. *Foraminiferal assemblage counts*

An assessment of the total foraminifera species diversity was carried out on a $1/8^{th}$ split of the >150 μm fraction. The sample was examined under a microscope on a picking tray marked with a grid, for each grid square the foraminifera were identified and their number recorded. It is standard in micropalaeontology that 300 specimens are counted (Buzas, 1990) since this should allow 95 % of species that are present at >1 % abundance to be identified (Dennison and Hay, 1967). However, it was found that the Hampden samples are unusually diverse, with over 50 % of the species being present at the <1 % level making 300 specimens inadequate to accurately characterise the samples. Instead, for two of these samples a cumulative plot of species number against total number of foraminifera was generated and counts were continued until the plots were approaching horizontal (very few new species being added). It was estimated that

between 500 and 600 specimens were required to obtain a representative assemblage in sample CB05HB079 (Figure 2.2). Four samples were analysed in this way.

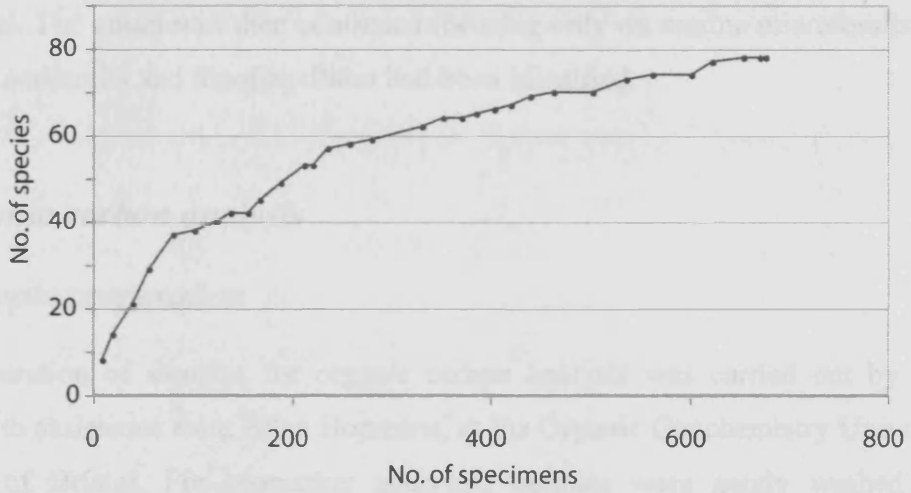

Figure 2.2. Cumulative diversity plot of number of species observed against number of specimens counted for sample CB05HB079.

Full assemblage counts were made of the planktonic foraminifera from the 212-250 μm fraction to place age constraints on the section. Seven eighths of the total sample was picked at this fraction and all planktonic foraminifera identified to species level. Alternate samples throughout the "long section" were counted.

2.8. Dinoflagellate assemblage counts

Palynological slides were prepared from approximately 10 g of dry sample by Natasja Welters at Utrecht University using their standard preparation method with no heavy liquid step or oxidation. The sample was dried overnight at 60 °C and accurately weighed then a known number of *Lycopodium* spores were added as a reference so that the concentration of organic microfossils in the sample could later be determined when counting the slide. The samples were then moistened with Agepon and hydrochloric (HCl) and hydrofluoric (HF) acids respectively were used to remove the calcareous and silicate components of the sample. The samples were initially treated with 10 % HCl, then twice with 40 % HF, rinsed with 30 % HCl between and after HF treatments. The remainder was rinsed and the residue sieved at 250 μm and 15 μm. The fraction retained between these two sieves was then mounted on a slide using resin.

The slides were then examined under a microscope. The first 100 organic microfossils were identified and categorised as spores, pollen grains, acritarchs or dinoflagellates. The dinoflagellates were identified to genus, and where possible, species level. The count was then continued focusing only on marine microfossils until 100 marine acritarchs and dinoflagellates had been identified.

2.9. Organic carbon analysis

2.9.1. Sample preparation

Preparation of samples for organic carbon analysis was carried out by Luke Handley with assistance from Ellen Hopmans, at the Organic Geochemistry Unit of the University of Bristol. For biomarker analyses, samples were gently washed with methanol, freeze-dried and powdered with a Retsch PM100 Ball Mill. The powdered samples were extracted via soxhlet extraction over 24 hours using dichloromethane/methanol (2:1 v/v) as the organic solvent. The total lipid extracts were separated into two fractions on an aminopropyl column by elution with dichloromethane/iso-propanol (3:1 v/v; neutral fraction) and 2 % (by volume) acetic acid in diethyl ether (acid fraction). The neutral fraction was further split using a column packed with (activated) alumina by elution with hexane (saturated hydrocarbon fraction), hexane/DCM (9:1 v/v; aromatic fraction) and dichloromethane/methanol (1:2 v/v; polar fraction) and all fractions were evaporated to dryness under a steady flow of nitrogen. The polar fraction was re-dissolved in 200 µl of hexane/isopropanol (99:1 v/v) and subsequently filtered through a 0.45 µm, 4 mm diameter PTFE filter attached to a 1 ml Luer syringe, ready for Liquid Chromatography (LC-MS) analysis.

2.9.2. Sample analysis

Analysis was performed by Stefan Schouten at the Royal Netherlands Institute for Sea Research (NIOZ) using a high performance (Palo-Alto, CA, USA) 1100 series High Performance Liquid Chromatography Mass Spectrometer (HPLC/MS) instrument equipped with an auto-injector and Chemstation chromatography manager software. Separation was achieved with a Prevail Cyano column (2.1 x 150 mm, 3 µm; Alltech, Deerfield, IL, USA), maintained at 30°C. Injection volume varied from 1 to 20 µl. Glycerol dialkyl glycerol tetraethers (GDGTs) were eluted isocratically with 99% hexane and 1% propanol for 5 min, followed by a linear gradient to 1.8% propanol over

45 min. Flow rate was 0.2 ml/min. After each analysis the column was cleaned by back-flushing hexane/propanol (90:10, v/v) at 0.2 ml/min for 10 min. Detection was achieved using atmospheric pressure positive ion chemical ionization mass spectrometry (APCI-MS) analysis of the eluent. Conditions were: nebuliser pressure 60 psi, vaporizer temperature 400 °C, drying gas (N2), flow 6 l/min, temperature 200 °C, capillary voltage -3 kV, corona 5 μA (~3.2 kV). GDGTs were detected via single ion monitoring (SIM) of their [M+H]+ ins (dwell time = 234 ms) and quantified by integration of the peak areas. Absolute concentrations were calculated using an external standard curve obtained with a crenarchaeol standard. The concentrations of GDGTs were corrected for the regular removal of incubation water (100 ml from 5 L) due to sampling for lipid analysis. TEX_{86} values were calculated according to (Kim et al., 2008).

2.10. X-Ray diffraction analysis

2.10.1. Complete sample analysis

X-ray diffraction requires a homogenous solid crystalline sample, so approximately 5 g of whole sample was crushed to a fine powder using a pestle and mortar. This powder was then packed into an aluminium sample holder and placed into the sample chamber of the diffractometer. The sample was bombarded with X-rays and the diffraction pattern recorded over a 2θ range of 2° to 70°.

The instrument used was a Phillips PW1710 automated Powder Diffractometer , which uses copper (CuKα) radiation at 35 kV 40 mA. The resulting diffraction patterns were recorded using PW1877 APD version 3.6 and the mineral phases contained within the samples were identified using PW1876 PC-Identify version 1.0b.

To generate semi-quantitative abundance estimates for the minerals, the area under the major peak for each mineral was measured using PW1877 APD version 3.0 and the relative % abundance of each mineral in the sample calculated.

2.10.2. Fine fraction analysis

To specifically identify the clay phases approximately 3 g of the crushed sample was processed to separate out the clay fraction. The samples were first added to 18 MΩ DI water and placed in an ultrasonic bath to disaggregate them, they were then washed through a 63 μm sieve and the coarse fraction discarded. The fine fraction was retained

and left to settle for approximately 10 minutes, the liquid containing the clay fraction was then poured off the silt residue. This liquid was placed in a centrifuge to bring the clays out of suspension and most of the water poured off. The clays were re-suspended into a small amount of water, transferred onto a glass slide using a pipette and left to dry.

The clay slides were analysed using the same instrument as the whole sample but the diffraction pattern was only recorded between 2θ angles of 2° and 32°, the range in which clay minerals produce peaks. The samples were then glycolated using ethylene glycolate and analysed again as glycolation affects specific clay minerals, allowing them to be discriminated from others that have very similar diffraction patterns.

2.11. Carbonate dissolution

To accurately determine the weight % calcium carbonate ($CaCO_3$) within the sediment, approximately 5 g of whole sediment from each sample was weighed accurately into a plastic sample bag. The bag was placed open into a 500 ml jar with the opening of the bag folded back over the mouth of the jar. Approximately 300 ml of 2 M Acetic acid was added to the sample and agitated gently, then left for ~24 hours. The acid was then siphoned off the top of the sediment being careful to minimise disturbance of the sediment, leaving ~1 cm covering the sediment. The acid addition and removal step was then repeated and as little acid as possible left covering the sediment.

After the final acid was siphoned off the samples, they were placed in an oven at 40 °C for several days until they were completely dry. The samples were then weighed, the difference between the initial weight and the final weight was determined and the % of the original weight lost was calculated to give the weight % $CaCO_3$.

3. Hampden Beach Field Section

3.1. Introduction

3.1.1. Location

Hampden is a small town on the east coast of South Island, New Zealand situated between Christchurch to the north and Dunedin to the south (Figure 3.1). The Hampden Section is a coastal cliff section approximately 2.5 km long situated at Hampden Beach, 2 km north of the town of Hampden. The section extends northwards from Park Gulch, with the cliff becoming progressively lower until it is obscured by beach gravels. The cliffs that outcrop along the Hampden Section consist of middle Eocene Hampden Formation calcareous siltstone overlain by Quaternary glacial sediment (McMillan, 1999).

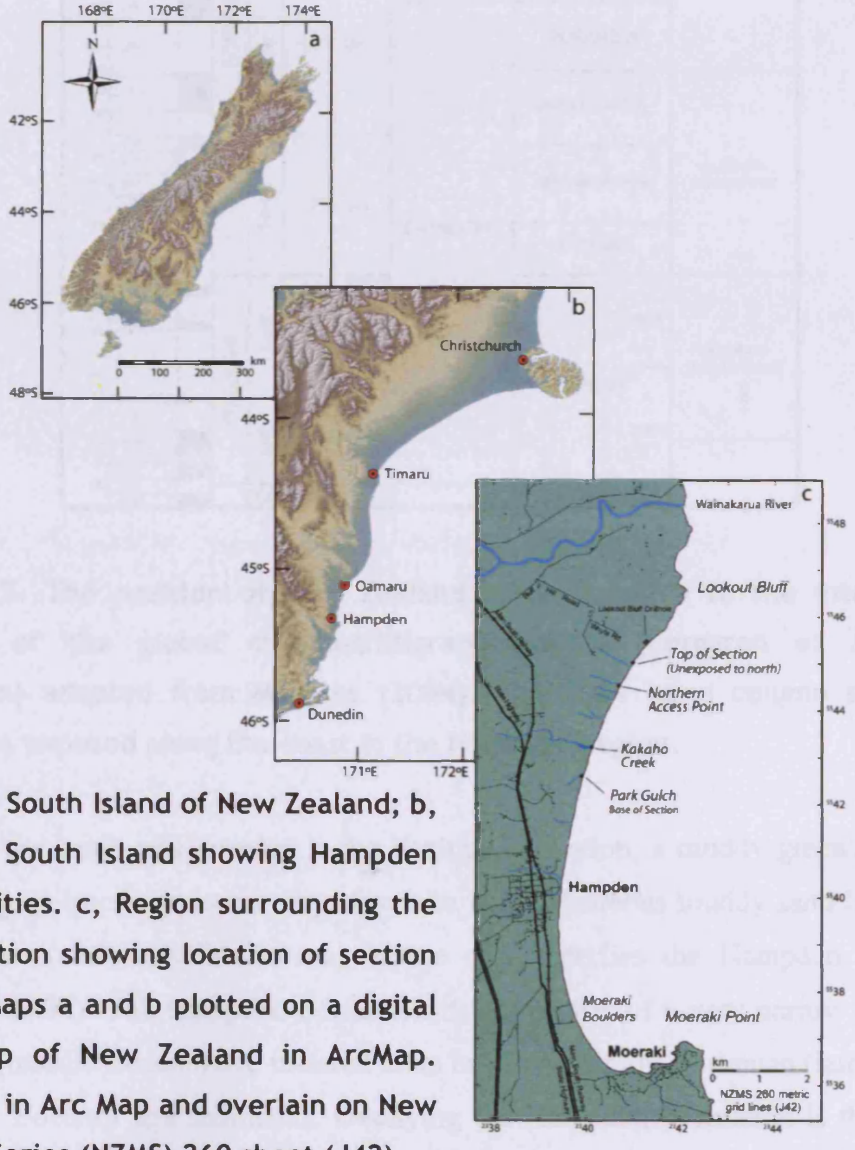

Figure 3.1. a, South Island of New Zealand; b, East coast of South Island showing Hampden and nearby cities. c, Region surrounding the Hampden Section showing location of section and access. Maps a and b plotted on a digital elevation map of New Zealand in ArcMap. Map c plotted in Arc Map and overlain on New Zealand Map Series (NZMS) 260 sheet (J42)

3.1.2. Geological setting

The locality at Hampden Beach is thought to comprise a middle Eocene sedimentary sequence bridging the New Zealand Dannevirke and Arnold Series (Morgans, 2004; Morgans, 2008, Figure 3.2). New Zealand stratigraphy is routinely discussed in relation to a series of local stages that are then correlated to globally accepted stages and the international timescale.

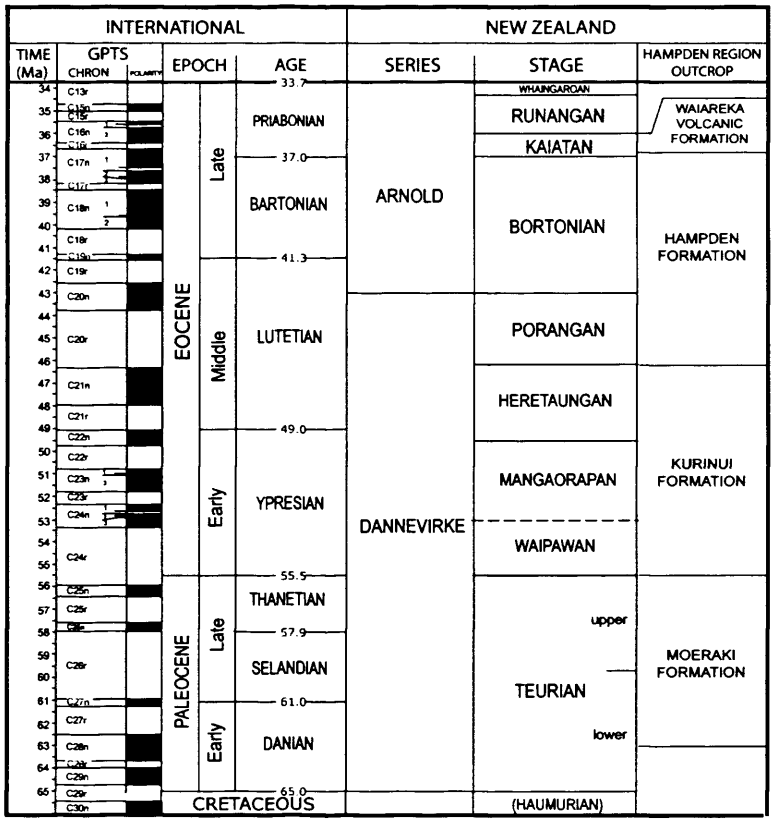

Figure 3.2. The position of New Zealand stages relative to the international divisions of the global chronostratigraphic scale (Berggren et al., 1995 calibration) adapted from Morgans (2004). The right hand column shows the formations exposed along the coast in the Hampden region.

To the south of Hampden is the Kurinui Formation, a muddy greensand at the base fining up into a smectitic silty claystone with calcareous muddy sand layers. It is Heretaungan (early middle Eocene) in age and underlies the Hampden Formation (Morgans, 2008). The Hampden Formation itself consists of a very narrow interval of Porangan (middle Eocene) age material at its base overlain by Bortonian (late middle to early Late Eocene) age sediments. Overlying the Hampden Formation is the Kaiatan (Late Eocene) age Waiareka Volcanic Formation, consisting of pyroclastic tuffs,

agglomerate and basalt (dykes, sills and pillow lavas) with lenses of chalk and diatomite. Dykes associated with this volcanism also penetrate into the upper part of the Hampden Formation (McMillan, 1999).

This study focuses specifically on the Hampden Formation. The bottom few metres of the formation is highly glauconitic and likely condensed; above this interval the sediment consists of grey-brown calcareous, micaceous, mudstone to very fine sandstone. There are numerous small faults within the section and several igneous dykes associated with the overlying Waiareka Volcanics in the upper part of the formation. The sediment exhibits clearly developed cyclicity on a ~1 m wavelength that persists throughout the section (Figure 3.3). The muddy facies enables exceptional microfossil fossil preservation (Pearson and Burgess, 2008) making the microfossils useful for environmental and palaeoclimatic analysis (Chapter 5).

Figure 3.3. View facing west of the cliffs towards the southern end of Hampden Beach showing clearly developed cyclicity. Hugh Morgans is standing at site 1 (trench 1) to the left of the photograph with a 1.5 m measuring stick for scale, the ladder marks the position of site 1 (trench 2).

3.1.3. Tectonic history

Hampden Beach is located at approximately 45°S, however during the middle Eocene, tectonic reconstructions suggest that New Zealand lay substantially further south (Nelson and Cooke, 2001). An Eocene tectonic reconstruction of New Zealand (King, 2000) indicates that while the Hampden Formation was deposited, Hampden Beach was located off the eastern coast of the New Zealand landmass in a region now referred to as the Canterbury Basin (Figure 3.4) at ~53 °S.

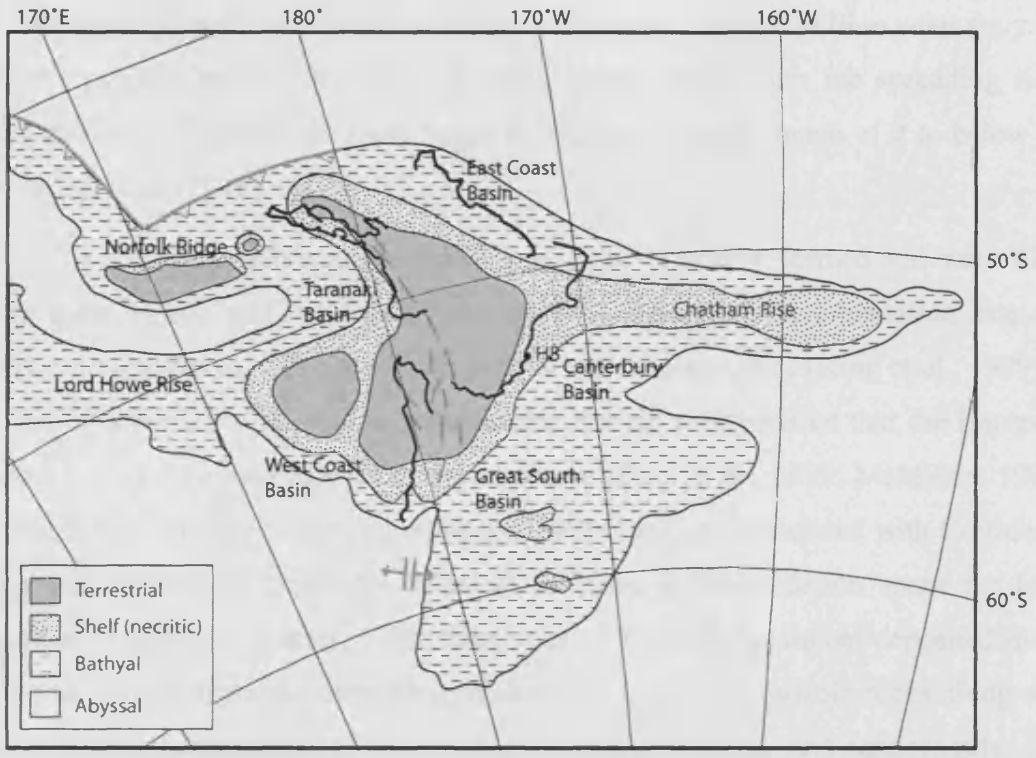

Figure 3.4. Palaeogeographic reconstruction of New Zealand at 40 Ma based on King (2000) with palaeobathymetry from GNS Science. The present day coastline is shown in bold, overlain on middle Eocene palaeobathymetry and major tectonic features. The Hampden Beach locality is at the site 'HB'.

New Zealand has an extraordinarily complex geological history (Suggate et al., 1978; King et al., 1999; McSaveney and Nathan, 2007) and is still tectonically active today. Present day New Zealand is the sub-aerially exposed portion of a larger continental shelf referred to as "Zealandia" that lies on the boundary between the Pacific and Indo-Australian tectonic plates. The oldest rocks forming this landmass were sediments deposited offshore to the north-east of the Gondwana supercontinent between the Cambrian and Devonian. These sediments were uplifted and accreted onto Gondwanan margin as the oceanic crust on which they were deposited was subducted beneath Gondwana during the late Devonian and Carboniferous (Suggate et al., 1978). Much of the sediment was metamorphosed in the collision zone to schist and gneiss, or melted to form granite and diorite although some sedimentary greywackes remained. By the middle Cretaceous these rocks formed a mountainous region along the Australian-Antarctic margin of Gondwana, which was being steadily eroded. During the Cretaceous rifting began in Gondwana and by approximately 85 Ma the sea had flooded into a rift separating Zealandia from the part of Gondwana that was to become Australia

and Antarctica (Suggate et al., 1978). This rift developed over 30 million years (m.y.) to form the present Tasman Sea. As Zealandia moved away from the spreading ridge during the early Cenozoic the crust began to cool and subside, much of it to below sea level (King et al., 1999).

The sedimentary basins around New Zealand primarily formed and were filled during these rifting and subsidence phases, with changes in sedimentation rate and occasionally pauses in sedimentation related to regional tectonics (King et al., 1999). It was during a period of thermal subsidence and marine transgression that the Hampden Formation was deposited in the Canterbury Basin (King et al., 1999; McMillan, 1999). This basin was initially developed in the extensional regime associated with Cretaceous rifting and subsequent thermal subsidence provided accommodation space for large quantities of sediment (Carter, 1988; King et al., 1999). The sediment deposited in the basin was derived from the remaining sub-aerially exposed Mesozoic rocks along with marine carbonates composed of the remains of calcareous micro- and nannofossils.

Within this broadly transgressional sequence, there is a regional unconformity that immediately underlies the Hampden Formation and is thought to relate to the onset of seafloor spreading and oblique extension to the south of New Zealand in the early middle Eocene (King et al., 1999). Following this unconformity, subsidence continued in the eastern basins reaching a maximum marine transgression in the middle part of the Oligocene with predominately carbonate deposition occurring (Carter, 1988). Rifting and the development of the new Australia–Pacific plate boundary began to take place in the middle of the Oligocene to the south-west of New Zealand and by the Late Oligocene this plate boundary had propagated through western South Island, splitting the single plate previously underlying Zealandia into the Pacific and Indo-Australian plates. Beginning in the Miocene, rotation of these plates lead to an oblique collision in which the Pacific plate subducted beneath the Australian plate in the north of New Zealand and the Australian plate subducted beneath the Pacific plate to the South of New Zealand, with a large strike-slip fault through South Island linking these zones (King, 2000). The onset of convergent tectonics, uplift and expansion of land area increased the terrigenous sedimentation within most basins. This phase of deformation is referred to as the Kaikoura orogeny and is still ongoing. This orogeny is responsible for the uplift of the western part of the Canterbury basin, including the Hampden Formation, to its present position just above sea level.

3.2. Field Section

3.2.1. The Hampden Section

The Hampden Section is accessed via land owned by Robyn & Lindsay McNicol who can be contacted (as of 2006) at;

Address; Wainakarua Coastal Farm,
377 Bluff Hill Road
10-ORD, Oamaru
Telephone; 03 439 4622
E-mail; wainak.farmsextra.co.nz

The access to the section is via two points, Kakaho Creek to the south of the section and a narrower dry creek cutting to the north (Figures 3.1 and 3.7). The base of the section is at the locality referred to as Park Gulch (45°18.25' S, 170°49.91' E) and the top of the section is at (45°16.96' S, 170°50.78' E), beyond which the Hampden Formation is unexposed (Figure 3.5).

Figure 3.5. Photograph facing northwest of the top of the Hampden Section. The Hampden Formation (grey calcareous siltstone) is approximately 1 m high at the south (left) of the photograph and is pinched out by the Quaternary sediments above and beach gravels below.

The basal contact was initially thought to be faulted, as a fault is visible in the cliff at Park Gulch, apparently between the dark brown-grey low cliffs of the Kurinui Formation to the south and the paler green-grey higher cliffs of the Hampden Formation to the north (Figure 3.6 A and B). However, on a single day during the 2005 field season, the wave cut platform below the cliff was exposed and it was seen that the fault could not clearly be traced in the platform (Figure 3.6 C). A suite of samples was collected along this platform by Hugh Morgans of IGNS and his analysis concluded that the contact was marked by a rapid coarsening upwards sequence from the claystones of the Kurinui to the basal glauconitic sandstone of the Hampden Formation. He arbitrarily placed the base of the Hampden at the point where glauconite exceeds 10% of the rock in hand specimen (Morgans, 2008).

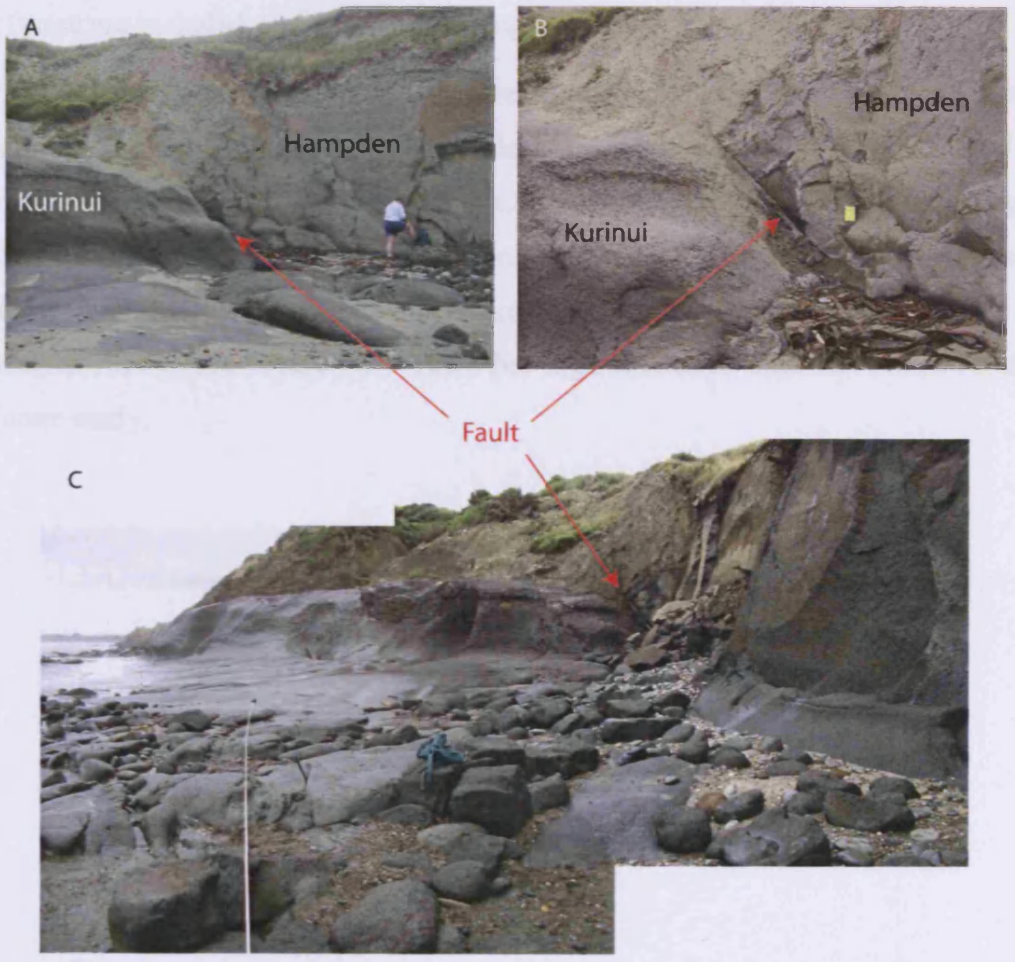

Figure 3.6. The basal contact of the Hampden Formation at Park Gulch. A, the contact that is typically visible (Hugh Morgans for scale); B, close up of the fault (yellow notebook for scale ~12x18 cm); C, panorama of two photographs showing the fault and exposed wave cut platform. Samples were collected by Morgans along the white measuring tape. Photographs by Burgess.

The sampling strategy employed at the section by Hugh Morgans and Catherine Burgess was to collect 1) a low-resolution suite of samples through the whole section to study long term trends and construct a biostratigraphic framework for the section and 2) a number of short high-resolution suites of samples to study the apparent cyclicity in detail.

The low-resolution samples (referred to throughout as the "long section") were collected every 50 m horizontally along the section. These samples were located (using photographs and field notes) to alternate with a sample suite collected by Hugh Morgans in 2001, to improve the combined sample spacing to every 25 m. The samples were located using a handheld global positioning system (GPS) unit with an estimated accuracy of ±15 m (Figure 3.7), the average dip of the sediment between samples was recorded and photographs were taken of the cliff viewing from one sample site to the next (these are included on the accompanying CD ROM).

High-resolution suites of samples were collected at four sites along the section (Figure 3.7), at each of these sites samples were collected up the cliff face in 5 cm intervals (see Section 2.1). The most southerly of these (Site 1) was the longest, totalling 5.2 m stratigraphic height and forms the basis of Chapter 7. Subsequent use of the term "high-resolution" section therefore refers to the section collected from two trenches at Site 1 (see Figure 3.3). The other high-resolution sites have been reserved for future study.

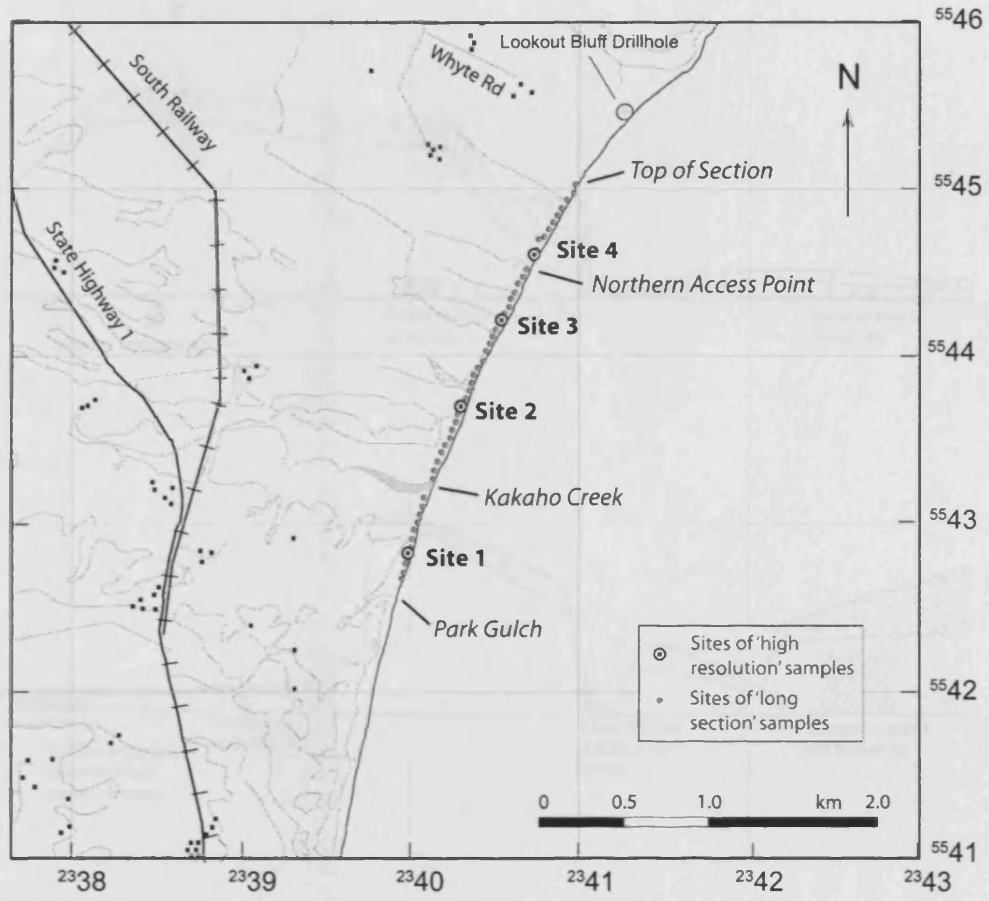

Figure 3.7. Map of Hampden Beach (NZMS260 metric grid, 1949 datum), overlain by an ArcMap plot of the sample sites and key features of the Hampden Section. The "high-resolution" section discussed in Chapter 7 was collected at Site 1.

The measurements and notes taken along the section have been used to sketch a view along the cliff face noting features of interest (Figure 3.9). The dip measurements and horizontal distances have then been used to calculate the stratigraphic thickness of the Hampden Section (table 3.1) using trigonometry (Figure 3.8).

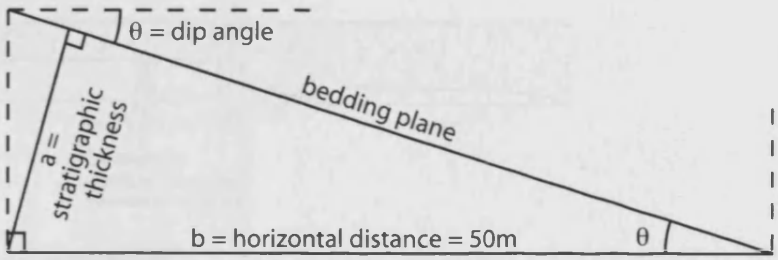

$a = b * \sin\theta$

Figure 3.8. Trigonometric method used for calculating the stratigraphic thickness between samples (a) from the horizontal distance (b) and dip angle (θ).

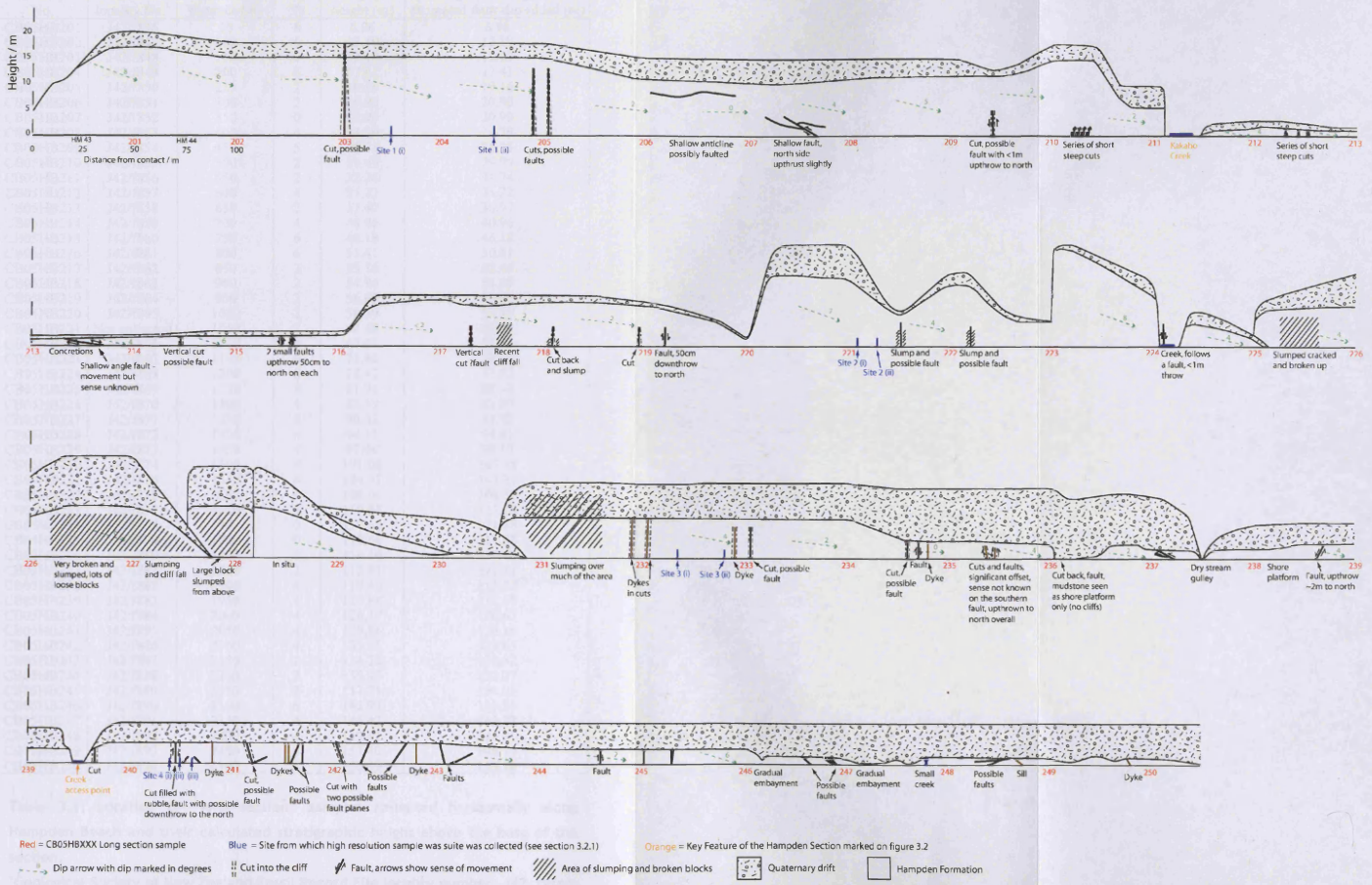

Figure 3.9. Annotated sketch of Hampden Section at 2.5x vertical exaggeration, showing the key features of the section, sample locations and dip measurement

CB Sample No.	NZ Fossil locality No.[1]	Horizontal distance (m)	Dip °N	Stratigraphic height (m)	Stratigraphic height with estimated fault slip added (m)
CB05HB201	J42/f846	50	8	6.96	6.96
CB05HB202	J42/f847	100	6	12.19	12.19
CB05HB203	J42/f848	150	0	12.19	12.19
CB05HB204	J42/f849	200	6	17.41	17.41
CB05HB205	J42/f850	250	2	19.16	19.16
CB05HB206	J42/f851	300	2	20.90	20.90
CB05HB207	J42/f852	350	0	20.90	20.90
CB05HB208	J42/f853	400	4	24.39	24.39
CB05HB209	J42/f854	450	5	28.75	28.25
CB05HB210	J42/f855	500	2	30.49	29.99
CB05HB211	J42/f856	550	2	32.24	31.74
CB05HB212	J42/f857	600	4	35.72	35.22
CB05HB213	J42/f858	650	2	37.47	36.97
CB05HB214	J42/f859	700	4	40.96	40.96
CB05HB215	J42/f860	750	6	46.18	46.18
CB05HB216	J42/f861	800	6	51.41	50.41
CB05HB217	J42/f862	850	2	53.16	52.16
CB05HB218	J42/f863	900	2	54.90	53.90
CB05HB219	J42/f864	950	2	56.65	55.65
CB05HB220	J42/f865	1000	2	58.39	57.89
CB05HB221	Not collected	1050	7	64.48	63.98
CB05HB222	J42/f866	1100	4	67.97	67.47
CB05HB223	J42/f867	1150	4	71.46	70.96
CB05HB224	J42/f868	1200	8	78.42	77.92
CB05HB225	J42/f869	1250	4	81.91	82.41
CB05HB226	J42/f870	1300	4	85.39	85.89
CB05HB227	J42/f871	1350	6	90.62	91.12
CB05HB228	J42/f872	1400	4	94.11	94.61
CB05HB229	J42/f873	1450	4	97.60	98.10
CB05HB230	J42/f874	1500	4	101.08	101.58
CB05HB231	J42/f875	1550	4	104.57	105.07
CB05HB232	J42/f876	1600	4	108.06	108.56
CB05HB233	J42/f877	1650	3	110.68	111.18
CB05HB234	J42/f878	1700	0	110.68	111.18
CB05HB235	J42/f879	1750	0	110.68	111.98
CB05HB236	J42/f880	1800	4	114.16	112.46
CB05HB237	J42/f881	1850	2	115.91	112.21
CB05HB238	J42/f882	1900	4	119.40	115.70
CB05HB239	J42/f883	1950	4	122.88	117.18
CB05HB240	J42/f884	2000	4	126.37	120.67
CB05HB241	J42/f885	2050	4	129.86	126.16
CB05HB242	J42/f886	2100	4	133.35	129.65
CB05HB243	J42/f887	2150	1	134.22	130.52
CB05HB244	J42/f888	2200	2	135.97	132.27
CB05HB245	J42/f889	2250	2	137.71	134.01
CB05HB246	J42/f890	2300	6	142.94	139.24
CB05HB247	J42/f891	2350	4	146.42	142.72
CB05HB248	J42/f892	2400	4	149.91	146.21
CB05HB249	J42/f893	2450	4	153.40	149.70
CB05HB250	J42/f894	2500	4	156.89	153.19

Table 3.1. Location of "long section" samples collected horizontally along Hampden Beach and their calculated stratigraphic height above the base of the section.

[1]Geological Society of New Zealand Fossil Record File locality number. J42 refers to New Zealand Map Series (NZMS) 260, a 1:50,000 topographical map series.

It should be noted that the stratigraphic thickness of the section has been estimated by a number of authors (Hornibrook et al., 1989; McMillan, 1999; Morgans, 2008) and these estimates vary significantly. This is a result of the low dip angle and extreme length of the section, small faults of uncertain throw and the difficultly in estimating an average dip over 50m intervals. Furthermore, it is unlikely that the dip visible in the cliff is always the true dip and the northern end of the section is covered by beach gravels that shift during storms, causing the extent of the exposure to change. Throughout this study the stratigraphic thickness used is 153 m, which is calculated using the method above and incorporates the movement on small faults recorded in the author's field notes. The stratigraphic column shown below (Figure 3.10) is adapted from Morgans (2008), to fit the stratigraphic thickness used here and includes the positions of the "long section" samples.

All samples collected for this study are referred to by their field collection number which has the form CB05HBXXX where XXX is a 3 digit identifying number, however they have also been assigned Geological Society of New Zealand Fossil Record File locality numbers (f-numbers), listed in Appendix 1. Since it is important to be able to refer this sample set to those previously collected, the stratigraphic column is also reproduced in Appendix 1, showing the samples used in this study referred to by their f- numbers along with previous sample collections curated by GNS Science. The samples of Morgans are positioned with respect to the studied samples and to field features noted on the horizontal sketch and stratigraphic column. Earlier collections are placed relative to the Morgans samples according to Morgans (2008). Note that sample heights read from this stratigraphic column for earlier collections will differ from those given by Morgans (2008) because he uses a different calculation for stratigraphic thickness; however their relative positions are accurate, which enables the integration of all 5 datasets.

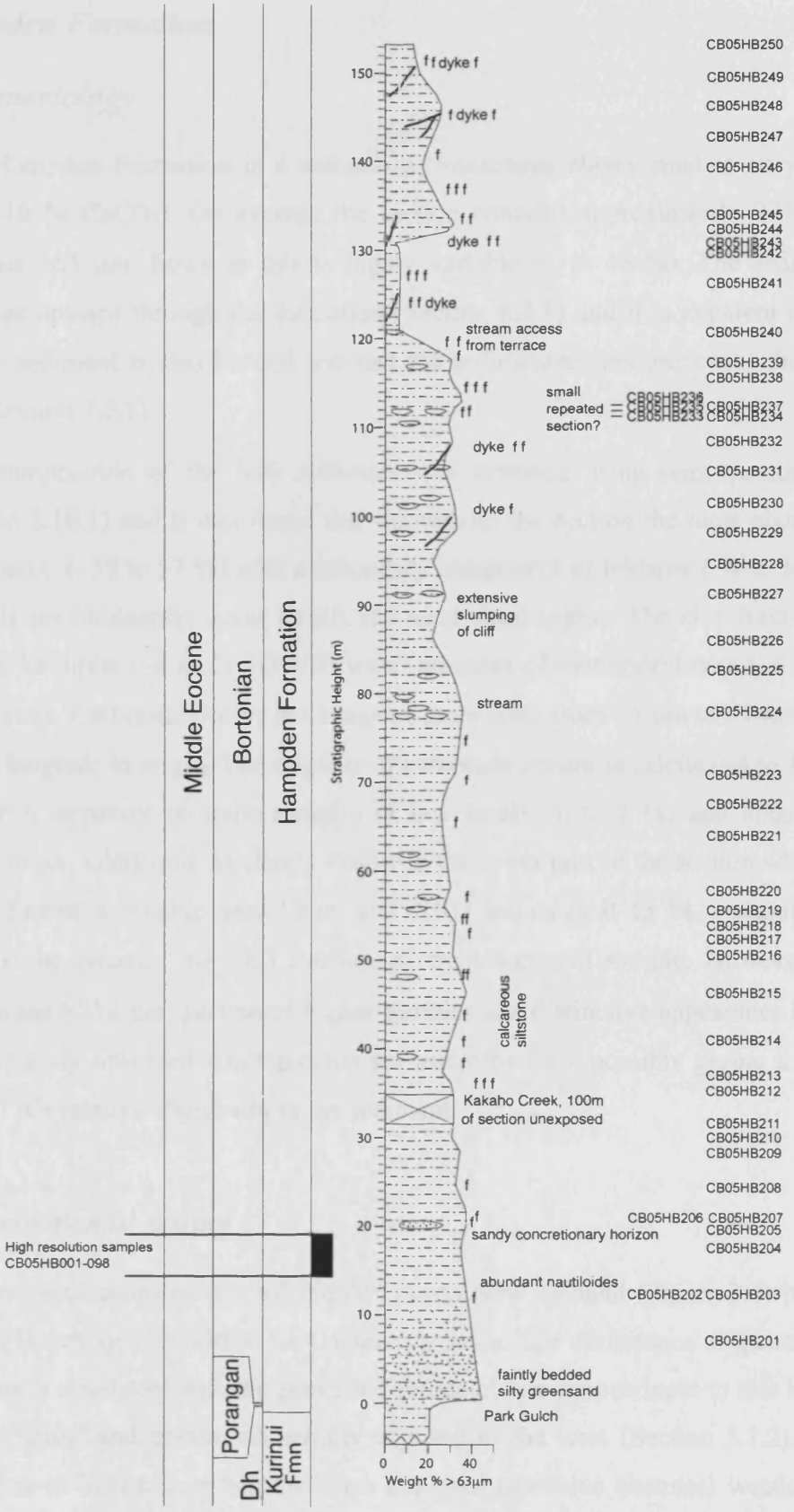

Figure 3.10. Stratigraphic log of the Hampden Section based on the weight % >63 µm and features noted in the field. The positions of "long section" samples and the "high-resolution" sampling interval are marked.

3.3. Hampden Formation

3.3.1. Sedimentology

The Hampden Formation is a calcareous, micaceous clayey mud to very fine sandstone (~10 % $CaCO_3$). On average the section contains approximately 27% (by weight) grains >63 μm, however this is highly variable (8 to 45 %). The sediment generally fines upward through the formation (Section 6.2.1) and it is apparent in the field that the sediment is also bedded and that the sedimentary texture varies through these beds (Section 7.2.1).

The composition of the bulk sediment was assessed using semi-quantitative XRD (Section 2.10.1) and it was found that throughout the section the most abundant mineral is quartz (~39 to 57 %) with a secondary component of feldspar (~8 to 34 %). Both minerals predominantly occur as silt and sand sized grains. The clay fraction is dominated by kaolinite (~8 to 21 %) with lesser amounts of montmorillonite (~4 to 10 %) and carbonate. Carbonate occurs at a range of grain sizes from <1 μm to >1 mm and much of it is biogenic in origin. The majority of carbonate occurs as calcite (~4 to 16 %) but aragonite is apparent in some samples at low levels (1 to 2 %) and aragonitic macrofossils occur. Glauconite is clearly visible in the lower part of the section where it gives the sediment a notable green hue, and XRD indicates it to be a significant component in the coarse (>63 μm) fraction of the lowermost sample. However, its occurrence in the >212 μm fraction of higher samples and distinctive appearance mean that it is frequently observed when picking for microfossils – possibly giving a false impression of it's relative abundance in the sediment.

3.3.2. Environmental setting

The tectonic reconstruction of middle Eocene New Zealand (Figure 3.4) places the Hampden Beach locality within the Canterbury basin. The dominance of quartz and feldspar grains is consistent with the presumed source of terrigenous input to this basin, the Mesozoic schist and gneiss sub-aerially exposed to the west (Section 3.1.2). The high proportion of kaolinite within the clays indicates extensive chemical weathering and leaching of this terrestrial rock (Curtis, 1990; Zachos et al., 1999) suggesting a relatively warm regional climate with high precipitation (discussed further in Chapters 6 and 7).

The benthic foraminiferal palaeodepth indicators used in this study (Section 4.2.4) were studied from samples in the lower part of the Hampden Formation and suggest a depositional environment around shelf – slope break (~300 m water depth). This agrees with the work of Morgans (2008) who studied further benthic foraminiferal species from throughout the Hampden Formation and concluded that they indicate similar to slightly deeper depths ranging from outer shelf to inner bathyal (~300 – 400 m). The low ratio of planktonic to benthic foraminifera seen in these samples (~0.2 : 1) (Section 7.2.3) also supports this relatively shallow palaeodepth (Gibson, 1989). It is possible that the water depth increased during the deposition of the formation as the Canterbury Basin continued to subside (Section 3.2.1) resulting in the grain size decrease upwards seen in the section (Section 6.2.1).

The depositional environment means that the sediment provides a sedimentary and palaeontological record of both terrestrial and marine environments. Furthermore, the large terrigenous clay component within the sediment decreases the permeability of the rock, reducing the diagenesis of calcareous microfossils contained within it, increasing their usefulness as palaeo-environmental proxies (Section 5). This makes the Hampden Section an excellent resource to study Eocene palaeoclimate and the environmental response to climatic changes both on land and in the ocean.

3.3.3. Biostratigraphy

The age constraints for the Hampden Section are limited. The sediment is so weakly magnetised that palaeomagnetic data are not available and the sediment contains no ash bands or other layers that could be used to generate absolute dates. Consequently the age model developed for the Hampden Section was initially biostratigraphic and based primarily on the lowest occurrence (LO) and highest (HO) occurrences of foraminifera and nannofossils. These are correlated to the global magnetic polarity timescale using the chronology of Berggren et al. (1995) unless otherwise specified. We employ specifically Antarctic biozones developed by Huber & Quillivéré (2005) for foraminifera and Wei (1992) for nannofossils (Figure 3.11).

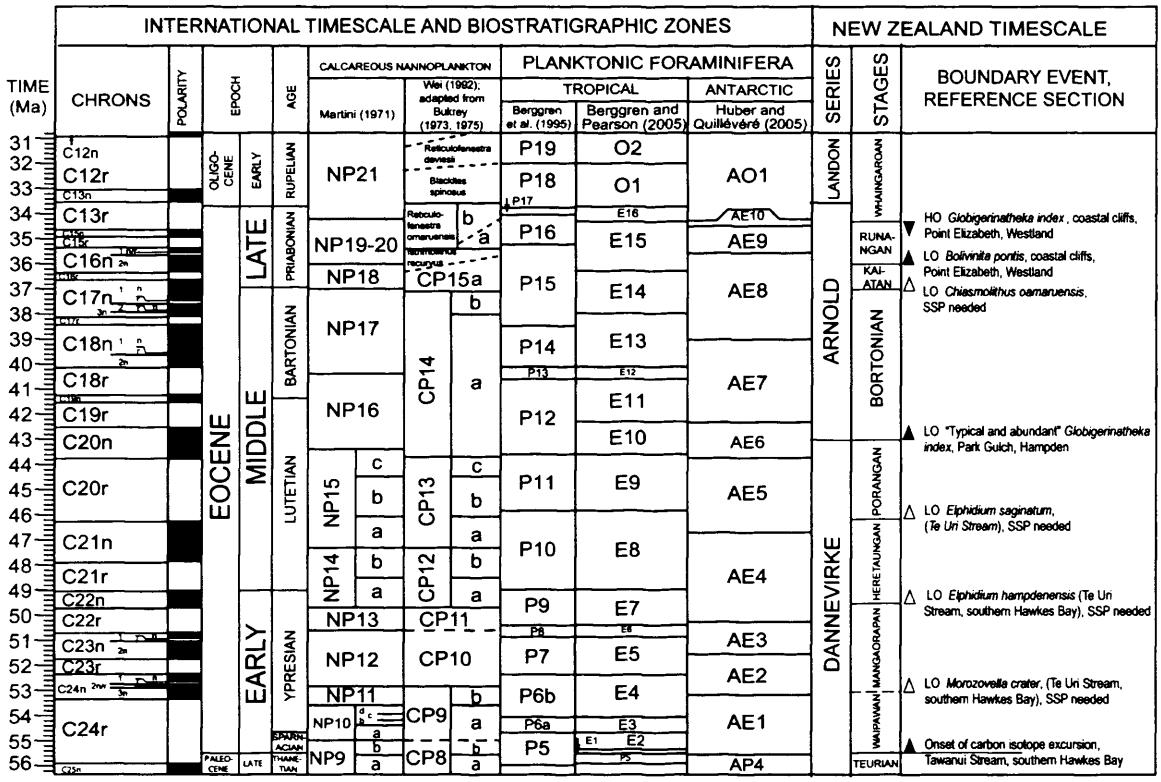

Figure 3.11. The Eocene timescale showing international biostratigraphic zones (adapted from Huber and Quillévéré, 2006) aligned with New Zealand regional stages and their biostratigraphic boundary events (after Morgans, 2004).

Counts were carried out on a 7/8ths split of the 212-250 μm component of the samples from the "long section" (table 3.2) and data from these were combined with the work of Morgans (2008).

The major biostratigraphic events recorded at Hampden Beach are summarised below and outlined in Table 3.3. Beneath the Hampden Formation lies the Kurinui Formation, which has been dated as Heretaungan (49.5 to 46.2 Ma) in age (Morgans, 2008). The lowermost biostratigraphic datum seen at Hampden is the LO of *Elphidium saginitum,* recorded by Morgans in his sample J42/f488 and which occurs without *Globigerinatheka index.* The LO of *E. saginitum* marks the Heretaungan-Porangan boundary (46.2 Ma) and the LO of *G. index* marks the Porangan-Bortonian boundary (43 Ma) indicating a Porongan age for this sample (Morgans, 2004). Field notes allowed the reference of sample f488 to the collection used in this study and determined that it came from within the northern part of Park Gulch, considered here to be the base of the Hampden Section and ~7 m stratigraphically below CB05HB201 (Figure 3.10).

Sample No.	*G. index*	*G. kulgeri*	*A. praetopilensis*	*A. mcgowrani*	*A. primitiva*	*A. collactea*	*A. bullbrooki*	*A. pseudosubspherica*	*C. unicavus*	*G. bassriverensis*	*G. martini*	*G. ouachitaensis*	*S. angiporoides*	*S. cf utilisindex*	*S. linaperta*	*S. senni*	*G. nuttalli*	*T. pomeroli*	*T. frontosa*	Others	Fragments
HB250	37	1									9		3	1	35				2	1	15
HB249	120		1	6	61	1		1		3	55	1	12		91			10	5	8	
HB248	19	1	1		1			2			15		2		49				2	4	
HB247	15	1			4					1?	6		1		19				1		
HB246	5				8						5				11						2
HB245	98		5	2	17			1			48	2	1		435			4	17	3	
HB244	15		1	2	6						8			4	64			2	3		
HB243	15									1	4				4			3	2	2	1
HB242	19			1	4						9				6			4	3	2	1
HB241	11										7				6				1		
HB240	6										1				3			1	1		
HB239	3														1						
HB238	31				7						12				3						
HB237	10			1	2	1		1			5	1			1					1	
HB236	48		3		4			1			15		2	1	15			2		1	
HB235	39				5						13		3	4	26			2	1		
HB234	70		2		4	2		3		1	14		13	9	80			7	2	1	
HB233	38		1		3					2	10		15	4	55			3	1		
HB232	12		1	3	2			2			8		1		31			2	16	2	
HB231	10		1	3	5							2	5	5	26			3	3		1
HB230	3		3	1	1	1		2			1		5	5	32			1	2		
HB229	32		1		3						9		13	11	51						
HB228	51		1		1	2		3	2		22		3	21					1	1	
HB227	77		2	2	2			1	1	3	29		5	9	67	?		1	1	2	
HB226	42	1	2	1	2		12	1	1	1	9	1	11	13	91			1	1		
HB225	5		2				1				1		2	1	16						
HB224	9			1						2	1	1	5	1	15						
HB223	51		10	1	10		2			4	26	3	13	2	4	2		1	1	4	2
HB222	5		1		2		8					4			5				2	2	
HB220	26		3		6		4			1	15	1	7		15	1		1	2	2	3
HB219	10		3	2	9		12			8	7	22	7	4	36			2	17	1	2
HB218	22		2		10		1			2	9	26	12	1	12	1		1	8	2	2
HB217	26			1	9	1	1			4	4	9	8	2	18	1		1	6	1	5
HB216	12		1	1	15	2	4				3	5	9	5	15	1				1	
HB215	12		2	2	18					9	3	18	2	1	2	3			6		
HB214	38		3	14	52	2				41	8	76	7	13	17		1	10	30	6	
HB213	11		3	7	17					1	3	11	5		14		1			2	
HB212	15		6	6	12					1	5	1	7		16					2	
HB211	3		5	7	18					3		4			3					4	
HB210	7		1	2	2					5	1	7	4		5					5	
HB209	7		8	9	14				1?	6	2	13	3		10	1				1	
HB208	8		8	10	31	1				4	2	5	1		6					1	
HB207	5		3	7	17					2	1	3	2		5					1	1
HB206	5		3	10	23	1				9	1	10	3		5					2	
HB205	21		2	2	10	2				9	5	9	6							4	
HB204	7		1	4	25					4	3	6	1		6	1					
HB203	7		2		10					2	2	1	3		3	1				1	
HB202	6		1	1	5					1	3									2	

Table 3.2. Planktonic foraminiferal count data from "long section" samples. Grey shading indicates the absence of taxa with a biostratigraphically significant highest occurrence; outlines indicate the presence of taxa with a biostratigraphically significant lowest occurrence.

The sample f489 (Morgans) immediately above sample f488 contained neither *E. saginitum* nor *G. index*. However, the next datum observed is the occurrence of abundant *Globigerinatheka index* (plate 4.2 a-h) in J42/f301 (Morgans) indicating an age of less than 43 Ma. This sample also contains a species identified as *Subbotina angiporoides minima*, which was regarded at a junior synonym of the species *Subbotina angiporoides* (plate 4.3 e-h) by Olsson et al. (2006a). The first occurrence of *S. angiporoides* marks the base of the Austral planktonic foraminiferal biostratigraphic zone AE7 dated at ~42.28 Ma (Huber and Quillévéré, 2006). The distance between samples f488 and f301 is only a few tens of centimetres (Morgans 2008, Figure 6), indicating a highly condensed Porangan and lower Bortonian interval, hiatus or faulting at the base of the Hampden Section. The co-occurrence of *G. index* and *S. angiporoides* is observed throughout the section (Samples CB05HB203-250 of this study).

The next datum observed in this study is the clear HO of *Acarinina bullbrooki* (Plate 4.1a-d) dated at 40.5 Ma (Berggren et al., 2006) in sample CB05HB226; this lies 89.5 m stratigraphically above the base of the section. Near the top of the section, a possible HO of *Acarinina primitiva* (Plate 4.1q-t) is seen. This would denote the top of the Austral planktonic foraminiferal biostratigraphic zone AE7 dated at 39.0 Ma (Huber and Quillévéré, 2006) and is identified in f336 in the Morgans collection and in the stratigrapically adjacent sample CB05HB249 in the current collection (stratigraphic height of 149.7 m). However, this species is only absent from the uppermost 4 samples and localised absences occur lower in the section, so it not considered a definite HO. Furthermore, the species *Turborotalia frontosa* (Plate 4.3 q-t) occurs in the uppermost samples of the section (CB05HB250 and Morgans f334, f333 & f332). This species has a HO of 39.3 Ma (Berggren et al., 1995) suggesting that to be the minimum age of top of the section. It should be noted though that this species makes a subtle transition to *T. pomeroli*, which has a much higher HO and that it is not a zone fossil and thus less rigorously dated than the HO of *A. primitiva*.

As foraminiferal data are limited, nannofossil biostratigraphy was also applied to the section. Preliminary counts of five samples through the "long section" were conducted by Dr Paul Bown at University College London as part of this study. He records the presence of *Reticulofenestra umbilicus* and *Discoaster bifax* in the lowermost samples and *Chiasmolithus solitus* throughout the section, suggesting the entire section falls within Nannofossil Subzone CP14a (Okada and Bukry, 1980), which is equivalent to upper Nannofossil Zone NP16 (Martini, 1971). The date for the top of

CP14a was given as 40.4 Ma by Berggren et al. (1995) which would disagree with the HO of *A. primitiva.* However, work by Arney & Wise (2003) redates the top of Subzone CP14a to 37.9 Ma, for the Southern Ocean, as a result of the co-occurrence of *Reticticulofenestra bisecta* (which has a LO at 38 Ma) and *Chiasmolithus solitus* (the HO of which defines the zone) at ODP Site 1138 on the Kerguelen Plateau (also observed at the Falklands Plateau, Wise, 1983). The revised age of subzone CP14a is in good agreement with the foraminiferal biostratigraphy presented in this study.

The foraminiferal and nannofossil biostratigraphic data are summarised in Table 3.3 and combined on the stratigraphic column below (Figure 3.12).

	Lowest Occurrence (LO)	Highest Occurrence (HO)	Chron	Age (Ma)	Reference	Occurrence at Hampden Beach	Stratigraphic height at Hampden Beach	Notes
Foraminifera								
Elphidium hampdense	X		N/A	49.5	Morgans (2008)	f300 (Morgans)	-?.0.2 m	Marker for the base of the Heretangun
Elphidium saginitum	X		N/A	46.2	Morgans (2008)	f488 (Morgans)	-? 0.1 m	Marker for the base of the Porongan
Globigerinatheka index	X		C20n	42.9	Bergerren et al (1995)	f301 - (Morgans) and **HB202-250**	~0 - ~156 m and **12.2 - 153.2 m**	Marker for the base of the Bortonian. Placed at at 44Ma (20n/20r boundary) in Pearson et al. (2006) based on it's occurance at Shatsky Rise. Hole 689B -Kerguelen has several hiatuses and the Anarctic zonation of Kennett & Stott (1990) has been revised by Huber & Quillivéré (2006) who follow Berggren et al. (1995) in placing the boundary at 43 Ma. Morgans (2004) also follows Bergerren (1995).
Subbotina angiporoides	X		N/A	42.28	Huber & Quillivéré (2005)	f301-333 (Morgans) and **HB203-250**	~0 – ~154.5 m **12.2 - 153.2 m**	
Acarinina bullbrooki		X	C18r	40.5	Bergerren et al. (1995)	**HB216-226**	**50.4 - 85.9 m**	Does not appear until sample HB216 in this study. HO at HB226
Turborotalia frontosa		X	C18n (mid)	39.3	Bergerren et al. (1995)	**HB214-250**	**41.0 – 153.2 m**	Range in Pearson et al. (2006) is based on Toumarkine & Bolli (1970) from Italy. *T. increbescens* is recorded in ocasional samples from f301 to f332 by Morgans - photos suggest this is actually *T. frontosa*. Morgans studied > 150μm size fraction, may be observing smaller specimens. Only absent from HB250 and f334,3,2 (Morgans 2008), may not represent true HO.
Acarinina primitiva		X	C18n	39.0	Bergerren et al. (1995)	f301-335 (Morgans) **HB202 to 249**	~0 – 148 m **12.2 – 149.7 m**	
Nannofossils								
Reticulofenestra umbilicus	X		C20n	43.7	Bukrey (1975)	**HB205-250**	**19.2 – 153.2 m**	Marks base of CP14a . HB205 was lowest sample studied for nannofossils
Chiasmolithus solitus		X	C17n (3n)	37.9	Wise (1992)	**HB205-250**	**19.2 – 153.2 m**	Marks top of CP14a - HO at 40.4 Ma in low latitudes (Bukrey 1975). Re-dated in high latitudes due to it's co-occurrence at several sites with *Reticulofenestra bisecta* (see Arney & Wise, 2003) which has a LO of 38.0 Ma (Bergerren 1995)

All calibrated to Berggren et al. 1995 timescale **Samples collected for this study in bold**

Table 3.3. Summary of biostratigraphic data in the Hampden Section from oldest (top) to youngest (bottom).

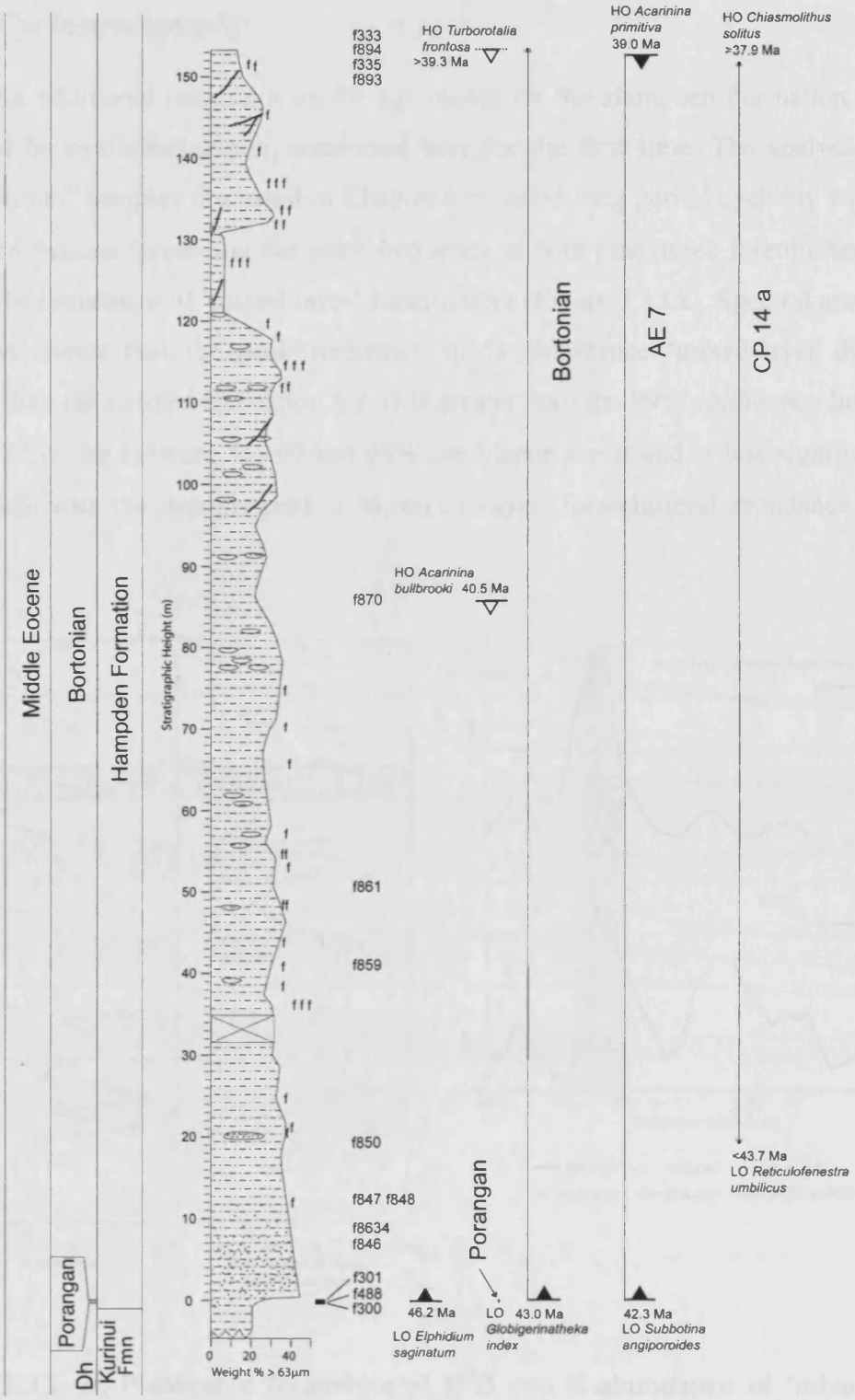

Figure 3.12 Hampden Section stratigraphic column showing key biostratigraphic data and the corresponding biozones and New Zealand stages. Closed triangles are events that define stages or biostratigraphic zones, open triangles are other events correlated to the palaeomagnetic record by Berggren et al. (1995). Arrows denote where the LO or HO occurs in the lowest or highest sample examined and thus the range of the taxon likely extends beyond the sampled interval.

3.3.4. Cyclostratigraphy

An additional constraint on the age model for the Hampden Formation may be provided by cyclostratigraphy, conducted here for the first time. The analysis of the "long section" samples discussed in Chapter 6 revealed long period cyclicity within the Hampden Section, present at the same frequency in both planktonic foraminiferal $\delta^{18}O$ and the % abundance of 'mixed-layer' foraminifera (Figure 3.13A). Spectral analysis of this data shows that the peak frequency in % abundance 'mixed-layer dwelling' foraminifera (as defined in Section 6.2.3) is greater than the 99% confidence limit. The peak in $\delta^{18}O$ lies between the 90 and 95% confidence limits and is less significant but co-incident with the stronger peak in % 'mixed-layer' foraminiferal abundance (Figure 3.13B).

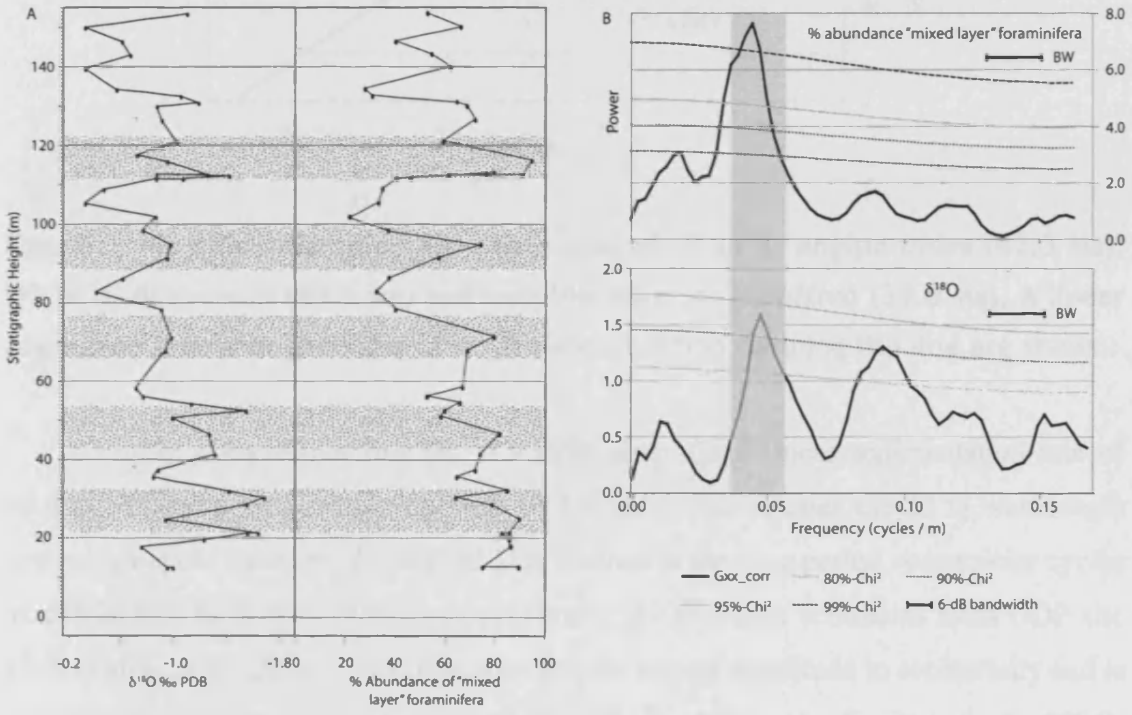

Figure 3.13. A, Planktonic foraminiferal $\delta^{18}O$ and % abundance of 'mixed-layer dwelling' foraminifera against stratigraphic height, stippled bands highlight the cyclicity; B, spectral analysis of $\delta^{18}O$ and % abundance of 'mixed-layer dwelling' foraminifera data, plotted with confidence intervals against a red noise background generated using REDFIT (Schulz and Mudelsee, 2002). Grey band highlights the dominant cyclicity at approximately 0.045 cycle/m.

The peak frequency of the cyclicity is ~0.045 cycles/m, which equates to a wavelength of 22.2 m. To establish whether this likely corresponded to a long period Milankovitch frequency it is necessary to translate the samples used in this study between depth and time domains. To do this, a simple age model was constructed by creating an age-depth plot of the three key biostratigraphic datums discussed in Section 3.3.3 which lie on a linear trend, albeit probably coincidentally (Figure 3.14).

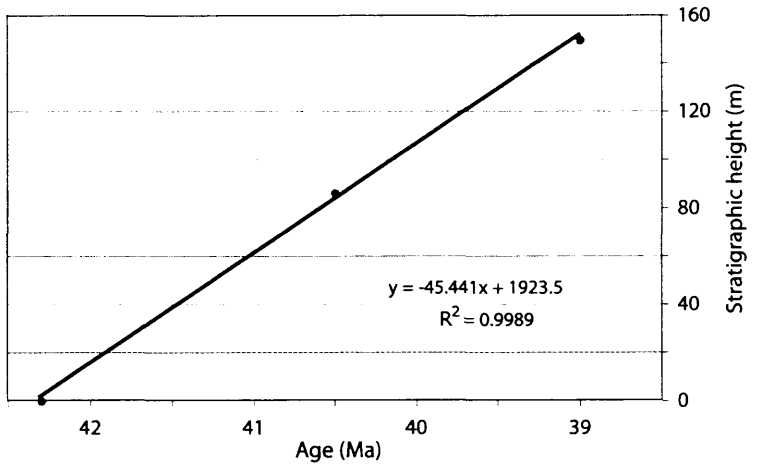

Figure 3.14. Biostratigraphic age-depth plot of LO of *S. angiporoides* (42.3 Ma), HO of *A. bullbrooki* (40.5 Ma) and possible HO of *A. primitiva* (39.0 Ma). A linear regression line with goodness of fit (R^2) and equation defining the line are shown.

Fitting a regression line (R^2 = 0.999) generates a linear sedimentation rate of 45.4 m/Ma and a total section duration of 3.37 Ma. This equates the 22 m wavelength cycles to a cycle duration of ~484 ka. This is close to the long period eccentricity cycles at 405 ka that have been recognised previously in Oligocene sediments from ODP site 1218 (Pälike et al., 2006). This frequency has the largest amplitude in eccentricity and is considered to have remained constant through the Mesozoic (Laskar et al., 2004). Furthermore, shorter period cycles have been identified in the "high-resolution" samples at a wavelength of ~1 m (discussed in Chapter 7), the ratio of 1:22 is a good fit to the ratio of short period precession cycles (~18 ka) to long period eccentricity cycles (405 ka). Consequently it is considered likely (although not proven) that the cycles observed in the "long section" samples at Hampden Beach are driven by these 405 ka orbital cycles. The sedimentation rate required to generate 405 ka cycles at the observed frequency (0.045 cycles/m) was then calculated to be 54.87 m/Ma (table 3.4).

Sedimentation rate from biostratigraphic age model	45.44	m/Ma
Observed frequency peak in % abundance 'mixed-layer' species	0.045	cycles/m
Corresponding wavelength	22.22	m
Duration of 22 m cycles	484.1	ka
Sedimentation rate adjusted to give 405 ka cyclicity	54.87	m/Ma

Table 3.4. Key calculations in developing cyclostratigraphy.

3.3.5. Combined age model

A combined age model was created by fixing the HO of *Acarinina bullbrooki* at 40.5 Ma because it is the clearest biostratigraphic datum in the section and applying the calculated linear sedimentation rate of 54.87 m/Ma above and below it. The results of this are shown in the age–depth plot below (Figure 3.15), which gives calculated ages for the base and the top of the section as 42.1 and 39.3 Ma respectively.

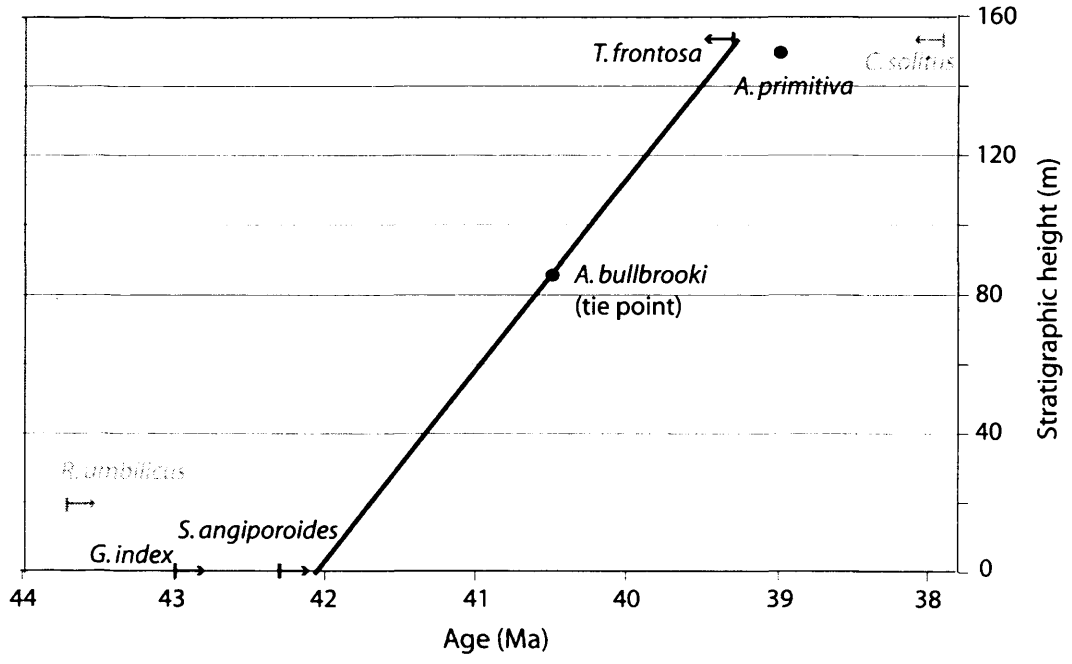

Figure 3.15. Linear age-depth plot of the Hampden Formation using the cyclostratigraphic sedimentation rate of 54.87 m/Ma and the HO of *A. bullbrooki* at 40.5 Ma. The biostratigraphic data discussed in Section 3.3.3. are shown as circles for a 'true' LO and HO and lines with arrows where the LO or HO at Hampden is the top or base of the Formation and thus only provides a constraint. Foraminiferal data are shown in black and nannofossil data in grey.

The age for the base of the section is in good agreement with the biostratigraphic data because the LO of *G. index* and *S. angiporoides* together suggest that it is younger than 42.3 Ma and that at least some time (43 – 42.3 Ma) is highly condensed or not recorded. These new dates suggest that the base of the section is slightly younger still, at 42.1 Ma and the condensed or missing interval is somewhat longer. The top of the section is slightly less clear; the HO of *T. frontosa* (39.3) is not recorded and samples from higher up the section would need to be collected to see how much higher the HO occurred. Furthermore the new age model suggests that the HO of *A. primitiva* observed in sample CB05B249 is not a true HO, which is not unexpected (discussed in Section 3.3.3.). Consequently although the age of the top section does not conflict significantly with the biostratigraphic data, it is more ambiguous.

Previous studies of the Hampden Formation have regarded the formation as Bortonian in age, contacting the underlying Porangan stage at Park Gulch and the overlying Kaiatan stage a few metres below the top of the section (Brown, 1954; Morgans, 2008). The Bortonian is a middle Eocene New Zealand specific stage dated at 43 to 37 Ma and approximately equivalent to the upper Lutetian and lower Bartonian international stages see Figure 3.11 (Morgans, 2004). This would suggest a younger age for the top of the section than determined in this study. However, the Bortonian – Kaiatan boundary has historically been poorly defined and the current date of this boundary is based on the LO of the nannofossil *Chiasmolithus oamaruensis* (Morgans, 2004). The LO of *C. oamaruensis* (dated at 37.0 Ma, Berggren et al., 1995) is known to occur above the HO of the benthic foraminifera *Bulimina bortonica* used by Morgans (2008) to define the boundary in the Hampden Formation. Furthermore the HO of *A. primitiva* (dated at 39.0 Ma, Berggren et al., 1995) is currently considered an intra-Kaiatan event and thus stratigraphically above the LO of *C. oamaruensis* (Morgans 2007, pers. comm.). This suggests that either the biostratigraphic definition of the stage or the associated dating in the standard New Zealand chronology needs to be revised and that the dates used in this study are valid. Figure 3.16 below shows the Hampden Section stratigraphic column plotted against time and indicates the relevant international and New Zealand stages.

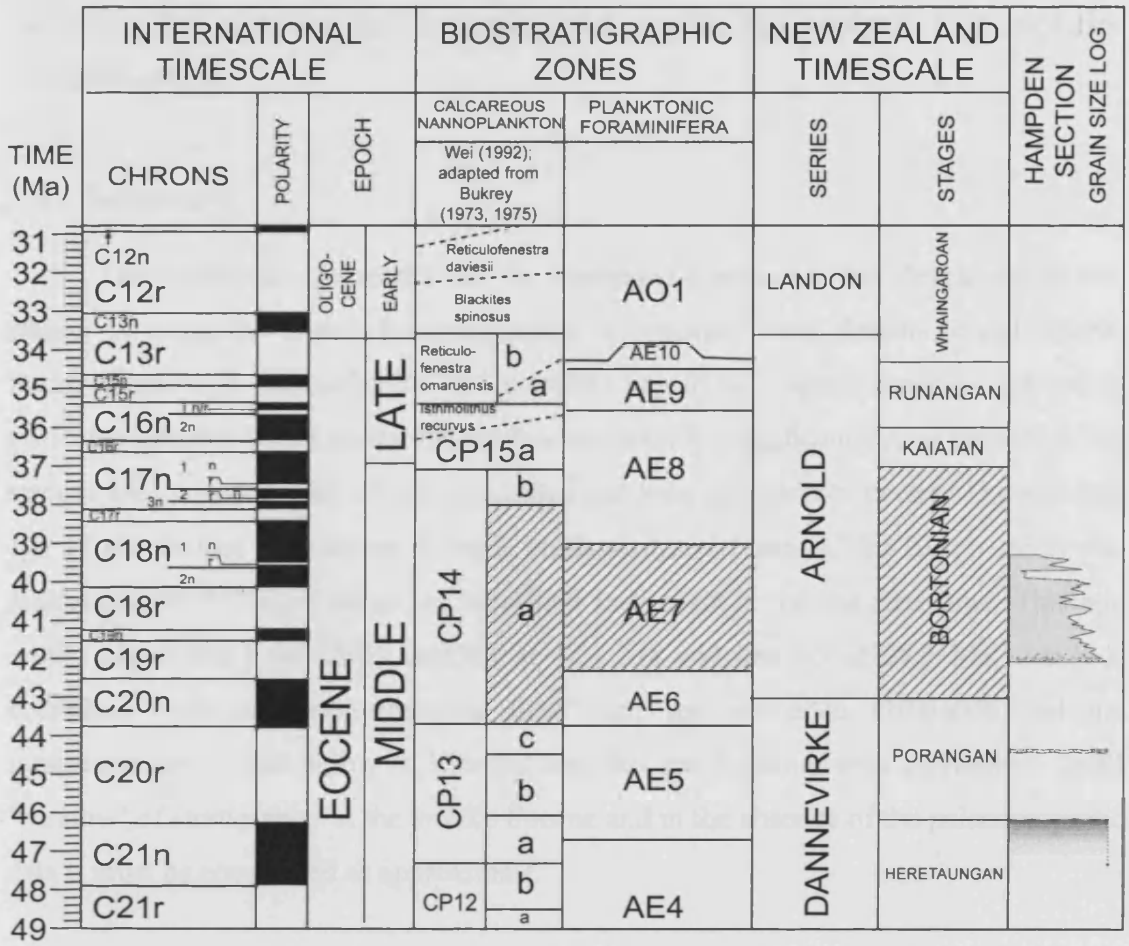

Figure 3.16. The Hampden Section stratigraphic column with grain size variation (right) according to the age model developed here, plotted against the international timescale and biostratigraphic zones (after Huber & Quillivéré, 2006) and New Zealand timescale (after Morgans, 2006). Hatched zones are those employed in the biostratigraphic analysis of the section.

This age framework is used during the palaeoenvironmental analysis of the Hampden Formation throughout later chapters. However, it is stressed that although the combination of biostratigraphy and cyclostratigraphy strengthens the age model, constraints on the dating and stratigraphic thickness are still relatively poor and there is a significant error associated with determining the peak frequency of the cyclicity. Furthermore, this model assumes a constant sedimentation rate throughout the section. It is known that the base of the section contains a hiatus or highly condensed interval since the Porangan period spans only a few centimetres and it is possible that the interval of fine sediment around 115-130 m is also condensed. Discussions related to the age of the section should therefore be treated with appropriate caution and the dating of the section would benefit from further study, possibly utilising improvements in

techniques for analysing palaeomagnetism or coring and applying high-resolution cyclostratigraphy.

3.4. Summary

The combined age model for the Hampden Formation was developed in two stages: 1) using the limited biostratigraphic information from planktonic and benthic foraminifera and nannofossils to provide an initial approximation; 2) using cyclostratigraphy, based on the theory that statistically significant cycles present in the section are caused by the orbital precession and long eccentricity cycles. The absolute age of the section is hung on a single well-constrained datum, the HO of *Acarinina bullbrooki* (40.5 Ma) at 86 m, as identified in this study for the first time. This age model places the base of the section at 42.1 Ma and the top at 39.3 Ma, which is consistent with the biostratigraphic data from the Hampden Formation and the formations above and below it. It is the best that can be done with a relatively small 'window' of stratigraphy in the middle Eocene and in the absence of the palaeomagnetic data it must be considered as approximate.

4. Taxonomic Palaeontology

4.1. Introduction

The Hampden Formation contains a diverse range of macro-, micro- and nannofossils making it an excellent site for studying the palaeoecology and palaeoenvironment of this region of the "Southern Ocean" during the middle Eocene. This study concentrates on microfossils, particularly foraminifera and dinoflagellates as their assemblages can be quantified and their environmental relationships have been extensively studied. For example, see Hemleben et al. (1989), Lipps et al. (1979) and Sluijs et al. (2004) for general introductions to the use of these groups as palaeoenvironmental indicators. Nannofossils are discussed briefly as they are used in biostratigraphy and support the foraminifera based age model of the Hampden Formation (Section 3.3.1). The presence of several genera of macrofossils are also recorded.

4.2. Foraminifera

4.2.1. Overview

Foraminifera are single celled protists that live either on the seafloor or among the marine plankton. They are heterotrophic, although some form symbiotic relationships with photosynthetic algae, and inhabit a wide range of environments. They consist of soft tissue (cytoplasm) enclosed by a hard test formed from either secreted organic matter (tectin), secreted minerals (calcite, aragonite or silica) or agglutinated particles. This study focuses on those species that secrete calcitic or aragonitic tests. Geochemical analyses of these tests are used here as palaeoclimatic proxies.

The foraminiferal test is thought to have a range of functions, protecting the organism from predation, damage by abrasion or turbulence and inhospitable water chemistry (extreme ranges of salinity, pH, CO_2 or O_2) and consequently shows specific environmental adaptations in some species. The test composition is important in foraminiferal classification and the calcareous species form the largest group. There are three main types of calcareous wall structure, porcellaneous (characteristic of the suborder Miliolina), microgranular (characteristic of the Fusulinina) and hyaline perforate (seen in all other suborders including aragonitic; Involutina and Robertinina,

calcitic; Spirillinina, Lagenina, Globerinina and Rotaliina). All the planktonic species are contained within the Globerinina (Lee et al., 2000; Armstrong and Brasier, 2005).

Foraminiferal taxonomy has undergone many revisions over the last 70 years since a key species in this study, *Globigerinatheka index,* was first described by Finlay (1939a) as *Globigerinoides index.* This chapter aims to illustrate and describe the species concept used to identify key species used in biostratigraphy and as palaeoclimatic and palaeoenvironmental proxies during this study.

4.2.2. Planktonic foraminiferal taxonomy

The taxonomy of Eocene planktonic foraminifera is based on Pearson et al. (2006a) with additional reference to Hornibrook at al. (1989) and Jenkins (1971). Only the common and/or biostratigraphically or environmentally interesting species are illustrated and described here. Full species lists are given in the foraminiferal assemblage studies carried out in Chapters 6 and 7. A glossary of the morphological terms used below is given in Appendix 2.

Order: FORAMINIFERIDA Eichwald, 1830

Superfamily: GLOBIGERINACEAE Carpenter, 1862

Family: TRUNCOROTALOIDIDAE Loeblich & Tappan, 1961

Genus: *Acarinina* Subbotina, 1953 see discussion in Berggren et al. (2006)
Species: *Acarinina bullbrooki* (Bolli, 1957) - Plate 4.1 (a) to (d).

Wall texture: muricate

Test morphology: Low trochospiral, quadrate, with 4 inflated chambers in the outer whorl, increasing in size but all sub-triangular in shape. Sutures are radial and straight, not deeply incised (less pronounced than in *A. primitiva*). Aperture has a distinct rim, is more open than that of *A. primitiva* in the centre and extends out towards, but does not reach, the margin above the earliest of the visible chambers. Spiral side flat with 2 to $2^1/_2$ whorls of chambers, sutures very shallow and curved. Angular in cross-section.

Distinguishing features: Spiral side notably flatter than in other species of *Acarinina* seen at Hampden. Test more quadrate and chambers more angular than *A. primitiva, A. mcgowrani* or *A. collactea.* Test more compressed and sutures shallower than in *A. praetopilensis.*

Size: >200 μm

Species: *Acarinina collactea* (Finlay, 1939) - Plate 4.1 (e) to (h)

Wall texture: muricate

Test morphology: Low trochospiral, rounded with 5 inflated, rounded to wedge shaped chambers of gradually increasing size in the final whorl. Sutures are radial and straight to slightly curved. Aperture is straight and slit like along the base of the last chamber. Spiral side shows rounded chambers in 3 whorls with radial sutures. Side view subrectangular to ovoid. Tiny openings commonly present at chamber junction margins.

Distinguishing features: Small size, 5 chambers in the final whorl.

Size: >150 μm (generally smaller than other *Acarinina* species)

Species: *Acarinina mcgowrani* Wade & Pearson, 2006 - Plate 4.1 (i) to (l)

Wall texture: densely muricate

Test morphology: Low to moderately trochospiral. Rounded to weakly lobate with 4 chambers in the final whorl increasing in size until the ultimate chamber, which is frequently smaller than the penultimate. Chambers are wedge shaped with the final chamber somewhat flattened. Deeply incised radial sutures. Aperture is open at the umbilicus and extends, narrowing, towards the margin but does not actually meet it. Spiral side shows 2 whorls of ovate chambers with radial sutures. Cross section subrectangular with more angular final chamber.

Size: >200 μm

Species: *Acarinina* cf. *praetopilensis* (Blow, 1979) - Plate 4.1 (m) to (p)

Wall texture: muricate

Test morphology: Low trochospiral, lobate in outline. Final whorl contains 4 inflated, wedge shaped, chambers with depressed radial sutures. Ultimate chamber is often more triangular with a flattened top. Aperture is wide at the umbilicus and extends in a straight line to the margin, with a slight apertural lip. Hampden specimens do not always show the 'rim' of partially fused muricae around the margin of the final chamber described by Blow (1979) as diagnostic of this species. Spiral side shows 2 to 2½ whorls of ovoid chambers with weakly curving sutures. Ovoid in cross-section

Distinguishing features: 4 very distinct and inflated chambers in the final whorl, final chamber may be notably more triangular in apertural view.

Size: >200 μm

Species: *Acarinina primitiva* (Finlay, 1947) - Plate 4.1 (q) to (t)

Wall texture: coarsely muricate

Test morphology: Low trochospiral, compact and rounded to subrectangular in outline. 3 to 4 chambers in the outer whorl gradually increasing in size. Deep incisions between the chambers in the final whorl, straight to slightly curved. Aperture straight, asymmetrically placed at the base of the final chamber extending out towards the margin. Area directly above the aperture is smoother and ornamented with short stout pustules or beads with no pores between them. Short pustules may be present in the mouth of the aperture. In the later stages of life the test may become heavily encrusted. Spiral side contains 2 whorls of chambers, sutures largely obscured by heavy muricae. Ovate to rounded cross-section.

Dinstinguishing features: Compact test with heavy muricate ornament. Deep sutures on umbilical side. Smooth or beaded face above the aperture.

Size: >200 μm

Plate 4.1. Scanning Electron Microscope (SEM) images of planktonic foraminifera from Hampden Beach, scale bar 100 μm. The 1st column shows a specimen in umbilical view and the 2nd the same specimen rotated to view the aperture, the 3rd column shows a different specimen in spiral view and the 4th, that specimen with the aperture rotated away. *Acarinina bullbrooki* a, b, c, d from CB05HB219; *Acarinina collactea* e, f from CB05HB228, g, h from CB05HB216; *Acarinina mcgowrani* i, j f, k, l from CB05HB206; *Acarinina* cf. *praetopilensis* m, n, o, p from CB05HB203; *Acarinina primitiva* q, r, s, t from CB05HB203.

Plate 4.1

Family: GLOBIGERINIDAE Carpenter, 1862

Genus: *Globigerinatheka* Brönniman, 1952, emended Premoli Silva et al. (2006)
Species: *Globigerinatheka index* (Finlay, 1939) - Plate 4.2 (a) to (h)

Wall texture: cancellate with cylindrical pores. Spinose with fine spines rarely preserved.

Test morphology: Low trochospiral, subrectangular in apertural view with 3 globular chambers in final whorl. Penultimate and antepenultimate chambers are approximately equal in size, final chamber is double this size and lying symmetrically above both making up half of the final whorl. Sutures are straight and radial, deeply incised. Aperture is a high arch at the base of the final chamber centred over the suture between the penultimate and antepenultimate chambers, often bordered by a think lip. Bullae are not common in Hampden specimens, although broken remains are occasionally seen and may cover the aperture. Secondary apertures although described in this species, are also rare at Hampden.

Size: >200 μm

Genus: *Globoturborotalita* Hofker, 1976 emended Olsson et al. (2006a)
Species: *Globoturborotalita bassriverensis* Olsson & Hemleben, 2006 - Plate 4.2 (i) to (l)

Wall texture: cancellate and spinose but spines rarely preserved

Test morphology: Low trochospiral, compact and globular, somewhat lobulate in outline. 4 inflated, globular chambers in final whorl, increasing very slightly in size, final chamber slightly wider than high. Aperture arched over the umbilicus and with a distinct lip, generally symmetrical but may be slightly asymmetric. In spiral view, 2 whorls of globular chambers with straight sutures. Rounded in side view.

Distinguishing features: Small size with 4 nearly globular chambers of nearly equal size. Umbilical aperture with a thickened lip.

Size: <250 μm

Plate 4.2. SEM images of planktonic foraminifera from Hampden Beach, scale bar 100 μm. The 1st column shows a specimen in umbilical view and the 2nd the same specimen rotated to view the aperture, the 3rd column shows a different specimen in spiral view and the 4th, that specimen with the aperture rotated away. *Globerinatheka index* a-h from CB05HB234; *Globoturborotalita bassriverensis* i, j from CB05HB206, k, l from CB05HB205; *Globoturborotalita martini* m, n ,o, p from CB05HB050; *Globoturborotalita ouachitaensis* q, r, s, t from CB05HB214.

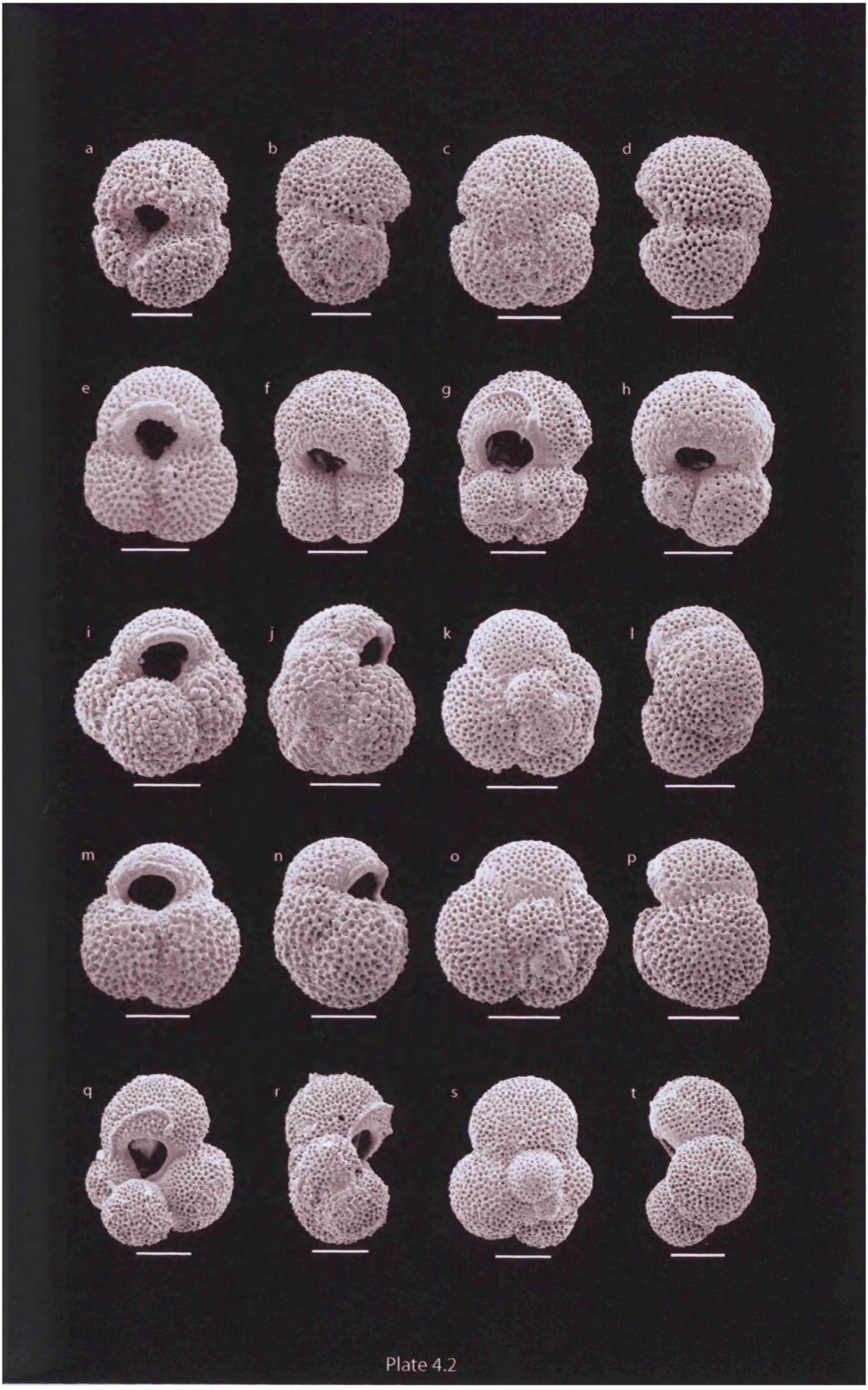

Plate 4.2

Species: *Globoturborotalita martini* (Blow & Banner, 1962) - Plate 4.2 Figures (m) to (p)

Wall texture: cancellate and spinose but spines rarely preserved.

Test morphology: Low trochospiral, lobulate in outline with 3 to 4 globular chambers increasing rapidly in size in the final whorl. Final chamber is significantly reduced in size and partially covers the umbilicus. Sutures are straight and depressed but not deeply incised giving an indistinct appearance to the apertural view of the test. Aperture is a low rounded arch bordered by a lip. Spiral view shows 2½ whorls of globular chambers with straight, slightly depressed sutures. Ovoid to rounded in side view.

Distinguishing features: Small, 3 to 4 chambers in the final whorl with ultimate chamber reduced in size and partially covering the umbilicus.

Size: <250 μm generally smaller than other similar species.

Species: *Globoturborotalita ouachitaensis* (Howe & Wallace, 1932) - Plate 4.2 (q) to (t)

Wall texture: cancellate and spinose, spines rarely preserved.

Test morphology: Moderately trochospiral, lobulate in outline with 4 inflated globular chambers increasing in size in the final whorl. Aperture is a medium to high arch above the large open umbilicus with a slightly thickened rim. In spiral view gobular chambers with straight sutures and a slightly elevated initial spire of chambers. Crescentic to ovate in side view.

Distinguishing features: 4 globular chambers increasing in size in the final whorl, large open umbilicus and moderately high arched aperture.

Size: <250 μm

Genus: *Guembelitriodes* El-Naggar, 1971 emended Olsson et al. (2006b)
Species: *Guembelitrioides nuttalli* (Hamilton, 1953) - Plate 4.3 (a) to (d)

Wall texture: cancellate, spinose

Test morphology: moderately to high spired trochospiral, lobate in outline. Final whorl consists of 3 globular chambers increasing moderately in size, with the ultimate chamber slightly wider than high. Aperture a medium arch with slight rim centred over the umbilicus. Spiral view shows 2 to 3 whorls of globular chambers in a high spire with moderately depressed sutures. Side view is triangular due to the high trochospiral form.

Distinguishing features: High spired morphology with globular chambers and medium arched aperture.

Size: >200 μm

Genus: *Subbotina* Brotzen & Pozaryska, 1961 emended Olsson et al. (2006a)
Species: *Subbotina angiporoides* (Hornibrook, 1965) - Plate 4.3 (e) to (h)

Wall texture: moderately cancellate, spinose but with spines rarely preserved.

Test morphology: Low trochospiral, spherical, rounded in apertural view with 4 globular chambers increasing s in size in the final whorl, chambers are radially compressed giving them a 'flattened' appearance. Ultimate chamber is slightly smaller and extends over the umbilical sutures resembling a bulla. Sutures are only weakly depressed, radial to slightly curved. Aperture is a low straight slit extending from the centre to the margin centred above the antepenultimate chamber and bordered by a distinct lip. Spiral view shows 2 to 3 whorls of globular chambers with weakly depressed radial sutures. In side view the outline is compact and rounded.

Distinguishing features: Compact globular form, 4 chambers in the final whorl with a smaller ultimate chamber and straight slit-like aperture.

Size: >250 μm

Species: *Subbotina linaperta* (Finlay, 1939) - Plate 4.3 (i) to (l)

Wall texture: coarsely cancellate and spinose but with spines rarely preserved.

Test morphology: Low trochospiral, subrectangular in apertural view, 3 to $3^1/_2$ globular chambers in the final whorl increasing rapidly in size with final chamber radially compressed. Sutures radial, straight to slightly curved and depressed. Aperture straight and slit like extending from the centre to close to the margin, bordered by a distinct narrow lip. In spiral view 2 to 3 whorls of globular chambers with weakly depressed radial sutures. Side view subrectangular.

Distinguishing features: 3 to 3½ chambers in final whorl rapidly increasing in size with flattened final chamber giving subrectangular outline. Slit like aperture bordered by distinct lip.

Size: >250 μm

Species: *Subbotina cf. utilisindex* (Jenkins & Orr, 1973) - Plate 4.3 (m) to (p)

Wall texture: cancellate, spinose

Test morphology: low trochospiral, lobate in outline with 4 globular chambers increasing moderately rapidly in size in the final whorl, final chamber significantly radially compressed. Aperture a very low arch with a slight lip, centred over the umbilicus. In spiral view, 3 whorls of globular chambers with moderately depressed radial to weakly curved sutures. Outline in side view is subrectangular to ovate.

Distinguishing features: Differs from *S. linaperta* in having 4 chambers in the final whorl, increasing less rapidly in size and having a slightly more open aperture centred above the umbillicus. Differs from *S. angiporoides* in having a less compact form, larger final chamber and more open aperture.

Size: >200 μm

Family: HEDBERGELLIDAE Loeblich & Tappan, 1961

Genus: *Turborotalia* Cushman and Bermúdez, 1949 emended Pearson et al. (2006b)
Species: *Turborotalia frontosa* (Subbotina, 1953) - Plate 4.3 (q) to (t)

Wall texture: weakly cancellate, raised pustules on earlier chambers becoming smoother on final chamber.

Test morphology: Low trochospiral with 3½ globular chambers increasing rapidly in size in the final whorl. Aperture is an asymmetric high arch, intra-extraumbillical in position extending almost to the margin and has a distinct thickened lip. In spiral view 2 whorls of globular chambers with weakly curving, slightly depressed radial sutures. Side view appears almost triangular when viewing the apertural side but rounded when viewing the non -apertural side as a result of the rapid increase in chamber size in the final whorl.

Distinguishing features: Rapid increase in chamber size in the final whorl and asymmetric high arched aperture.

Size: >200 μm

Turborotalia pomeroli (Tourmarkine & Bolli, 1970) - Plate 4.3 (u) to (x)

Wall texture: Smooth, normal perforate, weakly cancellate on early chambers.

Test morphology: Low trochospiral with 4 chambers in the final whorl increasing moderately in size with ultimate chamber smaller. Chambers are inflated and radially compressed, particularly apparent in the ultimate chamber. Aperture is an asymmetrical high arch, umbilical-extraumbillical, extending to the margin and with a distinct lip. Spiral view shows 3 whorls of chambers with weakly to moderately depressed radial to slightly curving sutures. Side view is ovate.

Distinguishing features: 4 chambers in the final whorl with smaller final chamber, asymmetric, high arched aperture.

Size: >200 μm

Plate 4.3. SEM and RLM images of planktonic foraminifera from Hampden Beach, scale bar 100 μm. The 1st column shows a specimen in umbilical view and the 2nd the same specimen rotated to view the aperture, the 3rd column shows a different specimen in spiral view and the 4th, that specimen with the aperture rotated away. *Guembelitrioides nuttalli* a, b, c, d all images of same specimen from CB05HB237; *Subbotina angiporoides* e, f, g, h from CB05HB234; *Subbotina linaperta* i, j, k, l from CB05HB234; *Subbotina c.f. utilisindex* m, n, o, p from CB05HB234; *Turborotalia frontosa* q, r, s, t from CB05HB232; *Turborotalia pomeroli* u, v, w, x from CB05HB214.

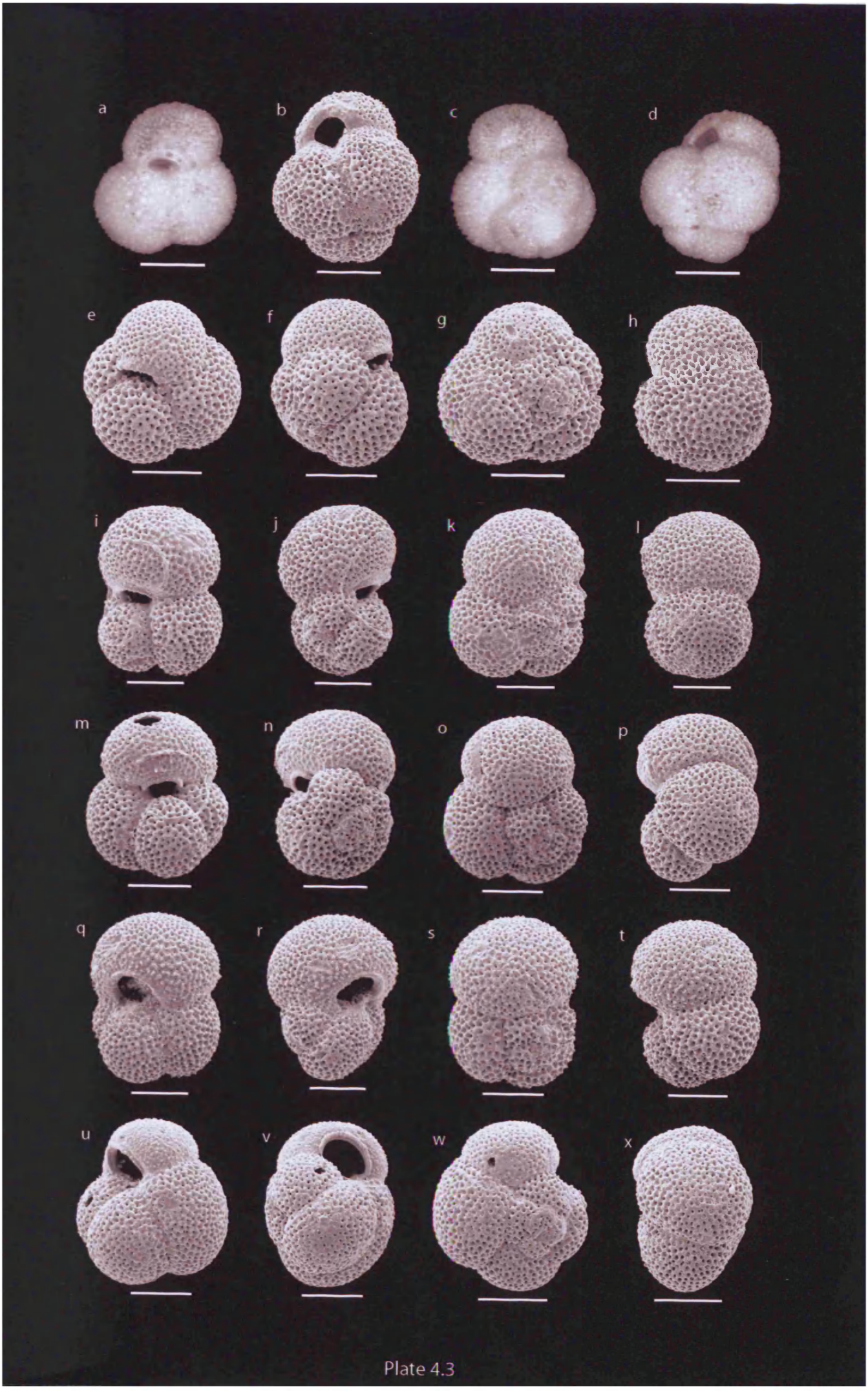

Plate 4.3

4.2.3. Benthic foraminiferal taxonomy

Hampden Beach contains diverse benthic foraminifera, with approximately 85 different species recorded in this study. Species level identification has not been attempted for the benthic foraminifera since they are used in this study as environmental indicators, based primarily on their gross test morphology. However, some individual genera also provide information regarding water-depth and environmental setting (Section 4.2.4) so taxa have been identified to genus level.

The genera used in the environmental interpretation and discussed in the assemblage work in Chapter 7 are listed here and illustrated in Plates 4.4 to 4.8. A detailed description is given of "*Cibicidoides* sp. A" as it is the benthic foraminifera species used for geochemical analysis in this study and consequently it is important that it can be identified accurately. Full descriptions of genera are available in Loeblich & Tappan (1988). Sketche s and notes used to discriminate species within genera are available in Appendix 3 to allow identification to species level.

The taxonomy used here is based on Loeblich & Tappan (1988) with additional reference to Lee et al. (2000), Hornibrook et al. (1989) and Loeblich & Tappan (1964). Although the classification of Lee et al. (2000) supersedes that of Loeblich & Tappan (1988) and makes a significant taxonomic change, promoting the Foraminifera to a class and consequently the suborders to orders, it deals only with modern genera and so cannot be used to produce a comprehensive taxonomy for the genera at Hampden Beach. Further descriptions and illustrations of all genera can be found in Loeblich & Tappan (1988) with more recent descriptions and classifications given for modern genera in Lee et al. (2000). The full reference to the originator of each taxonomic group, given here in brackets, can be found in Loeblich & Tappan (1964) but for conciseness are not repeated.

Order: FORAMINIFERIDA Eichwald, 1830

Suborder: TEXTULARIINA Delage & Hérouard, 1896

Superfamily: LITUOLACEA de Blainville, 1827

Family: HAPLOPHRAGMOIDIDAE Maync, 1952

Genus: *Haplophragmoides* Cushman, 1910
Species: *Haplophragmoides* sp. A. - Plate 4.4 (a)

Superfamily: SPIROPLECTAMMINACEA Cushman, 1927

Family: SPIROPLECTAMMINIDAE Cushman, 1927

Subfamily: SPIROPLECTAMMININAE Cushman, 1927

Genus: *Bolivinopsis* Yakovlev, 1891
Species: *Bolivinopsis* sp. A - Plate 4.4 (b)
Species: *Bolivinopsis* sp. B - Plate 4.4 (c)

Genus: *Spiroplectinella* Kisel'man, 1972
Species: *Spiroplectinella* sp. A - Plate 4.4 (d)
Species: *Spiroplectinella* sp. B - Plate 4.4 (e)

Superfamily: TEXTULARIACEA Ehrenberg, 1838

Family: EGGERELLIDAE Cushman, 1937

Subfamily: EGGERELLINAE Cushman, 1937

Genus: *Karreriella* Cushman, 1933
Species: *Karreriella* sp. A - Plate 4.4 (f)
Species: *Karreriella* sp. B - Plate 4.4 (g)

Suborder: MILIOLINA Delage & Hérouard, 1896

Superfamily: MILIOLACEA Ehrenberg, 1838

Family: HAUERINIDAE Schwager, 1876

Subfamily: HAUERININAE Schwager, 1876

Genus: *Quinqueloculina* d'Orbigny, 1826
Species: *Quinqueloculina* sp. A - Plate 4.4 (h)

Subfamily: MILIOLINELLINAE Vella, 1957

Genus: *Sigmoilina* Schlumberger, 1887
Species: *Sigmoilina* sp. A - Plate 4.4 (i)

Suborder: LAGENINA Delage & Hérouard, 1896

Superfamily: NODOSARIACEA Ehrenberg, 1838

Family: NODOSARIIDAE Ehrenberg, 1838

Subfamily: NODOSARIINAE Ehrenberg, 1838

Genus: *Dentalinoides* Marie, 1941
Species: *Dentalinoides* sp. A - Plate 4.4 (j)
Species: *Dentalinoides* sp. B - Plate 4.4 (k)

Genus: *Nodosaria* Lamark, 1812
Species: *Nodosaria* sp. A - Plate 4.4 (l)
Species: *Nodosaria* sp. B- Plate 4.4 (m)

Genus: *Pyramidulina* Fornasini, 1894
Species: *Pyramidulina* sp. A - Plate 4.4 (n)

Family: VAGINULINIDAE Reuss, 1860

Subfamily: LENTICULININAE Chapman et al. 1934

Genus: *Lenticulina* Lamarck, 1804
Species: *Lenticulina* sp. A - Plate 4.5 (a)
Species: *Lenticulina* sp. B - Plate 4.5 (b)
Species: *Lenticulina* sp. C - Plate 4.5 (c)
Species: *Lenticulina* sp. D - Plate 4.5 (d)

Genus: *Saracenaria* Defrance, 1824
Species: *Saracenaria* sp. A - Plate 4.5 (e)
Species: *Saracenaria* sp. B - Plate 4.5 (f)

Subfamily: MARGINULININAE Wedekind, 1937

Genus: *Vaginulinopsis* Silvestri, 1904
Species: *Vaginulinopsis* sp. A - Plate 4.5 (g)

Genus: *Marginulina* d'Orbigny, 1826
Species: *Marginulina* sp. A - Plate 4.5 (h)
Species: *Marginulina* sp. B - Plate 4.5 (i)

Subfamily: VAGINULININAE Reuss, 1860

Genus: *Vaginulina* d'Orbigny 1826
Species: *Vaginulina* sp. A - Plate 4.5 (j)
Species: *Vaginulina* sp. B - Plate 4.5 (k)

Plate 4.4 SEM images of benthic foraminifera from Hampden Beach, scale bar 100 μm. a) *Haplophragmoides* sp. A, CB05HB079; b) *Bolivinopsis* sp. A, CB05HB079; c) *Bolivinopsis* sp. B, CB05HB079; d) *Spiroplectinella* sp. A, CB05HB079; e) *Spiroplectinella* sp. A, CB05HB074; f) *Karreriella* sp. A, CB05HB079; g) *Karreriella* sp. B, CB05HB079; h) *Quinqueloculina* sp. A, CB05HB079; i) *Sigmolina* sp. A, CB05HB079; j) *Dentalinoides* sp. A, CB05HB079; k) *Dentalinoides* sp. B, CB05HB079; l) *Nodosaria* sp. A, CB05HB079; m) *Nodosaria* sp. B, CB05HB079; n) *Pyramidulina* sp. A, CB05HB079.

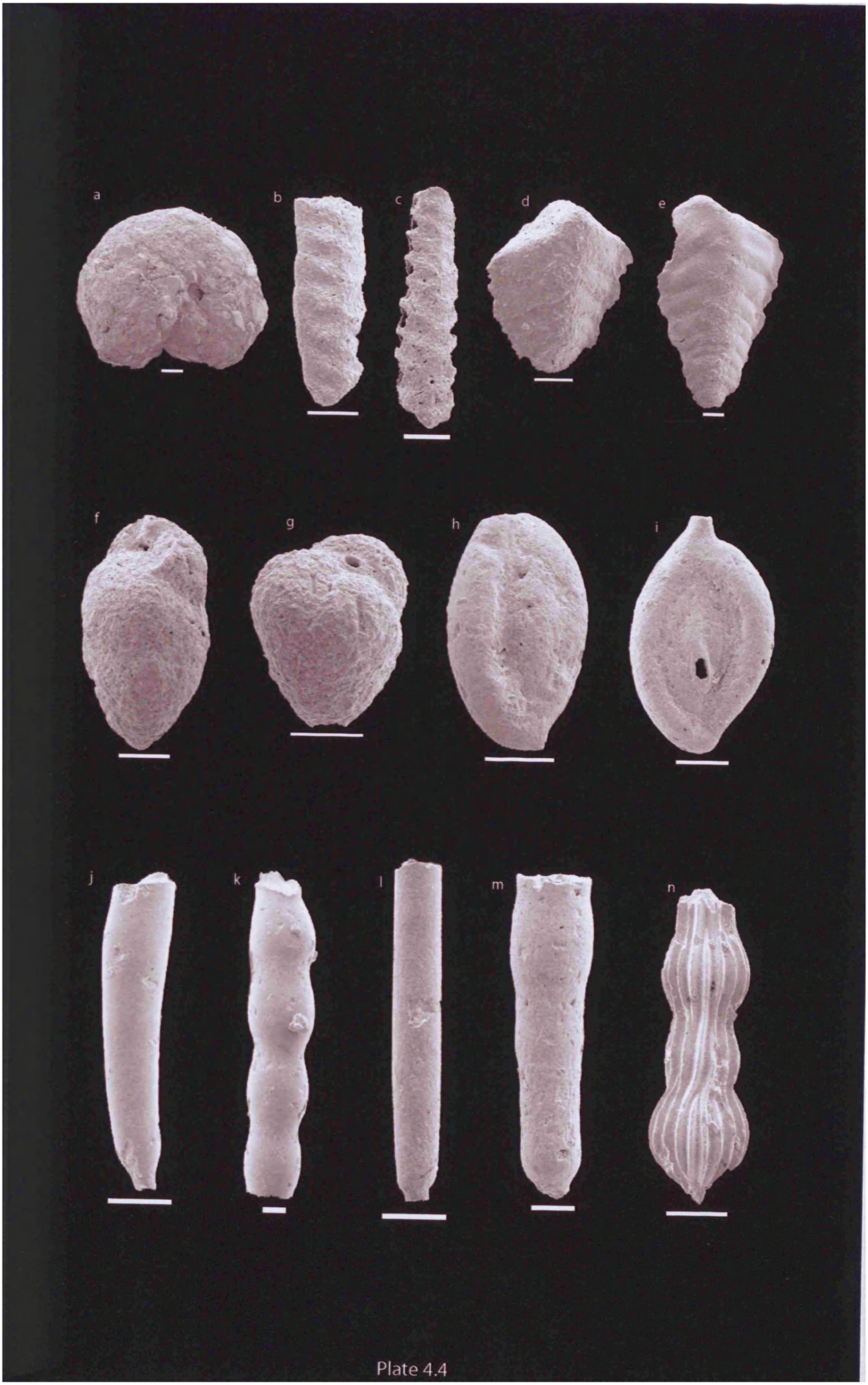

Plate 4.4

Family: LAGENIDAE Reuss, 1862

Genus: *Lagena* Walker & Jacob, 1798
Species: *Lagena* sp. A - Plate 4.5 (l)
Species: *Lagena* sp. B - Plate 4.5 (m)
Species: *Lagena* sp. C - Plate 4.5 (n)

Family: GLANDULINIDAE Reuss, 1860

Subfamily: GLANDULININAE Reuss, 1860

Genus: *Siphoglobulina* Parr, 1950
Species: *Siphoglobulina* sp. A - Plate 4.5 (o)

Family: POLYMORPHIDAE d'Orbigny, 1839

Subfamily: POLYMORPHININAE d'Orbigny, 1839

Genus: *Globulina* d'Orbigny, 1839
Species: *Globulina* sp. A - Plate 4.5 (p)

Genus: *Guttalina* d'Orbigny, 1839
Species: *Guttulina* sp. A - Plate 4.5 (q)

Suborder: ROBERTININA Loeblich & Tappan, 1984

Superfamily: CERATOBULIMINACEA Cushman, 1927

Family: CERATOBULIMINIDAE Cushman, 1927

Subfamily: CERATOBULIMININAE Cushman, 1927

Genus: *Ceratocrancris* Finlay, 1939
Species: *Ceratocancris* sp. A - Plate 4.5 (r)

Family: EPISTOMINIDAE Wedekind, 1937

Subfamily: EPISOMININAE Wedekind, 1937

Genus: *Epistomina* Terquem, 1883
Species: *Epistomina* sp. A - Plate 4.6 (a)

Plate 4.5. SEM images of benthic foraminifera from Hampden Beach, scale bar 100 μm. a) *Lenticulina* sp. A, CB05HB079; b) *Lenticulina* sp. B, CB05HB079; c) *Lenticulina* sp. C, CB05HB079; d) *Lenticulina* sp. D, CB05HB079; e) *Saracenaria sp.* A, CB05HB079; f) *Saracenaria* sp. B, CB05HB074; g) *Vaginulinopsis* sp. A, CB05HB079; h) *Marginulina* sp. A, CB05HB079; i) *Marginulina* sp. B, CB05HB074; j) *Vaginulina* sp. A, CB05HB079; k) *Vaginulina* sp. B, CB05HB079; l) *Lagena* sp. A, CB05HB079; m) *Lagena* sp. B, CB05HB074; n) *Lagena* sp. C, CB05HB074; o) *Siphoglobulina* sp. A, CB05HB079; p) *Globulina* sp. A, CB05HB079; q) *Guttulina* sp. A, CB05HB079; r) *Ceratocancris* sp. A, CB05HB079.

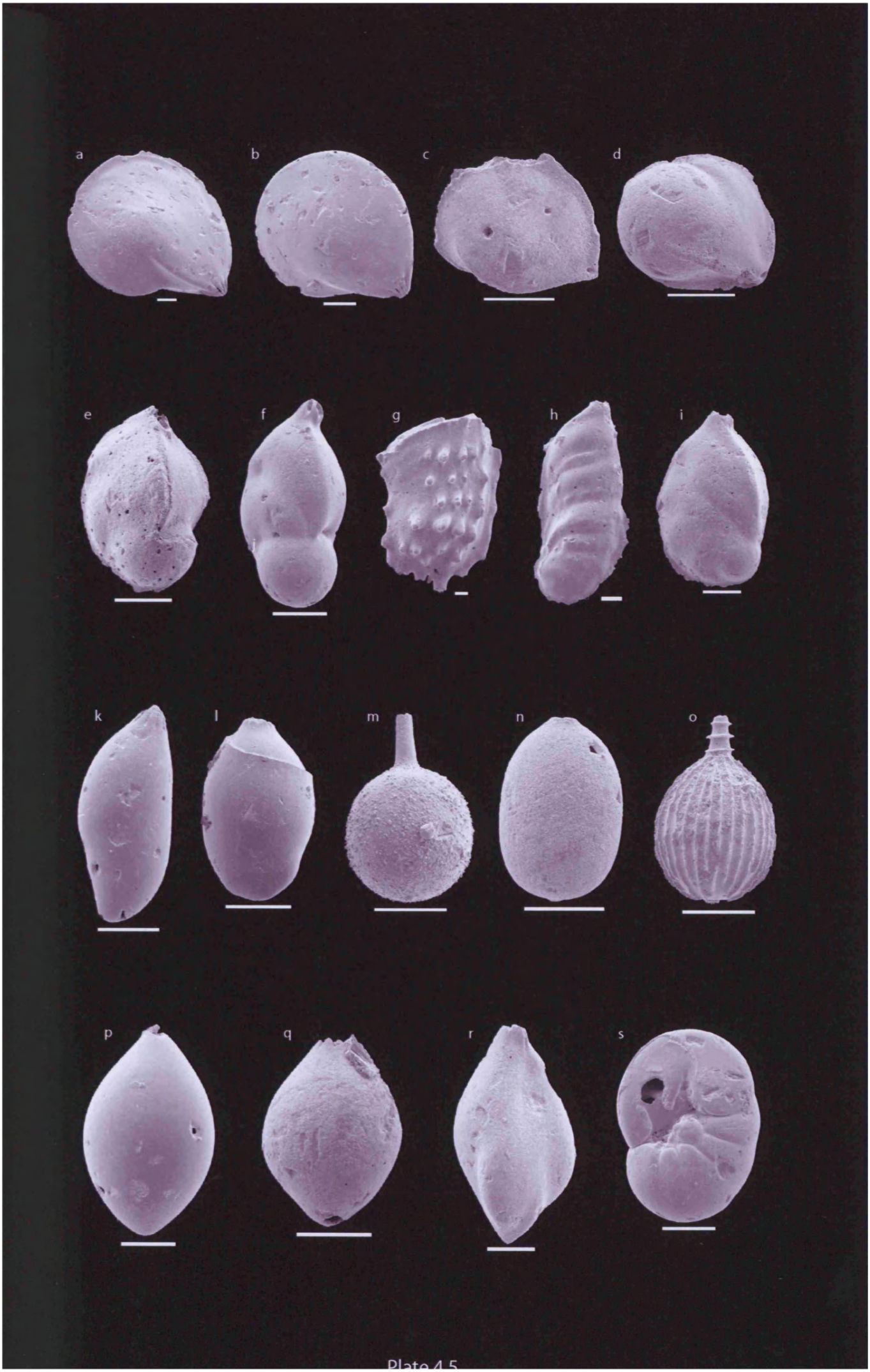

Plate 4.5

Suborder: ROTALIINA Delage & Hérouard, 1896

Superfamily: CASSIDULINACEA d'Orbigny, 1839

Family: CASSIDULINIDAE d'Orbigny, 1839

Subfamily: CASSIDULININAE d'Orbigny, 1839

Genus: *Globocassidulina* Voloshinova, 1960
Species: *Globocassidulina* sp. A - Plate 4.6 (b)

Superfamily: STILOSTOMELLACEA Finlay, 1947

Family: STILOSTOMELLIDAE Finlay, 1947

Genus: *Nodogenerina* Cushman, 1927
Species: *Nodogenerina* sp. A - Plate 4.6 (c)
Species: *Nodogenerina* sp. B - Plate 4.6 (d)
Species: *Nodogenerina* sp. C - Plate 4.6 (e)

Genus: *Siphonodosaria* Silvestri, 1924
Species: *Siphonodosaria* sp. A (f)

Genus: *Stilostomella* Guppy, 1894
Species: *Stilostomella* sp. A - Plate 4.6 (g)
Species: *Stilostomella* sp. B - Plate 4.6 (h)
Species: *Stilostomella* sp. C - Plate 4.6 (i)

Superfamily: BULIMINACEA Jones, 1895

Family: BULIMINIDAE Jones, 1895

Genus: *Bulimina* d'Orbigny, 1826
Species: *Bulimina* sp. A - Plate 4.6 (j)
Species: *Bulimina* sp. B - Plate 4.6 (k)
Species: *Bulimina* sp. C - Plate 4.6 (l)
Species: *Bulimina* sp. D - Plate 4.6 (m)

Genus: *Globobulimina* Cushman, 1927
Species: *Globobulimina* sp. A - Plate 4.6 (n)

Plate 4.6. SEM images of benthic foraminifera from Hampden Beach, scale bar 100 μm. a) *Epistomina* sp. A, CB05HB079; b) *Globocassidulina* sp. A, CB05HB079; c) *Nodogenerina* sp. A, CB05HB079; d) *Nodogenerina* sp. B, CB05HB079; e) *Nodogenerina* sp. C, CB05HB079; f) *Siphonodosaria* sp A, CB05HB079; g) *Stilostomella* sp. A, CB05HB079; h) *Stilostomella* sp. B, CB05HB074; i) *Stilostomella* sp. C, CB05HB079; j) *Bulimina* sp. A, CB05HB079; k) *Bulimina* sp. B, CB05HB079; l) *Bulimina* sp. C, CB05HB051; m) *Bulimina* sp. D, CB05HB051; n) *Globobulimina* sp. A, CB05HB074.

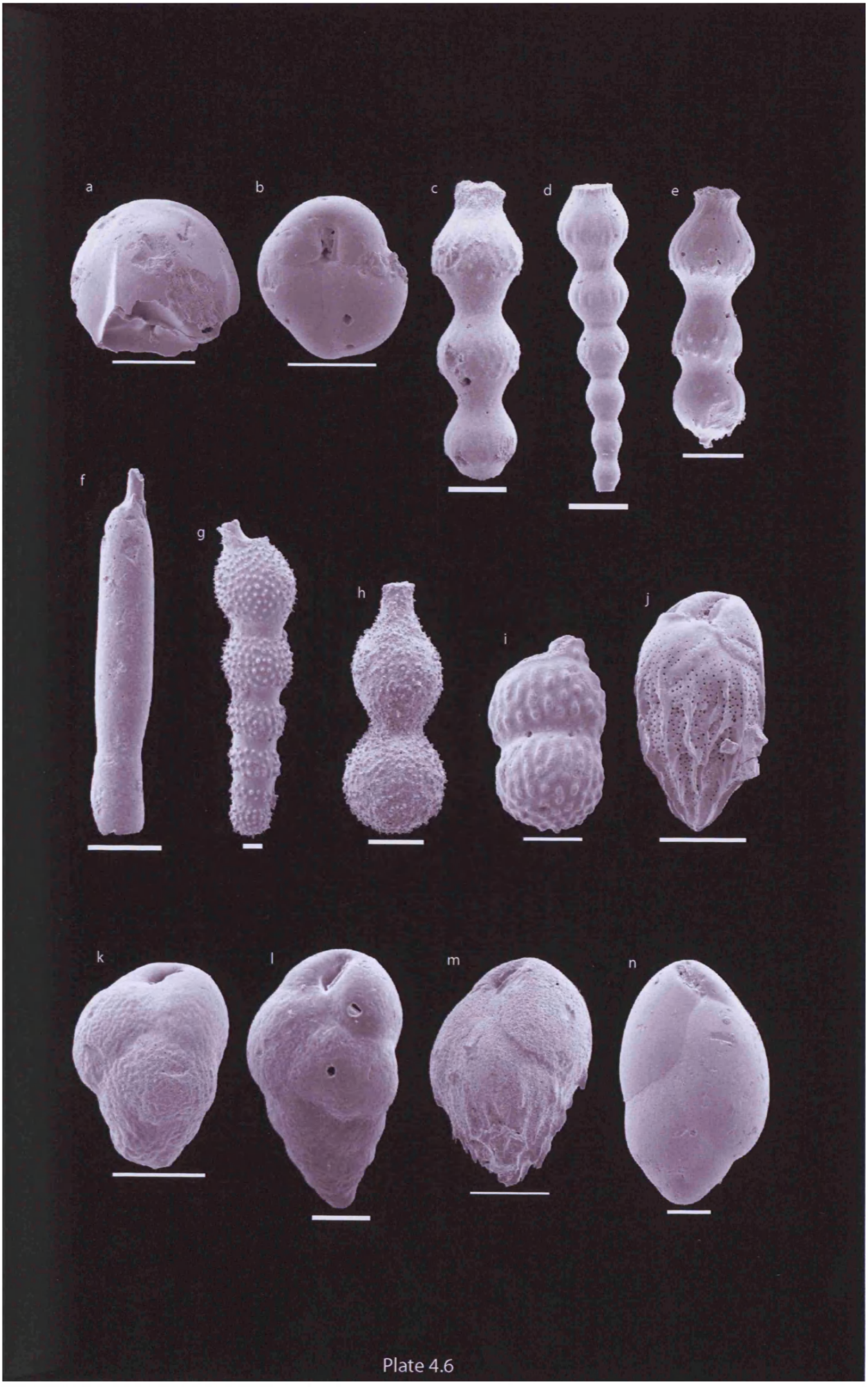

Plate 4.6

Family: UVIGERINIDAE Haeckel, 1894

Subfamily: Uvigerininae Haeckel, 1894

Genus: *Uvigerina* d'Orbigny, 1826
Species: *Uvigerina* sp. A - Plate 4.7 (a)

Subfamily: ANGULOGERININAE Galloway, 1933

Genus: *Kolesnikovella* Bykova, 1958
Species: *Kolesnikovella* sp. A - Plate 4.7 (b)
Species: *Kolesnikovella* sp. B - Plate 4.7 (c)

Superfamily: DISCORBINELLACEA Sigal, 1952

Family: PARRELLOIDIDAE Hofker, 1956

Genus: *Cibicidoides* Thalmann, 1939
Species: *Cibicidoides* sp. A - Plate 4.7 (i to n)

Used for trace metal and isotope geochemistry.

Test trochospiral, lenticular and biconvex with spiral side slightly flatter, 7 to 9 chambers in the final whorl. Sutures on spiral side curved, sutures on umbilical side almost straight. Both sides smooth, unornamented and perforate. Aperture a low equatorial arch extending further towards the margin of the umbilical side than the apertural side, bordered by a slight lip.

Species: *Cibicidoides* sp. B - Plate 4.7 (d)
Species: *Cibicidoides* sp. C - Plate 4.7 (e)
Species: *Cibicidoides* sp. D - Plate 4.7 (f)
Species: *Cibicidoides* sp. E - Plate 4.7 (g)
Species: *Cibicidoides* sp. F - Plate 4.7 (h)
Species: *Cibicidoides* sp. G
Species: *Cibicidoides* sp. H

Plate 4.7. SEM images of benthic foraminifera from Hampden Beach, scale bar 100 μm. a) *Uvigerina* sp. A, CB05HB079; b) *Kolesnikovella* sp. A, CB05HB079; c) *Kolesnikovella* sp. B, CB05HB074; d) *Cibicidoides* sp. B, CB05HB079; e) *Cibicidoides* sp. C, CB05HB079; f) *Cibicidoides* sp. D, CB05HB051; g) *Cibicidoides* sp. E, CB05HB079; h) *Cibicidoides* sp. F, CB05HB079; i) to k) *Cibicidoides* sp. A, CB05HB098 in a range of views; l) to n) *Cibicidoides* sp. A, CB05HB098 reflected light microscopy photographs corresponding to images i) to k).

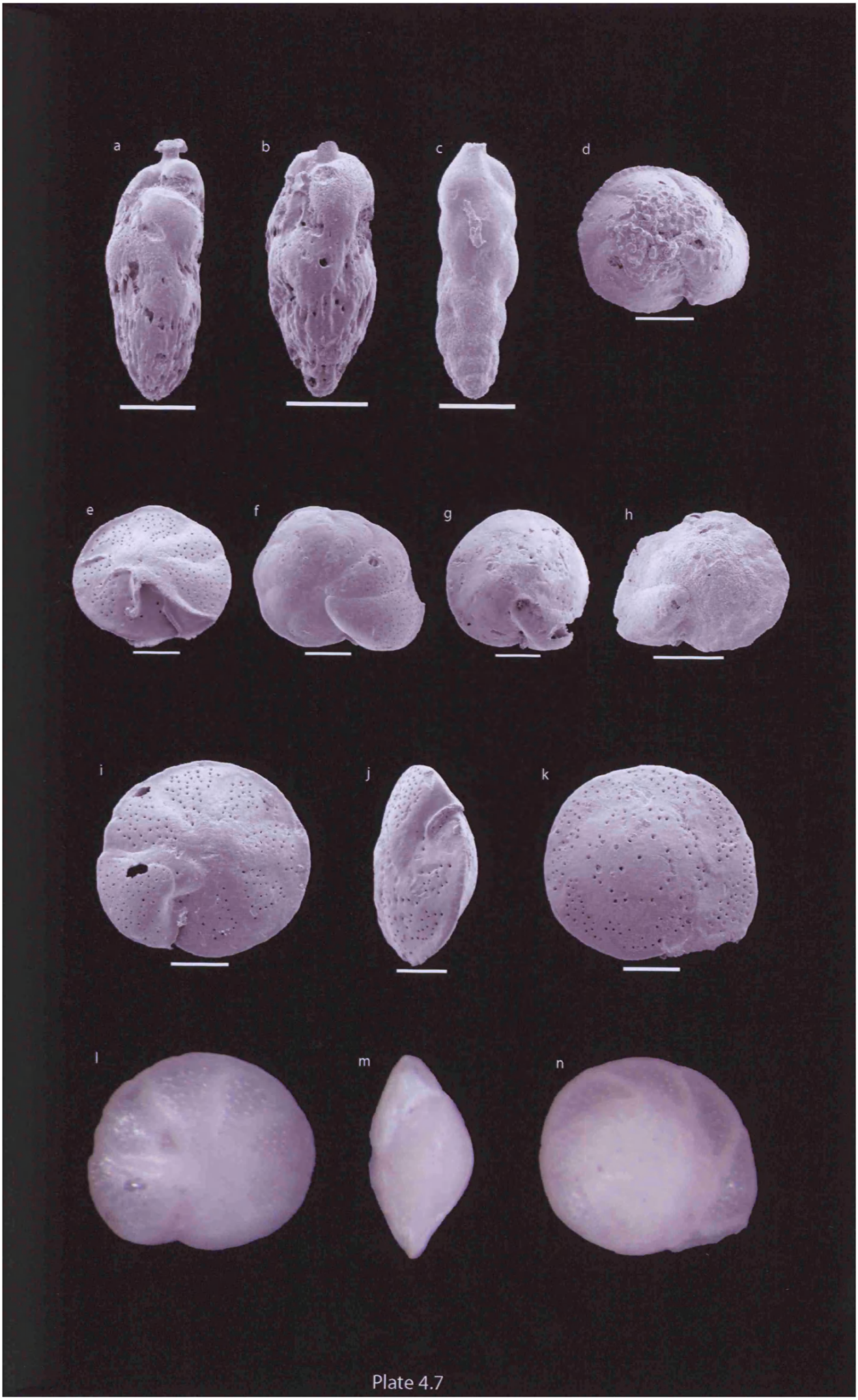

Plate 4.7

Superfamily: PLANORBULINACEA Schwager, 1877

Family: CIBICIDIDAE Cushman, 1927

Subfamily: CIBICIDINAE Cushman, 1927

Genus: *Cibicides* de Montfort, 1808
Species: *Cibicides* sp. A - Plate 4.8 (a)
Species: *Cibicides* sp. B - Plate 4.8 (b)
Species: *Cibicides* sp. C - Plate 4.8 (c)

Genus: *Lobatula* Fleming, 1828
Species: *Lobatula* sp. A - Plate 4.8 (d)

Superfamily: NONIONACEA Shulze, 1854

Family: NONIONIDAE Schultze, 1854

Subfamily: NONIONINAE Schultze, 1854

Genus: *Nonionella* Cushman, 1926
Species: *Nonionella* sp. A - Plate 4.8 (e)

Subfamily: PULLENIINAE Schwager, 1877

Genus: *Melonis* de Montfort, 1808
Species: *Melonis* sp. A - Plate 4.8 (f)

Genus: *Pullenia* Parker & Jones, 1862
Species: *Pullenia* sp. A - Plate 4.8 (g)
Species: *Pullenia* sp. B - Plate 4.8 (h)

Superfamily: CHILSTOMELLIDAE Brady, 1881

Family: ALABAMINIDAE Hofker, 1951

Genus: *Alabamina* Toulmin, 1941
Species: *Alabamina sp. A* - Plate 4.8 (i)

Family: ORIDORSALIDAE Loeblich & Tappan, 1984

Genus: *Oridorsalis* Anderson, 1961
Species: *Oridorsalis* sp. A - Plate 4.8 (j)

Family: HETEROLEPIDAE Gonzáles-Donoso, 1969

Genus: *Anomalinoides* Brotzen, 1942
Species: *Anomalinoides* sp. A - Plate 4.8 (k)

Family: GAVELINELLIDAE Hofker, 1956

Subfamily: GYROIDINOIDINAE Saidova, 1981

Genus: *Gyroidinoides* Brotzen, 1942
Species: *Gyroidinoides* sp. A - Plate 4.8 (l)

Subfamily: GAVELINELLINAE Hokfer, 1956

Genus: *Gavelinella* Brotzen, 1942
Species: *Gavelinella* sp. A - Plate 4.8 (m)

Genus: *Linaresia* Gonzáles-Donoso, 1969
Species: *Linaresia* sp. A - Plate 4.8 (n)

Superfamily: ROTALIACEA Ehrenberg, 1839

Family: ELPHIDIIDAE Galloway, 1933

Subfamily: ELPHIDIINAE Galloway, 1933

Genus: *Elphidium* de Montfort, 1808
Species: *Elphidium* sp. A - Plate 4.8 (o)

Plate 4.8. SEM images of benthic foraminifera from Hampden Beach, scale bar 100 μm. a) Cibicides sp. A, CB05HB079; b) Cibicides sp. B, CB05HB079; c) Cibicides sp. C, CB05HB079; d) Lobatula sp. A, CB05HB079; e) Nonionella sp. A, CB05HB079, f) Melonis sp. A, CB05HB079, g) Pullenia sp. A, CB05HB051; h) Pullenia sp. B, CB05HB079; i) Alabamina sp. A, CB05HB079; j) Oridorsalis sp. A, CB05HB079; k) Anomalinoides sp. A, CB05HB079; l) Gyroidinoides sp. A, CB05HB079; m) Gavelinella sp. A, CB05HB079; n) Linaresia sp. A, CB05HB074; o) Elphidium sp. A, CB05HB074.

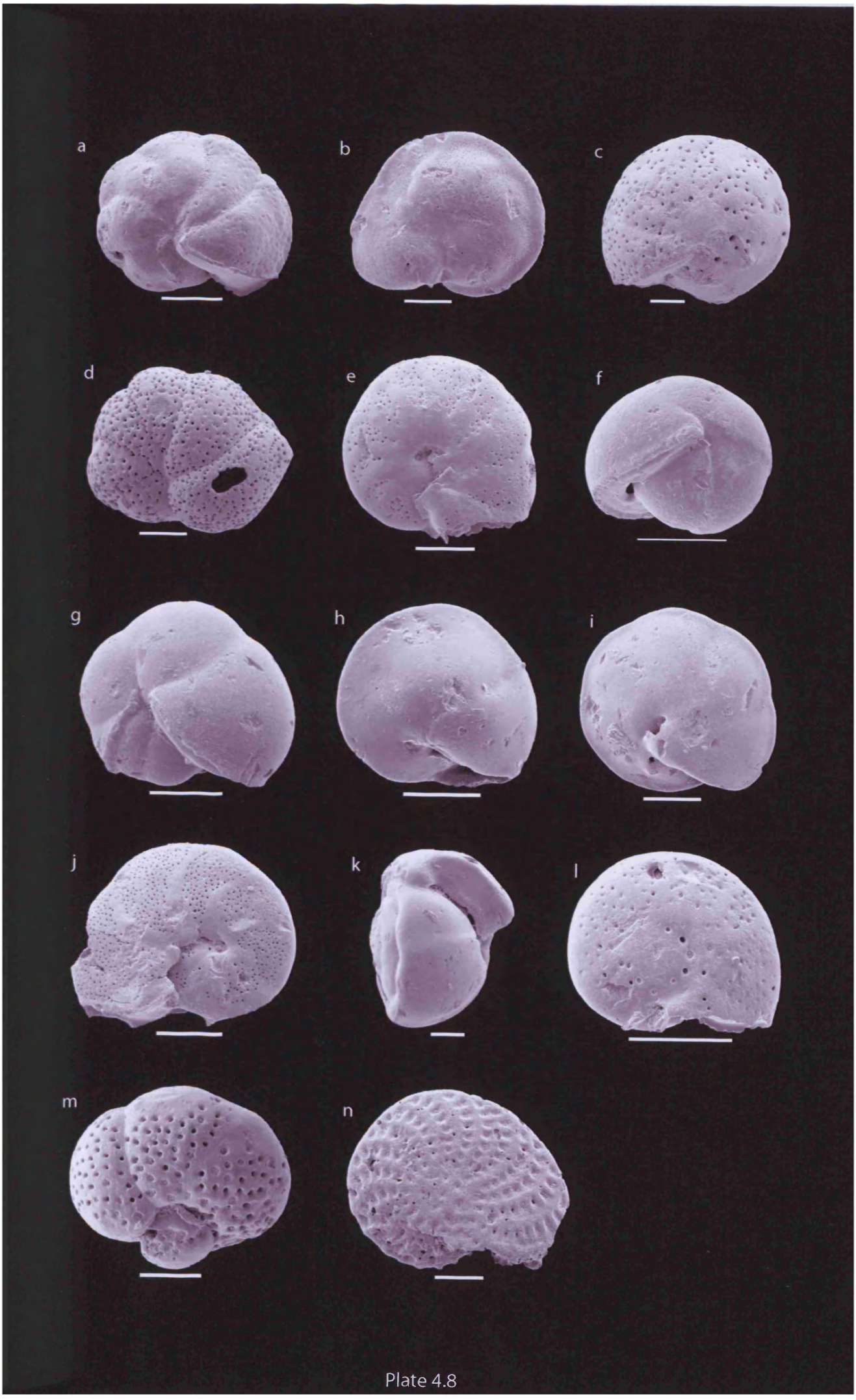

Plate 4.8

4.2.4. Foraminifera as environmental indicators

As discussed in Chapter 1, some species of planktonic foraminifera are known to have specific temperature preferences, with the range of high latitude species expanding during cold periods and retreating during warm periods. This has been extensively studied for the Pleistocene and numerical transfer functions have been developed to allow the determination of absolute sea surface temperature (SST) from planktonic foraminiferal assemblages (e.g. Imbrie and Kipp, 1971). The temperature preferences of Eocene foraminifera cannot be determined so precisely as they cannot be calibrated to modern core tops with a known SST. However, it is possible to consider the latitudes at which certain species are known to occur and draw temperature inferences from this. Most of the species seen at Hampden Beach are cosmopolitan but a number are most commonly associated with mid to low latitudes (*Acarinina* cf. *praetopilensis*, *Guembelitrioidies nuttalli* and all three species of *Globoturborotalita*) in contrast only one species (*A. primitiva*) is more commonly known from temperate to high latitudes (Pearson et al., 2006a). This environmental information is combined with geochemical proxy data to discuss the palaeoclimate at Hampden Beach in Chapters 6 and 7.

Different species of planktonic foraminifera spend the majority of their lives at different depths within the water column. For example, *Subbotina linaperta* tends to live at the thermocline (Pearson et al., 1993) whilst the majority of species seen at Hampden live within the mixed-layer (discussed in Chapter 5 below). The species selected for isotopic analysis, *Globigerinatheka index* is thought to be a mixed-layer dwelling species but there is some evidence that gametogenic calcite may be added to the shell at deeper depths during the final stage of the life cycle (Premoli Silva et al., 2006). The specimens picked for isotopic analysis in this study were from the 212-250 μm fraction that rarely contains individuals showing extensive gametogenic calcite hence the *G. index* specimens used in this study calcified primarily above the thermocline.

Some species of benthic foraminifera are also known to have preferred water depth habitats and since they live at or just below the sediment water interface, they can provide information about the depth to the sea floor. There are a number of genera seen at Hampden Beach that are linked to approximate water depths and environments, these generally indicate an outer shelf to upper slope environment; *Sigmolina* - mid-outer shelf to upper slope, *Haplophragmoides* – outer shelf to upper slope, *Karreriella* – outer shelf to upper slope (Murray, 1973, I. McMillan pers. comm. 2005). Single specimens

of the genera *Lobatula* and *Elphidium* are also seen at Hampden Beach, these are normally associated with high-energy wave or current dominated sites and shallow water environments respectively (Murray, 1973, I. McMillan pers. comm. 2005). However, since they are present only as single specimens and do not fit with the environment indicated by more common genera, they are likely to have been transported to the site. Consequently it is considered that the Hampden Formation represents an outer-shelf to upper-slope environment at approximately 300 m water depth, in good agreement with the work of Morgans (2008) (Section 3.3.2).

The general test morphology of calcareous benthic foraminifera can also indicate their environmental preferences, in particular the oxygenation level of the water. Kaiho (1994) divides calcareous benthic foraminfera into three types, oxic (O), suboxic (S) and dysoxic (D) based on their test morphology and relates the oxygen index (oxygen index = [O/(O+D)]x100) to the oxygen concentration in the water. Oxic indicators are generally large (>350μm), thick walled, epifaunal species; dysoxic indicators are small (<200μm for spiral forms), thin walled species with morphologies that have a high surface area to volume ratio and are deep infauna in high oxygen environments; suboxic indicators include smaller specimens of oxic indicators and forms intermediate in morphology between oxic and dysoxic indicators and include species that are both epifaunal and infaunal under high oxygen conditions but only epifaunal under low oxygen conditions. Most species recorded at Hampden Beach are oxic or suboxic indicators suggesting that the bottom waters were well oxygenated, this is discussed further in Section 7.2.3.

4.3. Dinoflagellates

4.3.1. Overview

Dinoflagellates are unicellular protists most of which are free-living in marine or freshwater environments although some species are either parasitic or symbiotic. Dinoflagellates are characterised by having a motile stage in during which they use two flagellae to propel themselves through the water. Approximately 50% of dinoflagellate species are autotrophic and form an important component of the marine primary productivity. Others are heterotrophic and feed by either ingesting food particles or absorbing dissolved food (Dodge and Lee, 2000; Williams et al., 2006).

Dinoflagellates have a variety of reproductive mechanisms and in some cases very complicated life cycles, many of which incorporate an encysting stage. These cysts may be vegetative, short-term temporary cysts or long-term resting cysts. Most motile dinoflagellate cells, vegetative and temporary cysts decay quickly, however in about 15% of modern species, resting cysts are formed from a resistant organic material (sporopollenin) that can be preserved in the fossil record. It is the fossilised remains of these resting cysts (dinocysts) that are observed at Hampden Beach.

4.3.2. Dinoflagellate taxonomy

The key dinoflagellate species recorded in the Hampden Formation are illustrated and described below. The systematic position of dinoflagellates is somewhat unclear as closely related forms may or may not be photosynthetic, some workers chose to classify them using the code of botanical nomenclature (Fensome et al., 1993) whereas others use the code of zoological nomenclature (Cavalier-Smith, 1998). The taxonomy given here is based on Fensome et al. (1993) with additional reference to Evitt (1985), Eisenack (1964), Wilson (1988), and Crouch & Brinkhuis (2005). Regardless of the taxonomic system used, the primary distinction usually made for the purpose of palaeoenvironmental study is between gonyaulacoid (G) cyst and peridinoid (P) cyst morphologies so this distinction is made clear below. Furthermore, dinoflagellates are identified here to species level where possible, as in some cases different species within the same genera have different environmental preferences (see 4.3.3).

Again, brief descriptions are given to illustrate the species concept used during this study and a glossary of the morphological terms used is given in Appendix 2. Full references are given to the originators of the species listed as they are not comprehensively available elsewhere, however the full references to the originators of genera and higher taxonomic level groups are given in Fensome et al. (1993) and only the name and date are shown here.

Division: DINOFLAGELLATA Bütschli, 1885
Subdivision: DINOKAYOTA Fensome, 1993
Class: DINOPHYCEAE Pascher, 1914
Subclass: PERIDINIPHYCIDAE Fensome et al. 1993

Gonyaulacoids (G-cysts)

Order: GONYAULACALES Taylor, 1980
Suborder: GONYAULACINEAE Taylor, 1980 (autonym)

Family: AREOLIGERACEAE Evitt, 1963

Genus: *Glaphyrocysta* Stover & Evitt, 1978
Species: *Glaphyrocysta spp.* - Plate 4.9 (a)

Sub-spherical cyst with finely reticulate surface. Membranous penitabular processes linked distally by fine trabeculae. Tabulation indistinct but gonyaulacacean in nature. Apical archeopyle with typical zig-zag margin.

Family: GONYAULACACEAE Lindemann, 1928
Subfamily: CRIBROPERIDINIOIDEAE Fensome et al. 1993

Genus: *Cordosphaeridium* Eisenack, 1963b
Species: *Cordosphaeridium fibrospinosum* Davey & Williams, 1966 - Plate 4.9 (b)

Near spherical cyst with smooth surface and no clear tabulation, however a gonyaulacaloid tabulation pattern can be deduced from the positions of the processes. Solid intratabular processes are formed from fine fibres that flare out distally. P-type archeopyle.

Genus: *Cribroperidinium* Neale & Sarjeant, 1962
Species: *Cribroperidinium spp.* - Plate 4.9 (c)

Sub-spherical cyst with slight apical-antapical compression and small apical projection. Sexiform tabulation clear with prominent ridges formed at the sutures surrounding the cingulum, 'growth lines' of tabulae visible on the plates. Clear pentagonal P-type archeopyle.

Genus: *Diphyes* Cookson, 1965
Species: *Diphyes colligerum* Deflandre & Cookson, 1955 - Plate 4.9 (d)

Sub-spherical cyst with numerous narrow hollow processes, closed distally with a capitate tip, aligned along the cingulum but otherwise in a non-tabular arrangement. Large hollow antapical process tapers slightly distally and has a ragged margin. Apical archeopyle with typical zig-zag margin.

Genus: *Hystrichokolpoma* Klumpp, 1953
Species: *Hystrichtokolpoma rigaudiae* Deflandre & Cookson, 1955 - Plate 4.9 (e)

Spherical cyst with smooth wall. Broad, hollow pre and post-cingular intratabular proceses tapering distally and open at the ends, similar but relatively longer and more pointed apical process, simple narrow cingular processes. Apical archeopyle.

Genus: *Lingulodinium* Wall, 1967a
Species: *Lingulodinium spp.* - Plate 4.9 (f)

Ovate cyst with finely granular surface texture. Numerous narrow hollow processes tapering distally and closed at the ends in a non tabular arrangement. Archeopyle apical.

Subfamily: GONYAULACOIDEAE Lindemann, 1928

Genus: *Impagidinium* Stover & Evitt, 1978
Species: *Impagidium dispertitum* Cookson & Eisenack, 1965 - Plate 4.9 (g)

Cyst subspherical to somewhat ovate with smooth to finely granulate surface. Low solid parasutural ridges highlight gonyaulacaloid tabulation pattern. Pentagonal P-type archeopyle. Smaller than the similar Early Eocene species *Impagidium crassimuratum*

Species: *Impagidium cf. dispertitum* - long ridges - Plate 4.9, (h)

Cyst subspherical to somewhat ovate with smooth to finely granulate surface, as for *I. dispertitum*, but with much taller, membraneous, parasutural septae. Archeopyle type not clear on the limited number of specimens observed.

Species: *Impagidium maculatum* Cookson & Eisenack, 1961 - Plate 4.9 (i)
Cyst subsperical with a distinct 'dotted' appearance resulting from closely spaced low granules on the cyst surface. Low solid parasutural ridges highlight gonyaulacaloid tabulation pattern. Pentagonal P-type archeopyle.

Genus: *Spiniferites* Mantell 1850
Species: *Spiniferites pseudofurcatus* Klumpp 1953, - Plate 4.9 (j)
Large subspherical cysts with a smooth wall. Gonyaulacaloid tabulation is outlined by low parasutural ridges, the junctions of ridges extend up into elongate hollow processes that flare out distally into broad open trifurcate structures. Apical archeopyle.
Species: *Spiniferites ramosus spp.* Ehrenberg, 1838 - Plate 4.9 (k)
Smaller somewhat ovate cysts with a smooth wall and low parasutural ridges. Narrow processes that terminate distally in delicate trifurcate 'fingers' arise from the junctions of ridges. Apical archopyle. Smaller and more delicate in appearance than *S. pseudofurcatus* with thinner processes, particularly distally.

Species: *Spiniferites spp* - Plate 4.9, (l)
Subspherical cysts with a smooth wall and parasutural ridges outlining gonyaulacaloid tabulation. Towards the junctions of sutures, the ridges become higher extending up into short processes that are flared at their bases and narrow distally with short trifurcate projections at their ends. The processes are shorter than those of either *S. pseudofurcatus* or *S. ramosus* and the parasutural ridges more pronounced.

Plate 4.9. Light microscope photographs of dinoflagellate cysts from Hampden Beach, scale bar 50 μm. a) *Glaphyrocysta spp*, CB05HB073; b) *Cordosphaeridium fibrospinosum*, CB05HB090; c) *Cribroperidinium spp*, CB05HB070; d) *Diphyes colligerum*, CB05HB046; e) *Hystrichtokolpoma rigaudiae*, CB05HB090, f) *Lingulodinium spp*, CB05HB030, g) *Impagidium dispertitum*, CB05HB090; h) *I. cf. dispertitum*, CB05HB090; i) *I. maculatum*, CB05HB046; j) *Spiniferites pseudofurcatus*, CB05HB090; k) *S. ramosus spp*, CB05HB090; l) *Spiniferites spp*, CB05HB030; m) *Enneadocysta partridgei*, CB05HB042; n) *Pyxidinopsis spp*, CB05HB030

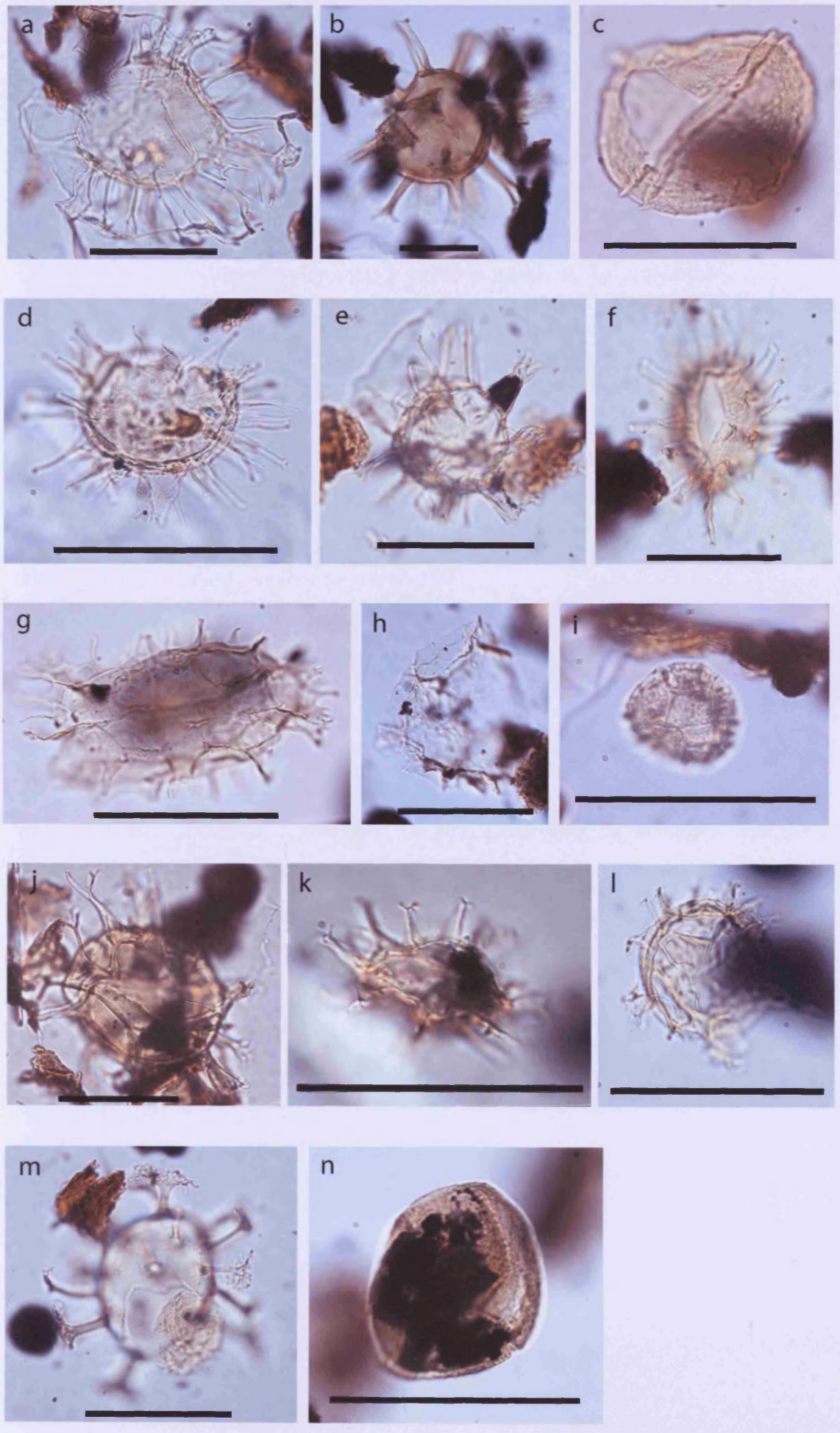

Plate 4.9

Subfamily: LEPTODINIOIDEAE Fensome et al. 1993

Genus: *Enneadocysta* Stover & Williams, 1995
Species: *Enneadocysta partridgei* Stover & Williams, 1995 - Plate 4.9 (m)
Sub-spherical to lenticular cyst with smooth to faintly granular surface texture. Position of intratabular processes suggest gonyaulacaloid tabulation. Processes have slender, solid, somewhat fibroid stems that are expanded at the distal ends to form a broad vasiform structure with an approximately circular outline. Apical archeopyle.

Subfamily: UNCERTAIN

Genus: *Pyxidinopsis* Habib, 1975
Species: *Pyxidinopsis spp.* Plate 4.9 (n)
Small sub-spherical cyst with fairly thick wall. The cyst wall has a fine, low, reticulate ornament with no clear tabulation. Archeopyle is P-type and pentagonal in outline.

Suborder: GONIODOMINEAE Fensome et al. 1993
Family: GONIODOMACEAE Lindemann, 1928
Subfamily: PYRODINIOIDEAE Fensome et al. 1993

Genus: *Hystrichosphaeridium* Deflandre et al. 1937b
Species: *Hystrichosphaeridium tubiferum* Ehrenburg, 1838 - Plate 4.10 (a)
Large sub-spherical cyst with smooth walls and no visible sutures, although gonyaulacaloid tabulation is indicated by the distribution of processes. The long, hollow, intratabular processes are much narrower at their base than the diameter of the plate they arise from, but widen distally and are open at the end, giving a 'trumpet like' appearance. Apical archeopyle.

Species: *Hystrichosphaeridium truswelliae* Wrenn & Hart, 1988 - Plate 4.10 (b)
Very similar in form to *H. tubiferum* but the distal ends of the processes are covered with a thin plate of ectophragm that reflects the shape of the plate on the main cyst body that the process arises from.

Suborder: UNCERTAIN

Genus: *Cleistosphaeridium* Davey et al. 1966
Species: *Cleistosphaeridium ancyreum* Cookson & Eisenack, 1965
- Plate 4.10 (c) operculum only

Sub-spherical cyst with smooth to very finely granulate surface and numerous non-tabular processes. The processes are slender, solid and approximately a third of the diameter of the cyst in length. The distal ends of some of the processes flare out slightly. Apical archeopyle.

Genus: *Dapsilidinium* Bujak et al. 1980

Species: *Dapsilidinium spp* – Plate 4.10 (d)

Sub-spherical to ovate cyst with a smooth surface, faint indications of tabulae and numerous non-tabulate processes. Processes are less than one third of the diameter of the cyst in length, slender and hollow, narrowing distally. Apical archeopyle.

Peridiniodes (P-cysts)

Order: PERIDINIALES Haeckel, 1894

Suborder: PERIDINIINEAE Haeckel, 1894

Family: PERIDINIACEAE Haeckel, 1894

Subfamily: DEFLANDREOIDEAE Bujak & Davies, 1983

Genus: *Deflandrea* Eisenack, 1938
Species: *Deflandrea antarctica* Wilson, 1967a - Plate 4.10 (e)

Circumcavate cyst somewhat dorsoventrally compressed with a single apical horn (broad at base and narrow at apex) and two short symmetrical antapical horns. Periphragm surface slightly granulose with tabulation not clear, endophragm near circular in outline with smooth surface. Archeopyle broad, intercalary and subhexagonal.

Subfamily: WETZELIELLOIDEAE

Genus: *Wilsonidium* Lentin & Williams, 1976
Species: *Wilsonidium echinosuturatum* Wilson, 1967b - Plate 4.10 (f)

Circumcavate cyst, dorsoventrally compressed and approximately rhombic in outline with the antapex separated into two angular, symmetrical, antapical horns. Low to medium ridges extend along the sutures with fine protrusions extending distally from them giving the ornament and the outline of the cysts a 'frilled' appearance. These sutures indicate a peridiniod tabulation pattern.

ACRITARCH:

Genus: *Tritonites spp.* - - Plate 4.10 (g)

Small acritarch with a rounded trifurcate morphology and smooth, transparent cyst wall.

Plate 4.10. Light microscope photographs of dinoflagellate cysts from Hampden Beach, scale bar 50 μm. a) *Hystrichosphaeridium tubiferum*, CB05HB030; b) *H. truswelliae*, CB05HB030; c) *Cleistosphaeridium ancyreum*, CB05HB030; d) *Dapsilidinium spp*, CB05HB038; e) *Deflandrea antarctica*, CB05HB030, f) *Wilsonidium echinosuturatum*, CB05HB070; g) *Tritonites spp*, CB05HB090

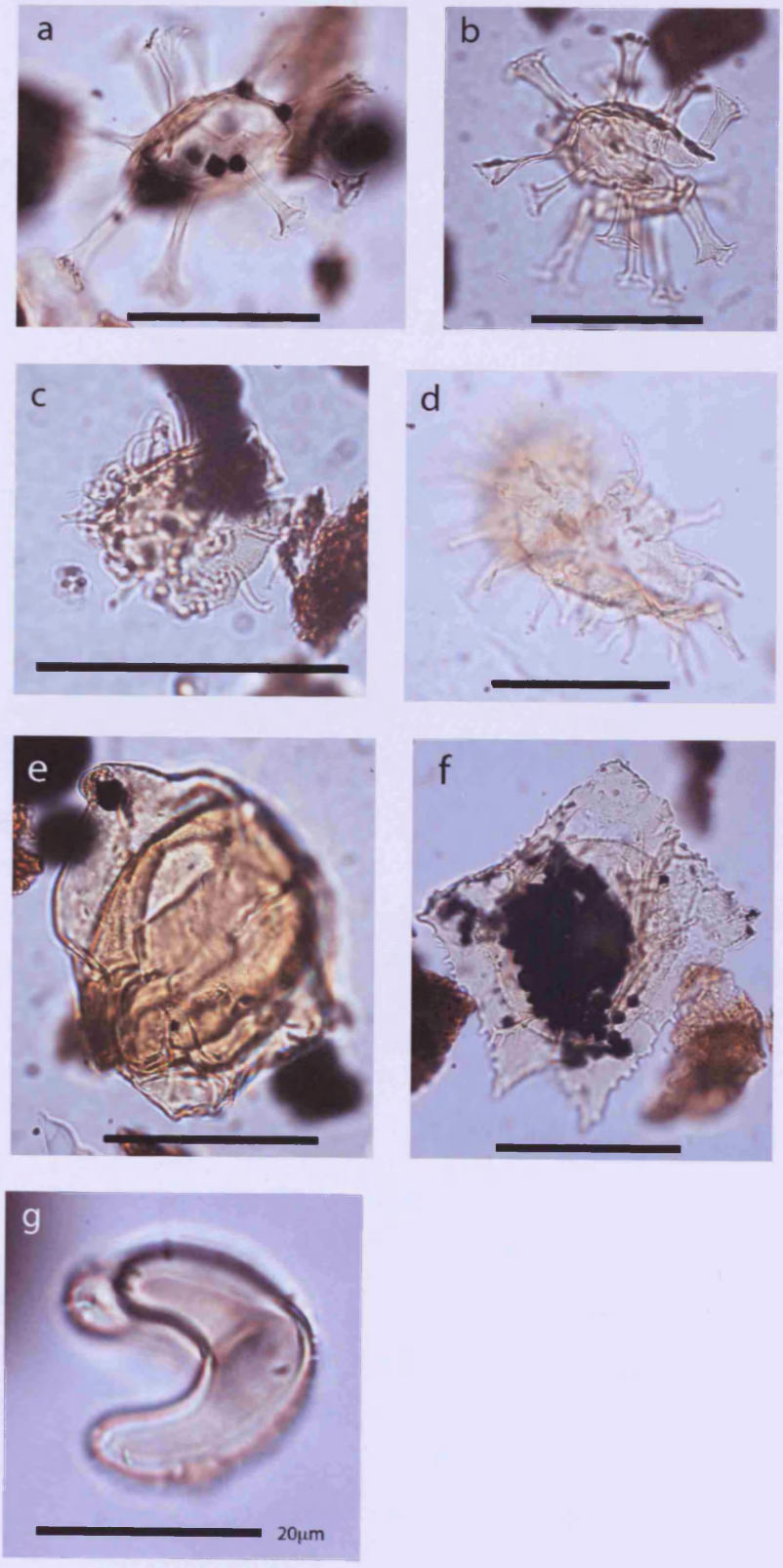

Plate 4.10

4.3.3. Dinoflagellates as palaeoenvironmental indicators

Dinoflagellates are particularly abundant in neritic environments so that palaeoclimatic and palaeoecological data derived from this group is complementary to that from typically more offshore groups such as planktonic foraminifera. Palaeoenvironmental analysis of dinoflagellate cysts originated in Quaternary studies where the high number of extant taxa allowed direct correlation between the taxa and their modern day environment. More recently however, dinocyst based palaeoenvironmental reconstructions have been extended back further in time and our understanding of Paleogene dinoflagellate ecology has increased considerably. An excellent review of these techniques is given in Sluijs et al. (2004).

The most commonly used Paleogene palaeoenvironmental reconstruction technique employs the ratio of peridiniod (P) to gonyaulacoid (G) cysts to estimate productivity (overview in Reichart and Brinkhuis, 2003). This is based on observations that the majority of P-cysts are formed by dinoflagellates with a heterotrophic feeding strategy whereas G-cysts are predominately formed by autotrophic dinoflagellates. Thus a dominance of P-cysts over G-cysts is commonly associated with a eutrophic environment, although there are further complications in areas where sea ice may be present. In different environments increased abundances of P-cysts may reflect increased nutrient input from terrestrial runoff e.g. (Crouch, 2001) or enhanced upwelling and mixing in the surface waters e.g. (Firth, 1996). Either of these causes may occur in a shelf edge setting such as Hampden Beach and consequently other techniques are required to distinguish them. For example, the strength of terrestrial runoff may be reflected by the ratio of terrestrial to marine palynomorphs or of organic compounds known to be terrestrial or marine in origin (BIT index).

In addition to providing information about palaeoproductivity, dinoflagellates can also be used to draw inferences about SST because (as with foraminifera) species have particular temperature preferences. Evaluating the proportions of high/mid latitude (cool water) taxa versus low latitude (warm water) taxa can indicate water temperature shifts at a site (e.g. Brinkhuis and Biffi, 1993; Crouch, 2001). While the majority of species in the Hampden Section are cosmopolitan, *Enneadocysta partridgei, Deflandrea antarctica* and *Hystrichosphaeridium truswelliae* have a predominantly high latitude distribution (*D. Antarctica* in particular considered to be an Antarctic endemic species). In contrast *Hystrichosphaeridium tubiferum, Hystrichtokolpoma rigaudiae, Cordosphaeridium fibrospinosum* and the representatives of the genus *Impagidinium* are

low latitude warm water species (Warnaar, 2006) and (Brinkhuis, 2007, pers. comm.). This agrees well with the temperature preferences known for the foraminifera and is discussed further in Chapter 7.

Finally, the preference of different dinoflagellate taxa for specific surface water environments has allowed the construction of a model for the composition of gonyaulacoid dinocyst assemblages along a proximal-distal transect (Brinkhuis, 1994). This places the *Impagidinium* group as the most distal, open ocean group seen at Hampden with *Enneadocysta* and *Spiniferities* intermediate and *Glaphyrocesta* most proximal and inshore. Changes in the proximal-distal composition of species may reflect sea level change or variation in terrestrial runoff and the transport of more proximal species.

Although dinoflagellates provide a great deal of environmental information, their interpretation is complex and consequently they are used in this study in conjunction with other palaeoenvironmental proxies that can help to constrain that interpretation.

4.4. Calcareous nannoplankton

4.4.1. Overview

The calcarous nannoplankton is a group comprising all forms of calcareous plankton less than 63μm in diameter, including juvenile foraminifera and calcareous dinoflagellates (Armstrong and Brasier, 2005). However, the overwhelmingly dominant group of calcareous nannofossils are the calcified remains of haptophyte algae. The majority of these are coccoliths, disc-like forms that are analogous to the calcified plates produced today by the coccolithophores but they also include morphologically variable nannoliths, the taxonomic affinities of which are less certain as they have no recent analogue (Bown, 1998).

The living coccolithophores are marine, unicellular phytoplankton characterised by the possession of a cell wall covering composed of coccoliths (a coccosphere). These can reproduce in a very large numbers creating blooms visible in satellite photographs and making them a very important part of global biogeochemical cycles. Furthermore, their coccoliths can undergo accelerated deposition in the faecal pellets of zooplankton or in aggregations known as "marine snow", making them very abundant in marine sediments above the calcite compensation depth (CCD). Coccolithophore cells may produce two types of coccoliths during different phases of their life cycle, heterococcoliths and holococcoliths. Heterococcoliths are built of large, variably shaped crystal units and are significantly more robust than holococcoliths, which are formed from minute equidimensional calcite crystallites, consequently the fossil record is dominated by heterococcoliths although some holococcoliths are recorded at Hampden Beach (see Chapter 5).

In this study the calcareous nannofossils observed at Hampden Beach have been used predominantly to study the preservation of the section (see Chapter 5) and their palaeoecology and palaeoenvironmental interpretation is not considered here, consequently taxonomic descriptions are not given. Dr Paul Bown of UCL carried out assemblage counts on 5 samples collected by Burgess (CB05HB202, 210, 220, 230, 240, 250) in collaboration with this study to aid in constraining the age model for the Hampden Section (Section 3.3.1). A species list of the calacareous nannofossils present in the Hampden Beach samples was compiled by Burgess from these counts.

4.4.2. Calcareous nannoplankton taxonomy

The list of species identified at Hampden Beach is given below using a taxonomic structure based on Young & Bown (1997) with additional reference to Arney and Wise (2003), Perch-Neilsen (1985) and Pospichal & Wise (1990). For reasons of space, full taxonomic references are not given here; see Young & Bown (1997) and references therin. Only calcareous nannofossil species that are highly abundant or of particular biostratigraphic significance are illustrated.

Division: HAPTOPHYTA Cavalier-Smith, 1986
Class: PRYMNESIOPHYCEAE Hibberd, 1976
Subclass: PRYMNESIOPHYCIDAE Cavalier-Smith, 1986
Order: ZYGODISCALES Young & Bown, 1997

Heterococcoliths

Family: HELICOSPHAERACEAE Black, 1971

Genus: *Helicosphaera* Kamptner, 1954
Species: *Helicosphaera bramlettei*
Species: *Helicosphaera clarissima*
Species: *Helicosphaera compacta*
Species: *Helicosphaera reticulata*

Family: PONTOSPHAERACEA Lemmermann 1908

Genus: *Pontosphaera* Lohmann, 1902 - Plate 4.11 (a) to (b)
Species: *Pontosphaera formosa*
Species: *Pontosphaera multipora*
Species: *Pontosphaera pectinata*
Species: *Pontosphaera pulcheroides*
Species: *Pontosphaera pulchra*

Family: ZYGODISCACEAE Hay & Mohler, 1967

Genus: *Neochiastozygus* Perch-Nielsen, 1971- Plate 4.11 (c)
Species: *Neochiastozygus imbriei*

Genus: *Neococcolithes* Sujkowski, 1931- Plate 4.11 (d)
Species: *Neococcolithes dubius*
Species: *Neococcolithes* sp.

Genus: *Nannotetrina* (Achuthan & Stradner, 1969)
Species: *Nannotetrina cristata*

Order: RHABDOSPHAERALES Ostenfeld, 1899

Family: RHABDOSPHAERACEAE Lemmermann, 1908

Genus: *Blackites* Hay & Towe, 1962 - Plate 4.11 (e) to (f)
Species: *Blackites amplus*
Species: *Blackites creber*

Species: *Blackites spinosus*
Species: *Blackites tenuis*
Species: *Blackites truncata*
Species: *Blackites vitreus*

Genus: *Rhabdolithus* Kamptner, 1952 - Plate 4.11 (g)
Species: *Rhabdolithus vitreous*

Order: PRINSALES Bown & Young, 1997

Family: PRINSIACEAE Hay & Mohler, 1967

Genus: *Toweius* Hay & Mohler, 1967
Species: *Toweius occultatus*

Family: NOELAERHABDACEAE Jerkovic, 1970

Genus: *Cyclicargolithus* Bukry, 1971 - Plate 4.11 (h)
Species: *Cyclicargolithus floridanus*
Species: *Cyclicargolithus* sp.

Genus: *Reticulofenestra* Hay, Mohler & Wade, 1966 - Plate 4.11 (i) to (o)
Species: *Reticulofenestra bisecta*
Species: *Reticulofenestra cribcrocentrum*
Species: *Reticulofenestra dictyoda*
Species: *Reticulofenestra filewicz*
Species: *Reticulofenestra lockeri*
Species: *Reticulofenestra macmillanii*
Species: *Reticulofenestra minuta*
Species: *Reticulofenestra reticulata*
Species: *Reticulofenestra reticulata (elliptical)*
Species: *Reticulofenestra umbilicus*

Order: COCCOSPHAERALES Haeckel, 1894

Family: COCCOLITHACEAE Poche, 1913

Genus: *Campylosphaera* Kamptner, 1963
Species: *Campylosphaera dela*

Genus: *Chiasmolithus* Hay, Mohler & Wade, 1966 - Plate 4.12 (a) to (c)
Species: *Chiasmolithus expansus*
Species: *Chiasmolithus grandis*
Species: *Chiasmolithus medius*
Species: *Chiasmolithus modestus*
Species: *Chiasmolithus solitus*

Plate 4.11. SEM images of nannofossils from Hampden Beach. a) *Pontosphaera multipora* CB05HB201; b) *Pontosphaera pulchra* CB05HB210; c) *Neochiastozygus imbriei* CB05HB245; d) *Neococcolithes dubius* CB05HB046; e) *Blackites spinosus* taken by TDJ at UCL; f) *Blackites sp.* CB05HB210; g) *Rhabdolithus vitreous* 230; h) *Cyclicargolithus floridanus* CB05HB230; i) *Reticulofenestra cribrocentrum.* CB05HB225; j) *Reticulofenestra umbilicus* CB05HB210; k) *Reticulofenestra macmillanii* CB05HB240; l) *Reticulofenestra minuta* CB05HB245; m) *Reticulofenestra reticulata* CB05HB201; n) *Reticulofenestra* sp. CB05HB250; o) *Reticulofenestra reticulata* CB05HB245.

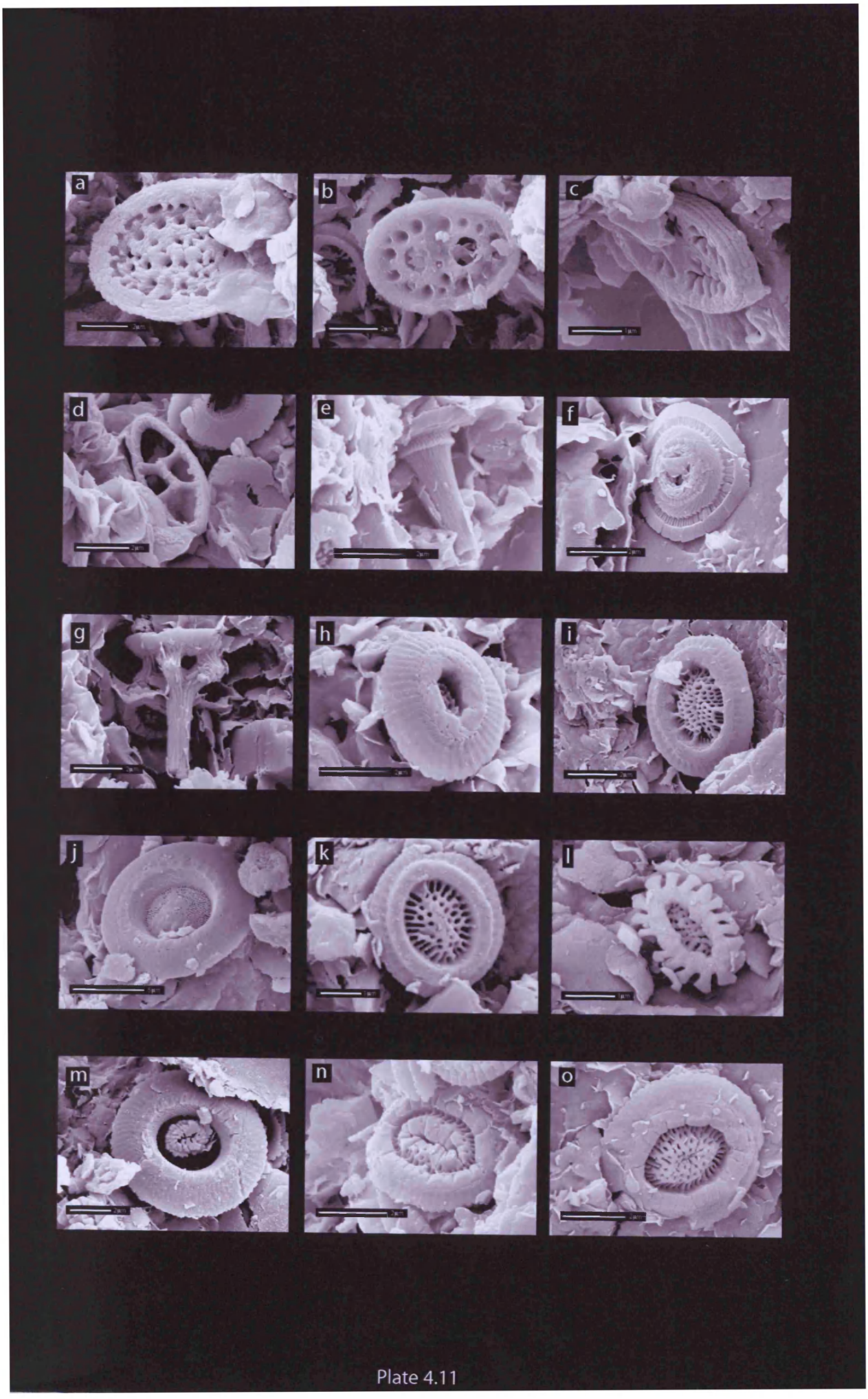

Plate 4.11

Genus: *Clausicoccus* Prins, 1979 - Plate 4.12 (c)

Species: *Clausicoccus fenestratus*
Species: *Clausicoccus subdistichus*

Genus: *Coccolithus* Schwartz, 1894 - Plate 4.12 (d) to (e)
Species: *Coccolithus cachaoi*
Species: *Coccolithus eopelagicus*
Species: *Coccolithus formosus*
Species: *Coccolithus pelagicus*

Genus: *Cruciplacolithus* Hay & Mohler, 1967
Species: *Cruciplacolithus primus*

Genus: *Coronocyclus* Hay, Mohler & Wade, 1966 - Plate 4.12 (f)
Species: *Coronocyclus bramlettei*

Genera incertae sedis:

Genus: *Markalius* Bramlette & Martini, 1964 - Plate 4.12 (g)
Species: *Markalius inversus*

Holococcoliths

Family: CALYTROSPHAERACEAE Boudreaux & Hay, 1969

Genus: *Holodiscolithus* Roth, 1970
Species: *Holodiscolithus geiseni*
Species: *Holodiscolithus macroporus*
Species: *Holodiscolithus solidus*

Genus: *Orthozygus* Bramlette & Wilcoxon, 1967
Species: *Orthozygus aureus*

Genus: *Dactylethra* Gartner, 1969 - Plate 4.12 (h)
Species: *Dactylethra probertii**
Species: *Dactylethra punctulata*
Species: *Dactylethra unitatus*

Genus: *Lanternilithus* Stradner, 1962
Species: *Lanternilithus minutes*

Genus: *Zygrhablithus* Deflandre, 1959 - Plate 4.12 (i)
Species: *Zygrhablithus bijugatus*
Species: *Zygrhablithus cf. bijugatus cornutus*
Species: *Sujkowskiella enigmatica*

Nannoliths

Family: BRAARUDOSPHAERACEAE Deflandre, 1947

Genus: *Braarudosphaera* Deflandre, 1947
Species: *Braarudosphaera bigelowii*
Species: *Braarudosphaera bigelowii* (large)
Species: *Braarudosphaera cf. hockwoldensis*

Genus: *Micrantholithus* Deflandre, 1954
Species: *Micrantholithus ornatus*

Genus: *Pemma* Klump, 1953
Species: *Pemma basquense*

Family: LAPIDEACASSACEAE Bown & Young, 1997

Genus: *Lapideacassis* Black, 1971
Species: *Lapideacassis* sp.

Order: DISCOASTERALES Hay, 1977

Family: DISCOASTERCEAE Tan, 1927

Genus: *Discoaster* Tan, 1927 - Plate 4.12 (j) to (l)
Species: *Discoaster barbadensis*
Species: *Discoaster bifax*
Species: *Discoaster deflandrei*
Species: *Discoaster distinctus*
Species: *Discoaster kuepperi*
Species: *Discoaster lodoensis*
Species: *Discoaster nodifer*
Species: *Discoaster saipanensis*
Species: *Discoaster salisburgensis*
Species: *Discoaster spinescens*

Family: FASCICULITHACEAE Hay & Mohler, 1967

Genus: *Fasciculithus* Bramlette & Sullivan, 1961
Species: *Fasciculithus involutus*

Family: SPHENOLITHACEAE Deflandre, 1952

Genus: *Sphenolithus* Deflandre, 1952
Species: *Sphenolithus moriformis*
Species: *Sphenolithus radians*
Species: *Sphenolithus runus*
Species: *Sphenolithus spiniger*

Family: LITHOSTROMATIONACEAE Deflandre, 1959

Genus: *Lithostromation* Deflandre, 1942
Species: *Lithostromation opersum*
Species: *Lithostromation simplex*

Genera incertae sedis:

Genus: *Tribrachiatus* Shamrai. 1963
Species: *Tribrachiatus orthostylus*

Plate 4.12. SEM images of nannofossils from Hampden Beach. a) *Chiasmolithus solitus* CB05HB046; b) *Chiasmolithus sp.* CB05HB250; c) *Chiasmolithus sp.* CB05HB078; d) *Clausicoccus fenestratus* CB05HB225; e) *Coccolithus pelagicus* CB05HB043; f) *Coccolithus pelagicus* (distal view) CB05HB034; g) *Markalius inversus* CB05HB201; h) *Dactylethra sp.* CB05HB210; i) *Zygrhablithus bijugatus* CB05HB245; j) *Discoaster barbadensis* CB05HB205; k) *Discoaster cf. deflandrei* CB05HB057; l) *Discoaster nodifer* CB05HB070.

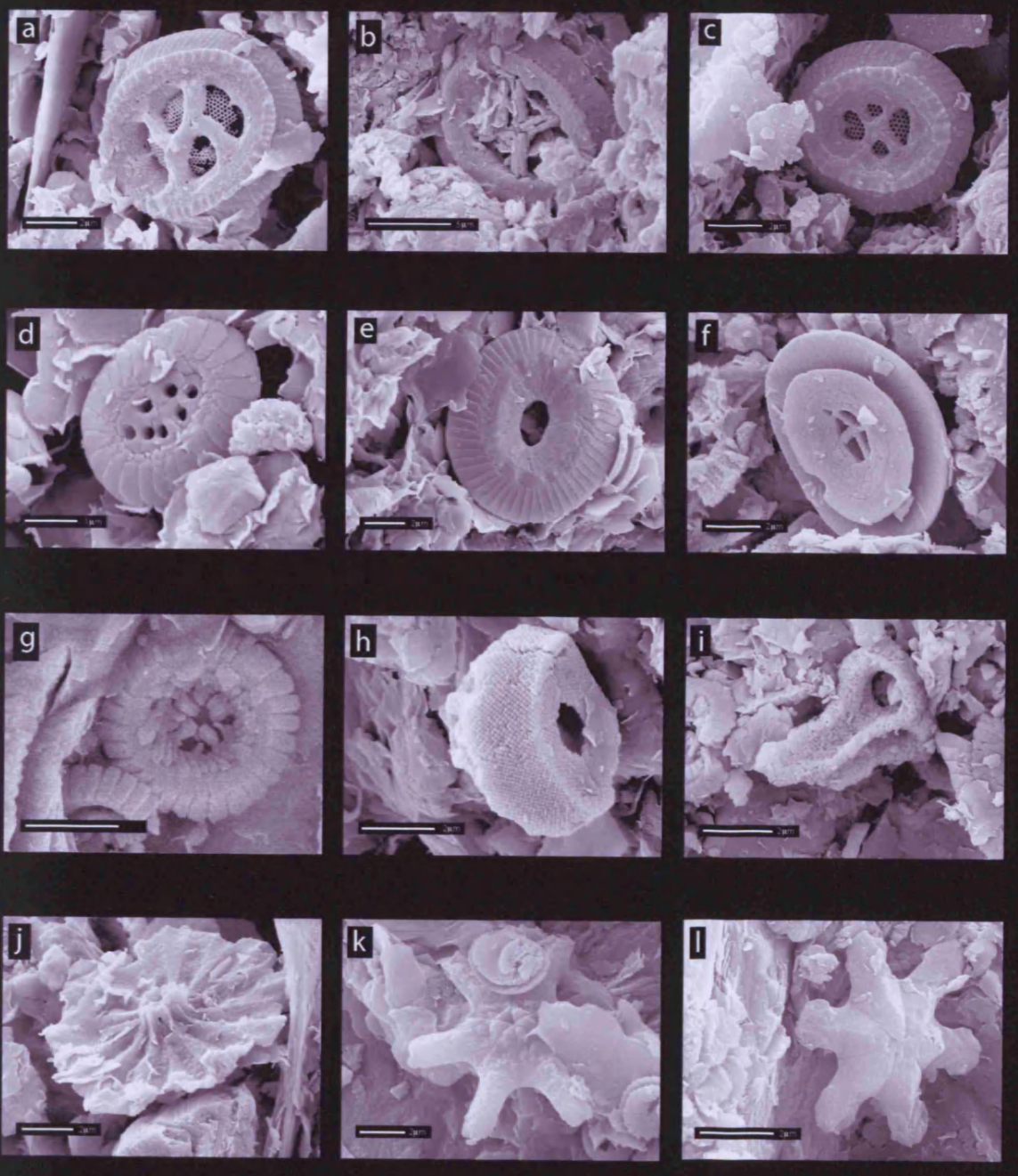

Plate 4.12

4.5. Macrofauna

Macrofossils are common at Hampden Beach and it is important to note their presence; however they are fragile and extremely difficult to recover intact from the sediment. Consequently macrofossils are illustrated in-situ in the cliff face and are only used in general terms for environmental, palaeoclimatic or biostratigraphic purposes.

The macrofossils observed were both organic and calcareous (Plate 4.13), particularly wood fragments, gastropods, nautiloids (*Aturia* Morgans, 2008), echinoids and scleractinian corals. The calcareous fossils all belong to groups that would have been composed originally of aragonite and the fossils remain aragonitic, no recrystallization to calcite was observed in any of the specimens seen (possibly contributing to their fragility). This supports the assertion that little alteration of calcareous fossils has occurred at Hampden Beach (discussed in Chapter 5).

The wood indicates proximity to a source of terrestrial material and is in keeping with the shelf edge environment inferred from benthic foraminifera. The molluscs are considered by Beu et al. (1990) to indicate outer shelf to upper bathyal water depths also supporting this depositional setting. The corals are solitary scleractinian forms and although the specimens seen at Hampden Beach have not been identified to species level, it is known that modern solitary corals are not restricted to the photic zone as colonial forms are, so these are also likely to be compatible with a shelf edge environment.

Plate 4.13. Photographs of macrofossils in the cliffside at Hampden Beach, the tip of a pencil is shown in each for scale. a) wood fragment (stratigraphic height ~18 m, level with CB05HB071); b) scleractinian coral (stratigraphic height ~15.5 m, level with CB04HB015); c) gastropod (stratigraphic height ~110 m, level with CB05HB267); d) echinoid plates (stratigraphic height ~134 m, level with sample CB05HB245); e) nautiloid in cross-section (stratigraphic height ~15 m, level with CB05HB010); f) nautiloid (stratigraphic height ~111 m, level with CB05HB280).

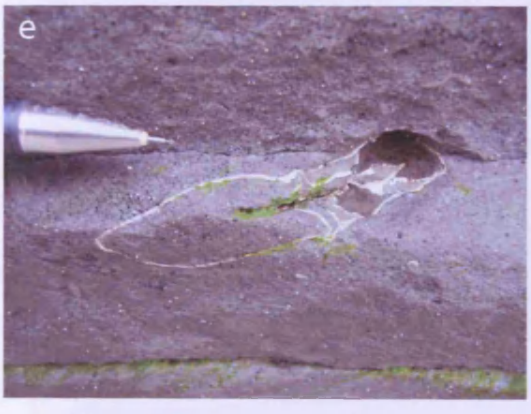

Plate 4.13

5. Calcareous Microfossil Preservation

5.1. Introduction

The preservation of microfossils is key to obtaining both accurate geochemical results and complete floral and faunal abundance data, and consequently to correctly interpreting the palaeoenvironment of a site. It is known that sites located on the continental shelf with a relatively high terrigenous input, resulting in a clay rich lithology can contain very well preserved microfossils (Norris and Wilson, 1998; Pearson et al., 2001; Wilson et al., 2002; Bown et al., 2008). A pilot study by Paul Pearson prior to this project showed that the microfossils in the clay rich Hampden Formation, at least at some levels, show good textural and geochemical preservation, thus making them suitable for use as proxies in generating palaeoenvironmental and palaeoclimatic reconstructions.

Diagenesis can affect species abundance data for nanno- and microfossil groups as dissolution preferentially removes particular species, for example those that are smaller, have thinner walls, or are composed of smaller crystals. In particular planktonic foraminifera are reduced in abundance relative to benthic foraminifera (Berger, 1979) and holococcoliths relative to heterococcoliths (Young et al., 2003). Such preferential dissolution can therefore affect the palaeoclimatic and palaeoecological conclusions drawn from floral and faunal assemblages.

Preservation is particularly important in calcareous groups. Recrystalisation and formation of diagentic calcite can substantially alter the isotopic composition of foraminiferal tests and thus generate spurious palaeoenvironmental interpretations (e.g. (Norris and Wilson, 1998; Pearson et al., 2001). It is also known that calcite with a relatively high Mg content is more soluble than carbonate with a lower Mg content and this can result in dissolution affecting the Mg/Ca ratio of foraminiferal tests, affecting the temperature reconstructed from the trace metal composition of the carbonate (Brown and Elderfield, 1996).

5.2. Nannofossils

The small size of nannofossils makes them prone to dissolution and therefore they act as a useful indicator of calcareous preservation in the sediment, although this study does not use them directly for geochemical analysis. As shown in this section, both the nannofossil assemblage composition and the appearance of individual nannofossils in the samples indicate that the calcareous preservation in the Hampden Formation is excellent.

The dominant components of the calcareous nannofossil assemblage in the Hampden Beach samples are coccoliths - the calcium carbonate plates that cover the cells of coccolithophores - some of which are still articulated into complete coccospheres. The vast majority of fossil coccolith specimens are heterococcoliths, the larger more robust plates associated with the diploid stage of the coccolithophore life cycle (Bown et al., 2008). These are the 'typical' coccoliths observed in a wide range of calcareous sediments and are composed of relatively large (0.1μm) crystals. However, the Hampden samples also contain a number of specimens of holococcoliths that are formed during the motile haploid stage of the lifecycle. These are much more delicate, being composed of very small (<0.1μm) crystals that disarticulate very easily and dissolve rapidly post deposition (see Plate 5.1). This makes them uncommon in the geological record, of 83 known modern species of holococcoliths only 2 are seen in the Pleistocene record (Young et al., 2003). However, large numbers of them have been recorded from Paleogene shelf sediments in Tanzania that also exhibit exceptional calcareous preservation (Bown et al., 2008).

The individual nannofossil specimens in the Hampden Beach samples are clearly well preserved. SEM photographs reveal the presence of a fine 'mesh' structure in the central area of some species; this is very delicate and prone to dissolution and is rarely observed in the fossil record, although again is seen in specimens from Tanzania (Bown et al., 2008). The slim cross-shaped structure in the centre of some taxa is also rarely observed in some species, for example *Coccolithus pelagicus*. In addition, the outlines of the coccoliths generally appear smooth and unbroken, whereas dissolution causes etching of the surface of the individual crystals producing 'ragged' margins. This is illustrated in Plate 5.2 comparing nannofossils from ODP sites 689 Maud Rise (Pospichal and Wise, 1990) and 1135 Kerguelen Plateau, (Arney and Wise, 2003) to those from Hampden Beach. These are all "Southern Ocean" sites of middle Eocene age

containing a number of the same species thus allowing as close a comparison as possible.

Overgrowths are more difficult to detect in nannofossils since additional calcite generally aligns its crystal axes with the original calcite laths, meaning that the overgrowths are difficult to distinguish using a light microscope. They are also not easily visible in SEM images; however none have been observed from Hampden Beach.

Plate 5.1. SEM images of calcareous nannofossils from Hampden Beach. Complete coccospheres a) *Clausicoccus sp.* from CB05HB074 and b) *Reticulafenestra* CB05HB022; heterococcoloiths with spines c) *Blackites spinosus* from CB05HB022 and d) *Blackites vitreus* from CB05HB230; heterococcoliths with intact central grills e) *Cyclococcolithus sp.* from CB05HB042 and f) *Reticulafenestra sp.* from CB05HB050; holococcoliths g) *Zygrhablithus bijugatus* from CB05HB245 and h) *Lanternithus* sp. from CB05HB230.

Plate 5.2. SEM images of calcareous nannofossils from ODP 1135 and 690 a) *Chiasmolithus solitus,* (113-690B-16H-5, 28-30 cm), b) *Chiasmolithus danicus,* (113-690C-14X-3, 28-30 cm), c) *Neococcolithes dubius* (113-690B-15H-4, 30-32 cm), d) *Neococcolithes dubius* (183-1135A-25R-1, 25-26 cm); compared with similar species from Hampden Beach e) *Chiasmolithus sp.* (CB05HB210), f) *Chiasmolithis sp.* (CB05HB046), g) *Neococcolithes sp.* (CB05HB046) and h) *Neococcolithes sp.* (CB05HB210).

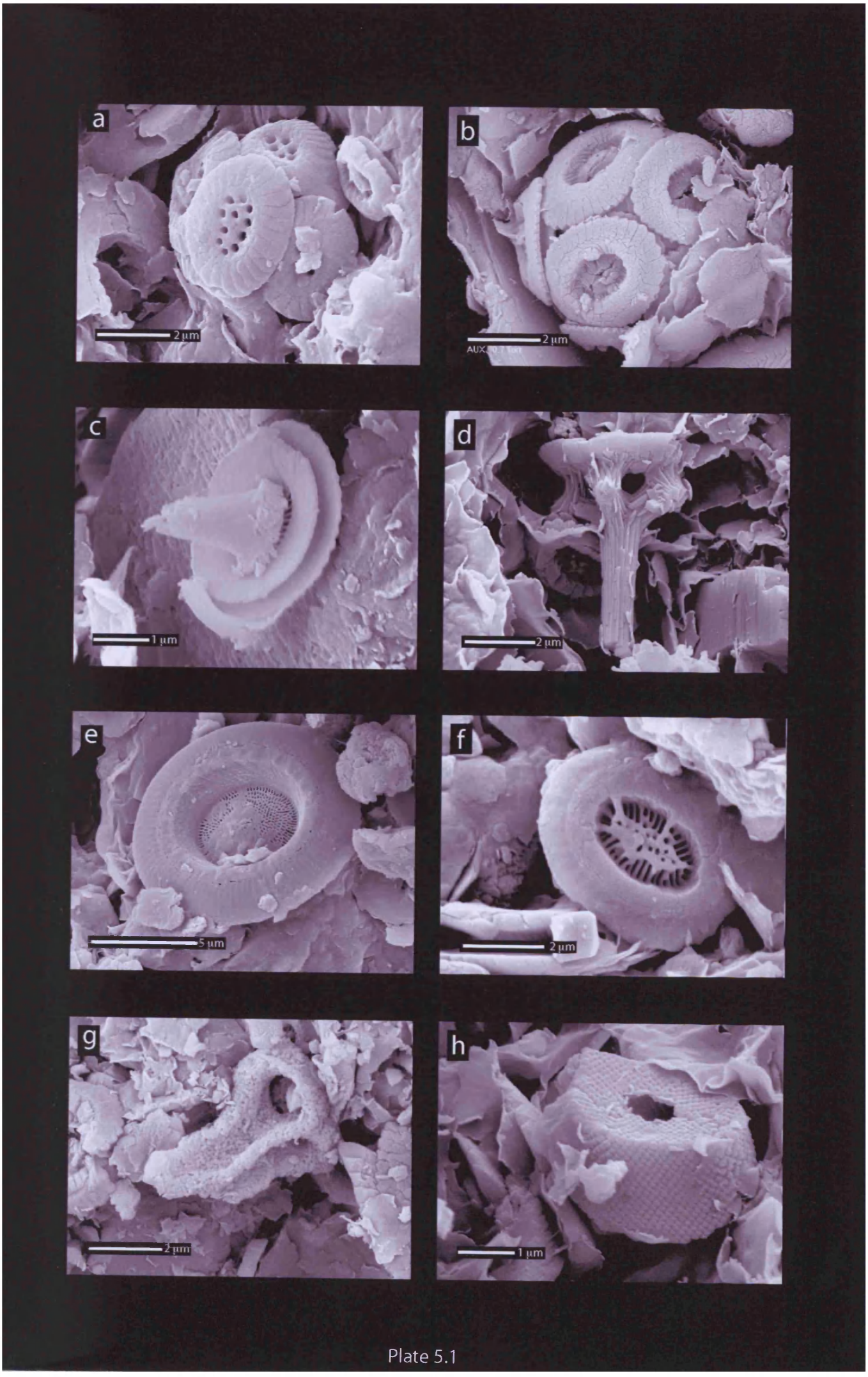

Plate 5.1

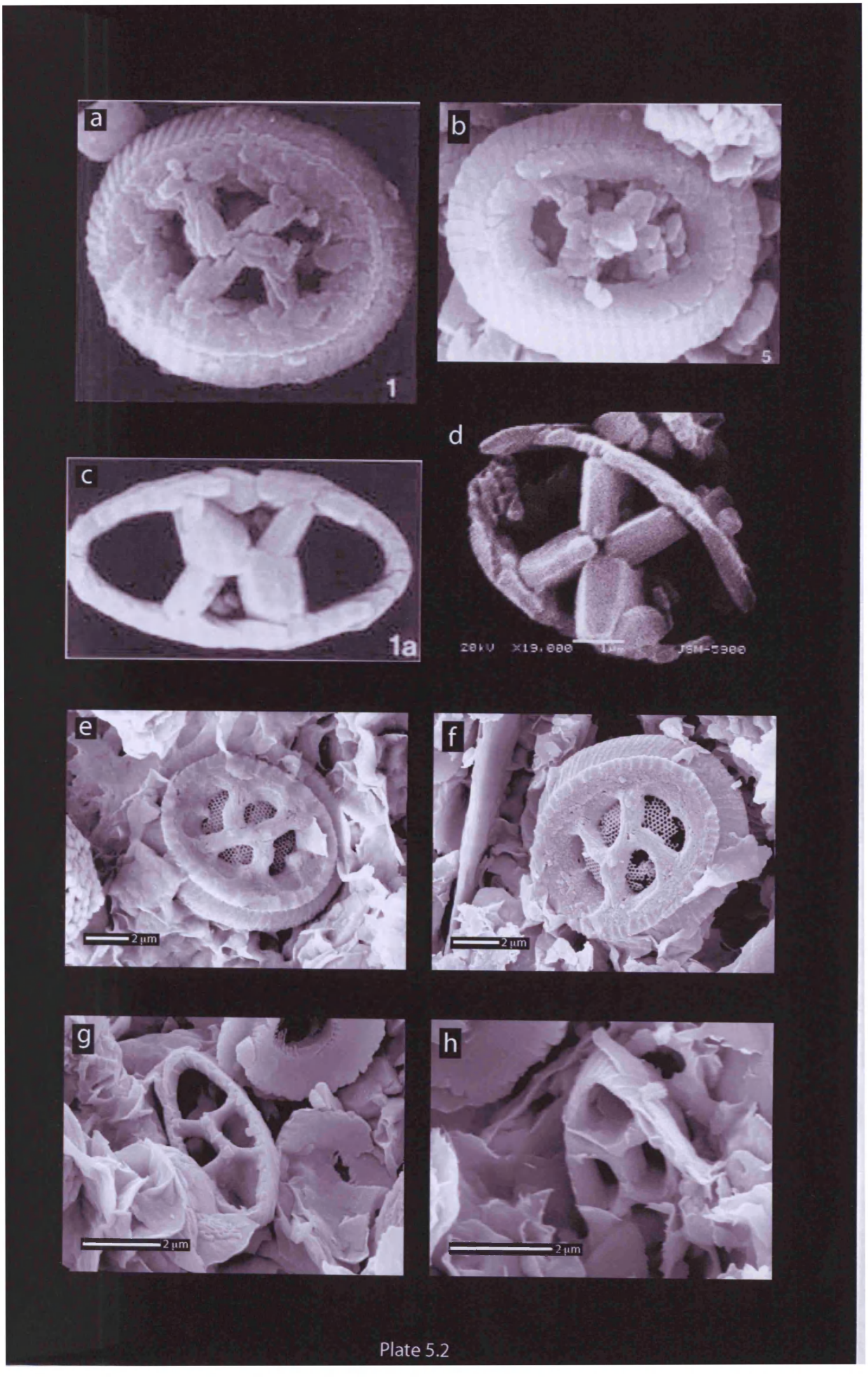

Plate 5.2

5.3. Foraminifera

The palaeoclimatic interpretation of foraminiferal trace metal and isotopic data forms a crucial part of this study, hence it is important to establish that the foraminifera are well-preserved and thus likely to record an original geochemical signature. This is done by using reflected light microscopy (RLM) and scanning electron microscopy (SEM) to image the specimens and by evaluating interspecific offsets of oxygen and carbon isotopic composition.

It has been realised over the last decade that foraminifera that were previously considered well preserved because they had not suffered serious dissolution or overgrowth may have in fact have undergone substantial micro-scale recrystallization. Pearson et al. (2001) propose that planktonic foraminifera from typical Paleogene and Neogene deep sea calcareous oozes comprise up to 50% diagenetic calcite. This new calcite is precipitated in deep ocean bottom waters and therefore records a substantially lower water temperature than that inhabited by the organism, particularly at low latitudes. It is now widely appreciated that better preservation can be found in clay rich sediments similar to those of the Hampden Formation (Huber et al., 1995; Norris and Wilson, 1998; Pearson et al., 2001; Wilson et al., 2002; Pearson et al., 2007). This is thought to result from the higher sedimentation rate burying the microfossils more rapidly than occurs at most open ocean sites and the impermeable nature of the clay limiting the diagenetic alteration of calcium carbonate by pore waters or overlying seawater (Pearson and Burgess, 2008). However, the use of these hemipelagic sediments remains controversial as their proximity to the continent may result in a terrestrial influence on the palaeoenvironmental signal (Zachos et al., 2002).

5.3.1. Imaging

The tests of foraminifera are composed of microgranules of calcite with a diameter of approximately 0.1μm and no clear crystal faces (Blow, 1979; Hemleben et al., 1989). The test walls are very smooth on a sub-micron scale both inside and outside although different wall textures and ornamentation are displayed by different foraminiferal genera. Tests may suffer overgrowth, dissolution and recrystallization in a number of ways, these can be difficult to detect using low-resolution RL and SEM imaging (Hemleben and Olsson, 2006; Sexton et al., 2006b). In particular it is difficult to detect neomorphism, where the calcite microgranules are replaced by larger more equant micron scale crystals, as the appearance of the surface texture is preserved at low

magnification. For example, *Acarinina* species that have muricae (fine surface pustules (Blow, 1979)) retain their mucricate appearance but the fine granules comprising the muricae are replaced by large blocky crystals (Plate 5.6).

Neomorphism is common in deep ocean sediments as illustrated in Plates 5.3 to 5.6, these compare foraminifera of the same species from Hampden Beach and a site with a similar lithology (ODP 647 in the North Atlantic), with those from typical calcareous deep ocean ODP sites 1135 (Kerguelen Plateau) and 689 (Maud Rise), all of which are middle Eocene in age. The images show clearly that specimens that appear similar under low-resolution SEM have undergone widely different degrees of digenesis. This difference is visible at high magnification when imaging the specimens on a micron scale (scale bars between 2 and 10 μm), as the larger equant crystals are then apparent in neomorphised foraminifera. Furthermore, when the specimens are submerged in water and photographed using RLM, specimens that have undergone recrystallization appear white and opaque whereas those that retain their original crystal structure are more transparent and 'glassy'. The use of RLM provides an excellent quick check on the preservation state of many foraminifera in a short period of time; for example it should be noted that although only single specimens of *Acarinina* from each sample are illustrated in Plates 5.8 and 5.10 for conciseness, many more were observed during processing (between 10 and 50 specimens from each sample) and consequently it is known that those specimens subsequently selected for imaging were representative of the whole sample. RLM also provides an excellent check on preservation in the field when SEM facilities are not available. However, RLM alone must be treated with a degree of caution as infilling of the tests with sediment can also cause them to appear opaque even when test wall preservation is good.

Plate 5.3. Comparison of four specimens of *Subbotina linaperta* from four localities, ODP Site 689 - Maud Rise (a,e,i,m,q,u), ODP Site 1135 - Kergeulen Plateau (b,f,j,n,r,v), Hampden Beach (c,g,k,o,s,w), ODP Site 647 - North Atlantic (d,h,l,p,t,x). RLM photos taken with the specimens submerged in water (a-d) are compared to SEM photographs of the same specimens (e-x). Scale bar is 200 μm for (a-h). Scale bars are 10 μm in (i-l) and 2 μm in (m-x). (Pearson & Burgess, 2008; imaged by Burgess)

Plate 5.4. Comparison of three specimens of *Globoturborotalita* sp. from three localities, ODP Site 1135 - Kergeulen Plateau (a,d,g,j,m), Hampden Beach (b,e,h,k,n), ODP Site 647 - North Atlantic (c,f,i,l,o). RLM photos taken with the specimens submerged in water (a-c) are compared to SEM photographs of the same specimens (d-o). Scale bar is 200 μm for (a-f). Scale bars are 10 μm in (g-i) and 2 μm in (j-o). (Pearson & Burgess, 2008; imaged by Burgess)

Plate 5.5. Comparison of three specimens of *Globeriginatheka index* from three localities, ODP Site 689 - Maud Rise (a,d,g,j,m), ODP Site 1135 - Kergeulen Plateau (b,e,h,k,n), Hampden Beach (c,f,i,l,o). RLM photos taken with the specimens submerged in water (a- c) are compared to SEM photographs of the same specimens (d-o). Scale bar is 200 μm for (a-f). Scale bars are 10μm in (g-i) and 2μm in (j-o). (Pearson & Burgess, 2008; imaged by Burgess)

Plate 5.6. Comparison of two specimens of *Acarinina bullbrooki* from two localities, ODP Site 1135 - Kergeulen Plateau (a,c,e,g,i), Hampden Beach (b,d,f,h,j). RLM photos taken with the specimens submerged in water (a,b) are compared to SEM photographs of the same specimens (c-j). Scale bar is 200 μm in (a-d). Scale bars are 10 μm in (e,f) and 2 μm in (g-j). (Pearson & Burgess, 2008; imaged by Burgess)

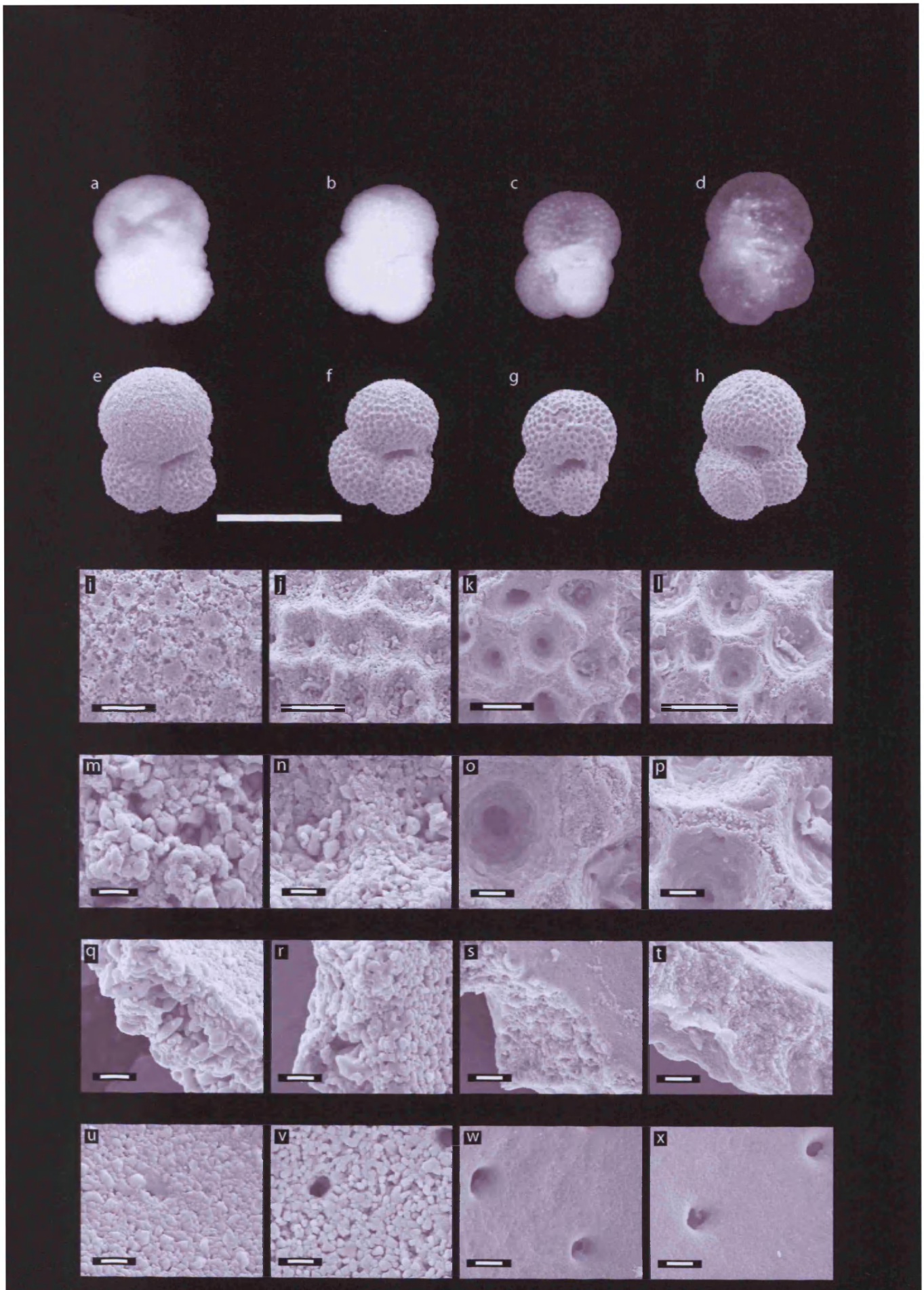

Plate 5.3

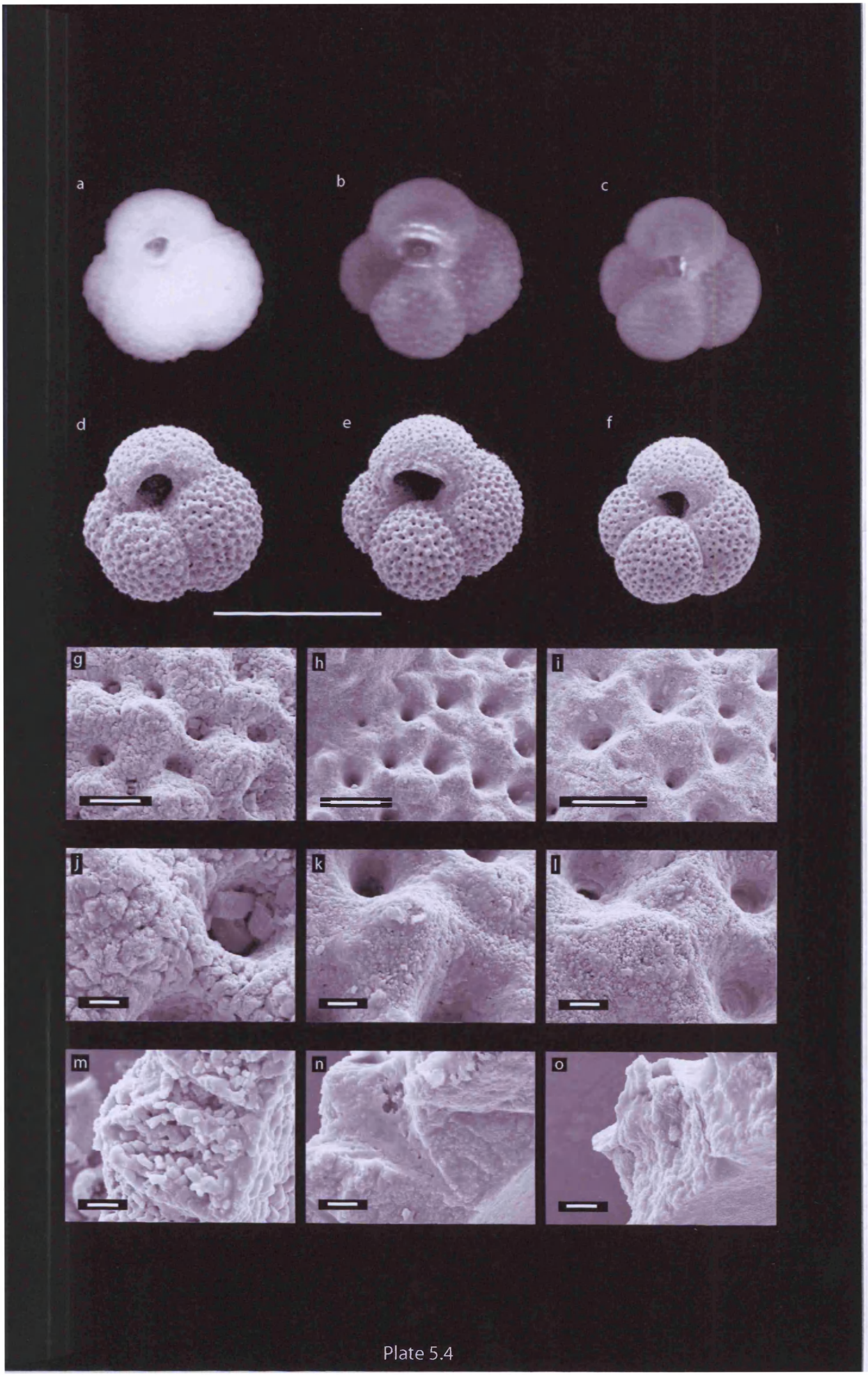

Plate 5.4

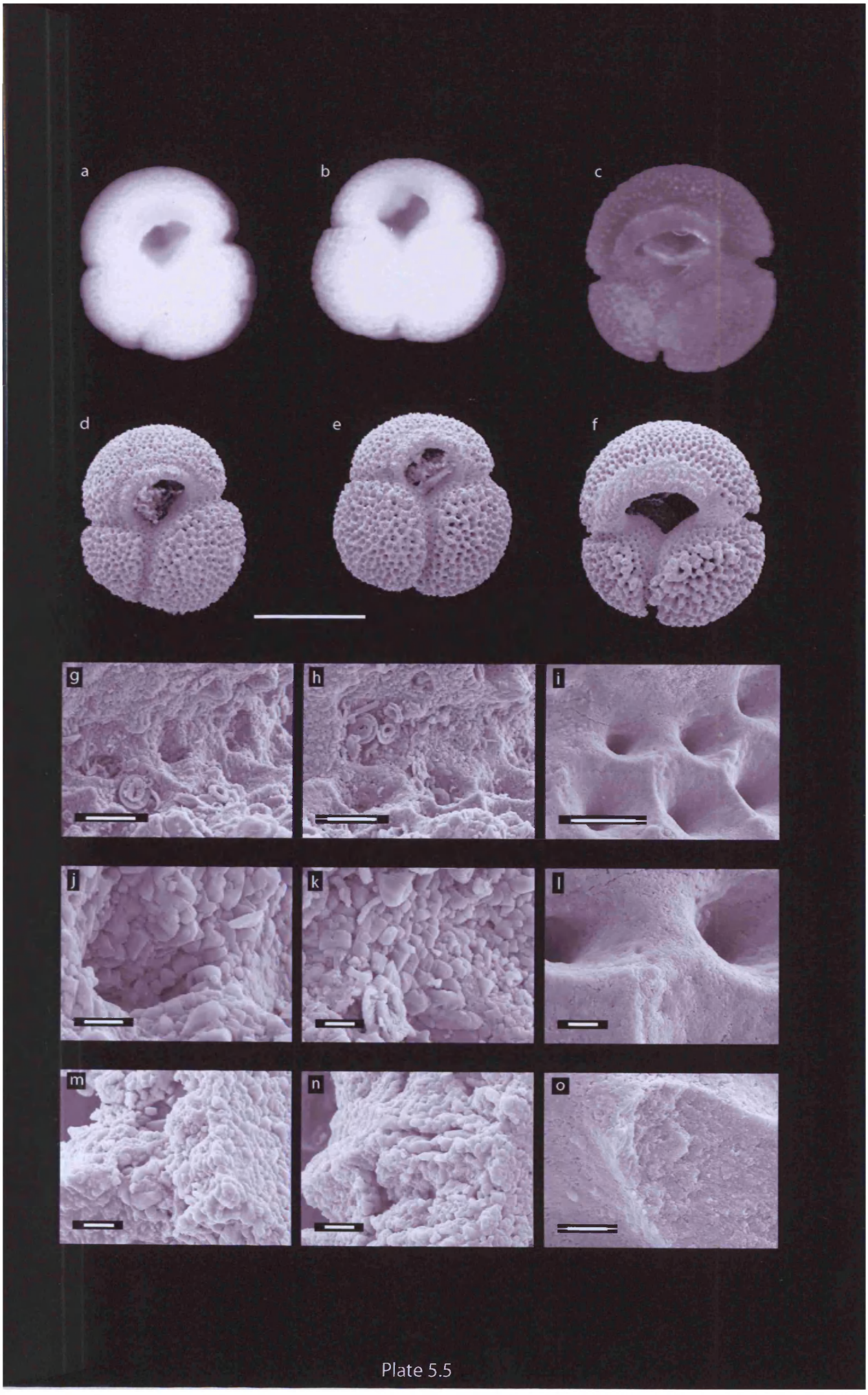

Plate 5.5

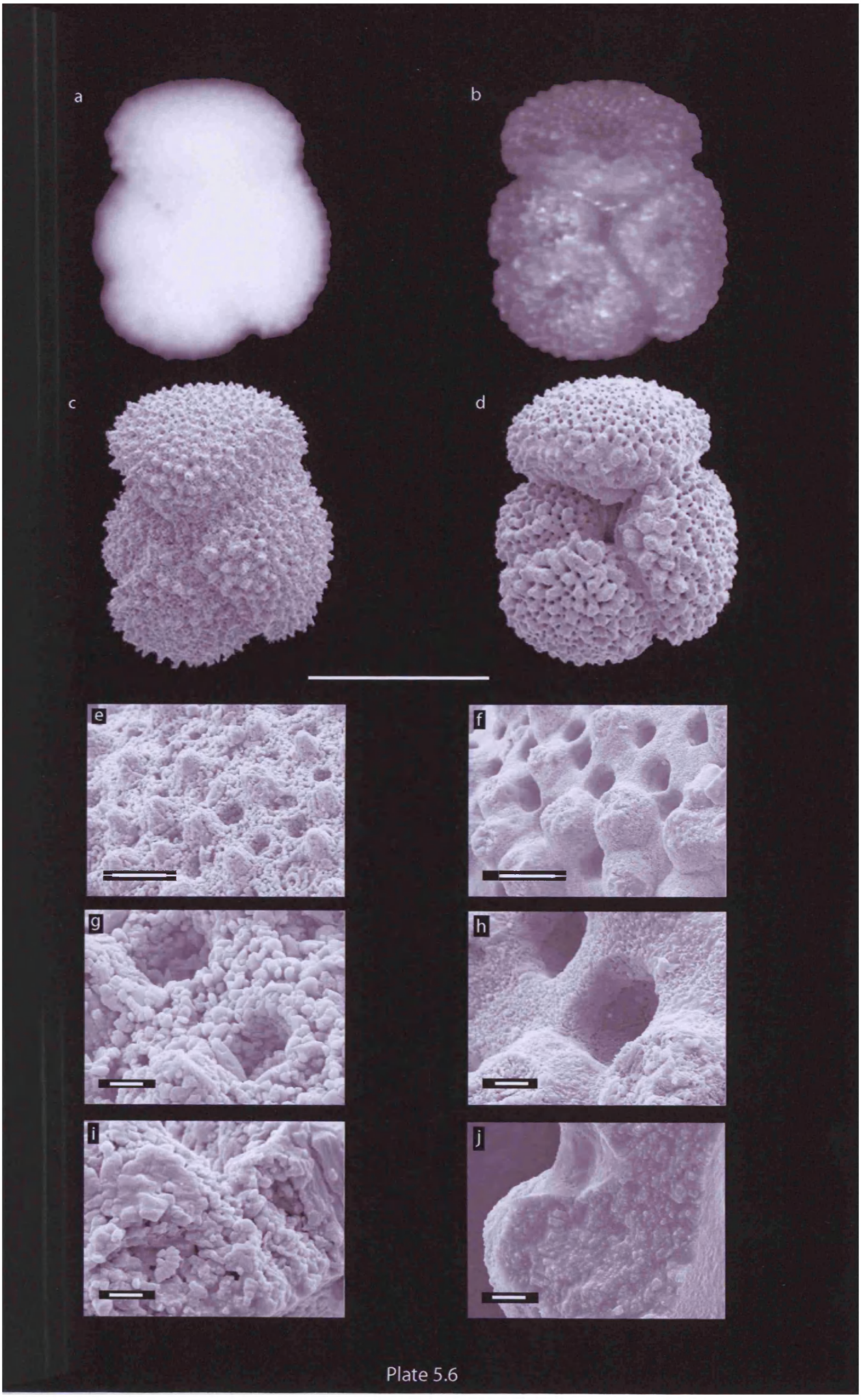

Plate 5.6

Four criteria can be used to demonstrate good preservation in foraminifera (Pearson and Burgess, 2008):

(1) Is the shell translucent and reflective under RLM, especially when in water or oil?

(2) Do ultrafine features such as spines (if originally possessed) survive?

(3) Under SEM, are originally smooth parts of the shell such as the outer surface (in some species), the inner surface (in most species), apertural lips and sutures still smooth on a submicron scale?

(4) Can the submicron microgranular texture be identified in cross section

The samples from Hampden Beach clearly exhibit features (1), (3) and (4) (e.g Plate 5.7). Ultrafine features such as spines are rare because they are very delicate and easily broken, both during burial and during sample processing. Damage during processing may be a particular problem in clay-rich sediments where cohesive sediment must be agitated whilst being washed through a sieve. Despite this problem, a fine pustule is visible in one specimen of *Acarinina primitiva* (Plate 5.7; image d) and short but fine pustules with a diameter of approximately 1 μm are seen around the apertures of a number of *Acarinina* (Plate 5.7).

Plate 5.7. Examples of foraminifera from Hampden Beach exhibiting the characteristic features of good preservation as set out in Pearson and Burgess (2008). RLM photographs taken underwater showing the translucent, reflective shell a) *Acarinina primitiva* CB05HB205, b) *Globigerinatheka ouchitaensis* CB05HB074, c) *Globigerinatheka index* CB05HB042. Ultrafine features d) pustule near the aperture of *A. primitiva* CB05HB205, e) short fine pustules around the aperture of *A. primitiva* CB05HB042, f) close up of these pustules. Smooth parts of the shell g) inner surface of *G. index* CB05HB042, h) apertural lip of *Subbotina angiporoides* CB05HB050, i) apertural lip of *A. primitiva* CB05HB215. Cross section showing microgranular texture j) *S. angiporoides* CB05HB050, k) *G. index* CB05HB042, l) *A. primitiva* CB05HB050

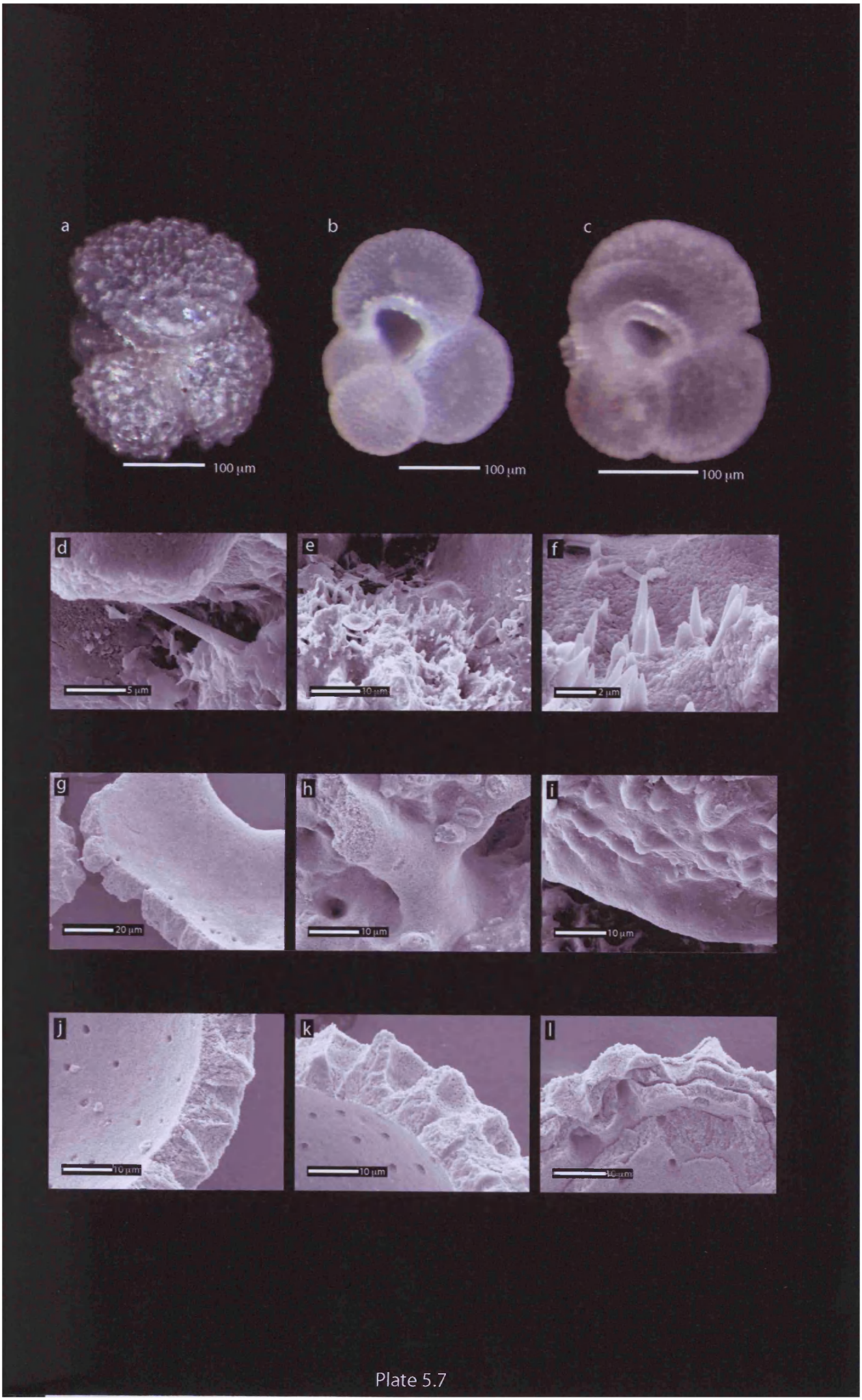
a
100 µm
b
100 µm
c
100 µm
d
5 µm
e
10 µm
f
2 µm
g
20 µm
h
10 µm
i
10 µm
j
10 µm
k
10 µm
l
10 µm

Plate 5.7

5.3.2. Geochemical signature

In addition to using imaging to assess textural preservation, interspecies offsets in oxygen and carbon isotopic composition of specimens in a sample can be used to assess geochemical preservation (Pearson et al., 2001). Foraminifera live at different depths within the water column and should record the differing geochemical signatures of the water they inhabit. As described in Chapter 1, in the modern ocean, surface waters are depleted in ^{12}C relative to ^{13}C because biological productivity in the photic zone preferentially removes the lighter carbon. A proportion of this is then returned to the water at the seafloor when the resulting organic matter decays, enriching deep water in ^{12}C (Ruddiman, 2001). Furthermore, surface waters are warmer than deep and consequently surface dwelling foraminifera will precipitate calcium carbonate with a lighter oxygen isotopic composition (Emiliani, 1955). This should result in surface dwelling species having heavier $\delta^{13}C$ and lighter $\delta^{18}O$ than deeper dwelling species. However, if the specimens have undergone recrystallization at the sea floor they will become partially homogenised, converging on a geochemical profile of diagenetic calcite (Pearson et al., 2001). Plotting the $\delta^{18}O$ against $\delta^{13}C$ for a range of foraminiferal species in a single sample allows an assessment of whether the species preserve these original offsets or whether they have undergone homogenisation.

A sample from Hampden Beach using 6 to 8 specimens each of 8 species of foraminifera clearly shows variation not only between planktonic and benthic species but that they can be further subdivided into shallow dwelling (mixed-layer) species and deep (sub-thermocline) species (Figure 5.1). The depth habits indicated by their isotopic composition agrees well with those given for the species in (Pearson et al., 2006a). This indicates that during the time recorded by this sample, the water column at Hampden was well-stratified and that the isotopic composition of the foraminiferal tests reflects their depth habitats. There remains however, significant variability in isotopic compostion between mixed-layer dwelling planktonic species that may reflect differences in preferred depth habitat and late stage calcification at depth of some species (Premoli Silva et al., 2006) or a difference in the timing of the species bloom meaning that they record a somewhat different season. This is a further indication that the foraminiferal preservation at Hampden Beach is excellent and well suited to palaeoclimatic analysis.

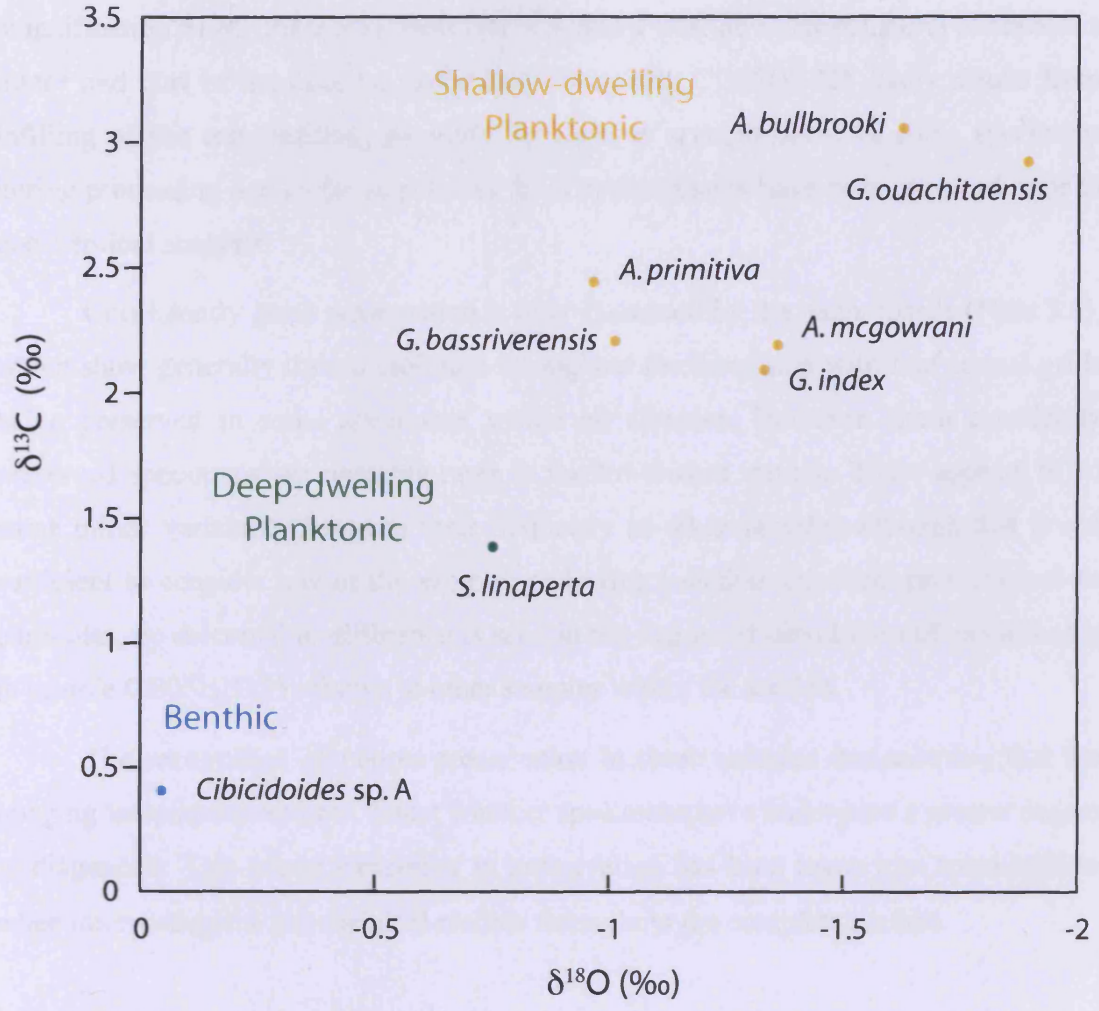

Figure 5.1. The oxygen and carbon isotopic compositions of 8 species of foraminifera from sample CB05HB097. These can be clearly differentiated into shallow dwelling planktonic species with light $\delta^{18}O$ and heavy $\delta^{13}C$, a sub-thermocline species with intermediate values and a benthic species with heavy $\delta^{18}O$ and light $\delta^{13}C$, outlined in orange, green and blue respectively.

5.4. Variability of preservation

5.4.1. Hampden Formation

Light microscopy and high-resolution SEM photographs of calcareous micro- and nannofossils were taken from samples throughout the whole of the Hampden Formation (Plates 5.8 and 5.9). The samples show good preservation through almost all of the section but with slightly poorer than average preservation in the lowermost sample (CB05HB202) and in sample CB05HB225. Specimens from these samples are more opaque under RLM and show signs of dissolution and recrystallization under high

magnification SEM (Plate 5.8). However it is noted that the microstructural alteration is minor and part of the opacity, particularly in sample CB05HB225 likely results from infilling of the test. Infilling by pyrite or clays is seen to occur in some specimens during processing and as far as possible these contaminants have been removed prior to geochemical analysis.

Consistently good preservation is also illustrated by the nannofossils (Plate 5.9), which show generally little dissolution throughout the formation with fine central grills being preserved in some specimens within all samples. However, these excellently preserved specimens are noteably rarer in the lowermost sample. There appears to be some minor variability between their frequency in other samples although this is not sufficient to consider any of the samples as having less than excellent preservation. In particular, no discernable difference is seen in the degree of dissolution of nannofossils in sample CB05HB225 relative to other samples within the section.

The recognition of poorer preservation in these samples demonstrates that the imaging techniques used can detect whether specimens have undergone a greater degree of diagenesis. This minor variability in preservation has been taken into consideration when interpreting the geochemical records throughout the complete section.

Plate 5.8 Stratigraphic column of Hampden Beach section showing images of *Acarinina prmitiva* from samples throughout the section with the sample number marking their stratigraphic postion (scale on stratigraphic column in m). For each sample from left to right; RLM photograph of the specimen underwater, SEM photograph of the specimen (scale bar = 100 μm), close up of the specimen showing the muricate wall texture (scale bar = 10 μm) and ultra close up showing the microgranular wall texture (scale bar = 2 μm).

Plate 5.9. SEM images of calcareous nannofossils from the same samples illustrated in Plate 5.8 also plotted against the straigraphic column (scale in m).

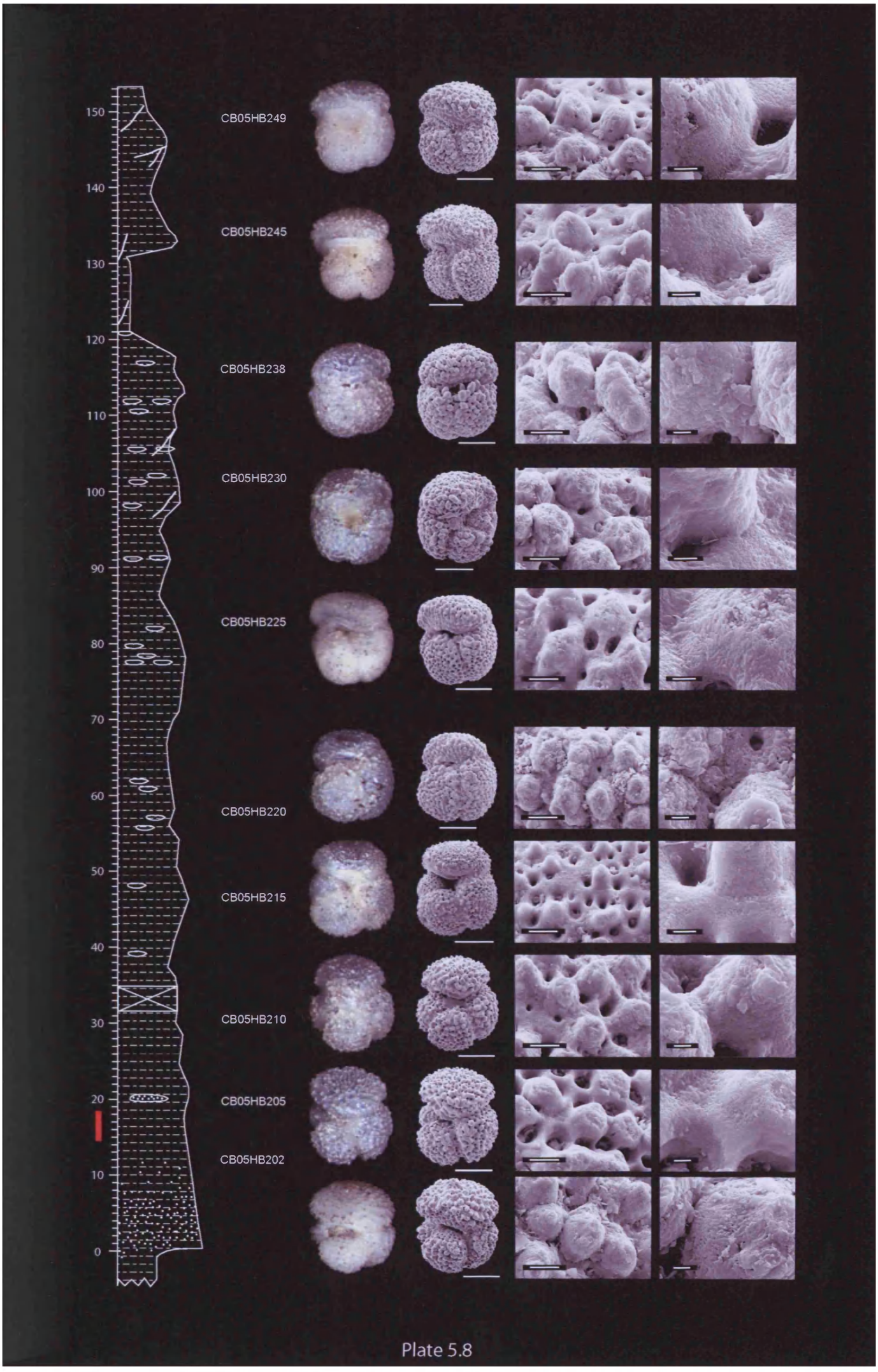
150
140
130
120
110
100
90
80
70
60
50
40
30
20
10
0
CB05HB249
CB05HB245
CB05HB238
CB05HB230
CB05HB225
CB05HB220
CB05HB215
CB05HB210
CB05HB205
CB05HB202

Plate 5.8

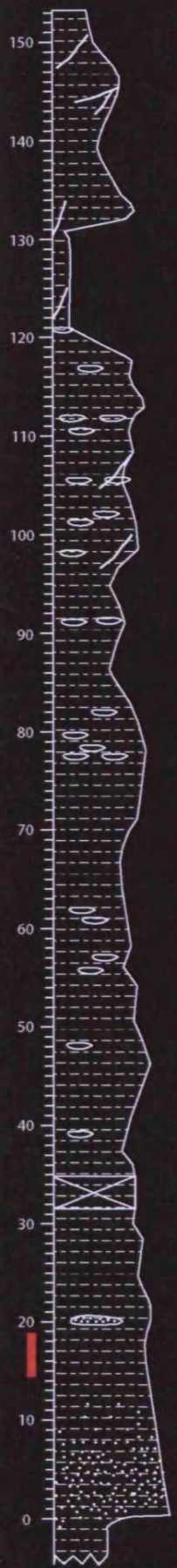

CB05HB250

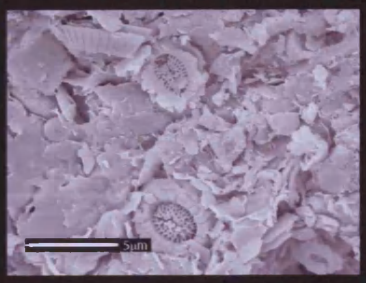

CB05HB245

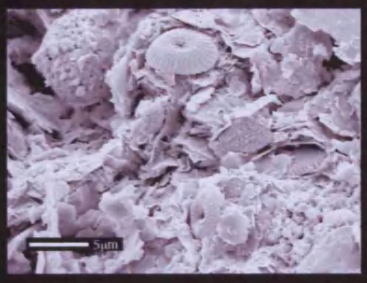

CB05HB240

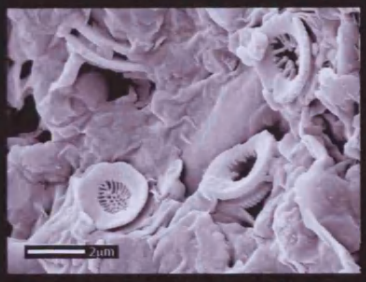

CB05HB235

CB05HB230

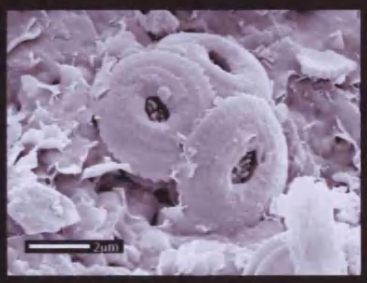

CB05HB225

CB05HB220

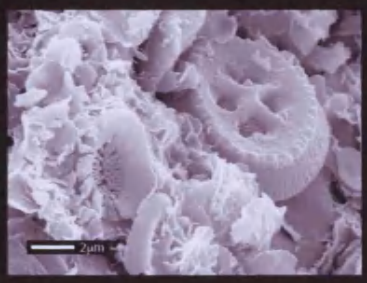

CB05HB215

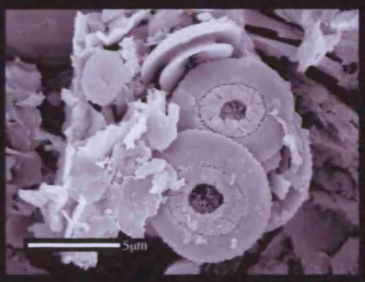

CB05HB210

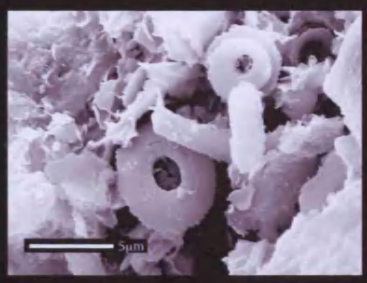

CB05HB205

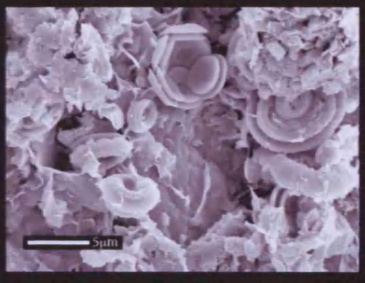

CB05HB201

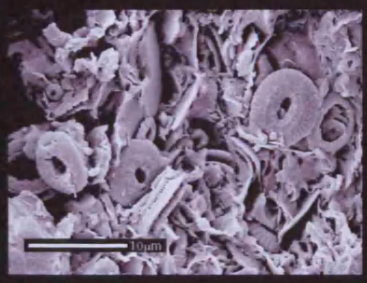

Plate 5.9

5.4.2. "High-resolution" section

A major part of the study of the Hampden Section involved looking at the geochemical, palaeontological and sedimentological variability through a short interval towards the base of the Hampden Section (the "high-resolution" section) the results of which are given in Chapter 7. Therefore, it was important to establish that the geochemical and palaeontological variability exhibited through the section was not a consequence of preservational change through the section related to changing lithology. For example, it is possible that where the average grain size of a rock was higher, the rock would be more permeable and thus expose the microfossils to greater dissolution and recrystallization.

To establish the preservation state of the calcareous micro- and nannofosils, high magnification SEM photographs of the nannofossils were taken from every fourth (stratigraphically) "high-resolution" sample. One typical foraminifer from each of these samples was also photographed in water under RLM and at high magnification with the SEM. Although some specimens have undergone a small degree of dissolution, significant recrystallization has not occurred and there is no systematic variation in preservation through the "high-resolution" section (Plates 5.10 and 5.11).

Plate 5.10. Photograph of the cyclic "high-resolution" section studied in Chapter 7 showing images of *Acarinina primitiva* from samples throughout the section with the sample number marking their stratigraphic position. For each sample from left to right; RLM photograph of the specimen underwater, SEM photograph of the specimen, close up of the specimen showing the muricate wall texture and ultra close up showing the microgranular wall texture.

Plate 5.11. SEM images of calcareous nannofossils from equally spaced samples throughout the "high-resolution" section shown against stratigraphic column (scale in m).

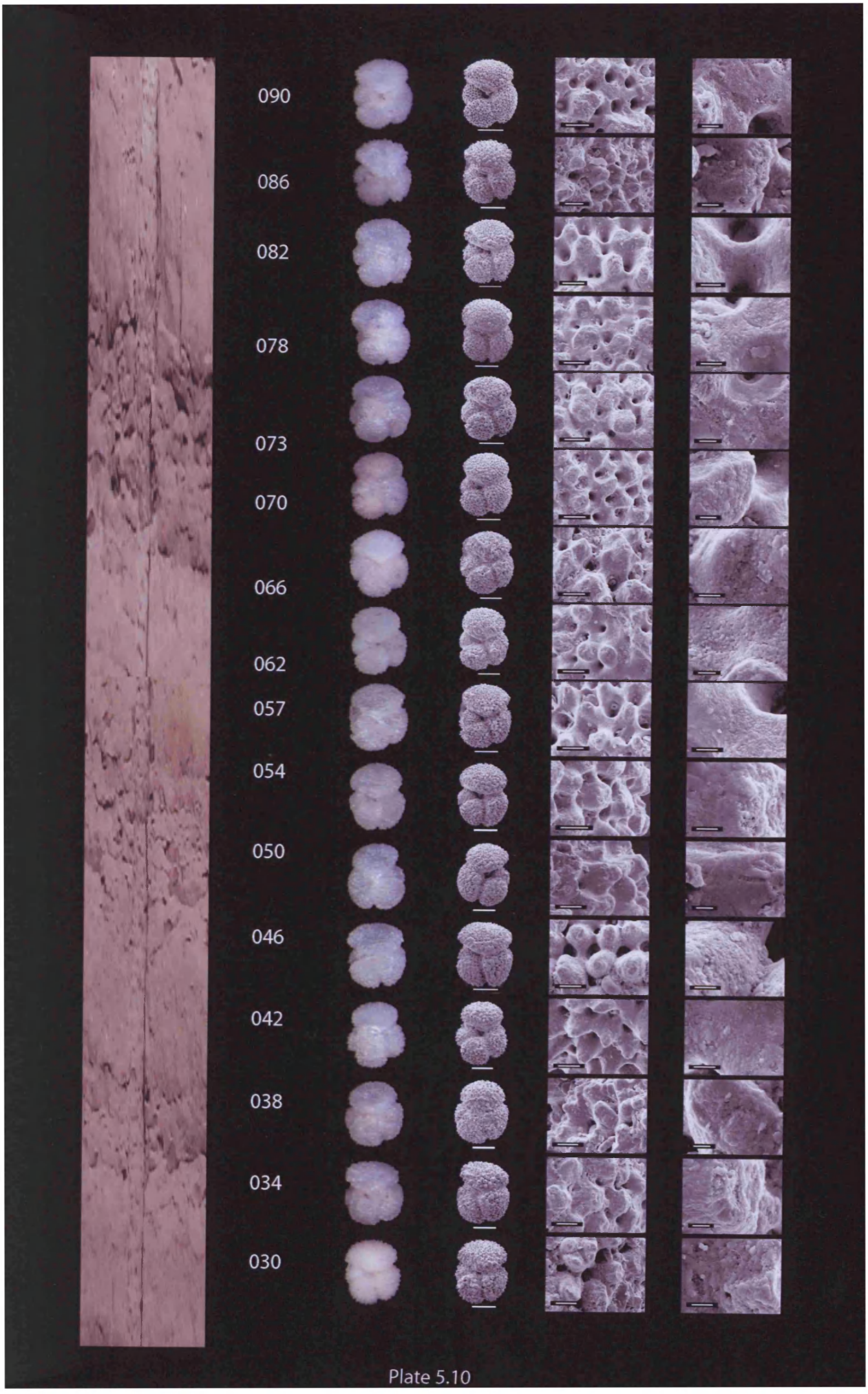

Plate 5.10

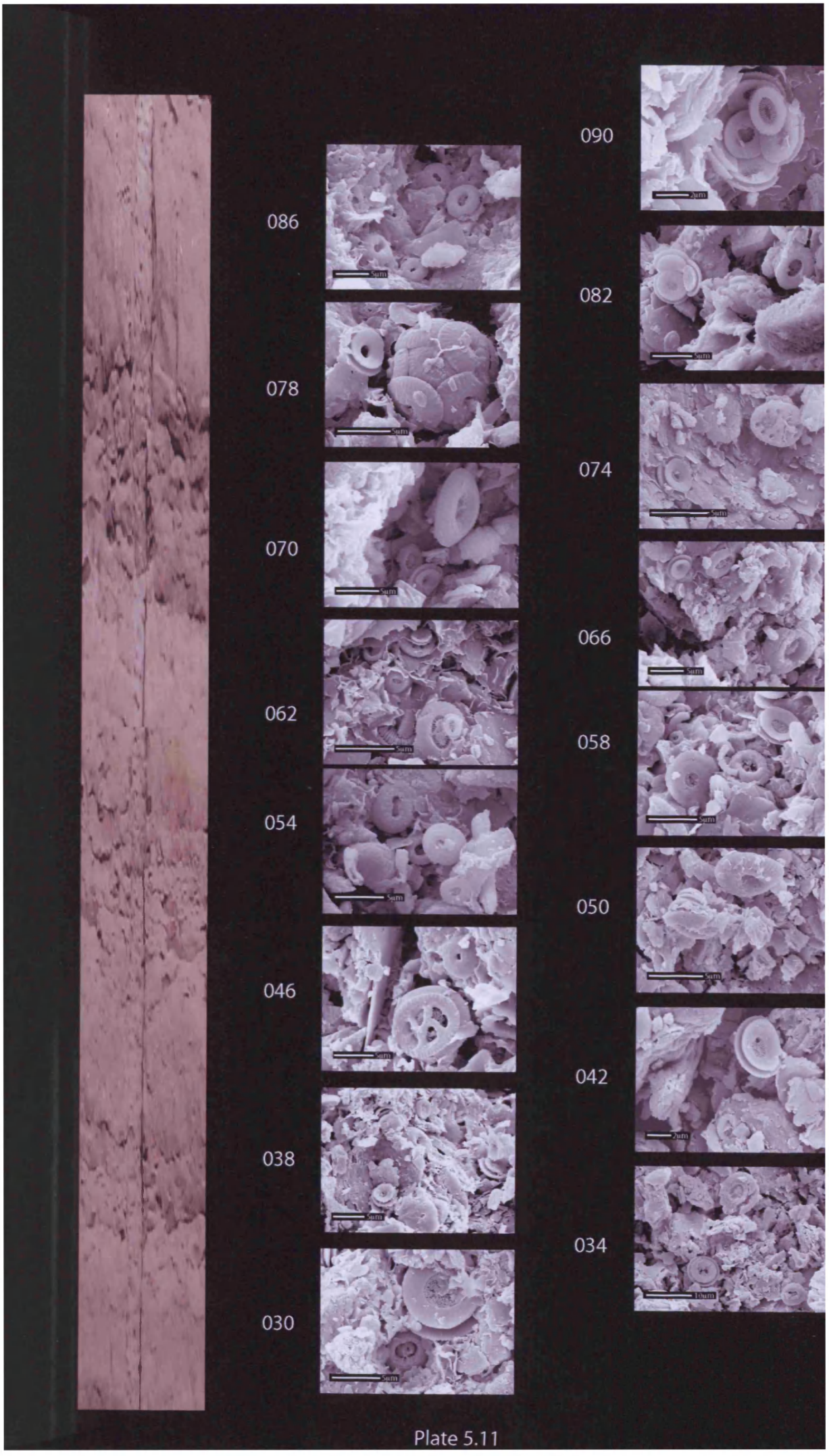

Plate 5.11

5.5. Summary

The Hampden Formation contains excellently well-preserved calcareous micro- and nannofossils suitable for palaeoenvironmental analysis using both geochemical techniques and faunal and floral assemblage data. Imaging techniques illustrate exceptional textural preservation, which is rarely observed in samples of this age and nowhere else in the Eocene "Southern Ocean" region to date. RLM observations and photographs of numerous specimens show them to be transparent and 'glassy'. Very high-resolution SEM images confirm that this 'glassy' appearance results from excellent sub-micron scale preservation. This good textural preservation indicates that the calcite composing the tests is original and has not been neomorphised, dissolved or overgrown with diagenetic calcite. Isotopic analysis further demonstrates that foraminiferal tests of different species retain an original isotopic signature, characteristic of the temperature and isotopic composition of the water in which they formed. The preservation is consistent throughout the section and also through the metre-scale lithologic cycles that characterise the formation.

6. Long-Term Cooling and an Abrupt Warm Event in the Hampden Beach Section

6.1. Introduction

This chapter aims to develop a ~3 million year record of middle Eocene climate and ocean ecology from the Hampden Section with particular focus on long term trends and transient events. Specifically, the study aims to identify whether the Middle Eocene Climatic Optimum (MECO, Bohaty and Zachos, 2003) is recorded at this site and if so, to understand its nature and the mechanisms by which it is expressed.

The middle Eocene palaeoclimate of the Southern Ocean is currently known primarily from Ocean Drilling Program (ODP) sites at Maud Rise (689 and 690) and Kerguelen Plateau (738, 744 and 748). These areas both sample open ocean waters; Sites 689, 744 and 748 are positioned at palaeodepths between ~1500 and 1800 m and Sites 690 and 738 are slightly deeper at ~2000 to 2500 m. These sites have been used by Bohaty and Zachos (2003) to generate a compilation palaeoclimate record that shows the general trend of middle Eocene Southern Ocean climate and identifies a transient warm event, termed by them the 'Middle Eocene Climatic Optimum' (MECO). This record shows a trend of ocean cooling from the Early Eocene Climatic Optimum to the onset of major Antarctic glaciation near the Eocene-Oligocene boundary. Within this cooling trend the MECO is a transient warm interval with a duration of ~600 ka representing a warming of ~4 °C in both surface and deep water (Bohaty and Zachos, 2003).

Hampden Beach allows detailed study of a shallower site with excellent microfossil preservation. This provides the opportunity to study the geochemistry of well preserved foraminiferal calcite along with the foraminiferal assemblage change, to obtain an ocean palaeoclimate signal and also to use the terrestrial sediment input to this shelf edge site to infer information about the terrestrial climatic conditions. The Hampden Formation has long been known to contain occurrences of the warm-water planktonic foraminifera genus *Hantkenina* (Finlay, 1939b). The same species as originally described from Hampden (*H. australis*) is also known to occur briefly in the northern high latitudes at ODP Site 647 and occurs across the northern Pacific (V. Beniamovski quoted in Coxall and Pearson, 2006). Hence the hypothesis is proposed that the *Hantkenina* incursion might correspond to the MECO and provide a useful global marker for this event.

The record through the Hampden Section was generated using the "long section" samples collected at Hampden Beach (Section 3.2.1). These span the period from approximately 42 to 39 Ma according to the age model developed in Section 3.3.5, which is within the upper part of the middle Eocene. The sampling technique means that that samples are not evenly spaced but coverage through the section is generally good (Figure 6.1).

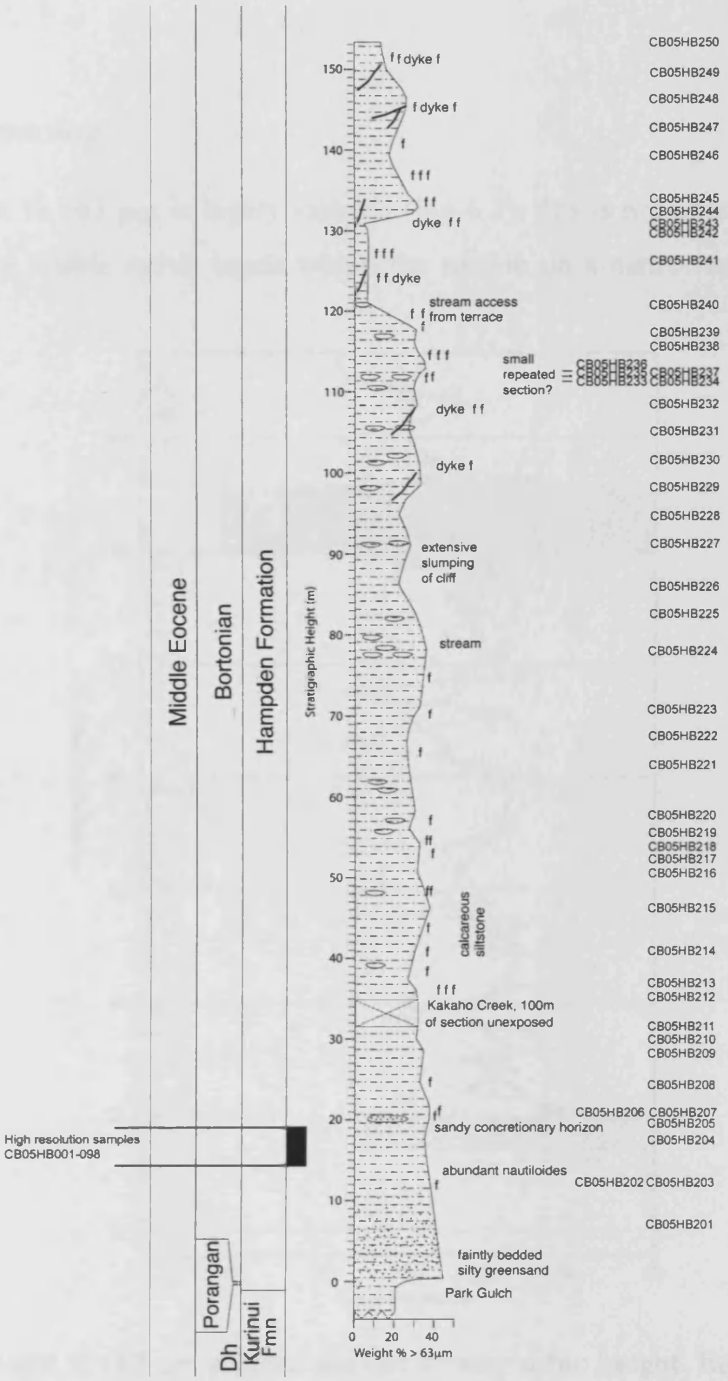

Figure 6.1. Stratigraphic log of the Hampden Section showing "long section" samples and the "high-resolution" sampling interval.

The samples were analysed using a range of techniques (outlined in Chapter 2) to study the sedimentology, ecology and geochemistry of the section. The results of these analyses are described below and used to develop an understanding of the palaeoclimate and palaeoenvironment at Hampden Beach and its development through the middle Eocene.

6.2. Results

6.2.1. Sedimentology

The weight % >63 μm is highly variable (Fig 6.2), this is not unexpected because there are clearly visible cyclic bands within the section on a metre scale (explored in Chapter 7).

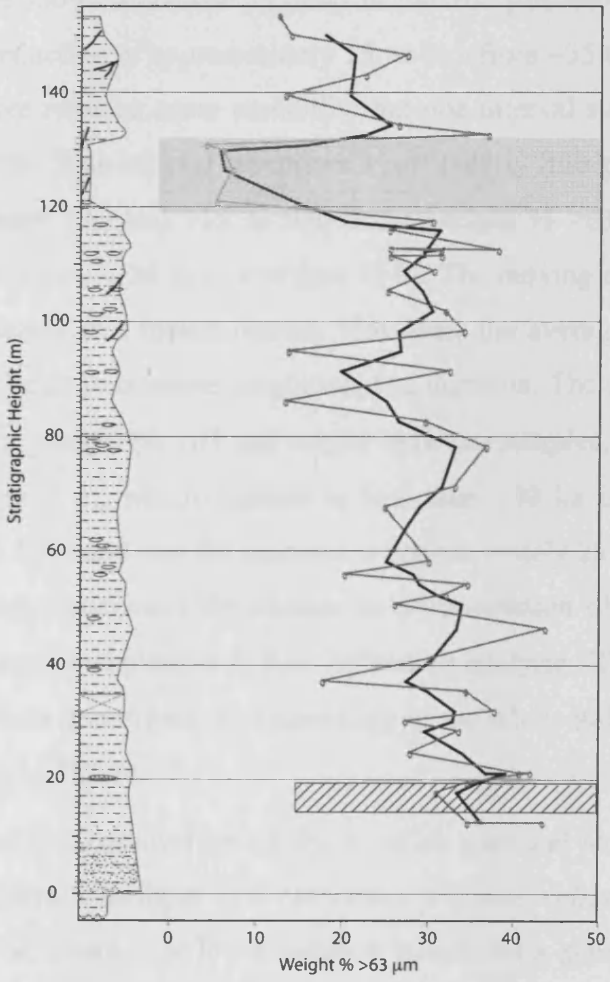

Figure 6.2. Weight % >63 μm plotted against stratigraphic height, heavy black line is a 3 point moving average. Hatched area shows the extent of "high-resolution" variability (discussed in Chapter 7). Grey shading shows the fine interval discussed below. The stratigraphic column is shown for reference.

The metre scale bands vary in their grain size composition (Section 7.2.1) and this high frequency signal is randomly sub-sampled by the low frequency "long section" samples. Therefore, the "long section" exhibits the whole of the variability seen through the metre scale bands (discussed further in Chapter 7), the range of this variability is marked on Figure 6.2. It is interesting to note that this inter-sample variability is of similar magnitude throughout the section (with the exception of the interval between approximately 110 m and 120 m), suggesting that the cycles studied at the base of the section persist, with a similar magnitude, throughout the Hampden Section. This agrees with the field observation that cycles are visible all the way along the cliff section until the cliff becomes too low to see them.

A three point moving average is placed through the record shown in Figure 6.2 to allow the identification of significant events and trends within the highly variable record. This average shows a decreasing trend in the >63 μm fraction upward through the section, with a reduction of approximately 15 wt % (from ~35 to 20 %). Within this general decrease there remains some variability but one interval stands out beyond this background variability. This interval comprises a particularly fine-grained series of beds between approximately 120 and 135 m where the weight % >63 μm shows a rapid decrease from approximately 30 % to less than 10 %. The moving average suggests that this fine-grained interval is a robust feature. However, the average also smoothes the feature making it difficult to estimate magnitude and duration. The raw data suggest that this rapid decrease in weight % >63 μm occurs between samples, over a stratigraphic distance of only 2 to 3 m, which equates to less than 100 ka using the age model discussed in Section 3.3.5 and that the decrease is approximately 25 %.

In order to better understand the change in sedimentation observed as changing weight % >63 μm, semi-quantitative X-Ray diffraction analysis (XRD) was carried out on every fifth sample to investigate the mineralogy of the whole sediment; the results of this are shown below in Figure 6.3.

The sediment is comprised primarily of silica (silt and sand) with significant amounts of clay minerals, feldspar and carbonate, a minor component of micas and occasional pyrite. The record is at low-resolution but shows a general trend of slightly decreasing clay, carbonate and mica input and increasing feldspar and quartz, upwards through the section with the ratio of feldspar to quartz varying. Since the quartz and feldspar occur primarily as sand and silt sized grains, this increase in their abundance

along with the decreasing trend in weight % >63 μm suggest that the average grain size for these quartz and feldspar grains is decreasing.

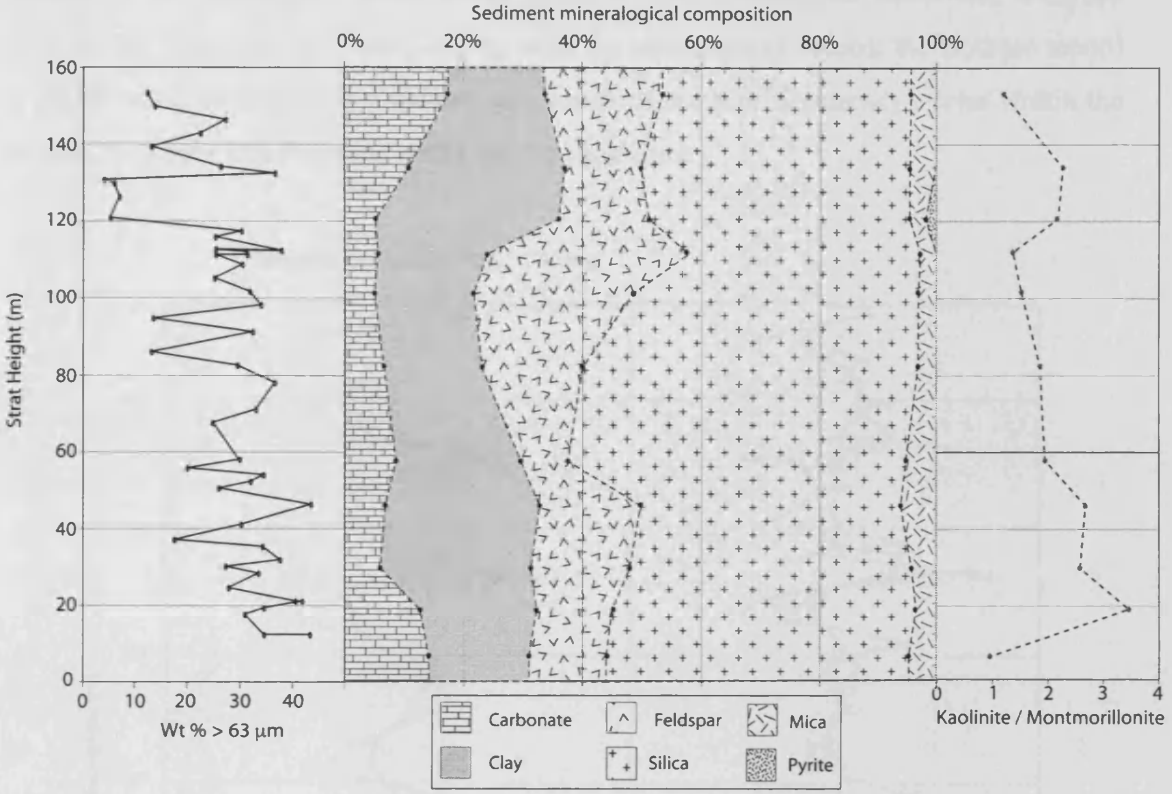

Figure 6.3. Left panel, weight % >63 μm; Centre panel, sediment composition by mineralogical group from semi-quantitative XRD; Right panel, ratio of kaolinite to montmorillonite.

The change in sediment composition between 120 and 135 m is not very apparent, possibly because only one sample falls within this interval due to the lower sample frequency of the record. However, there is an increase in the percentage of clay minerals and to a lesser extent carbonate minerals at this level. This increase in clay is balanced by a relative decrease in feldspar with little change in the silica or micas. There is also a transient appearance of pyrite at this level, however XRD does not easily enable the quantification of minerals occurring at less than ~5% abundance so although pyrite is only recorded in this one sample, it is also observed to occur in the washed residues throughout the section. Knowing that pyrite is indeed present throughout the section, the pyrite is still at sufficiently low percentage abundance that caution should be exercised in drawing conclusions from its presence.

6.2.2. Geochemistry

The oxygen and carbon isotopic composition of calcite of 6 to 8 specimens per sample of the planktonic foraminifera species *Globigerinatheka index* was analysed from all the "long section" samples. As with the sedimentary record, the isotopic record is highly variable (Figure 6.4 below) as a result of the high frequency cycles within the section, however trends and features can be identified.

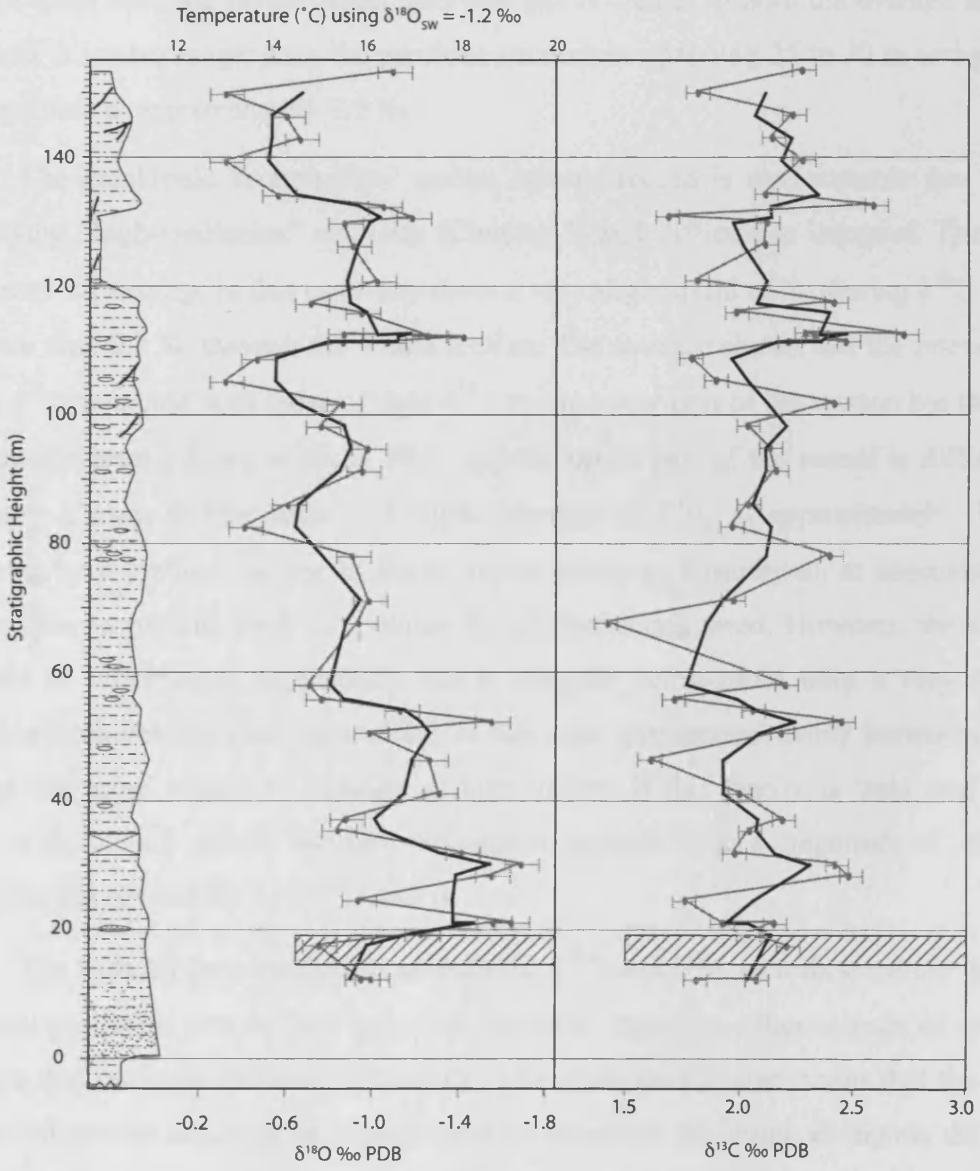

Figure 6.4. $\delta^{18}O$ (left) and $\delta^{13}C$ (right) isotopic composition of calcite from *Globigerinatheka index* measured relative to PDB, is plotted against stratigraphic height. Heavy black line is a three point moving average. Error bars show the analytical error from the mass spectrometer. The stratigraphic column is shown for reference.

The three point moving average through the oxygen isotope record shows a trend upwards through the section of increasingly heavy $\delta^{18}O$ values, from approximately -1.5 ‰ at the base of the section to -0.5 ‰ at the top, a total increase of ~1 ‰. Within this trend there is still significant variability, in the form of cycles in $\delta^{18}O$ with a magnitude of between 0.2 and 0.4 ‰ and wavelength of approximately 20 m (discussed in Section 3.3.4 and 6.2.4). There is then a particular light $\delta^{18}O$ excursion between 110 and 130 m, broadly coincident with fine layer observed in the sedimentary record. This has a much sharper onset than the earlier warm intervals and is clearer in both the average and the raw data, it is also longer than the previous excursions spanning 25 to 30 m and greater in magnitude at approximately 0.5 ‰.

The planktonic foraminiferal carbon isotope record is also variable due to the underlying "high-resolution" cyclicity (Chapter 7) and difficult to interpret. The three point moving average in this case may show a very slight trend of increasing $\delta^{13}C$ but of no more than 0.2 ‰ through the whole section. The average shows that the intervals of heavy $\delta^{18}O$ coincide with those of light $\delta^{13}C$ in the lower part of the section but that this relationship breaks down at about 70 m and the upper part of the record is difficult to interpret. It may be that there is a subtle increase in $\delta^{13}C$ at approximately 110 m, followed by a gradual decline to lower values reaching a minimum at approximately 125 m then recovering back to continue the gradual rising trend. However, the sudden increase at 110 m may be partially due to samples being taken from a very similar stratigraphic level (because the bedding in this area was approximately horizontal) and thus giving more weight to a cluster of high values. If this feature is 'real' and not a result of the closely spaced samples, the positive excursion has a magnitude of ~0.2 ‰ and spans approximately 110 m to 140 m.

The features described above in both the $\delta^{18}O$ and $\delta^{13}C$ records stand out beyond the analytical error plotted on Figure 6.4, however, there are other sources of error in the data that are more difficult to quantify. The small sample size means that the intra-sample variability resulting from individual foraminifera calcifying at slightly different depths or times may be a significant source of error. Diagensis or infilling of foraminifera can also affect isotopic composition, the foraminiferal preservation at Hampden Beach is generally excellent (Chapter 5) and any specimens not translucent under RLM were not selected for analysis, reducing this source of error. It is considered that despite these possible sources of error, the trends and excursions described are robust.

6.2.3. Ecology

Full counts were carried out of the planktonic foraminifera in the 212 – 250 μm size fraction of 500 g sediment samples (see table 3.2) to determine the abundance (foraminifera per gram) and the species composition of the assemblage (Figure 6.5).

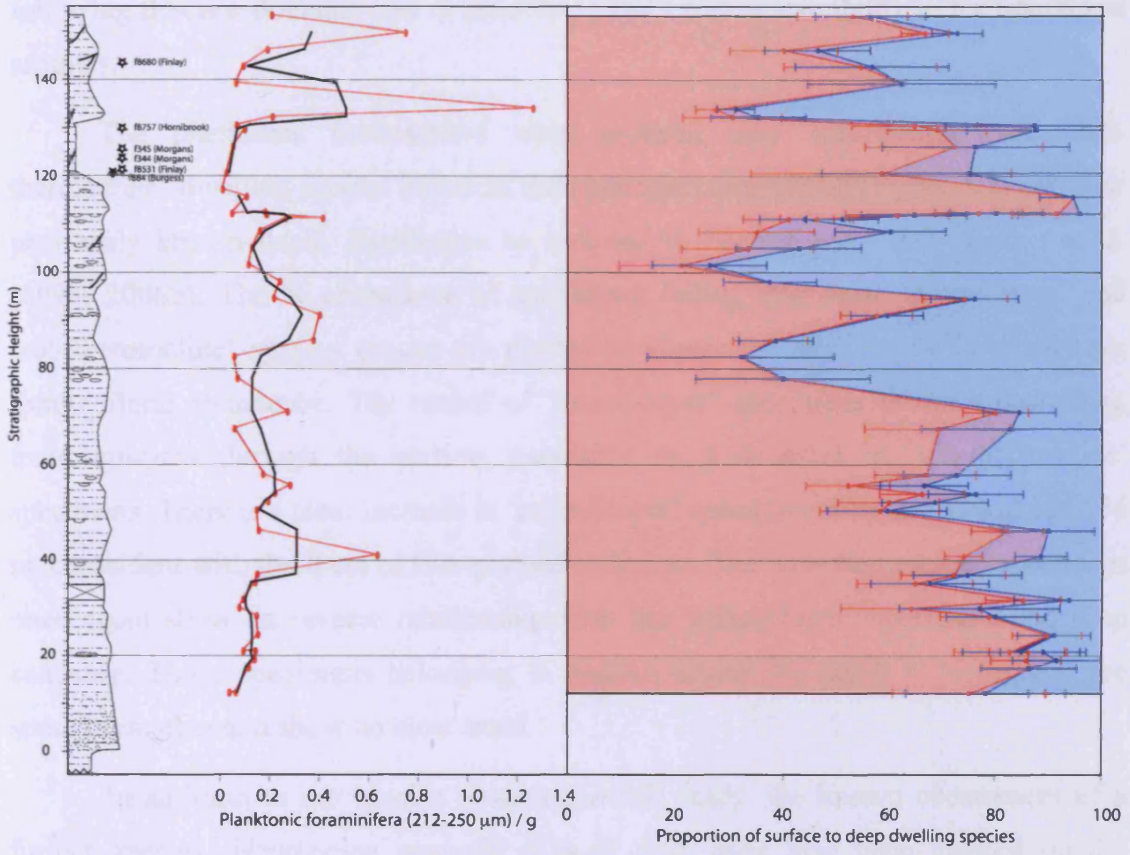

Figure 6.5. Left, planktonic foraminiferal abundance in the 212 - 250 μm fraction, red line shows raw data, thick black line is a 3 point moving average; right, % abundance of planktonic foraminifera species associated with different depth habitats, red - 'mixed-layer' (*Globigerinatheka index*, *Globoturborotalita martini*, *G. bassriverensis*, *G. ouachitaensis*, *Guembelitriodes nuttalli*, *Acarinina praetopilensis*, *A. primitiva*, *A. mcgowrani*, *A. bullbrooki*); purple - 'unknown depth' (*Turborotalia frontosa*, *T. pomeroli*); blue - 'sub-thermocline' species (*Catpsydrax unicavus*, *Subbotina angiporoides*, *S. linaperta*, *S. senni*, *S. cf utilisindex*). Error bars show 95% confidence intervals for the % abundances as the sample size varies. A stratigraphic column is shown for reference and stars mark the positions at which samples containing *Hantkenina* have been collected in this study (filled) and previously (hollow).

The planktonic foraminiferal abundance varies dramatically from less than 0.05 foraminifera per gram to more than 1.2 foraminifera per gram. The 3 point average shows no real change through the lower part of the section, with significant variability in the raw data. Between approximately 110 m and 130 m there is a slight fall in abundance coincident with the planktonic foraminiferal oxygen isotope excursion, following this is a dramatic rise in abundance and extreme variability in the uppermost samples.

The planktonic foraminifera were grouped into 'mixed-layer' and 'sub-thermocline' dwelling species based on their isotopic composition (Figure 5.1) and their previously known depth distribution as outlined in Section 4.2.4 and Pearson et al. (1993; 2006b). The % abundance of specimens falling into these 'mixed-layer' and 'sub-thermocline' species groups are plotted in Figure 6.5 adjacent to the planktonic foraminiferal abundance. The record of 'mixed-layer' specimens shows a decreasing trend upwards through the section, paralleled by a decrease in 'sub-thermocline' specimens. There is a clear increase in 'mixed-layer' specimens between 120 m and 135 m, coincident with the level of fine-grained sediment. The 'sub-thermocline' specimens once again show an inverse relationship with the 'mixed-layer' specimens and drop suddenly. Those specimens belonging to species where the depth is 'unknown' are small in number and show no clear trend.

In addition to the species observed in this study, the known occurrences of a further species, *Hantkenina australis* (Figure 6.6), have also been marked on the stratigraphic column (hollow stars) placed according to work by Finlay (1939) and Morgans (2008).

Figure 6.6. *Hantkenina australis* from CB05HB240. Scale bar 100 μm; poorly preserved specimen with characteristic spines broken off

Hantkenina australis was first described from Hampden Beach (Finlay, 1939b) and rare occurrences have been recorded by a number of authors (summarised by Morgans, 2008). This species is of particular note as the genus *Hantkenina* has a primarily tropical distribution (Coxall and Pearson, 2006) and as noted here, a restricted occurrence in the Hampden Section, occurring almost exclusively within the fine sediment layer. A single poorly preserved specimen of *Hantkenina australis* (Figure 6.6) was observed in this study within the 150 – 212 μm fraction of sample CB05HB240 (the lowest sample in the fine sediment layer) the position of which is marked by a solid star.

6.2.4. Comparison

Figure 6.7 below, shows the records discussed above compared side by side, the transient event seen in the weight % >63 μm and foraminiferal carbonate $\delta^{18}O$ record is highlighted in grey and the possible cyclic variation in $\delta^{18}O$ is marked by stippled bands. These records clearly show a trend through the section of decreasing weight % > 63 μm and 'mixed-layer' species foraminifera, and a co-incident increase in planktonic foraminiferal carbonate $\delta^{18}O$ and possibly $\delta^{13}C$.

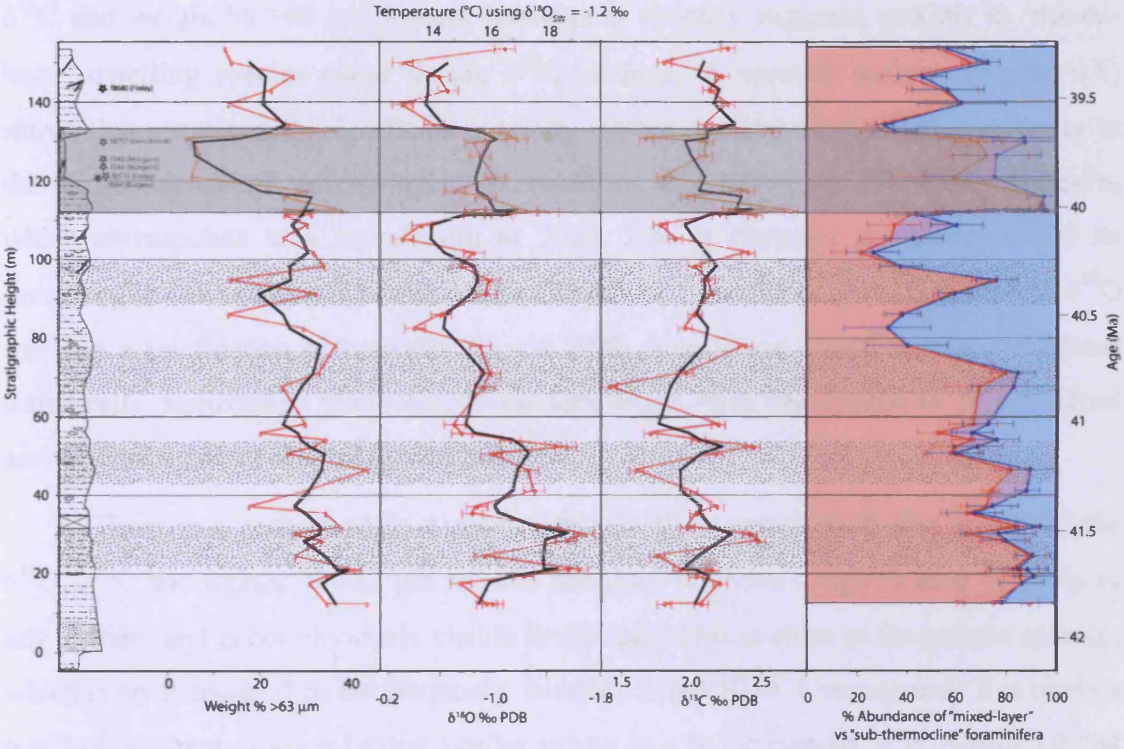

Figure 6.7 A comparison of the palaeoclimate proxy records from Hampden Beach plotted against stratigraphic height. From left to right; stratigraphic column; positions of samples containing *Hantkenina australis*; weight % >63 μm; planktonic foraminiferal $\delta^{18}O$; planktonic foraminiferal $\delta^{13}C$; % abundance of 'mixed-layer' (red), 'unknown depth' (purple) and 'sub-thermocline' (blue) dwelling planktonic foraminifera. The grey band highlights the stratigraphic level at which the excursion in $\delta^{18}O$ occurs. The stippled bands highlight the cyclicity in $\delta^{18}O$ and 'mixed-layer' species % abundance.

A solid grey band is used to highlight the excursion towards light $\delta^{18}O$ that occurs between 110 and 135 m. This shows that the excursion in $\delta^{18}O$ begins approximately 10 m below the fine layer and ends simultaneously with the rise in weight % >63 μm. The record also shows that there is a peak in the % abundance of 'mixed-layer' dwelling foraminiferal species co-incident with the fine sediment layer and that 5 of the 6 recorded occurrences of *Hantkenina australis* occur within this layer.

The possible cyclic variation in $\delta^{18}O$ noted in Section 6.2.2 is highlighted by stippled bands. This indicates visually that there is no coincident cyclic variation in the $\delta^{13}C$ and weight % >63 μm record, however it strongly suggests maxima in 'mixed-layer' dwelling species occur during $\delta^{18}O$ minima. A spectral analysis (Figure 6.8) shows that a statistically significant cyclicity, with a confidence of >99% does occur in the % abundance of 'mixed-layer' foraminifera at a frequency of ~0.045 cycles/m, which corresponds to a wavelength of 22m. This is assumed to equate to 405 ka according to the age model developed in Chapter 3. There is a co-incident peak in $\delta^{18}O$ that has a confidence of between 90 and 95‰, this alone would not be considered statistically significant, however it's co-occurrence with the cycles in foraminiferal assemblage suggests that it is a real feature.

There is a second peak at approximately 10 m wavelength that occurs in the $\delta^{18}O$, $\delta^{13}C$ and weight % >63 μm records that does not have a significance of >95% in any of them and is not obviously visible in the data. This is close to the sample spacing, which is on average ~3 m but frequently between 5 and 10 m. Consequently it is likely a result of adjacent samples having similar values in a few instances. It is considered that only the 22 m cycles in the $\delta^{18}O$ and % abundance of 'mixed-layer' species can be confidently identified in this record.

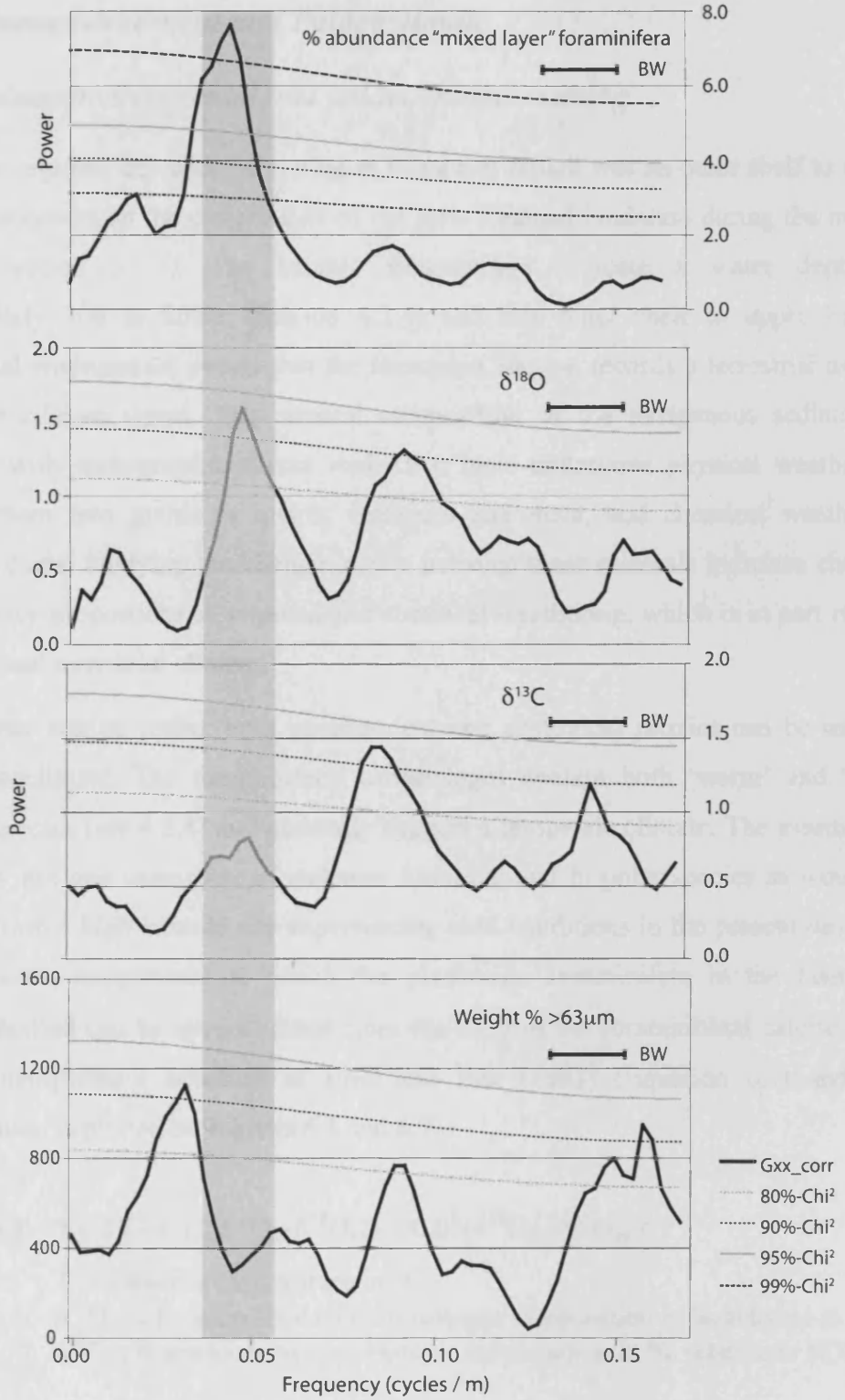

Figure 6.8. Spectral analysis of the % abundance 'mixed-layer' dwelling foraminifera, planktonic foraminiferal $\delta^{18}O$, planktonic foraminiferal $\delta^{13}C$ and weight % >63 μm records plotted with confidence intervals against a red noise background generated using REDFIT (Schulz and Mudelsee, 2002). BW indicates the 6-dB bandwidth A grey band highlights the dominant frequency, which equates to a wavelength of ~22 m

6.3. Palaeoenvironment and Palaeoclimate

6.3.1. Palaeoenvironmental and palaeoclimatic setting

The regional depositional setting at Hampden Beach was an outer shelf to upper slope environment on the eastern side of the New Zealand landmass during the middle Eocene (Section 3.1.3). The benthic foraminifera indicate a water depth of approximately 300 to 500m (Section 4.2.4) and this outer shelf to upper bathyal depositional environment means that the Hampden Section records a terrestrial as well as oceanic climate signal. The mineral composition of the terrigenous sediment is consistent with metamorphic source rocks that have undergone physical weathering, breaking them into grains of quartz, feldspars and mica, and chemical weathering producing clays. Studying the changing ratio between these minerals indicates changes in the relative proportions of physical and chemical weathering, which is in part related to the regional terrestrial climate.

In the marine realm, both geochemical and ecological proxies can be used to infer palaeoclimate. The foraminiferal assemblages contain both 'warm' and 'cold' indicator species (see 4.2.4) and generally suggest a temperate climate. The assemblage is certainly not one consisting of endemic Antarctic and bi-polar species as would be expected from a high latitude site experiencing cold conditions in the present day. The absolute water temperature at which the planktonic foraminifera in the Hampden Section calcified can be approximated from the $\delta^{18}O$ of the foraminiferal calcite using the palaeotemperature equation of Erez and Luz (1983) (Equation 6.1) and this approximation is plotted on Figures 6.4 and 6.7.

Equation 6.1 $$T = 17 - 4.52(\delta^{18}O_C - \delta^{18}O_{sw}) + 0.03(\delta^{18}O_C - \delta^{18}O_{sw})^2$$

T is seawater temperature in °C
$\delta^{18}O_C$ is foraminiferal oxygen isotopic composition in ‰ relative to PDB
$\delta^{18}O_{sw}$ is seawater oxygen isotopic composition in ‰ relative to PDB

Work discussed in Chapter 7 suggests there was little or no ice present towards the base of the section where the "high-resolution" samples were collected and that a $\delta^{18}O_{sw}$ value of -1.2 ‰ is appropriate (Chapter 7). This produces seawater temperature values from the "long section" samples in the lower part of the section of between 15 and 20 °C with a mean of approximately 18 °C. Towards the top of the section there is no independent proxy for seawater temperature and it has been suggested by some

authors that ice may have begun to develop at around 40 Ma e.g. Billups & Schrag (2003). This means it is not possible to accurately constrain the $\delta^{18}O_{sw}$ although the magnitude of the variability in $\delta^{18}O$ of foraminiferal carbonate remains similar to that at the bottom of the section, suggesting that the cyclicity has not obviously begun to be amplified by the waxing and waning of ice sheets. Using $\delta^{18}O_{sw}$ = -1.2 ‰ in the upper part of the section produces seawater temperatures of 13 - 17 °C with an average of approximately 15 °C. This places a constraint on the minimum seawater temperature at Hampden Beach at approximately 39Ma, if some ice had developed by this time, increasing the $\delta^{18}O_{sw}$, this would mean the seawater temperatures were slightly higher.

The minimum seawater temperature calculated from the Hampden Section is significantly warmer than the present day coastal sea surface temperature which varies seasonally between ~8 and 13 °C with an annual mean of just above 10 °C (Locarnini et al., 2006). This is despite the fact that during the middle Eocene, New Zealand lay approximately 10° south of its present position. Hence the climate appears to have been much warmer than modern, consistent with evidence from the middle Eocene around the world (e.g. Zachos et al., 2001).

The temperatures calculated at Hampden Beach are also warmer than those previously calculated for similar latitudes during the Eocene from ODP drilling sites. There are few records from the New Zealand region that have been analysed for the $\delta^{18}O$ of planktonic foraminiferal carbonate. However, a study carried out by Zachos et al. (1994) using planktonic foraminifera from a number of Deep Sea Drilling Program (DSDP) sites across a range of latitudes suggests water temperatures of between 5 and 15 °C through the middle Eocene at the palaeolatitude of New Zealand. Zachos (1994) incorporates earlier work by Kennett and Stott (1975) that calculates temperatures of approximately 13°C through the middle Eocene from DSDP site 277, 5 to 10° south of New Zealand. More recently, work by Bohaty and Zachos (2003) using fine fraction carbonate from ODP sites at Kerguelen Plateau and Maud Rise, which are also slightly further south, gives temperatures of 8 to 13 °C through the same period. However, none of these previous estimates were based on demonstrably 'glassy' or non-recrystallized foraminiferal carbonate. It is therefore considered that lower planktonic foraminiferal $\delta^{18}O$ temperatures recorded for this latitude from DSDP and ODP sites are likely to be a result of the addition of diagenetic carbonate to foraminifera at the seafloor and during shallow burial in slowly deposited carbonate oozes (Pearson et al., 2001; Pearson and Burgess, 2008).

During the middle Eocene, New Zealand was located at approximately 55° south in a region where the ocean circulation is still not well constrained. A study by Nelson and Cooke (2001) produced palaeoceanographic maps of the southern Pacific region using DSDP based studies of sediment facies, microfossil assemblages and diversity, and stable isotope records, as well as from evidence in onland New Zealand Cenozoic sequences. This indicates that New Zealand lay in the path of a current that flowed southwards past New Zealand and turned eastwards. However, a recent ocean circulation model suggests that New Zealand lay in the path of an Antarctic gyre, which is supported by biogeographic records from ODP leg 189 (Huber et al., 2004). These contrasting reconstructions were discussed briefly in Section 1.7 and are illustrated below in Figure 6.9.

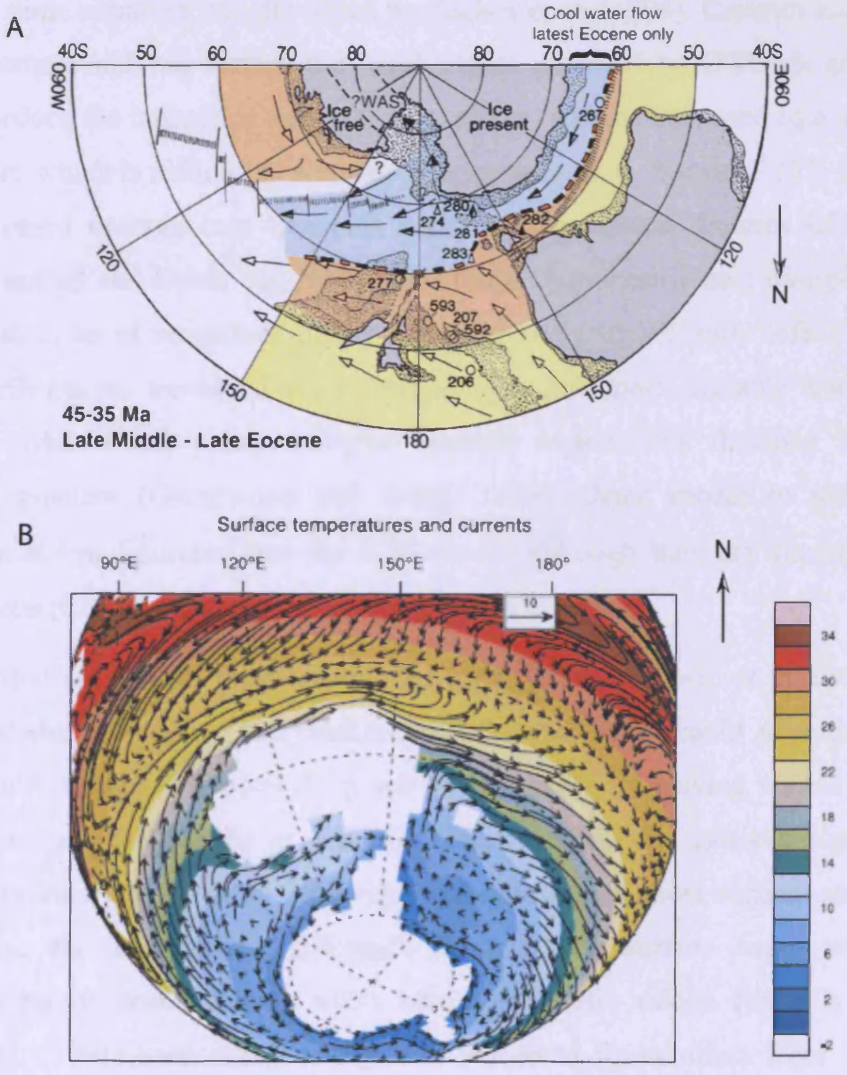

Figure 6.9 A. Palaeoceanographic reconstruction of the New Zealand sector of the "Southern Ocean" during the middle Eocene taken from Nelson & Cooke, 2001; B. Modelled middle Eocene ocean circulation taken from Huber et al., 2004.

The surface water temperatures recorded by planktonic foraminiferal $\delta^{18}O$ at Hampden Beach are more consistent with a warm southward flowing current passing New Zealand during the middle Eocene (although they are even warmer than the temperatures suggested by Nelson and Cooke, 2001) than an Antarctic gyre. However, Eocene General Circulation Models (GCMs) assessing the effect of elevated atmospheric pCO_2 find it difficult to reach such warm temperatures at high latitudes without unrealistically high temperatures in the tropics (Sloan and Rea, 1995: Huber pers. comm., 2008; Huber and Sloan, 2001). The phenomenon of polar temperatures much higher than today during the greenhouse world of the Cretaceous and early to middle Eocene without equally elevated tropical temperatures, leading to a much reduced latitudinal temperature gradient, was first observed by Shackleton and Boersma (1981). The same situation was described by Zachos et al. (1994), Crowley and Zachos (2000) and others and was termed the 'cool tropics paradox' by D'Hondt and Arthur (1996). To reduce the latitudinal temperature gradient requires increased equator to pole heat transport, which is difficult to simulate in climate models. Barron (1987) found that forcing increased oceanic heat transport could replicate some features of Antarctic warmth but not all and Huber and Nof (2006) found that oceanic heat transport would need to be an order of magnitude higher than present to significantly affect Antarctic climate. Furthermore, terrestrial fossil assemblages are more variable than marine records and while some palaeontological records support this flattened latitudinal temperature gradient (Greenwood and Wing, 1995) others appear to give higher temperatures at low latitudes than the $\delta^{18}O$ record although they are similar in high latitude regions (Crowley and North, 1991; Frakes et al., 1992)

A partial solution to this paradox was proposed by Pearson et al. (2001) who demonstrated that microscale recrystallization of foraminifera could alter the test to 50% diagenetic calcite in typical deep sea samples without leaving classic signs of alteration such as overgrowths or infilling. This can shift the isotopic signature of affected foraminifera towards cooler temperatures and is of most consequence in the tropics where the temperature difference between the surface water where the foraminifera calcify and the deep water where diagenetic calcite forms is greatest. Pearson et al. (2001) used exceptionally well-preserved foraminifera from Tanzania, Mexico and the Adriatic to derive much warmer Late Cretaceous and Eocene tropical temperatures than had previously been estimated. This reduced the problem of generating the flattened oceanic latitudinal temperature gradient by increasing low latitude temperatures. Earlier work by Norris and Wilson (1998) and Wilson and Norris

(2001) also showed that exceptionally well-preserved foraminifera from the tropical Cretaceous recorded warmer than present day sea surface temperatures (SSTs). However, these authors did not record significantly warmer temperatures than some diagentically suspect deep sea material (Norris and Wilson, 1998) suggesting that diagenesis does not provide a complete solution to the 'cool tropics paradox'.

The temperatures calculated here from exceptionally well-preserved foraminifera at Hampden Beach suggest that middle Eocene SSTs at high southern latitudes were also somewhat higher than have previously been calculated. This is probably because during this period SSTs were sufficiently warm that there was a large difference between surface and deep water temperatures, so alteration of foraminifera to diagenetic calcite occurring at depth has an impact on the calculated temperature, as in the tropics. Recent work from the ACEX coring expedition has used the organic carbon TEX_{86} SST proxy as an alternative to $\delta^{18}O$ and also indicates relatively warm temperatures of ~5 to 8 °C in the middle Eocene of the northern high latitude Arctic Ocean (Brinkhuis et al., 2006; Sangiorgi et al., 2008a).

The Hampden samples however, are ~5 °C warmer than those previously calculated for the middle Eocene at this latitude, whilst the tropical temperatures are ~10 °C warmer (Figure 6.10). This means that although these results return us to a situation with a somewhat reduced latitudinal temperature gradient during the middle Eocene, it is not as dramatic as originally proposed (e.g. Shackleton and Boersma, 1981). A number of possible mechanisms for decreasing the remaining data model mismatch are under investigation. These include increased polar stratospheric cloud cover, which produces increased warming at high latitudes (Sloan and Pollard, 1998), the impact of enhanced tropical storms in increasing the equator to pole heat transport (Huber 2006, pers. comm.) and biological cloud feedbacks (Kump and Pollard, 2008).

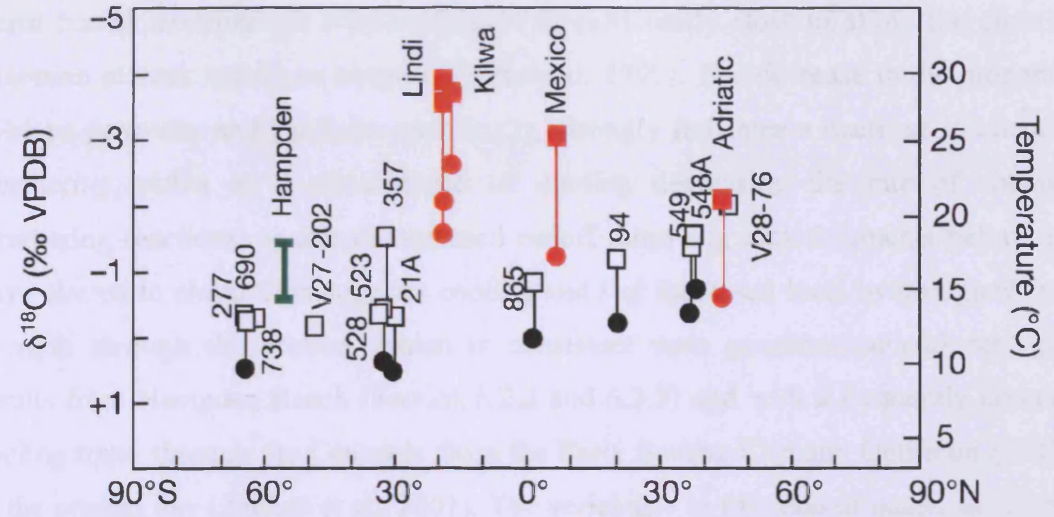

Figure 6.10. Middle Eocene (planktonic foraminfera zones P11-P14) zonal profile of planktonic foraminifera $\delta^{18}O$ as a function of palaeolatitude (adapted from Pearson et al. 2001). Squares, 'mixed-layer' dwelling species; circles, deeper dwelling species; red, well preserved material analysed by Pearson et al. (2001); green, 'mixed-layer' dwelling species from in this study (lines show the average values at the base and top of the Hampden Section). Temperature scale is amended to show the calibration of Erez & Luz (1983) with $\delta^{18}O_{sw}$ = -1.2 ‰ as used in this study.

6.3.2. Palaeoclimatic trends

The trend of decreasing weight % >63 μm (Figure 6.2) is due to a greater proportion of the quartz and feldspar grains being <63μm in size rather than a decrease in the abundance of these minerals (Figure 6.3). This is likely the result of the continual thermal subsidence of the sedimentary basin (outlined in Chapter 3) causing an isostatic sea level increase and marine transgression (King et al., 1999) even at a time of global cooling (Zachos et al., 2001) and reported eusatic sea level fall (Kominz et al., 1998). If this is the case, the depositional site became more distal from the sediment source decreasing the proportion of grains >63 μm reaching the site.

The gradual decrease in clay input relative to quartz and feldspar (Figure 6.3) is probably due to decreased weathering of the sub-aerially exposed source rocks. Further analysis of the clay minerals indicates that there is a gradual decrease in the ratio of kaolinite to montmorillonite upwards through the section (Figure 6.3). Kaolinite is a clay derived from chemical weathering of silicate minerals, particularly feldspars, in a

warm humid environment where transport is sufficiently slow to allow the chemical alteration of rock before its removal (Birkeland, 1999). The decrease in the proportion of clays generally and kaolinite specifically, strongly indicates a decrease in chemical weathering, either as a direct result of cooling decreasing the rate of chemical weathering reactions, or due to increased runoff removing rock fragments before they were altered to clays. This suggests cooling and / or increased local hydrological cycle strength through the section, which is consistent with geochemical and ecological results from Hampden Beach (Section 6.2.2 and 6.2.3) and with a frequently observed cooling trend through the Cenozoic from the Early Eocene Climatic Optimum (EECO) to the present day (Zachos et al., 2001). The variability in the ratio of quartz to feldspar in the samples is likely to result primarily from changes in the mineralogy of the source rocks.

The planktonic foraminiferal carbonate $\delta^{18}O$ record shows a trend of becoming heavier upwards through the section with the average shifting from approximately -1.5 ‰ to -0.5 ‰ (Figure 6.4). This increase may result from a trend of decreasing temperature and / or increasing ice volume. The trend of declining abundance of 'mixed-layer' foraminiferal species upwards through the section (Figure 6.5) suggests that either the depth or the seasonal duration of the thermocline above which they are thought to live (Pearson et al., 1993) was decreasing, which is suggestive of a cooling trend rather than the formation of an ice sheet. However, the ecological change cannot be used to estimate the magnitude of the temperature decrease and thus whether the whole of the $\delta^{18}O$ increase can be attributed to the cooling. Furthermore, during the Eocene warmer temperatures than present mean that the hydrological cycle was likely to have been enhanced, leading to reduced fractionation during transport of water from low to high latitudes and consequently a heavier $\delta^{18}O$ isotopic composition of ice. This would result in the build up of ice having a smaller impact in the $\delta^{18}O$ of seawater and therefore being more difficult the detect. A trend of decreasing temperature from the Early Eocene Climatic Optimum to the present day has been observed globally in both single core records (e.g. Kennett et al., 1975; Sexton et al., 2006a) and multisite compilation records (Zachos et al., 2001; Bohaty and Zachos, 2003). If the whole of the $\delta^{18}O$ shift observed between the base and the top of the Hampden Section (~1 ‰) is a result of changing temperature it equates to ~4 °C. However, if some proportion of the $\delta^{18}O$ change results from ice sheet development, the temperature shift is reduced. A number of authors have suggested the development of transient ice sheets during the

later part of the middle Eocene and Late Eocene based on isotopic (e.g. Tripati et al., 2005) and sedimentological (Ehrmann and Mackensen, 1992; Browning et al., 1996) data. Models also indicate that transient ice sheets may have begun to develop under middle to late Eocene conditions (e.g. Crowley, 1998; DeConto and Pollard, 2003) so they can not be ruled out without the use of an independent temperature proxy. However, the magnitude of the high frequency variability in the samples remains approximately constant between the base of the section where it is inferred that little to no ice is present (see Chapter 7) and the top of the section. This means it is unlikely that the high frequency cycles are being substantially amplified at the top of the section by the waxing and waning of ice sheets.

The $\delta^{18}O$ trend observed at Hampden is consistent with most Cenozoic records, suggesting that the underlying cause of the rise in foraminiferal carbonate $\delta^{18}O$ was a global climatic change rather than a local shift in the oceanographic regime. Recent work by Pearson et al. (2007) suggests that this trend of increasing $\delta^{18}O$ through the Eocene was less pronounced in the tropics than the high latitudes and shows stable low latitude temperatures from well preserved planktonic foraminifera and TEX_{86} analyses throughout the Eocene. These authors suggest that the observed trend in the planktonic foraminifera of low latitude deep sea sites results from increased diagenetic overprint by increasingly cold, corrosive bottom water. Their work also indicates that since there was no large change in $\delta^{18}O$, there was no substantial development of permanent ice sheets through this period, although transient glacials cannot be ruled out. The $\delta^{18}O$ and 'mixed-layer' foraminiferal species abundance trends seen at Hampden Beach provides good evidence from well-preserved foraminifera that high latitude surface waters did experience a real cooling through the Eocene in contrast to the tropics.

6.3.3. Climate cyclicity

The cycles observed in the % abundance of 'mixed-layer' dwelling foraminifera (Figure 6.5) and the $\delta^{18}O$ record of one of these species (*Globigerinatheka index*) (Figure 6.4) are very interesting as they likely result from orbital forcing, possibly long period eccentricity cycles with a period of 405 ka (see Section 3.3.4). Long period eccentricity cycles have been recorded from the Southern Ocean during the Eocene in benthic foraminiferal $\delta^{18}O$, $\delta^{13}C$ and abundance records from Maud Rise (ODP Site 689) (Diester-Haass and Zahn, 1996). All the main orbital frequencies are also observed

in the benthic foraminiferal $\delta^{18}O$ and $\delta^{13}C$ records from slighter younger early Eocene and Oligocene sediments in the tropical Pacific Ocean (ODP Site 1218) with power concentrated at obliquity and ~400 ka eccentricity cycles (Coxall et al., 2005; Pälike et al., 2006). Long and short period eccentricity cycles (405 ka and 100 ka) were also identified during the Paleocene and lower Eocene at Walvis ridge in the southern Atlantic Ocean (ODP Sites 1262, 1263, 1265 and 1267) in the records of colour reflectance and iron (Fe) intensity data (Kroon and Zachos, 2007). This suggests that long period orbital forcing has affected oceanic climate globally during the Paleogene.

At Hampden Beach the oxygen isotope shifts in the 'mixed-layer' dwelling planktonic foraminifera *Globigerinatheka index* suggest that the climatic change caused by the orbital forcing takes the form of either a cyclic warming and cooling of the surface ocean or fall and rise in global ice volume. The co-incident increase in the abundance of foraminifera belonging to 'mixed-layer' dwelling species relative to 'sub thermocline' species during the lighter parts of the $\delta^{18}O$ cycles, suggests that this cyclicity is likely due predominantly to temperature changes in the surface water column rather than global ice volume. The 'mixed-layer' dwellers are thought to occur primarily above a seasonal thermocline, which occurs in the modern day subtropical and temperate oceans through the warmer months when the upper ocean is heated by solar input and wind driven mixing reduces. In the modern Southern Ocean, no thermocline develops above approximately 60° south because the surface temperature is too cold and large scale upwelling mixes cold deep water to the surface (Segar, 2007).

In the middle Eocene Southern Ocean there was no deepwater flow around Antarctica and GCMs indicate that an Antarctic gyre occurred to the south of New Zealand in the surface water (Huber et al., 2004). This gyre is thought to have contained much colder water than the southward flowing current to its north (Figure 6.9 B) and therefore is considered less likely to have developed a strong thermocline. The ocean temperature and foraminiferal abundance changes through the middle Eocene seen at Hampden could thus be explained by changes in this gyre system. A gradual expansion of the gyre between 42 and 40 Ma may explain both the gradual cooling and decrease in 'mixed-layer' species by increased mixing of cooler water from the gyre into the surface waters at Hampden (Figure 6.11A) and a resulting shallowing of the thermocline. The observed cycles could then result from cyclic contractions of the gyre (Figure 6.11B).

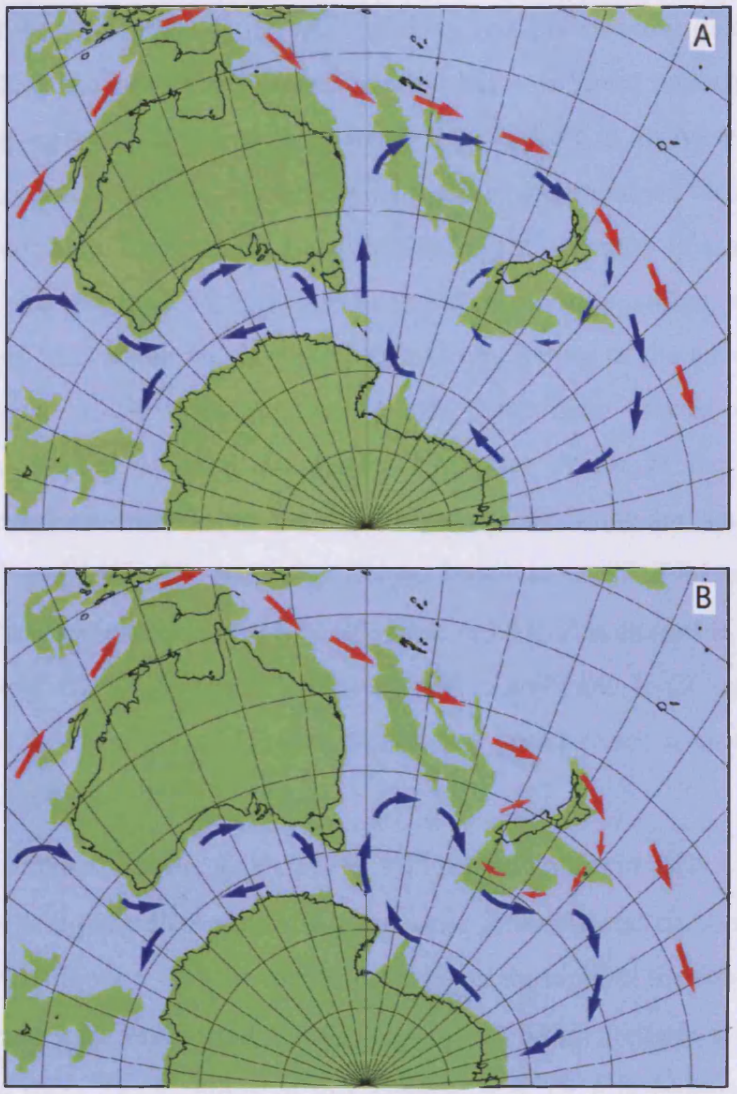

Figure 6.11. Hypothesised middle Eocene oceanic circulation modes for the southern Pacific region. The continental positions are reconstructed on an azimuthal projection for 40 Ma using a magnetic reference frame (modified from Ocean Drilling Stratigraphic Network Web site (www.odsn.de)). A. Cold mode gyre system (adapted from Huber et al., 2004); B. Warm mode gyre system (adapted from Nelson & Cooke, 2001).

6.3.4. Transient events

A transient event between approximately 110 m and 135 m is seen in sedimentary, ecological and geochemical records of the Hampden Beach "long section". In the foraminiferal assemblage and $\delta^{18}O$ records this appears to be an extreme and prolonged 'high' in the cyclicity described above, however the event is also seen in records that are apparently unaffected by the cyclicity. In the sediment record this transient event is observed as a rapid decrease in the weight % >63 μm, resulting from

an increase in the % abundance of clay in the section and a decrease in feldspar (Figure 6.3). The mineralogy indicates that this fine interval has a different underlying cause to the general fining up trend of the section, which results from a decrease in the % of silica and feldspar grains that are >63 μm in size and is accompanied by a decrease in the % abundance of clay. Through the transient fine event, the ratio of clay to feldspar in the sediment and the ratio of kaolinite to montomorillonite within the clay both increase. Both may indicate an increase in chemical weathering of the terrestrial source rocks. This increase in chemical weathering may have been caused by increased temperature or decreased physical weathering by water or ice in the source area. However, Hampden Beach was located at approximately 55° South and source area was a relatively small and low lying landmass (King, 2000) surrounded by water with an approximate surface temperature of 14 °C (Section 6.3.1). This makes it unlikely that the middle Eocene 'New Zealand' landmass had significant local ice cover and consequently that the increase in chemical weathering could result from a decrease in physical weathering by ice.

Prior to the sharp decrease in weight % >63 μm, at approximately 110 m, a rapid shift occurs towards lighter $\delta^{18}O$ values in planktonic foraminiferal carbonate, from ~ -0.6 ‰ to ~ -1.1 ‰ (Figure 6.4). This excursion persists throughout the fine interval and ends at approximately the same time that the weight % >63 μm returns to its pre-event values. There are three likely causes of this change in $\delta^{18}O$; a decrease in global ice volume, an increase in freshwater input or an increase in temperature. Work discussed in Chapter 7 suggests that global ice volume was low or absent during the lower part of the Hampden Section where the "high-resolution" samples were collected. However, without an independent proxy for temperature through the "long section" it is not possible to determine whether the trend towards heavier $\delta^{18}O$ upwards through the section results solely from temperature decrease or whether there is a component of ice volume build up (see Section 6.3.2). This means that it is possible that high-latitude ice had developed by the top of the section, which then melted causing the transient shift in $\delta^{18}O$ and rapidly returned at the end of the interval to slightly greater than it's former volume. However, a decrease in ice volume would increase sea level and although this would be expected to decrease the weight % >63 μm it would do so by decreasing the fraction of silica and feldspar grains >63 μm (as occurs upwards through the section due to the gradual subsidence of the basin), rather than increasing the ratio of clay to feldspar. It is possible that a decrease in ice in the immediate source area could decrease

the physical weathering of rock by ice, resulting in the observed increase in the ratio of clay to feldspar. However, the landmass was low lying and the relatively warm surrounding SSTs make it unlikely that the middle Eocene 'New Zealand' had significant local ice cover and therfore that the increase in chemical weathering could result from a decrease in physical weathering due to loss of that ice cover.

The possibility that the decrease in $\delta^{18}O$ results from increased freshwater input is unlikely, as increasing terrestrial runoff would probably result in both an increase in the weight % >63 μm in the sediment and a decrease in the ratio of clay to feldspar resulting from the more rapid transport of weathered material. This means that the 0.5 ‰ decrease in planktonic foraminiferal carbonate $\delta^{18}O$ is most likely to result from a warming of the surface ocean. The 0.5 ‰ shift is equivalent to 2.5 °C (using the calibration of Erez and Luz (1983) as in Section 6.3.1) if there is no ice volume change through the interval.

As with the cyclicity discussed above, the hypothesis that the $\delta^{18}O$ excursion records a transient warm interval is supported by the foraminiferal species abundance data. There is a marked increase in the relative abundance of specimens of 'mixed-layer' species (thought to inhabit the warm water above a seasonal thermocline) through this interval and a decrease in the abundance of 'sub thermocline' species. Furthermore, specimens of the tropical species *Hantkenina australis* occur almost exclusively within the fine sediment layer at Hampden Beach. This form was recorded as moderately abundant in the Hampden Section sample from which the type was described by Finlay (1939b). However, recent work (Morgans, 2008) and this study have found only single small specimens within the samples. This may indicate that the Hampden Section was on the edge of the range of this species during the warm interval and major incursions only occurred briefly, likely during the warmest parts of the high frequency cycles (Section 7.2.6). No *Hantkenina australis* have been recorded at the more southerly sites on the Kerguelen Plateau and Maud Rise (Stott and Kennett, 1990; Berggren, 1992). However, another species of the same genus *Hantkenina alabamensis* is observed at Agulhas Ridge, south of South Africa for a brief period at ~40.5 Ma and this is also hypothesised to represent a transient warm interval (Galeotti et al., 2002).

The earlier onset of the $\delta^{18}O$ shift compared to the change in grain size suggests that the warming drove the change in sedimentation. The very sudden change in the weight % >63 μm might indicate the passing of a climate controlled threshold affecting the mode of weathering or sediment transport.

Combining the ecological, geochemical and sedimentological characteristics of this interval enables a better understanding what occurred at Hampden Beach during this transient event. The co-occurrence of light $\delta^{18}O$ values with abundant 'mixed-layer' foraminifera and an excursion of a tropical species of foraminifera suggest significant oceanic warming. It is possible that this oceanic warming around New Zealand occurred by a transient contraction of the Antarctic gyre, similar to that discussed previously as a possible cause for the cyclic variability in marine temperature, but larger in magnitude and longer in duration. However, evidence from the additional proxies affected during this event suggests that the climate change that occurred during the transient warm interval was not purely an oceanographic effect. The increase in clays, particularly kaolinite, within the sediment likely results from increased chemical weathering due to increased temperature and / or decreased runoff due to decreased precipitation. This indicates that the event was a large scale climatic change affecting the terrestrial as well as the oceanic realm. This is supported by the records of similar and possibly co-incident, transient warm events from other Southern Ocean sites with a different oceanographic settings (Bohaty and Zachos, 2003), a low latitude site (Sexton et al., 2006a; Edgar et al., 2007) and northern hemisphere sites (Jovane et al., 2007; Spofforth et al., 2008). A global temperature increase explains the geochemical and sedimentological shifts seen during the transient event at Hampden very effectively and would also explain the invasion of a tropical foraminiferal genus, as water temperatures at the site rose to levels at which it could survive.

There are two mechanisms by which a global warm event could increase the abundance of 'mixed-layer' foraminifera at Hampden Beach, the first is to increase the maximum thermocline depth and the second to increase the duration of the seasonal thermocline. Increasing the temperature of the surface ocean would naturally lead to the warmth penetrating deeper which may deepen the maximum extent of thermocline. This would provide more 'space' for 'mixed-layer' species to inhabit and in relatively shallow water such as occurred at Hampden, may also decrease the 'space' in which 'sub thermocline' species could live (Figure 6.12A). Increasing the surface ocean temperature may also increase the duration over which a seasonal thermocline occurs if that thermocline develops above a certain threshold temperature (Figure 6.12B). This would provide a longer period for 'mixed-layer' species to live and reproduce. However, it should be noted that the thermocline may also require other climatic or oceanographic conditions, for example low wind driven mixing that may or may not be related to temperature (Kershaw, 2000).

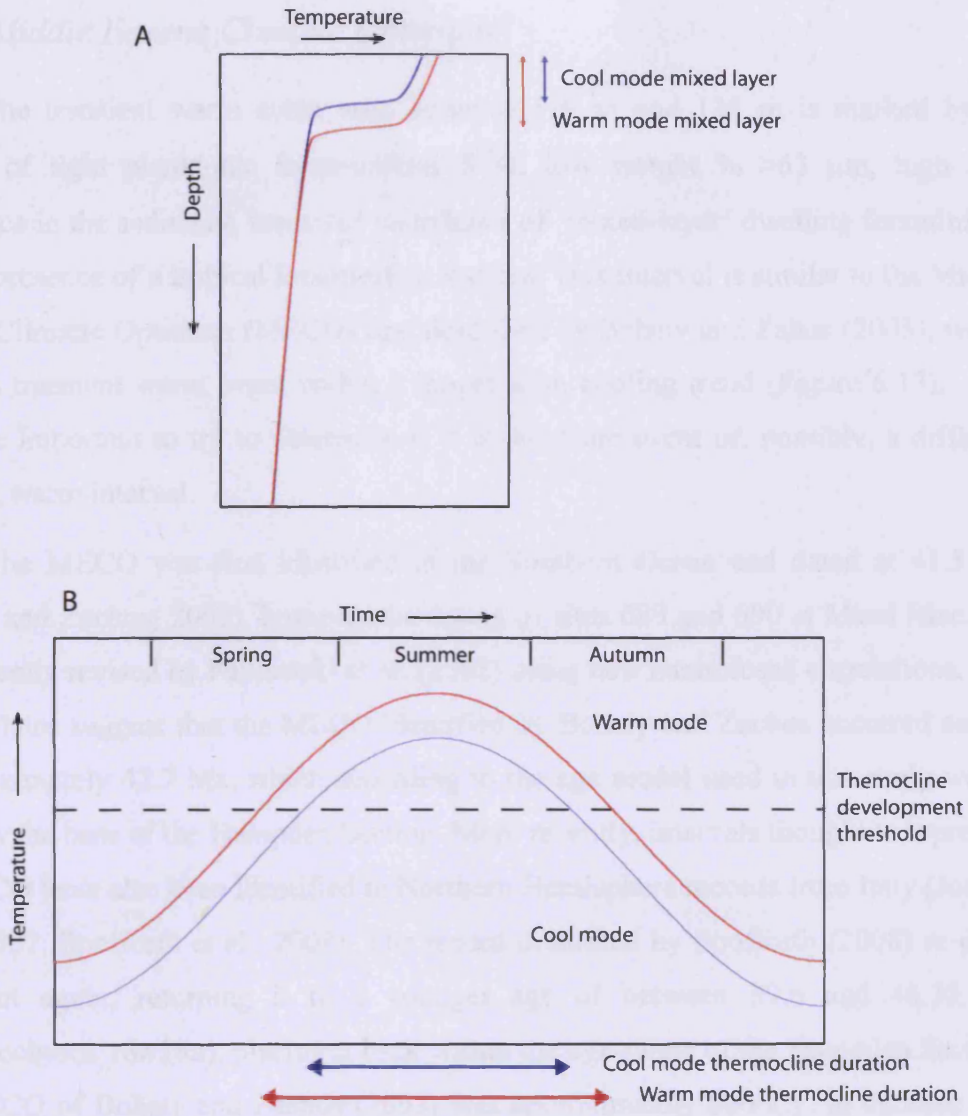

Figure 6.12. Mechanisms by which warming can expand the mixed-layer. A, Warm mode has higher surface temperature and greater mixed-layer depth; B, Warm mode has extended seasonal thermocline duration.

There is no significant negative excursion in $\delta^{13}C$ coincident with that in $\delta^{18}O$ at the top of the Hampden Section (Figure 6.4). This suggests that the warming was not the result of a massive methane hydrate release as proposed for the Late Paleocene Thermal Maximum (LPTM) (Dickens et al., 1995). A possible alternative is an increase in atmospheric carbon dioxide (pCO_2) due to tectonic processes (Bohaty and Zachos, 2003). However, we note here that the onset of this transient warm event occurs during the warming phase of the long period eccentricity cycles discussed in Section 6.3.3 above, indicating that orbital forcing may have had a role in triggering the transient event.

6.3.5. Middle Eocene Climatic Optimum?

The transient warm event seen between 110 m and 135 m is marked by an interval of light planktonic foraminiferal $\delta^{18}O$, low weight % >63 μm, high clay abundance in the sediment, increased abundance of 'mixed-layer' dwelling foraminifera and the presence of a tropical foraminifera species. This interval is similar to the Middle Eocene Climatic Optimum (MECO) first described by Bohaty and Zahos (2003), which is also a transient warm event within a longer term cooling trend (Figure 6.13). It is therefore important to try to determine if it is the same event or, possibly, a different transient warm interval.

The MECO was first identified in the Southern Ocean and dated at 41.5 Ma (Bohaty and Zachos, 2003), however the dating of sites 689 and 690 at Maud Rise was subsequently revised by Falkowski et al. (2005) using new nannofossil correlations. The revised dates suggest that the MECO identified by Bohaty and Zachos occurred earlier at approximately 42.7 Ma, which according to the age model used in this study would be below the base of the Hampden Section. More recently, intervals thought to represent the MECO have also been identified in Northern Hemisphere records from Italy (Jovane et al., 2007; Spofforth et al., 2008). The record described by Spofforth (2008) re-dates the event again, returning it to a younger age of between 39.6 and 40.35 Ma (magnetochrons 18r/18n), placing it back within the age-range of the Hampden Section. The MECO of Bohaty and Zachos (2003) was approximately 600 k.y. in duration and had a magnitude of ~1 ‰ in $\delta^{18}O$ corresponding to a temperature shift of ~4 °C; this is slightly longer in duration than the event seen at Hampden and with a somewhat greater isotopic shift (Figure 6.13). There is no major $\delta^{13}C$ excursion associated with the MECO identified by Bohaty and Zachos (2003), again similar to the situation observed at Hampden, although there is a very brief negative $\delta^{13}C$ excursion towards the end of the MECO possibly resulting from a brief interval of methane hydrate release.

The age model used here places the transient warm excursion in this section between approximately 39.6 and 40 Ma, significantly younger than the MECO is currently dated (Figure 6.13). However, the age model dates given for the MECO have varied, so it is possible that the transient warm event seen in the upper part of the Hampden Section is the same MECO observed by Bohaty and Zachos (2003).

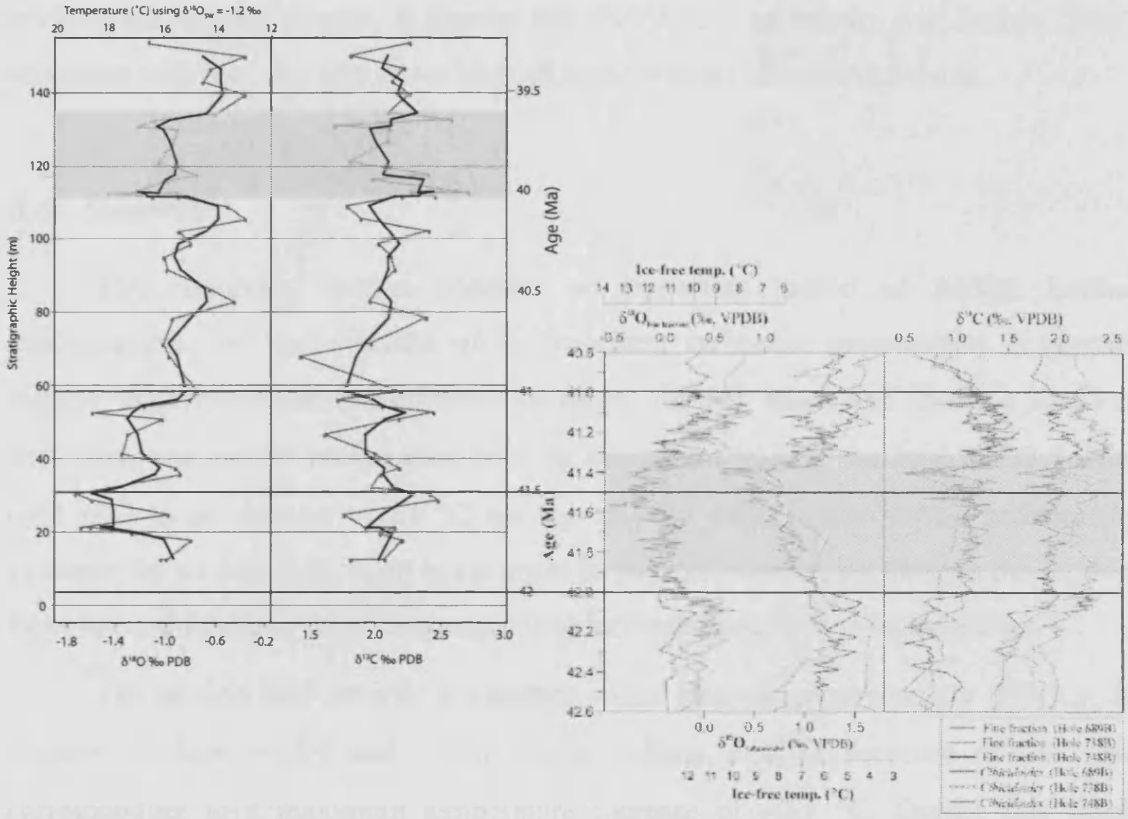

Figure 6.13. Left, foraminiferal oxygen and carbon isotopic record through Hampden Beach; Right, a multicore oxygen and carbon isotopic record through the MECO (from Bohaty and Zachos, 2003). The MECO record is plotted according to the age model used in Bohaty and Zachos (2003). Grey bands highlight the oxygen isotopic excursions in both records and the offset in time between them.

It is also possible that the transient event is an unnamed warm excursion. Sexton et al. (2006a) identified a broad warm interval between 40 and 42 Ma in the tropical western Atlantic (Demerara Rise) and a shorter but substantial transient warm interval at approximately 40.35 Ma. Edgar et al. (2007) also identified a number of negative $\delta^{18}O$ excursions during the middle Eocene in the record from Demerara Rise. Within foraminiferal assemblage records, Galeotti et al. (2002) observed a transient incursion of warm water species to Agulhas Ridge at ~40.5 Ma and Jenkins (1993) reported a warm event in foraminiferal assemblages in the southwestern Pacific at a similar time. It is possible that improved dating of the sites will show that some of these records are of the same event but it is also possible that there are multiple transient warm events throughout the middle Eocene that are extreme occurrences of the underlying long period climate cyclicity. Hence, at present it is not possible to definitively correlate

between the various records. It may be that the MECO of Bohaty and Zachos (2003) correlates with the relatively warm interval at the bottom of the long section.

6.4. Summary

The Hampden Section contains an important record of middle Eocene palaeoclimate, not least because of the excellent carbonate preservation. It records warmer temperatures than previously estimated for 55° south and shows a trend of decreasing sea surface temperature from an average of ~18 °C the base of the section (~42 Ma) to an average of 14 °C the top at (~39 Ma). It also shows sedimentary evidence for a relative decrease in chemical to physical weathering through the section, more likely due to decreased temperatures or increased runoff than increased ice.

The section also records a transient warm interval approximately 450 k.y. in duration between ~40.1 and ~39.6 Ma exhibiting a $\delta^{18}O$ decrease of ~0.5 ‰, corresponding to a maximum temperature increase of ~2.5 °C. During this warm interval in the marine record there is an incursion of *Hantkenina australis*, a tropical foraminfera species and an increase in % abundance of foraminifera belonging to 'mixed-layer' species. There is also an increase in the ratio of chemical to physical weathering in the terrigenous source area seen as a dramatic decrease in the weight % >63 μm of the sediment, largely due to an increase in the ratio of clays to feldspars.

This transient event records a brief global warm interval set against the longer term cooling trend of Eocene high latitudes. The impact of the warming at Hampden was to increase mixed-layer ocean temperature allowing the incursion of a tropical foraminifera, deepen or prolong the seasonal thermocline and increase the ratio of chemical to physical weathering in the terrestrial source region. The underlying cause of the warming is unlikely to be an injection of methane hydrate as has been suggested for the LPTM (Dickens et al., 1995) as there is no significant negative carbon isotope excursion. Instead it may result from an injection of CO_2 as proposed to explain the MECO (Bohaty and Zachos, 2003).

It is not possible to determine with current dating constraints whether the transient event observed at Hampden is the same one first described by Bohaty and Zachos (2003) as the MECO, but the geochemical record is broadly similar and the event falls within the upper part of the range of dates given to 'MECO' events (Spofforth et al., 2008).

It would be extremely interesting to carry out further work on the Hampden Section at higher resolution using both benthic and planktonic species and with an independent temperature proxy such as Mg/Ca in foraminifera to separate temperature and ice volume effects. Higher-resolution data would enable the identification of higher frequency orbital cyclicity, increasing confidence in the assignment of the 22 m cycles to the long period eccentricity forcing. It would also provide more information regarding the nature and timing of the transient event, its duration and the details of leads and lags during its onset and termination; all of which may increase the understanding of its underlying cause and any feedbacks within the event. This information could be very important in improving our understanding of the current anthropogenic CO_2 driven transient warm event. Although such a study is beyond the scope of a NERC PhD project, it is hoped that this study will stimulate further work on the Hampden Section on these lines.

7. High-Resolution Climate Cyclicity

7.1. Introduction

When viewing the cliff at Hampden Beach, it is immediately apparent that the sediment is banded and that rather than forming discrete beds, these bands grade into one another, see Figure 3.3. Furthermore, in some of the taller sections of cliff, it appears that these bands may be bundled into groups. This is reminiscent of localities where sedimentation is influenced by Milankovitch cycles, for example the Blue Lias Formation in southern England (Weedon, 1986) or the Massignano section in central Italy (Jovane et al., 2006). Milankovitch cyclicity is observed in a number of geochemical and ecological proxy records from the Paleogene across the full range of orbital frequencies (e.g. Wade et al., 2001; Pälike et al., 2006; Warnaar, 2006). However, relatively little is known of the mechanisms or nature of the orbital forcing in the Eocene greenhouse period compared with the Neogene icehouse.

Studies of both benthic (Hurley and Fluegeman, 2003) and planktonic (Wade et al., 2001; Wade and Kroon, 2002) foraminifers in the middle Eocene have shown large amplitude variability in $\delta^{18}O$ values on orbital timescales, on the order of 1‰, similar to that seen in the full glacial-interglacial variability of the Pleistocene. Hurley and Fluegeman (2003) argued for a glacio-eustatic interpretation, but as discussed by Wade et al. (2001) these records may equally reflect temperature and salinity changes related to the local oceanographic regimes (Wade et al., 2001). Milankovitch scale cyclicity is also observed in palynomorph assemblages on a precessional timescale in the New Zealand sector of the "Southern Ocean" during the Eocene (Warnaar et al., 2006). Warnaar et al. (2006) integrate palynomorph assemblage data with the results of a global circulation model (GCM) and suggest that the assemblage changes are related to fluctuations in austral summer temperature and precipitation.

The aim of this work is to establish whether the sedimentary banding observed at Hampden Beach is caused by orbital scale climatic forcing and to understand how this forcing is expressed in the sedimentological and palaeoclimatic record. The relatively high sedimentation rate at Hampden enables good resolution sampling through the cycles and the excellent microfossil preservation provides an outstanding palaeoclimatic proxy record. The work uses a multiproxy approach in order to most fully understand the climatic and ecological changes through the section.

Geochemical proxies, particularly isotopic and trace metal analysis of foraminiferal calcite are combined to generate a record of seawater temperature and global ice volume. Foraminiferal and dinoflagellate assemblage records are used to investigate whether there is any change in water column environment through the cycles that may be related to climatic changes. Together with a sedimentological record these may also indicate cyclic changes in the terrestrial realm and / or the ocean circulation.

The "high-resolution" samples were collected at 5 cm vertical intervals at Site 1 (see Section 3.2.1). The base of the section (the level of the sand at the bottom of the cliff on the first day that samples were collected) is 13.85 m above the base of the Hampden Formation. The first sample (CB05HB001) was collected 45 cm above the base of the "high-resolution" section and the sample heights are all given relative to the base of the section. According to the age model given in Section 3.3.5 the sedimentation rate at Hampden Beach is ~5.5 cm/k.y. so 13.85 m equates to ~0.25 Ma, dating the base of the section at ca. 41.81 Ma. The sampled interval spans ca. 41.80 to ca. 41.72 with a total duration of ~87 k.y. and a sample spacing of ~0.9 k.y.

7.2. Results

7.2.1. Sedimentology

The appearance of the cycles seen in the cliffs at Hampden Beach is enhanced by weathering and erosion, particularly in the lower part of the cliff where they are washed by the sea at high tide. The sediment alternates between more and less eroded bands as it is more and less resistant. This resistance is a result of a changing grain size through the sediment, the more resistant bands have a greater weight % >63 μm (sand fraction) (Figure 7.1). The record of weight % >63 μm through the section ranges from ~15 to 45 % and is clearly visibly cyclic on a wavelength of approximately 1 m.

Spectral analysis confirms that this cyclicity is significant to above the 99 % confidence interval at a frequency of 1.02 cycles/m (98 cm wavelength) (Figure 7.2). Using the combined age model developed in Section 3.3.5, this equates to a period of 18 k.y., which is close to the orbital precession frequencies of 19, 23 and 24 k.y..

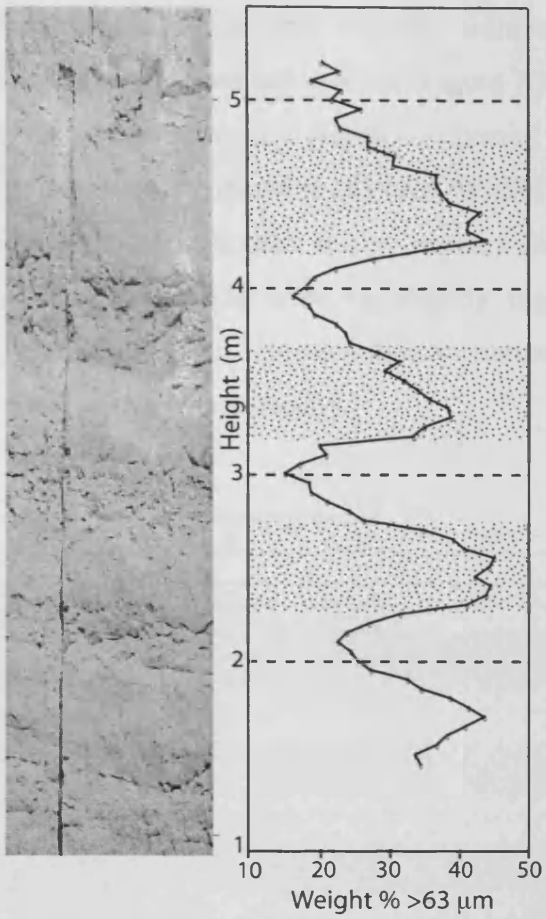

Figure 7.1. Record of weight % >63 μm through the high-resolution samples against field photographs showing the sample collection trench. Resistant bands are stippled.

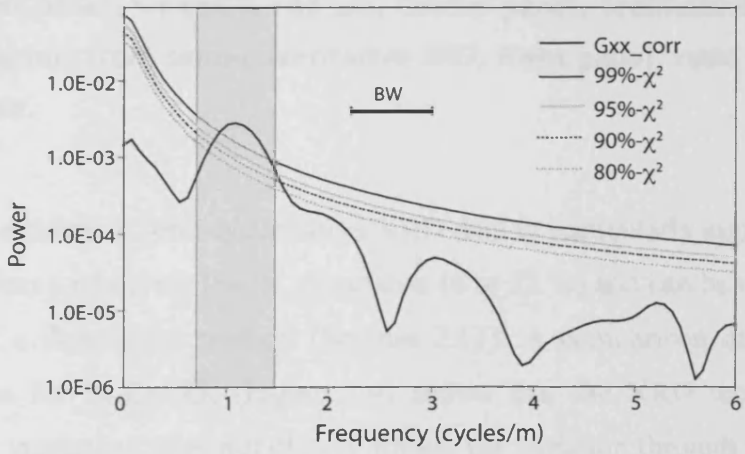

Figure 7.2. Spectral analysis of the weight % >63 μm plotted with confidence intervals against a red noise background generated using REDFIT (Schulz and Mudelsee, 2002). BW = 6-dB Bandwidth. The grey band highlights the cyclicity at a wavelength of ~1 m.

To better understand the nature of this varying sedimentation, the mineral composition was analysed using semi-quantitative XRD (Figure 7.3). This indicates that during periods of high coarse weight there is a slightly increased proportion of quartz and feldspar and a slightly decreased proportion of clays. Within the clays, there is a decreased ratio of kaolinite to montmorillonite. It also appears from the XRD data in Figure 7.3 that the % carbonate ($CaCO_3$) may be slightly higher during the fine intervals. However, the low-resolution and semi-quantitative nature of this record mean that it is difficult to draw conclusions with certainty.

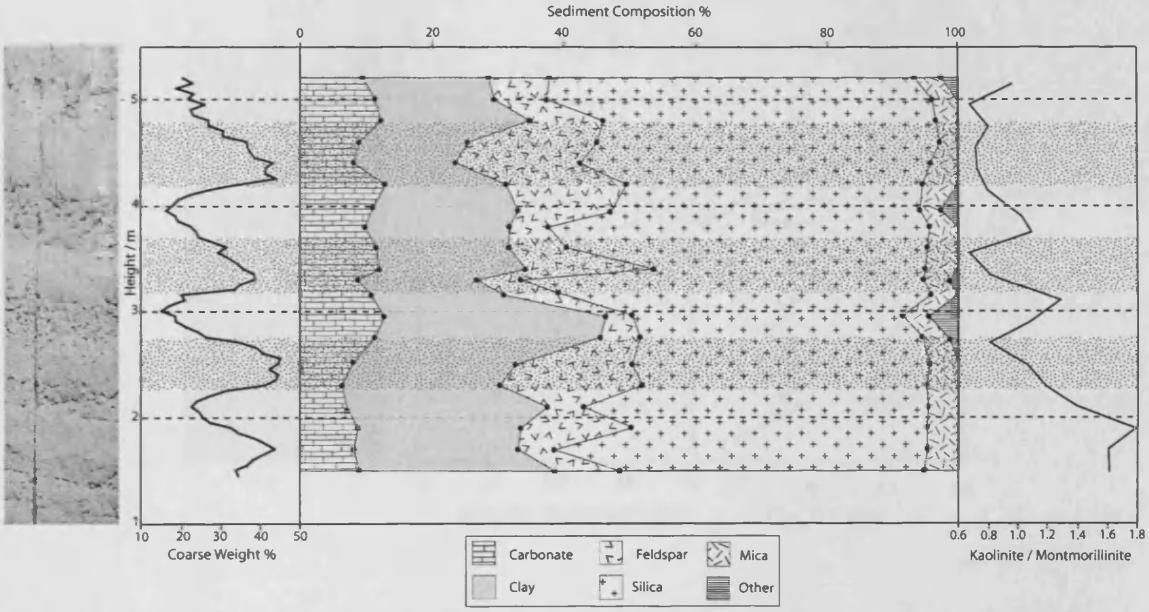

Figure 7.3. Left panel, weight % >63 μm; Centre panel, sediment composition by mineralogical group from semi-quantitative XRD; Right panel, ratio of kaolinite to montmorillonite.

The uncertainty in semi-quantitative XRD data is particularly apparent for the % $CaCO_3$, which has a relatively low % abundance (6 to 12 %) and can be more accurately analysed using a dissolution method (Section 2.11). A comparison of the XRD and dissolution data for % $CaCO_3$ (Figure 7.4) shows that the XRD technique records broadly similar values but does not closely follow the variation through the section that is shown when using the more accurate dissolution method. Furthermore, rather than showing variability on a ~1 m wavelength as occurs with the weight % >63μm, the dissolution record appears to show variability on an ~2 m wavelength. The 2 m wavelength would equate to a period of ~40 ka using the age model developed in

Section 3.3.5, however with only 1.5 possible 'cycles' recorded this is not a statistically significant cyclic variation.

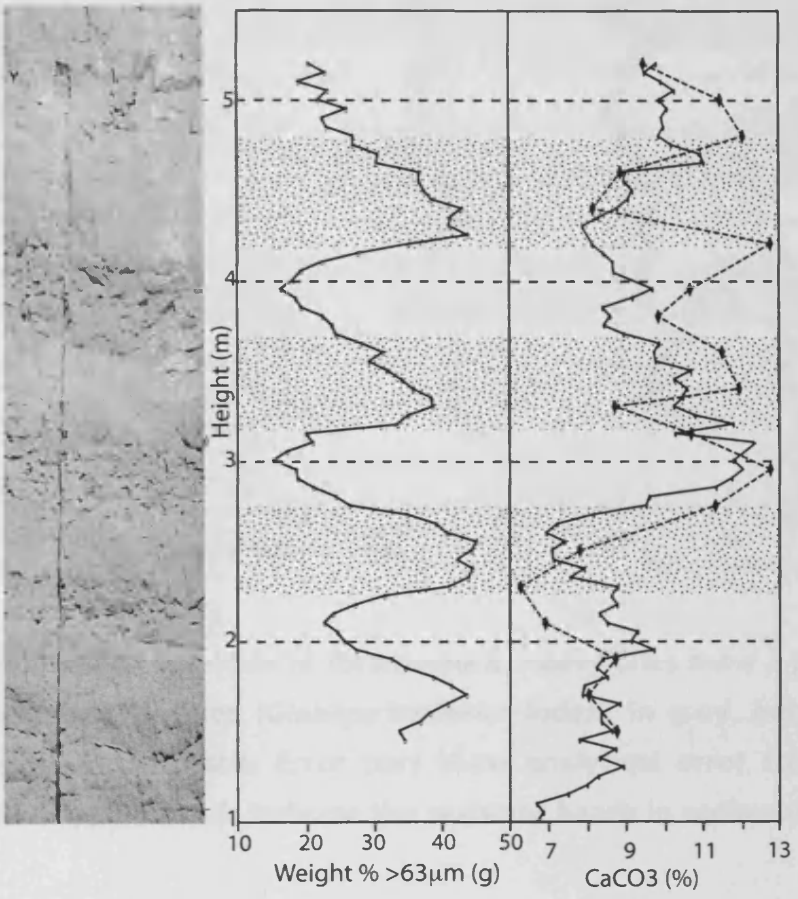

Figure 7.4. Left panel, weight % >63 μm; Right panel, % abundance $CaCO_3$, solid line from dissolution method, dashed line from semi-quantitative XRD method. Resistant bands are stippled.

7.2.2. Geochemistry

7.2.2.1. Isotope geochemistry

Oxygen and carbon isotopic analyses (Section 2.2) were carried out on samples composed of 6–8 specimens of the planktonic foraminifera *Globigerinatheka index* from the 212–250 μm size fraction and 10–20 specimens of the epifaunal benthic foraminifera *Cibicidoides* sp. A (see Section 4.2.3) from the 250–355 μm size fraction. Samples that gave an initial reading of 1.5 kV or less on the mass spectrometer were considered to be unreliable and disregarded then the remaining data were plotted on Figure 7.5 below.

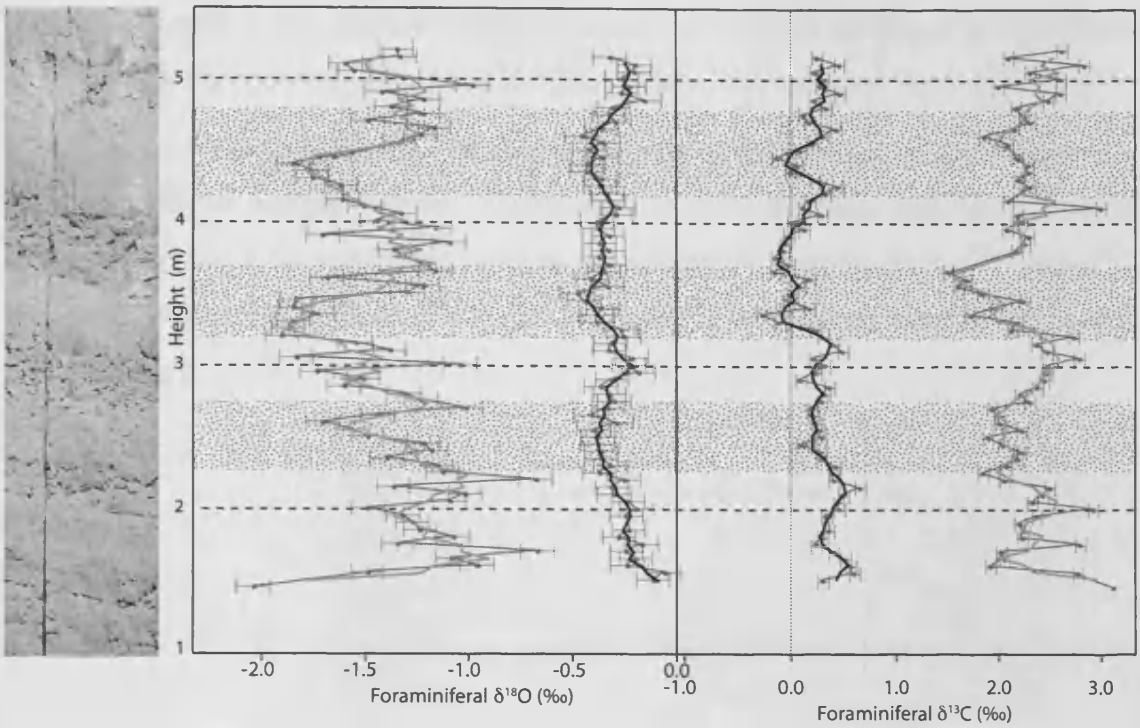

Figure 7.5. Isotopic composition of foraminifera, heavy lines show 3 point moving averages, planktonic species (*Globigerinatheka index*) in grey, benthic species (*Cibicidoides* sp. A) in black. Error bars show analytical error from the mass spectrometer. Stippled bands indicate the resistant bands in sediment.

Planktonic foraminiferal oxygen isotope values range from -0.7 to -2.1 ‰ at the extremes with the 3 point average varying between -0.9 and -1.9 ‰. The benthic foraminiferal oxygen isotope values range between -0.5 and -0.1 ‰ with the 3 point average between -0.1 and -0.4 ‰. The planktonic foraminifera have much lighter and more variable oxygen isotope values, which reflect the higher temperatures and greater variability in temperature and salinity of the surface water, compared to deeper water. Both planktonic and benthic foraminifera show visible cyclicity in oxygen isotopes on approximately the same wavelength as the sedimentary cyclicity.

The carbon isotope ratios of planktonic foraminifera range from 1.5 to 3.0 ‰ with the 3 point average between 1.6 and 2.6 ‰. The benthic foraminifera range between -0.3 and 0.6 ‰ with the 3 point average between -0.1 and 0.5 ‰. The planktonic foraminifera have a heavier isotopic composition than the benthic foraminifera, which likely results from organic productivity in surface water preferentially taking up ^{12}C leaving surface water enriched in ^{13}C. The planktonic foraminifera are also more variable and show cyclicity on the same wavelength as the

sedimentary cycles. The benthic foraminifera are less variable making it more difficult to see any cyclicity, however spectral analysis (Figure 7.6) indicates that it is present.

Spectral analysis (Figure 7.6) shows cyclicity at a frequency of approximately 1 cycle/m in all the isotopic records. The spectral analysis confirms that the cyclicity is significant to the 95% confidence level in the planktonic foraminiferal $\delta^{18}O$ and $\delta^{13}C$ and in benthic foraminiferal $\delta^{13}C$, and to the 90% confidence interval in benthic foraminiferal $\delta^{18}O$.

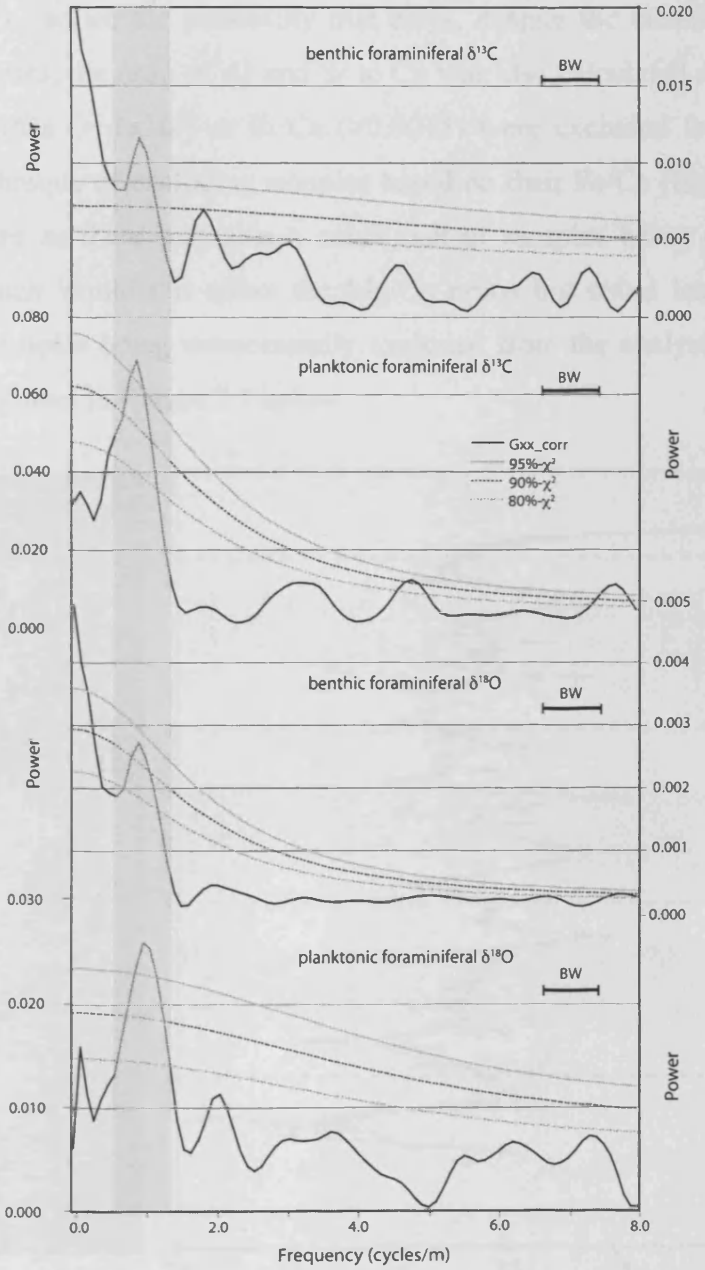

Figure 7.6. Spectral analysis of the isotopic composition of foraminiferal carbonate plotted with confidence intervals against a red noise background generated using REDFIT (Schulz and Mudelsee, 2002). BW = 6-dB bandwidth. Grey band highlights the dominant cyclicity at a wavelength of ~1 m.

7.2.2.2. Trace metal geochemistry

Trace metal analysis was carried out on splits of the same samples of 6 to 8 specimens of *Cibicidoides* sp.A as used for benthic foraminiferal isotope analysis (Section 2.2). The abundance of a number of metals was recorded and the ratio of magnesium (Mg) to calcium (Ca) was calculated ($^{25}Mg/^{43}Ca$) for study. Mg/Ca data can be potentially contaminated by clay minerals as they contain high levels of Mg, however they also contain high levels of metals such as iron (Fe), aluminium (Al) and strontium (Sr). To reduce the possibility that clays, despite the cleaning process, may contaminate samples, the ratio of Al and Sr to Ca was also calculated and samples with high levels of Al/Ca (> $1x10^4$) or Sr/Ca (>0.0015) were excluded from the analysis. The standard technique of excluding samples based on their Fe/Ca (Barker et al., 2003) was not used here as there was also a small risk of samples being contaminated by pyrite (FeS_2) which would not affect the Mg/Ca ratios but could lead to high Fe/Ca ratios and thus samples being unnecessarily excluded from the analysis. The results of this analysis are shown in Figure 7.7 below.

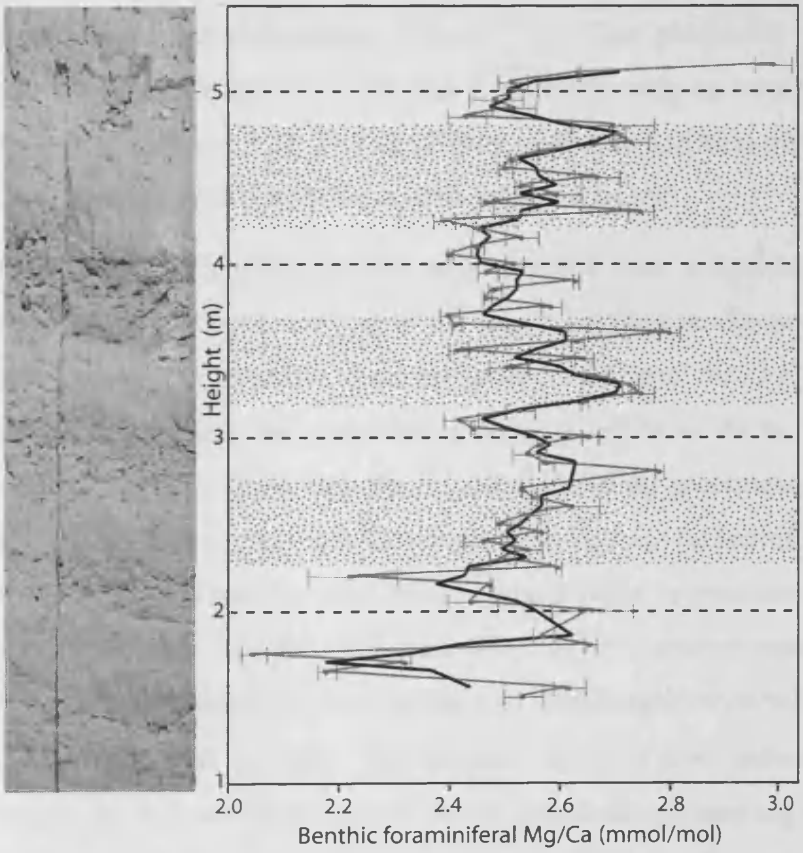

Figure 7.7. Mg/Ca ratio of calcite from *Cibicidoides* sp.A plotted against stratigraphic height. Heavy black line is a three point moving average, error bars show standard error in 3 repeat analyses of each sample.

The Mg/Ca ratio is highly variable through the section and somewhat 'noisy', which is typical of Mg/Ca data. The extreme values range from 2.0 to 3.0 mmol/mol with the 3 point average lying between 2.2 and 2.7 mmol/mol. The record appears to show variability on the same wavelength as the sedimentary banding with higher values during the coarse bands and lower during the fine bands. However, the 'noise' in the data means that this cyclicity is not detectable by spectral analysis. The mean value of samples that lie within the coarse bands is 2.6 and within the fine bands, slightly lower at 2.5, confirming that the Mg/Ca values of the coarser bands is indeed generally higher. The range between the extremes of the cycles can only be estimated by eye and is considered to be approximately 0.3 to 0.4 mmol/mol.

7.2.3. Ecology

7.2.3.1. Foraminifera

Full counts were carried out of planktonic foraminifera in the 212-250 μm size fraction of 500 g samples to determine the abundance (foraminifera per gram) and species composition of the assemblage (Figure 7.8). The planktonic foraminiferal abundance is low and varies between 0.05 and 0.5 specimens/g as would be expected for a shelf edge site (Section 3.3.2). The variability in abundance does not appear to be cyclic and shows no relationship with the coarse sediment bands.

The planktonic foraminifera species were divided into 'mixed-layer' dwelling and 'sub-thermocline' dwelling according to the depth distribution discussed in section 4.2.4. This assemblage composition data are plotted adjacent to the foraminiferal abundance data on Figure 7.8, the assemblage consists of 70 to 90 % 'mixed-layer' dwelling specimens and 5 to 20 % 'sub-thermocline' dwelling specimens. The relative abundances of 'mixed-layer' and 'sub-thermocline' dwelling foraminifera appear to vary cyclically through the section with more 'mixed-layer' specimens in the more resistant sedimentary bands. The data are somewhat 'noisy' however spectral analysis (Figure 7.9) does indicate a weak cyclicity at the 1 m wavelength recorded in the weight % >63μm and geochemical proxies. The spectral analysis also indicates a higher frequency cyclicity at ~0.3 m wavelength, however with a sample spacing of 10 cm this is likely to be an artifact of the sample spacing and relatively small number of samples rather than a real ecological signal.

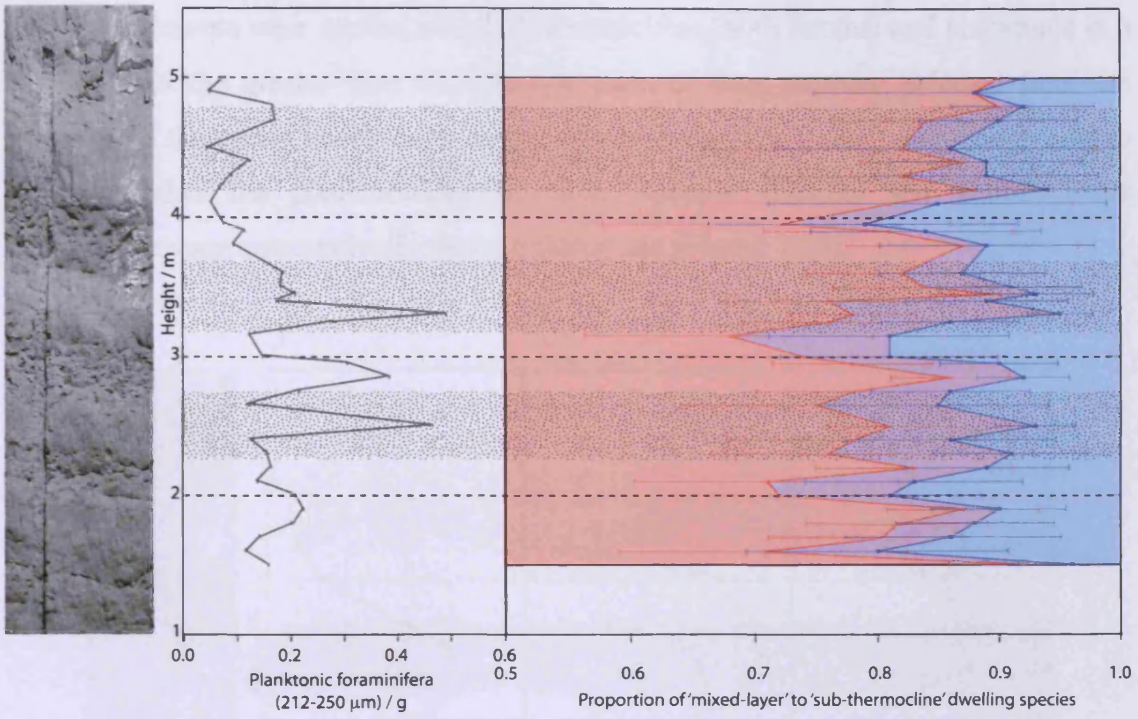

Figure 7.8. Left, planktonic foraminiferal abundance in the 212 - 250 µm fraction; right, % abundance of planktonic foraminifera species associated with different depth habitats, red - 'mixed-layer' (*Globigerinatheka index*, *Globoturborotalita martini*, *G. bassriverensis*, *G. ouachitaensis*, *Acarinina collactea*, *A. primitiva*, *A. mcgowrani*, *A. bullbrooki*); purple - 'unknown depth'; blue - 'sub-thermocline' species (*Catpsydrax unicavus*, *Subbotina angiporoides*, *S. linaperta*, *S. senni*). Error bars show 95% confidence intervals for the % abundances. A photograph of the section is shown for reference and the resistant sedimentary bands are highlighted in pale grey.

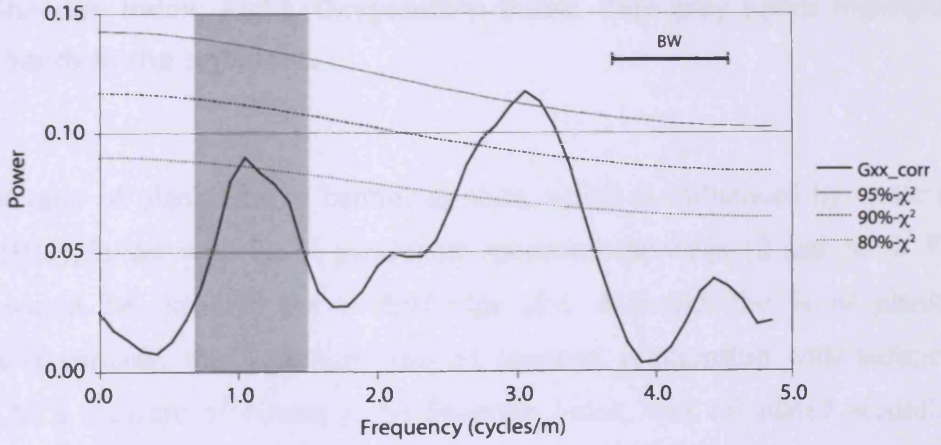

Figure 7.9. Spectral analysis of the % abundance 'mixed-layer' dwelling foraminifera, plotted with confidence intervals against a red noise background generated using REDFIT (Schulz and Mudelsee, 2002). BW = 6-dB bandwidth. Grey band highlights the cyclicity at a wavelength of ~1 m.

Full counts were carried out of all foraminifera, both benthic and planktonic in a $1/8^{th}$ split of the greater than >150 μm fraction of four samples, selected from the extremes of the cycles in sediment weight (see Section 2.7). These counts were used to assess whether the planktonic:benthic ratio, species diversity and bottom water oxygenation vary systematically through the cycles (Figure 7.10).

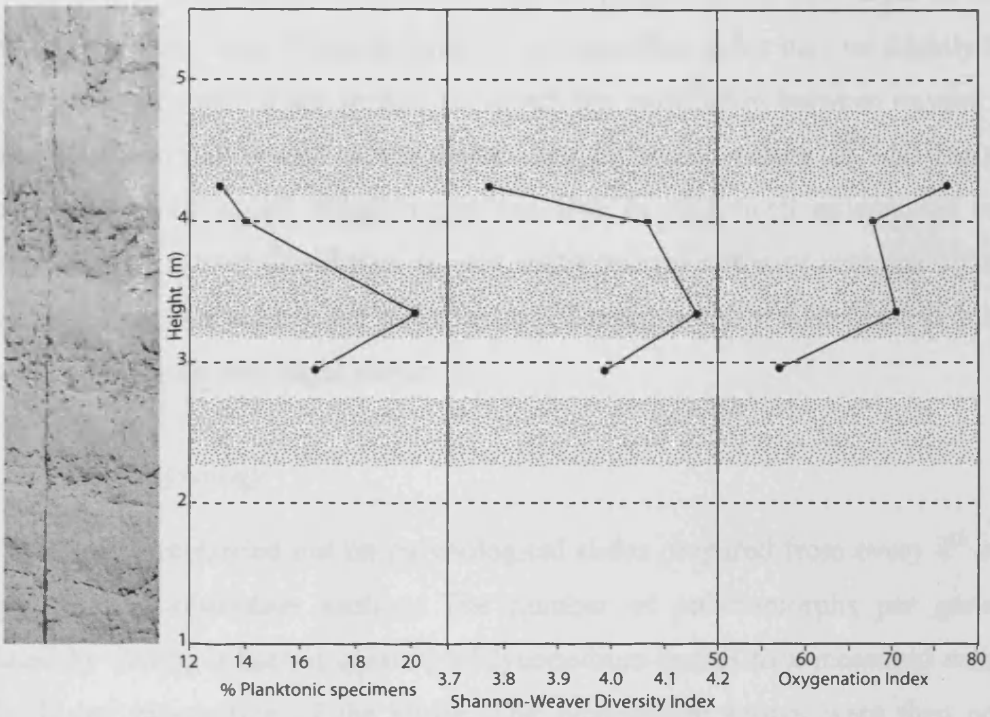

Figure 7.10. Ecological proxies from foraminiferal assemblages plotted against stratigraphic height. Left, Ratio of planktonic to benthic foraminifera specimens; Centre, Shannon Index; Right, Oxygenation index. Pale grey bands highlight the resistant bands in the sediment.

The ratio of planktonic to benthic species, which is influenced by water depth (Gibson, 1989), is low with the % planktonic specimens between 12 and 20 % (Figure 7.10) as would be expected for a shelf-edge site. Although the % of planktonic specimens is variable, this variability has no apparent relationship with sedimentary cyclicity. As a measure of diversity, the Shannon Index, was calculated according to equation 7.1 below (Magurran, 2004) and found to be very high, varying between 3.7 and 4.2, but again showing no consistent relationship with the cycles in sedimentation (Figure 7.10).

Equation 7.1. $H' = - \Sigma (n_i/N)*\ln(n_i/N)$

H' is the Shannon Index,
n_i is the number of specimens belonging to the i^{th} species
N is the total number of specimens

Finally, the benthic foraminifera were used to determine the oxygenation index of the bottom water according to the method of Kaiho (1994) outlined in Section 4.2.4. The oxygenation index ranges between 55 and 80 (Figure 7.10) and values above ~50 indicate highly oxic water. It appears that the oxygenation index may be slightly higher during the coarser parts of the cycles. However, the calibration between oxygen index and dissolved oxygen breaks down above oxygen index values of ~50 (dissolved oxygen ~3.0 mL/L) as all morphotypes can live in such well oxygenated surface sediments. Kaiho (1994) found that oxygen index values can vary between 50 and 95 due to changes in food supply and other factors. Consequently, it is difficult to draw any clear conclusion from this slight variability.

7.2.3.2. Palynology

Counts were carried out on palynological slides prepared from every 4^{th} sample through the high-resolution section. The number of palynomorphs per gram was calculated by adding a known quantity of lycopodium spores to a measured weight of sample during preparation of the slides. The lycopodium spores were then counted along with the palynomorphs on the slide and relative abundance of palynomorphs to lycopodium spores was then used to calculate the palynomorph abundance in the sample (equation 7.2).

Equation 7.2. $P = (L_A/W)*(P_O/L_O)$

P is the number of palynomorphs per gram
L_A is the number of Lycopodium spores added to the sample
W is the sample weight in grams
P_O is the number of palynomorphs observed
L_O is the number of Lycopodium spores observed

The palynomorph abundance varies between ~2000 and 5500 per gm with the higher abundance generally coinciding approximately with the finer, less resistant bands in the sediment.

The percentage of observed palynomorphs that were marine in origin (dinoflagellates, acritarchs or foraminiferal test linings) rather than terrestrial (spores or

pollen) was calculated from the 1st 100 palynomorphs and is plotted on Figure 7.11 below. The percentage of marine palynomorphs ranges from ~40 to 65% and may have a slightly decreasing trend through the section (Figure 7.11). The variability of the % marine palynomorphs relative to terrestrial ones does not appear to occur cyclically or coincide with the sedimentary variability.

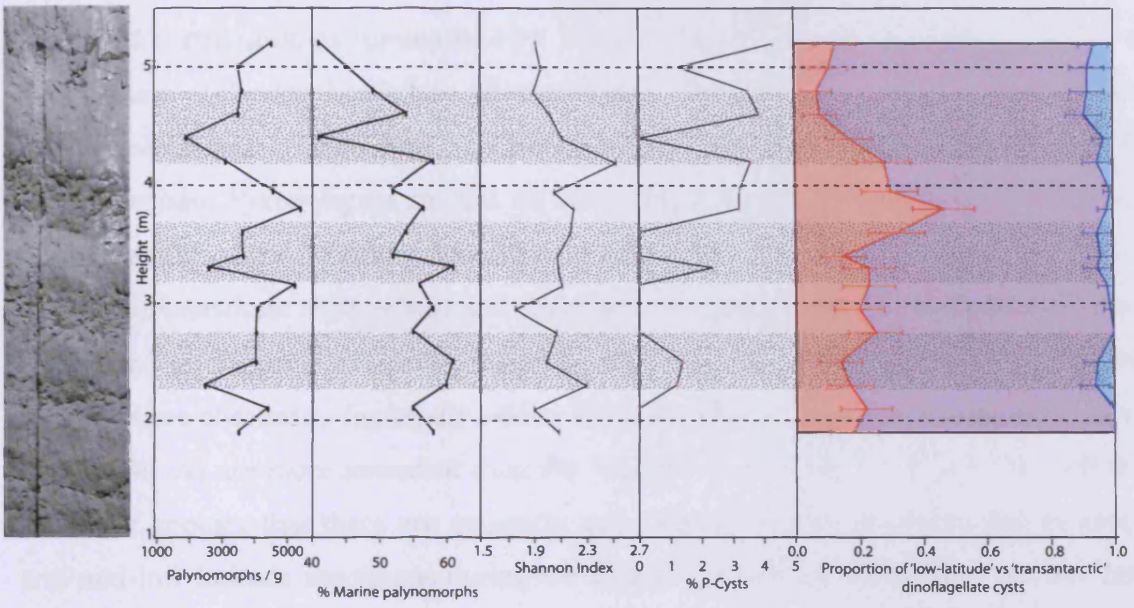

Figure 7.11. Palynological analysis from left to right; Total palynomorphs per gram; % marine relative to terrestrial palynomorphs; Shannon Index; % dinoflagellate cysts belonging to peridinioid species relative to gonyaulacoid species; Proportion of cysts belonging to 'low-latitude', 'cosmopolitan' and 'transantarctic' species as summarised by Warnaar (2006). Error bars show 95% confidence intervals for the % abundances. A photograph of the section is shown for reference and the resistant sedimentary bands are highlighted in pale grey.

The focus was then placed on dinoflagellates with the aim of better characterising the marine ecology. The Shannon index was calculated according to the method described for foraminifera above (see equation 7.1) as a measure of diversity. The values calculated for dinoflagellates are lower than for foraminifera but still moderately high, ranging between approximately 1.7 and 2.6 (Figure 7.11). The Shannon index is variable through the section, however it does not have any overall trend or follow the cyclicity seen in the sediment. The percentage of the dinoflagellate cysts that belong to peridinioid (P) rather than gonyaulacoid (G) species was also calculated as P cysts are predominately heterotrophic whereas G cysts are

predominantly autotrophic, so changes in this ratio may indicate changes in dinoflagellate feeding strategy. It is observed (Figure 7.12) that the % P-cysts is very low (<5 % and frequently 0 %) and although it is variable, this variability has no relationship with the cyclicity and only amounts to 2 or 3 cysts in the sample of 100 counted.

The dinoflagellates were then divided into categories according to their latitudinal distribution as summarised by Warnaar (2006). These categories are 'low to mid-latitude' (*Cordosphaeridium fibrospinosum, Hystrichosphaeridium tuberiferum, Hystrichokolpoma rigaudiae, Corrundinium incompositum, Wilsonidinium echinosuratum, Pyxinodopsis* sp. and all observed species of the genus *Impagidinium*), 'transantactic flora' (*Areosphaeridium partridgei*, *Deflandrea antarctica* and *Hystricosphaeridium truswelliae*) and cosmopolitan (all other observed species). These are plotted on Figure 7.11 above, it can be seen that the assemblage is dominated by cosmopolitan specimens (generally ~65 to 85%) and that mid to low-latitude specimens (~10 to 30 %) are more abundant than the 'transantarctic flora' (<10 %). Through the section it appears that there are generally more transantarctic specimens and possibly less mid-low latitude specimens during the coarser part of the sedimentary cycles. The correspondence with the cyclicity is strongest in the relative abundance of the transantarctic dinoflagellates, however these are represented by less than 10 specimens, so caution should be exercised in interpreting these data.

7.2.4. Foraminiferal test weights

The combined weight of the tests of 10 specimens of *Acarinina primitiva* were measured in alternate samples and used to calculate the mean weight of a single test from each of those samples. The mean test weight is plotted on Figure 7.11 below and it varies between ~6 and 9 mg with no overall trend or relationship to the cyclicity.

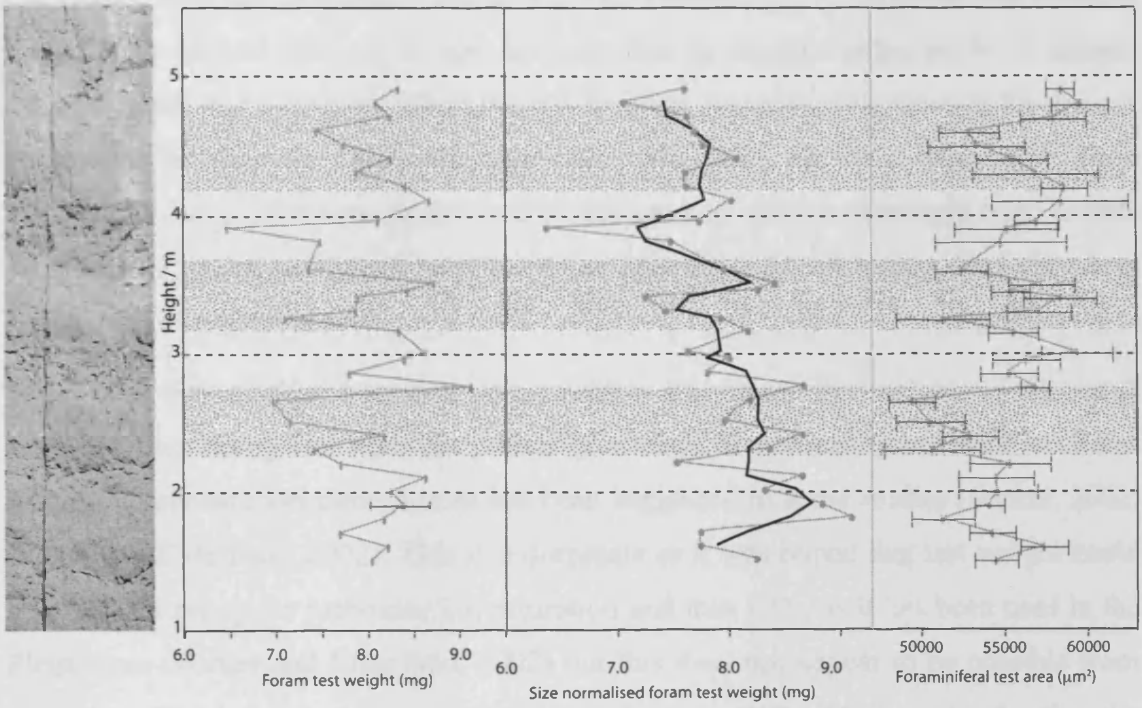

Figure 7.12. Planktonic foraminiferal test weight records. Left, mean weight of ~10 foraminiferal tests; Centre, mean weight of foraminifera normalised to mean size of the same specimens; Right, mean cross sectional area of foraminiferal tests. Error bars show intra-sample variability.

The test weight is determined by a combination of test density and test size, to remove the effect of size difference the test weights were size normalised (Section 2.4) and plotted on Figure 7.12. The errors shown on Figure 7.12 derive from the intra-sample variability as discussed in section 2.4.1 and 2.4.2. The difficulty in measuring this variability for test weight means that it is not possible to calculate the error on size normalised test weight. However, the magnitude of the errors in test area and in the single measured error of test weight mean that caution should be exercised in interpreting the size normalised test weight, although the variability in size and weight

will be linked. The much smaller analytical errors (Section 2.4) have not been plotted as they are far outweighed by the larger errors resulting from intra-sample variability.

The size normalised weights show that again the weight varies between ~6 and 9 mg but the random variability between samples appears to have been reduced to well within the likely errors and instead is replaced with an overall trend of a slight decrease upwards, again with no cyclicity related to the sedimentary cycles. The occurrence of this trend in the size-normalised weights is very interesting as it suggests that upwards through the section there is a size increase that is exactly balanced by a density decrease, such that it does not affect the raw weights. A possible explanation for this co-variation is that since the foraminifera are not solid objects, but are instead formed from a series of hollow chambers; as the foraminifer grows it adds increasingly large hollow chambers so larger specimens may indeed be less dense because their final chambers contain more 'empty' space.

This would suggest the decreasing trend in size normalised weight is an effect of a trend in increasing test size, not primarily a result of decreasing test wall thickness linked to carbonate ion saturation as has been suggested in some studies (Barker, 2002; Barker and Elderfield, 2002). This is unfortunate as it was hoped that test weight could be used as a proxy for carbonate ion saturation and thus CO_2, as it has been used in the Pleistocene (Barker and Elderfield, 2002) but this does not appear to be possible from these data. Since the samples are all selected from the 212 - 250 μm size fraction the trend in increasing mean size may be a result of a slight shift in population structure or the size at which they add additional chambers. Other studies looking at the use of foraminiferal test weight as a pCO_2 proxy have also found that the weight may be controlled by a complex range of interlinked environmental variables (de Villiers, 2004) and thus it is not entirely surprising that they do not behave here as a simple pCO_2 proxy.

7.2.5. Comparison

The sedimentary cycles in the Hampden Section reflect cyclic variations in grain size. Statistically significant cyclicity of the same wavelength (λ ~1m) is also present in the planktonic and benthic foraminiferal isotope records and to a lesser extent in the foraminifera assemblage composition. Similar cyclicity appears to be present in the Mg/Ca record although the signal to noise ratio in this record is too low for spectral

analysis. Using the age framework for the section (Section 3.3.5), this wavelength equates to a frequency of ~18 k.y., which is suggestive of precessional forcing.

The proxies showing the clearest patterns and trends are compared on Figure 7.13 below to highlight the relationships between them. It can be seen from Figure 7.13 that the weight % >63 μm shows the strongest cyclicity and that the coarser parts of the cycles coincide with the more resistant bands in the cliff, these are highlighted by stippled bands on Figure 7.13. Within the coarser bands the clay component of the sediment is comprised of more montmorillonite and less kaolinite. The geochemical analyses all show cyclicity on approximately the same wavelength as the sedimentology, which is stronger in the foraminiferal calcite isotopes than in the Mg/Ca. The results show lower $\delta^{18}O$ (more negative values) and lower $\delta^{13}C$ corresponding to the coarser parts of weight % >63 μm cycles and higher Mg/Ca during the same periods. Looking at the correspondence between the geochemical cycles on the plot and the stippled bands marking the coarse parts of the cycles, it appears that the planktonic $\delta^{18}O$ decrease slightly leads the % >63μm increase whereas the benthic $\delta^{18}O$ and Mg/Ca correspond more closely with the sediment change. The $\delta^{13}C$ decrease then slightly lags the % >63μm increase.

The ecological records are less clear than the geochemical records but they also show signs of cyclicity on the same frequency as the sedimentological cycles. The planktonic foraminifera show slightly higher proportion of mixed-layer species during the coarser parts of the sedimentary cycle and the rise in the proportion of the mixed-layer species slightly lags the increase in weight % >63μm. The palynomorphs show a decrease in the number of palynomorphs in the coarser parts of the sedimentary cycles and a slight decrease in the proportion of 'low-latitude' relative to 'transantarctic' dinoflagellate cysts.

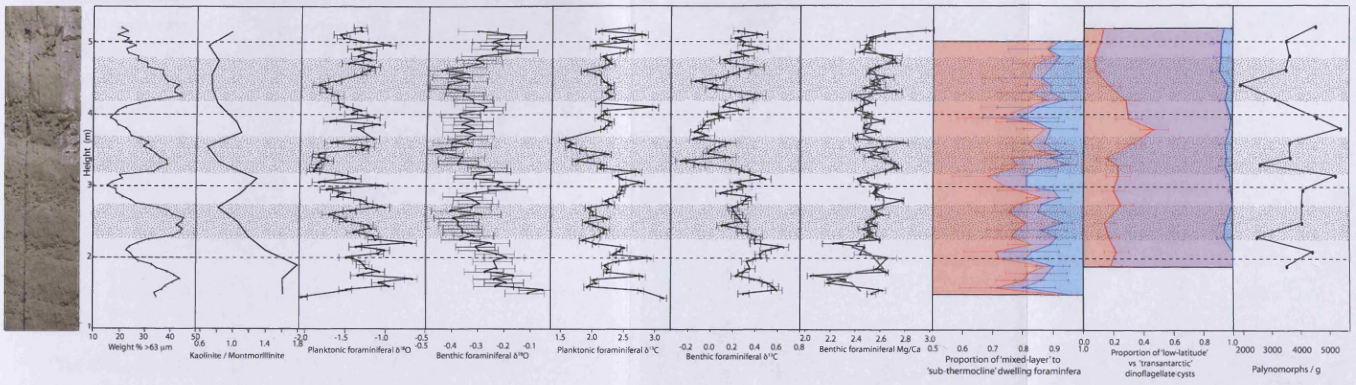

Figure 7.13. Comparison of sedimentary, geochemical and ecological proxies from left to right; weight % >63 µm; ratio of kaolinite to montmorillonite; planktonic foraminiferal $\delta^{18}O$; benthic foraminiferal $\delta^{18}O$; planktonic foraminiferal $\delta^{13}C$, benthic foraminiferal $\delta^{13}C$, benthic foraminferal Mg/Ca; proportion of 'mixed-layer' vs 'sub-thermocline' dwelling planktonic foraminifera; proportion of 'low-latitude' vs 'transantarctic' dinoflagellate cysts; palynomorph abundance. Stippled bands mark the resistant sediment bands.

7.3. Palaeoenvironmental interpretation

7.3.1. Regional temperature and global ice volume

To determine bottom water temperatures, the calibration of Lear et al. (2002) (equation 7.3) was applied to the benthic foraminiferal Mg/Ca record. The Mg/Ca values were first corrected to account for the difference between modern and Eocene seawater Mg/Ca by multiplying by $(Mg/Ca)_{modernsw}/(Mg/Ca)_{Eocenesw}$, using a modern seawater Mg/Ca value of 5.16 mmol/mol and modeled Eocene seawater Mg/Ca value of 4.07 mmol/mol (Wilkinson and Algeo, 1989). The water temperature was then calculated using equation 7.3, below.

Equation 7.3. $Mg/Ca = 0.867 * (e^{(0.109 * T)})$

$\Rightarrow$ $T = (Ln ((Mg/Ca) / 0.867)) / 0.109$

T is bottom water temperature in °C.
Mg/Ca is the measured foraminiferal Mg/Ca in mmol/mol corrected for Eocene seawater Mg/Ca.

The $\delta^{18}O_{sw}$ was then calculated using the Mg/Ca temperatures and the benthic foraminiferal $\delta^{18}O$ values in the paleotemperature equation of Kim and O'Neil (1997) (equation 7.4).

Equation 7.4. $T = 16.1-4.64 (\delta^{18}O_C-\delta^{18}O_{sw}) + 0.09(\delta^{18}O_C -\delta^{18}O_{sw})^2$

$\Rightarrow$ $\delta^{18}O_{sw} = \delta^{18}O_C - (4.64 \pm (\sqrt{(4.64^2-(0.36*(16.1-T)))))) / 0.18$

T is bottom water temperature in °C
$\delta^{18}O_C$ is foraminiferal oxygen isotopic composition in ‰ relative to PDB
$\delta^{18}O_{sw}$ is seawater oxygen isotopic composition in ‰ relative to PDB

The mean of these bottom water $\delta^{18}O_{sw}$ values (-1.20 ± 0.02 ‰) is then used to calculate mixed-layer temperatures from the planktonic foraminiferal $\delta^{18}O$ record, assuming no vertical gradient in $\delta^{18}O_{sw}$, using the equation of Erez and Luz (1983) (equation 6.1). SSTs have also been derived from TEX_{86} measurements carried out on the high-resolution samples by Handley and Pancost at the Univeristy of Bristol (Section 2.9) and the results are given in Burgess et al. (2008). All the calculated temperatures and seawater $\delta^{18}O$ record are plotted on Figure 7.14 below.

The measured analytical errors in $\delta^{18}O$ and Mg/Ca are also plotted on Figure 7.14 and these errors have been propagated (Equations 7.5 to 7.7) to produce an error in $\delta^{18}O_{SW}$, which gives an idea of the limit of variability $\delta^{18}O_{SW}$ that could be detected. The error in $\delta^{18}O_{SW}$ is a combination of the error in $\delta^{18}O_{SW}$ due to the error in $\delta^{18}O_C$ and the error in $\delta^{18}O_{SW}$ due to the error in Mg/Ca according to equation 7.5 below.

Equation 7.5. $\delta sw = \sqrt{(\delta sw_C^2 + \delta sw_M^2)}$

δsw is the error in $\delta^{18}O_{SW}$
δsw_C^2 is the error in $\delta^{18}O_{SW}$ due to the error in $\delta^{18}O_C$
δsw_M^2 is is the error in $\delta^{18}O_{SW}$ due to the error in Mg/Ca

To find the contribution of error due to $\delta^{18}O_C$ and Mg/Ca, $\delta^{18}O_{SW}$ must first be expressed as a function of $^{\delta 18}O_C$ and Mg/Ca (Equation 7.6 below). This is achieved by substituting the Mg/Ca calibration (Equation 7.3 above) into the inverse palaeotemperature equation (Equation 7.4 above), The result is then differentiated with respect to $\delta^{18}O_C$ and multiplied by the error in $\delta^{18}O_C$ to give the contribution of the error due to $\delta^{18}O_C$ (Equation 7.7A) and the procedure is repeated with respect to Mg/Ca to obtain the error due to Mg/Ca (Equation 7.7B). Not that the terms used for $\delta^{18}O_{SW}$, $\delta^{18}O_C$ and Mg/Ca have been simplified in the following equations for clarity.

Equation 7.6. $T = (\text{Ln}\,(M / 0.867)) / 0.109$

$$\delta^{18}O_{sw} = C - (4.64 \pm (\sqrt{(4.64^2 - (0.36*(16.1-T))}))) / 0.18$$

$$\Rightarrow \quad SW = C - (4.64 \pm (\sqrt{(4.64^2 - (0.36*(16.1-((\text{Ln}\,(M / 0.867)) / 0.109))))})) / 0.18$$

T is bottom water temperature in °C.
M is the measured foraminiferal Mg/Ca in mmol/mol corrected for Eocene seawater Mg/Ca.
C is foraminiferal oxygen isotopic composition in ‰ relative to PDB
SW is seawater oxygen isotopic composition in ‰ relative to PDB

Equation 7.7A. $$\delta sw_c = \left|\frac{\partial sw}{\partial c}\right| * \delta c$$

$$\Rightarrow \quad \delta sw_C = 1 * \delta c$$

δsw_C is the error in $\delta^{18}O_{SW}$ due to the error in $\delta^{18}O_C$
δsw is the error in $\delta^{18}O_{SW}$
δc is the measured error in $\delta^{18}O_C$

Equation 7.7B. $$\delta sw_M = \left|\frac{\partial sw}{\partial M}\right| * \delta M$$

$$\Rightarrow \quad \delta sw_M = \frac{-1}{0.109M\sqrt{\left(4.64^2 - \left(0.36 * \left(16.1 - \frac{1}{0.109}\left(Ln\left(\frac{M}{0.867}\right)\right)\right)\right)\right)}} * \delta M$$

δsw_M is the error in $\delta^{18}O_{SW}$ due to the error in Mg/Ca
δsw is the error in $\delta^{18}O_{SW}$
δM is the measured error in Mg/Ca
M is the measured foraminiferal Mg/Ca in mmol/mol corrected for Eocene seawater Mg/Ca.

These calculations produce an analytical error in $\delta^{18}O_{SW}$ of between ±0.080 and ±0.111 ‰ and demonstrate that the analytical error in $\delta^{18}O_{SW}$ results primarily from the analytical error in $\delta^{18}O_C$ with a relatively small contribution from the smaller error in Mg/Ca.

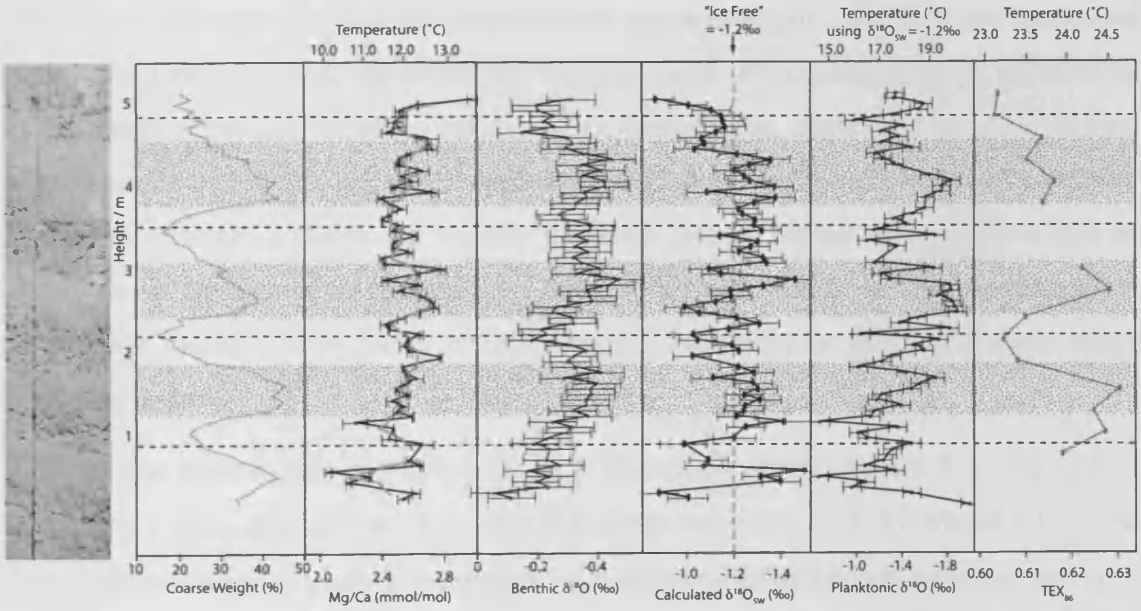

Figure 7.14. Palaeoclimatic proxies from left to right; weight % >63μm; benthic foraminiferal Mg/Ca showing calculated bottom water temperature; benthic foraminiferal $\delta^{18}O$; calculated $\delta^{18}O_{sw}$; planktonic $\delta^{18}O$ showing calculated sea surface temperature; TEX_{86} showing calculated sea surface temperature. Error bars show analytical and calculated errors as discussed above.

The TEX_{86} temperatures range between 23 and 25 °C, and temperatures produced from the planktonic foraminiferal $\delta^{18}O$ record, assuming constant $\delta^{18}O_{sw}$ (= −1.2‰ relative to PDB), range from 16 to 20 °C. An offset of ~5 °C between SSTs and *G. index* palaeotemperatures has previously been observed (Pearson et al., 2001) and is expected because *G. index* underwent late-stage calcification at depth (Premoli Silva et al., 2006). These data are consistent with the good agreement seen between TEX_{86} and planktonic foraminiferal $\delta^{18}O$ temperatures from well-preserved foraminifers at other sites (Schouten et al., 2003; Pearson et al., 2007). Mg/Ca derived bottom water temperatures vary between 11 and 13 °C (Figure 7.14); however, absolute temperatures depend upon species-specific vital effects and seawater Mg/Ca which are not well constrained for the Eocene.

The planktonic foraminiferal assemblage data also shows an increase in 'mixed-layer' relative to 'sub-thermocline' species during these warmer intervals as occurs during the warmer intervals in the long record (discussed in Section 6.2.7). Interestingly the dinoflagellate cysts appear to show a higher abundance of 'transantarctic' species relative to 'low-latitude' species during these warm intervals, which is the reverse of what would be expected. However, the interpretation of dinoflagellates is difficult as assemblages are also affected by salinity and nutrient input, the species considered here to be 'transantarctic' are generally eutrophic, shelf-dwelling species whereas a number of the 'low-latitude' species, particularly the genus *Impagidinium* are associated with an open ocean environment (Brinkhuis, 1994; Warnaar, 2006) so the dinoflagellate assemblage changes more likely reflect nutrient availability or freshwater input rather than temperature.

If the sedimentary cyclicity visible at Hampden Beach (Figure 7.1) was glacio-eustatic in origin, it would be likely that the lower weight % >63 μm would reflect sea level highstands as the study site became more distal to the terrestrial sediment source. I would therefore expect the lower weight % >63 μm to be coincident with lower $\delta^{18}O$ values, but instead the opposite occurs (Figure 7.14). Furthermore, the calculated $\delta^{18}O_{sw}$ from the combined benthic foraminiferal Mg/Ca and $\delta^{18}O$ records produces an average value of −1.2‰, considered to be appropriate for an ice free world (Shackleton and Kennett, 1975) and there is no evidence for cyclic variability of the $\delta^{18}O_{sw}$ on the ~1m wavelength as would be expected from glacio-eustasy. However, calculated error in $\delta^{18}O$ of ~±0.1 ‰ means that variations of up to 0.2‰ in $\delta^{18}O_{sw}$ could go undetected, If high latitude ice had a similar isotopic composition to today ($\delta^{18}O_{ICE}$ ~-50 ‰) this

would equate to slightly less than 25 % present Antarctic ice volume (Edgar et al., 2007). However, if the higher Eocene temperatures resulted in an enhanced hydrological cycle and reduced fractionation, high latitude ice would have a heavier isotopic composition (e.g. $\delta^{18}O_{ICE}$ -30 ‰). In this case a variation of 0.2 ‰ in $\delta^{18}O_{SW}$ would equate to ~40 % present Antarctic ice volume (Edgar et al., 2007). Furthermore, the analytical errors in $\delta^{18}O_{SW}$ are minimum estimates of error as intra-sample variability of foraminiferal Mg/Ca and $\delta^{18}O_C$ will increase the possible errors (particularly with small samples of 10-20 specimens) as will errors in the modelling of Eocene seawater Mg/Ca and in the calibrations of Mg/Ca and $\delta^{18}O_C$ with temperature. Despite the possible sources of error in the $\delta^{18}O_C$ measurements, the mean value of -1.2 ‰ indicates that total global ice volume during this period was low and it is unlikely that the sedimentary cycles in the study section reflect glacio-eustatic sea level changes, although fluctuations of up to ± 20 % of present Antarctic ice volume cannot be ruled out.

The Mg/Ca and TEX_{86} records combined with the record of weight % >63 μm indicate that the cyclicity in the benthic foraminiferal $\delta^{18}O$ record is predominately a result of temperature variability rather than ice volume change. The cycles have a magnitude of ~0.3‰ in benthic foraminiferal $\delta^{18}O$, 0.6–0.8‰ in planktonic foraminiferal $\delta^{18}O$ and ~0.3-0.4 mmol/mol in Mg/Ca. The full extent of the benthic foraminiferal $\delta^{18}O$ cycles can be accounted for by the ~1.5 °C temperature variability indicated by Mg/Ca bottom water temperatures, with no contribution from changing ice volume or salinity. The surface water data are more complex; the TEX_{86} data indicate that the temperature variability in surface waters is also ~1.5 °C, whereas the planktonic foraminiferal $\delta^{18}O$ change of 0.6–0.8‰ would equate to ~3–4 °C if it were purely a temperature effect. The discrepancy between TEX_{86} and planktonic foraminiferal $\delta^{18}O$ variability may have a number of causes including a 0.3–0.5‰ (0.6–1 psu) freshening of surface waters during the warmer periods (cf. Duplessy et al., 1991) and/or rhythmic alteration of the ocean thermal structure, possibly linked to changes in seasonality.

7.3.2. Terrestrial environment and hydrology

The cyclicity in the weight % >63 μm is very clear within the section and appears to be linked to cyclicity in temperature. However, it has been established that the variation in grain size is not caused, or amplified, by global ice-volume change so it is important to understand what alternative processes could cause this grain size variability.

There are no sedimentary features within the Hampden Formation to suggest that the site is in close proximity to a submarine channel or other submarine structure. This indicates that the site lay towards the distal edge of a sediment fan, making it likely that it received relatively steady sediment input (Leeder, 1999). Furthermore, it is highly unlikely that the grain size variability results from the physical process that transports sediment to the site (for example turbidites) as the age model indicates that the grain size cycles occur over an 18 k.y. timescale and are accompanied by geochemical and ecological changes. There are no physical transport processes that, alone, could generate cyclicity incorporating these features and over a timescale of k.y.. This indicates that the sedimentary variation must be caused either by a change in the composition of the terrestrial sediment input or in the transport of sediment by ocean currents during or shortly after deposition.

The most likely cause for a change in terrestrial sediment composition is a change in the precipitation in the source areas leading to variation in the weathering regime and runoff. Generally the increase in weight % >63 μm is associated with a slight increase in quartz and feldspar relative to clays and within the clay fraction, a slight dominance of montmorillonite over kaolinite. Quartz and feldspar both form clay minerals as a result of chemical weathering and kaolinite is considered to be a more advanced weathering stage than montmorillonite (White, 1987). Kaolinite is generally associated with warmer and more humid tropical environments than montmorillonite (White, 1987), which is in contrast to the situation observed here where it is more abundant during cooler periods. However, kaolinite often forms above montmorillonite in the same soils and thus the montmorillonite may be exposed if the soil is rapidly eroded (Birkeland, 1999).

The sediment composition therefore hints at an increase in physical relative to chemical weathering and increased runoff during the warm intervals, this would input more fragments of quartz and feldspar that have not been chemically altered to clays and may increase the transport energy, leading to the increased grain size that is

observed. This would agree with the hypothesised freshening of the surface water during the warm intervals, discussed in Section 7.3.1 above. However, there is no change in the proportion of terrestrial to marine palynomorphs indicating that either any increase in the abundance of terrestrial palynomophs is matched by a corresponding increase in marine palynomophs or that the source area from which the coarser grains were derived was not heavily vegetated. Furthermore, additional work by Handley (2008) shows that the BIT Index, a ratio of terrestrial to marine organic carbon in the sediment, shows a dominance of marine over terrestrial input during the coarse parts of the sedimentary cycles.

The apparent contradictions between the sedimentary and carbonate geochemistry records and the organic carbon and ecological records can be explained in a number of ways. The first is that increased precipitation and runoff increased the terrestrial organic input and provided a source of nutrients that fertilised shelf waters. This in turn increased marine productivity, leading to an overall productivity increase and a dominance of marine over terrestrial carbon in the organic geochemical record. The additional input of terrestrial organic carbon during the warm periods could also lead to the corresponding decrease seen in $\delta^{13}C$, as organic carbon has a light carbon isotope composition. However, there is no evidence from the foraminiferal and palynomorph abundances for a major increase in both marine and terrestrial productivity, the foraminiferal abundance shows no change on the same frequency as the cycles and the palynomorphs show a decrease during coarser parts of the cycles. The lack of a productivity signal in the palynomorphs and foraminifera may be due to the increase in the terrigenous sediment grains drowning out the increased productivity, or to increased decay of organic carbon where there is less clay to seal it from the overlying water column (although no change is seen in carbonate preservation through the cycles). However, the assemblage results do not support the hypothesis of increased productivity. Furthermore, cycles in $\delta^{13}C$ are seen globally on Milankovitch frequencies during the middle Eocene (Section 1.6) and likely reflect global changes in the carbon cycle rather than being associated with a local variation in terrestrial input. Finally, additional work by Handley (pers. comm.) indicates a lower soil pH during the warmer part of the cycles, which he hypothesises, is a result of lower runoff.

The second explanation for the apparent contradiction between different proxies is that the terrestrial sediment input remains constant and that changes in ocean circulation change the deposition of sediment on the shelf edge. In Section 6.2.7 it was

hypothesised that warmer intervals at Hampden Beach may represent a contraction of the 'Antarctic' gyre system resulting in a greater input of warm southward flowing water. If this resulted in a strengthening of the currents along the shelf, it may cause winnowing of the sediment, preferentially removing the lighter clay particles and the associated organic carbon and possibly palynomorphs (Figure 7.15). However, this cannot explain the changes observed in the composition of the remaining clays and organic carbon, these require a mechanism that impacts the terrestrial environment.

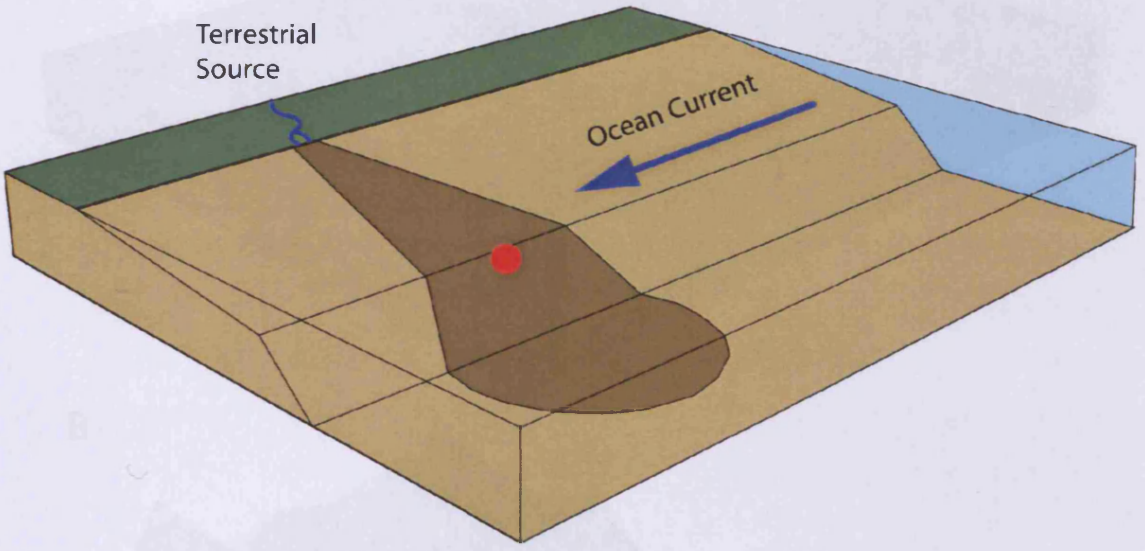

Figure 7.15. Block diagram showing the position of the Hampden Formation in red and the hypothesised sediment input and ocean circulation.

The final explanation for the apparently different climatic signals generated by different proxies is that the balance of the sediment to the site is being altered through the cycles. The site at Hampden Beach is thought to be on the shelf edge, distant from the sediment source, and it is possible that the sediment is influenced by two or more sources onto the shelf, for example two large rivers (Figure 7.16 A). The variation in sediment composition and terrestrial organic carbon may reflect an increasing and decreasing dominance of one source over the other. For example the catchment area of one source could comprise steep rocky slopes with little terrestrial vegetation, where during warm periods there may be increased orographic precipitation or melt of some high level snow cover leading to meltwater runoff. Increased input from this site would have a coarser grain size and higher montmorillonite as the energy of the runoff

increased, but relatively low terrestrial organic carbon and palynomoph abundance. The other source could be lower lying and become warmer and dryer, continuing to input finer more clay based material with high levels of kaolinite. The organic carbon, which is predominately associated with the finer material and therefore with this source may then show increased pH due to decreased rainfall and maybe a decrease in input.

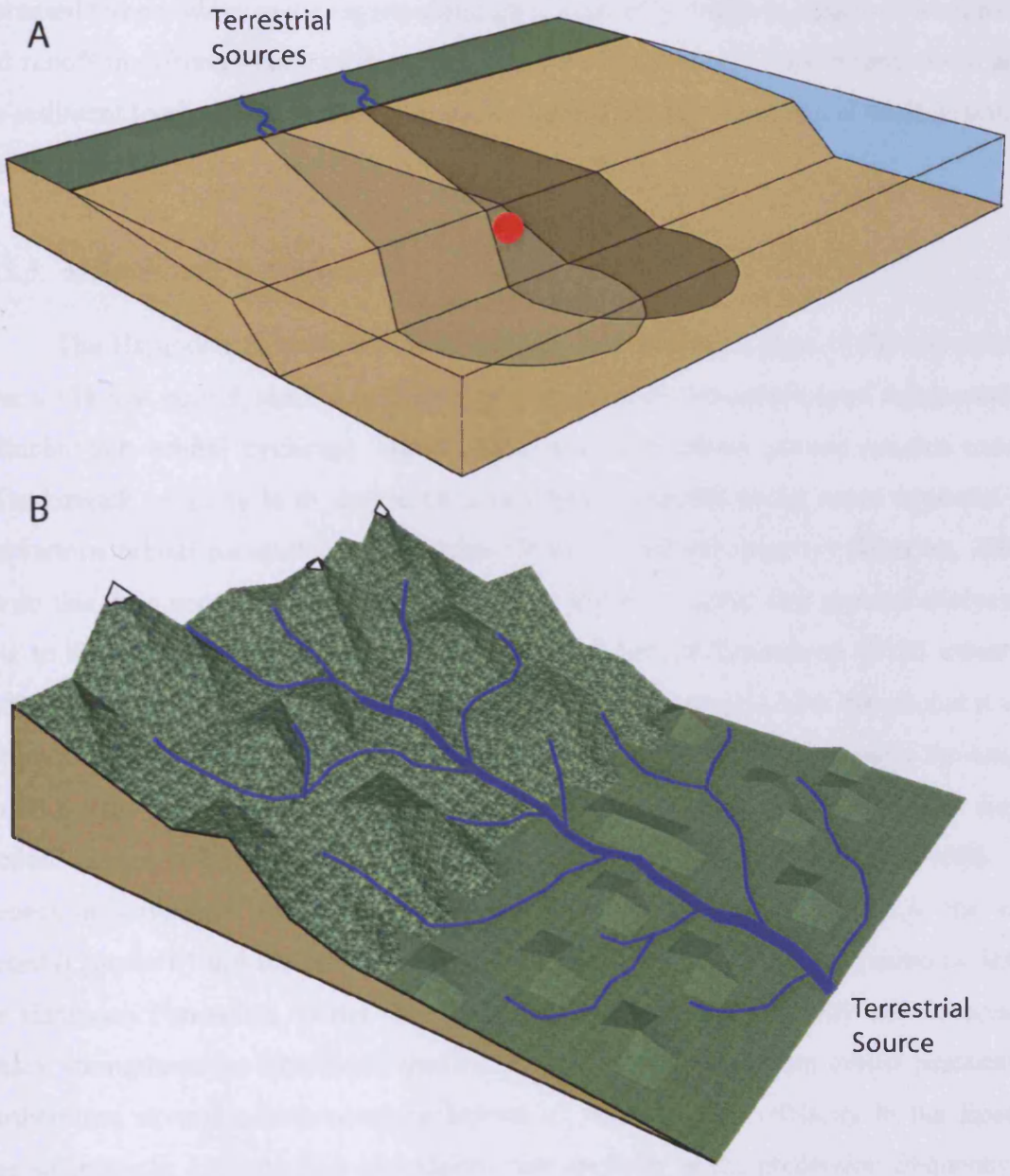

Figure 7.16. Block diagrams showing mechanisms by which the sediment input to the Hampden Formation may be altered. A, a change in the dominance of one sediment source over another; B, a single source with a complex catchment area.

A slight variation on the multiple source hypothesis and one that is equally likely, is that the Hampden Formation may receive sediment from only one point source but the catchment area of this source may include very different environments (Figure 7.16 B). In many rivers the source and early tributaries occur in upland areas with characteristics similar to those described for the first sediment source above, the lower parts of the course may then cross lower lying, flatter areas similar to those described for the second sediment source. Consequently, applying a change in climate such as increased temperature, to the region could have markedly different effects of weathering and runoff in different parts of the catchment for a single river. This in turn would alter the sediment load carried by the river and deposited onto the continental shelf in similar ways to those described above for two separate sources.

7.3.3. Milankovitch cyclicity

The Hampden Formation clearly exhibits cyclicity in a range of climatic proxies over a ~18 k.y. period, similar to the period generated by the precessional component of Milankovitch orbital cyclicity. The standard test of whether climate records exhibit Milankovitch cyclicity is to demonstrate multiple cyclicities at the ratios expected for the various orbital parameters (precession, obliquity and eccentricity) (Weedon, 2003). To do this, it is necessary to generate a sufficiently long record that spectral analysis is able to distinguish these ratios. In this study, the physical limitations of the extent of cliff exposure and the restricted time and scope of a PhD project have meant that it was not possible to generate a sufficiently long high-resolution section to capture the longer period cycles and to distinguish the necessary range of cycle frequencies in a single section. Hence it can only be demonstrated that the observed cycles fall within the precession waveband. However, the occurrence of longer period cycles in the long record (Chapter 6) and the similarity of the ratio between long and short period cycles in the Hampden Formation, to the ratio between long period eccentricity and precession cycles, strengthens the hypothesis that the 18 k.y. cycles result from orbital precession. Furthermore several occurrences are known of Milankovitch cyclicity in the Eocene (see summary in 1.6) and they all exhibit clear cyclicity at the precession frequency so this forcing clearly had a significant climate impact during the Eocene. Consequently it is considered that the 18 k.y. cycles observed at Hampden Beach are most likely forced by orbital precession although a longer high-resolution section is necessary to test this.

7.4. Summary

The high latitude Hampden Section in the southern Pacific experienced surface water temperatures in the region of 23–25 °C and deeper water temperatures around 11–13 °C at ~42.3 Ma during the middle Eocene. There is no evidence of large-scale glaciation during this snapshot of the middle Eocene 'doubthouse' interval. This demonstrates that although transient ice may have been present, extensive permanent ice sheets had not developed on Antarctica or elsewhere in the middle Eocene. If extreme bipolar glaciation did occur during the middle Eocene, as suggested by Tripati et al. (2005), it was not present during the high-resolution interval . This work also indicates that what are interpreted as Milankovitch scale temperature cycles in the southern Pacific Ocean, were not amplified by major waxing and waning of ice sheets. Foraminiferal shell weight data has proved inconclusive in determining whether CO_2 provides an alternative amplifier for the solar insolation changes generated by Milankovitch cyclicity. However, this mechanism certainly merits further investigation, perhaps using a narrower size fraction of foraminifera for shell weight analyses or by using a different proxy such as boron isotopes or alkenones in organic carbon.

The temperature changes appear to have an important impact on the terrestrial climate, altering the sedimentary input to the Hampden Section and possibly influencing both marine and terrestrial productivity. The sediment deposited at the Hampden Section is ultimately a result of a very complex interplay of the climatic and sedimentary systems on a regional and global scale. This section provides a unique insight into the effects of orbital cyclicity on both the terrestrial and marine climate in a brief snapshot of a greenhouse world.

8. Conclusion.

8.1. The Hampden Section

The Hampden Section was deposited during the middle Eocene on the shelf-slope break of a thermally subsiding tectonic basin on the eastern edge of the 'Zealandia' continental fragment at approximately 53 °south. Biostratigraphy indicates that the section was deposited during the AE7 Antarctic biostratigraphic zone (Huber and Quillévéré, 2005) and cyclostratigraphy has been used to further refine the age constraints. The resulting age model places the base of the Hampden Section at 42.1 Ma and the top at 39.3 Ma with a sedimentation rate of 54.9 m/M.y (Section 3.3.5)).

The Hampden Section is primarily composed of the Hampden Formation, a calcareous silt to very fine sandstone containing a diverse range of macro-, micro- and nannofossils (Chapter 4). In particular, the Hampden Formation contains excellently well-preserved calcareous micro- and nannofossils, likely a result of the high proportion of clay in the sediment, which is impermeable and seals the fossils from surrounding fluid. Foraminifera meet the criteria set out in Pearson & Burgess (2008) for good preservation; the tests appear 'glassy' and exhibit excellent textural preservation under both reflected light microscopy (RLM) and high magnification scanning electron microscopy (SEM). They retain their original microgranular texture and in a few cases, original ultrafine features such as spines can be observed, indicating that the test is original and has not been dissolved, overgrown or neomorphised by diagenetic calcite (Section 5.3.1). Furthermore, a multispecies $\delta^{18}O$ - $\delta^{13}C$ cross plot demonstrates that the tests of different foraminiferal species retain differing isotopic signatures, characteristic of the water mass in which they calcified (Section 5.3.2). This indicates that the foraminifera are suitable for geochemical analysis and likely to accurately record the palaeoenvironmental conditions in which they calcified. Consequently, Hampden Beach provides an excellent, high-resolution window into middle Eocene palaeoclimate and can improve our understanding of a number of issues in Cenozoic palaeoclimate studies on both a regional and global level.

8.2. Long term palaeoclimatic record

Using the Mg/Ca of benthic foraminiferal carbonate as a temperature proxy in the "high-resolution" samples has allowed the calculation of $\delta^{18}O_{sw}$ from the benthic foraminiferal $\delta^{18}O$ record. This gives a mean value of $\delta^{18}O_{sw}$ = -1.2 ‰, which is in turn used to produce temperature estimates from the planktonic foraminferal $\delta^{18}O$ in the 'long record'. This record spans ~3 M.y. and shows a trend of decreasing temperature from an average of ~18 °C at the base of the section (~42.1 Ma) to ~14 ° C at the top (~39.3 Ma), consistent with the deep-water cooling trend observed from the Early Eocene Climatic Optimum to the Eocene-Oligocene boundary (Zachos et al., 2001). The temperatures calculated from the Hampden Section are significantly warmer than those previously calculated from $\delta^{18}O$ of planktonic foraminifera from deep-sea sites at similar latitudes (e.g. Zachos et al., 1994). As none of the previous sites demonstrated 'glassy' foraminiferal preservation with tests retaining their original microstructure (Pearson and Burgess, 2008), it is considered that this temperature discrepancy likely results from diagentic overprinting of foraminiferal carbonate in the previously sampled deep sea oozes and that the Hampden Section provides a more accurate temperature record.

This record of middle Eocene high latitude warmth suggests that the observed 'flattening' of the latitudindal temperature gradient during greenhouse climate periods (e.g. Shackleton and Boersma, 1981; Zachos et al., 1994) is not purely an artefact of foraminiferal carbonate diagenesis reducing apparent tropical temperatures, although that has an effect. This returns us to a somewhat reduced 'cool tropics paradox' (D'Hondt and Arthur, 1996) and suggests that further work is still required to reconcile the data-model mismatch between the temperatures estimated from proxy records and those produced by Eocene General Circulation Models (GCMs). Furthermore, these temperatures indicate that the locality at Hampden Beach lay in the path of a warm current, likely flowing south, rather than in the path of an Antarctic gyre, helping to constrain the alternative ocean circulation models proposed for the middle Eocene southern Pacific Ocean (Nelson and Cooke, 2001; Huber et al., 2004, see Section 6.3.1).

The "long section" record from Hampden Beach also records long-period cyclicity in temperature (calculated from planktonic foraminiferal $\delta^{18}O$) and in the abundance of 'mixed-layer' dwelling foraminifera on a wavelength of ~22 m. These are thought to result from orbital forcing and the biostratigraphy suggests that they

correspond to long period eccentricity cycles with a period of ~405 k.y. This indicates that there was significant cyclic change occurring within the water column through the middle Eocene, possibly resulting directly from the increased solar radiation heating the upper water column but more likely, forcing change indirectly through a subtle alteration of ocean circulation patterns (Figure 6.11) or seasonality (Figure 6.12).

8.3. Transient events

The "long section" record from Hampden Beach exhibits a clear transient event between ~110 and 135 m stratigraphic height. This is marked by a decrease in $\delta^{18}O$ of ~0.5 ‰ (equating to a temperature increase of ~2.5 °C) and is accompanied by a dramatic decrease in the weight % >63 μm, an increase in the % 'mixed-layer' dwelling foraminifera and an incursion of *Hantkenina australis*, a tropical foraminifera. These proxies indicate a substantial warm excursion in both the marine and terrestrial realm with the decrease in weight % >63 μm probably resulting from a shift from physical to chemical weathering in the source area.

Conflicting dating of different records means that it is not yet clear whether the Hampden Section records a southern Pacific occurrence of the Middle Eocene Climatic Optimum (MECO) first identified in the "Southern Ocean" by Bohaty & Zachos (2003) and subsequently recorded in the northern hemisphere (Jovane et al., 2007; Spofforth et al., 2008) and possibly at lower latitudes (Sexton et al., 2006a; Edgar et al., 2007). If this is the case, Hampden will provide the first evidence of the terrestrial impact of this transient warm interval. However, it is also possible that a number of warm excursions occur during the middle Eocene, possibly coinciding with combined peaks in orbital cyclicity, as occur during the Late Paleocene and early Eocene (Lourens et al., 2005). To determine this it is necessary to improve the dating constraints across widely spatially distributed sites and to seek out sites where a sufficiently long climatic record occurs to identify multiple transient warm events at intervals of 1.2 or 2.4 M.y.

8.4. High-Resolution Cyclicity

The rapid sedimentation rate at Hampden Beach made it possible to collect a high-resolution section with a sample spacing of 5 cm equating to ~0.9 k.y. per sample according to the age model established in Section 3.3.5. A wide selection of proxy

records were obtained from this section in order to constrain the palaeoclimate and palaeoecology as far as possible.

Cyclicity with a wavelength of ~1 m, equating to a period of ~18 k.y. was observed in a large number of the proxy records. Although it can not be conclusively demonstrated that this is as a result of precessional forcing, the period of the cycles and widespread existence of other Eocene precessional cycles means that it is the most probable forcing mechanism. These cycles are clearest in the weight % >63 μm and this is what causes the sedimentary banding visible in the cliff face at Hampden. The cycles show a variability of ~0.3 ‰ in benthic foraminiferal $\delta^{18}O$, ~0.6-0.8 ‰ in planktonic foraminiferal $\delta^{18}O$ and ~0.3-0.4 mmol/mol in benthic foraminiferal Mg/Ca with the highest Mg/Ca and lowest $\delta^{18}O$ occurring during the coarser parts of the cycles.

The Mg/Ca records produce deepwater temperatures of between 11 and 13 °C and a variability through the cycles of ~1.5 °C, with the maxima of the temperature cycles approximately coinciding with the maxima of the weight % >63 μm cycles. The Mg/Ca temperatures were then used with the benthic foraminiferal $\delta^{18}O$ record to establish a record of $\delta^{18}O_{sw}$. The $\delta^{18}O_{sw}$ record shows no cyclic variability indicating that the whole of the benthic $\delta^{18}O$ changes result from temperature change and that these cycles are not amplified by the waxing and waning of ice. Furthermore, the mean value of $\delta^{18}O_{sw}$ = ~ -1.2 ‰, indicating that there were no significant ice sheets during this period of the middle Eocene. However, the poor signal to noise ratio in the Mg/Ca record means that small transient ice sheets cannot be ruled out.

Surface water temperatures were obtained for a number of samples through the high-resolution section using the TEX_{86} organic carbon proxy (Burgess et al., 2008). These show temperatures of ~23-24 °C, whereas temperatures produced using the calculated value of $\delta^{18}O_{sw}$ = -1.2 ‰ and the planktonic foramiferal $\delta^{18}O$ data are slightly lower and more variable at ~16-21 °C. The surface water temperature variability seen in TEX_{86} is ~1.5 °C, which agrees well with the deepwater temperature variability seen in the Mg/Ca record. However, this temperature change can not fully account for the 0.6-0.8 ‰ variabilty in planktonic foraminiferal $\delta^{18}O$ and it is suggested that the remaining decrease during the warm parts of the cycles is a result of a freshening of surface water.

The increase in weight % >63 μm and the hypothesised freshening of surface waters, combined with a change in the clay mineral composition of the sediment, which

indicates s shift towards physical rather than chemical weathering, all initially indicated enhanced precipitation and runoff during the warm parts of the cycles. This idea is also possibly supported by a slight increase in dinoflagellates species that indicate eutrophic conditions although no change in the ratio of marine to terrestrial palynomorphs or the foraminiferal abundance is observed. However, additional organic carbon records (Handley, 2008) indicate that in fact soil pH was higher during the warm parts of the cycles, suggesting dryer conditions and that there was a dominance of marine over terrestrial carbon. This suggests that a more complex mechanism lies behind the variation in the terrigenous component of the Hampden Formation. The apparent contradiction between proxies can be explained if the organic carbon component of the sediment, which is usually associated with fine fraction clays, is sourced from an area that responds differently to the temperature increase than the source of the coarser quartz and feldspar grains. The simplest way in which this could occur is for the coarse grains to be sourced from an upland area, with relatively little vegetation cover, that experiences increased orographic precipitation precipitation during warm periods and hence increased physical weathering and sediment transport energy. In contrast, the organic carbon could be sourced from a low lying flood plain or sediment fan where precipitation decreased during warm periods. This would lead to the 'swamping' of finer material with coarser and the differing climatic signals observed in the different proxy records.

This "high-resolution" section illustrates the complexity of the climatic system and the importance of obtaining as much information as possible in trying to understand palaeoclimates. The high-resolution palaeoclimatic record presented here demonstrates that significant climatic cyclicity occurred during the greenhouse world of the middle Eocene. The temperature cyclcity was likely forced by orbital precession cycles and despite having little or no amplification from ice, they had a major and complex effect on both the marine and the terrestrial environment.

8.5. *Further work*

The Hampden Section offers a wealth of opportunities for further work. The transient warm event recorded in the upper part of the section is unique among possible MECO records in containing influences from both terrestrial and marine environments. It would be very interesting to use organic geochemistry and foraminiferal Mg/Ca to determine the magnitude of the temperature shift through this excursion and establish whether there was any influence of ice volume on the $\delta^{18}O$ shift. The high sedimentation rate also means that the onset of the excursion and the return to a pre-excursion state could be studied in detail.

The high-resolution record also shows very interesting climate cyclcity and having established that the grain size variation is climatically influenced it would be possible to use the weight % >63 μm at high-resolution through a much longer record, for example a drill core, to observe the cyclicity over a longer period. This would enable a better assessment of whether the cycles exhibit the multiple frequencies characteristic of Milankovitch cyclcity and show conclusively whether they are orbitally forced.

Beyond the Hampden Section itself, the presence of both organic carbon and 'glassy' foraminiferal calcite in the Hampden Formation has enabled the offset between TEX_{86} derived SSTs and planktonic foraminiferal $\delta^{18}O$ derived "mixed-layer" temperatures, to be estimated for the southern Pacific region during the middle Eocene. This provides significant scope for work using TEX_{86} as a SST proxy in spatially and temporally close sections where foraminifera are poorly preserved or absent, enabling these temperatures to be more accurately related to the global Cenozoic planktonic foraminiferal $\delta^{18}O$ temperature record.

8.6. *Summary*

This study has used the Hampden Section to generate palaeoclimate records on two timescales that give an insight into the middle Eocene southern Pacific. These show warm seawater temperatures with a gradual cooling trend, punctuated by a transient warm interval lasting ~450 k.y. that affected both the marine and terrestrial realm. The seawater temperatures strongly suggest that the Hampden Beach locality lay in the path of a warm southward flowing current rather than a cold Antarctic gyre, helping to constrain the regional oceanography. The section also records both long and short period climate cyclicity, likely to be orbitally forced. These cycles have an impact not

only on seawater temperatures and marine ecology but also on the terrestrial environment and terrigenous sediment input.

The Hampden Formation provides a unique geological archive of past climate, environment and ecology in the New Zealand region of the southern Pacific during the middle Eocene. No other site in mid or high southern latitudes is known with such excellent microfossil preservation, clear cyclicity and high sedimentation rate. By combining multiple techniques ranging from organic and inorganic geochemistry to the taxonomy of calcareous microfossils and dinoflagellates, it has been possible to obtain a detailed snapshot of southern high latitude climate and climate change in a greenhouse world.

9. Bibliography

Armstrong, H. A. and Brasier, M. D. (2005). *Microfossils*, Blackwell Publishing.

Arney, J. E. and Wise, S. W. (2003). Paleocene-Eocene Nannofossil Biostratigraphy of ODP Leg 183, Kerguelen Plateau. *Proceedings of the Ocean Drilling Program, Scientific Results.* Frey, F. A., Wallace, M. F. and Quilty, P. G. **183:** 59.

Arrhenius, S. (1896). On the Influence of Carbonic Acid in the Air upon the Temperature of the Ground *Philosophical Magazine and Journal of Science* **41**: 237-276.

Barker, S. (2002). Planktonic foraminiferal proxies for temperature and pCO_2. *Department of Earth Sciences*. Cambridge, University of Cambridge: 35.

Barker, S. and Elderfield, H. (2002). Foraminiferal Calcification Response to Glacial-Interglacial Changes in Atmospheric CO_2. *Science* **297**: 833-836.

Barker, S., Greaves, M. and Elderfield, H. (2003). A study of cleaning procedures used for foraminiferal Mg/Ca paleothermometry. *Geochemistry, Geophysics, Geosystems* **4**(9): 20.

Barrera, E. and Huber, B. T. (1993). Eocene to Oligocene oceanography and temperatures in the Antarctic Indian Ocean. *The Antarctic Paleoenvironment: A perspective on global change*, American Geophysical Union. **60:** 49-65.

Barron, E. J. (1987). Eocene equator-to-pole surface ocean temperatures: a significant problem? *Paleoceanography* **2**: 729-739.

Beerling, D., J and Royer, D. L. (2002). Reading a CO_2 signal from fossil stomata. *New Phytologist* **153**: 387-397.

Bemis, B. E., Spero, H. J., Bijma, J. and Lea, D. W. (1998). Reevaluation of the oxygen isotopic composition of planktonic foraminifera: Experimental results and revised paleotemperature equations. *Paleoceanography* **13**(2): 150-160.

Berger, W. H. (1979). Preservation of Foraminifera. *Foraminiferal Ecology and Paleoecology.* Lipps, J. H., Berger, W. H., Buzas, M. A., Douglas, R. G. and Ross, C. A. Housten, Society of Economic Paleontologists and Mineralogists: 105-155.

Berggren, W. A. (1992). Paleogene Planktonic Foraminifer Magnetobiostratigraphy of the Southern Kerguelen Plateau (Sites 747-749). *Proceedings of the Ocean Drilling Program, Scientific Results*. Wise, S. W. and Schlich, R. **120:** 551-568.

Berggren, W. A., Kent, D. V., Swisher, C. C. and Aubry, M.-P. (1995). A revised Cenozoic geochronology and chronostratigraphy. *Geochronology, Time Scales and Global Stratigraphic Correlation*. Berggren, W. A., Kent, D. V., Aubry, M.-P. and Hardenbol, J., Society for Sedimentary Geology: 129-212.

Berggren, W. A., Pearson, P. N., Huber, B. T. and Wade, B. S. (2006). Taxonomy, Biostratigraphy, and Phylogeny of Eocene *Acarinina*. *Atlas of Eocene Planktonic Foraminifera*. Pearson, P. N., Olsson, R. K., Huber, B. T., Hemleben, C. and Berggren, W. A., Cushman Foundation for Foraminiferal Research: 257 - 326.

Bernstein, L., Bosch, P., Canziani, O., Chen, Z., Christ, R., et al. (2007). IPCC, 2007: Summary for Policymakers. *Climate Change 2007: Synthesis Report*. Cambridge, Cambridge University Press: 22.

Beu, A. G., Maxwell, P. A. and Brazier, R. C. (1990). Cenozoic Mollusca of New Zealand. *New Zealand Geological Survey Paleontological Bulletin* **58**: 518.

Bianchi, G. G., Hall, I. R., McCave, I. N. and Joseph, L. (1999). Measurement of the sortable silt current speed proxy using the Sedigraph 5100 and Coulter Multisizer IIe: precision and accuracy. *Sedimentology* **46**: 1001-1014.

Bianchi, G. G. and McCave, I. N. (1999). Holocene periodicity in North Atlantic climate and deep-ocean flow south of Iceland. *Nature* **397**: 515-517.

Bice, K. L., Barron, E. J. and Peterson, W. H. (1998). Reconstruction of Realistic Early Eocene Palaeobathymetry and Ocean GCM Sensitivity to Specified Basin Configuration. *Tectonic Boundary Conditions for Climate Reconstructions*. Crowley, T. J. and Burke, K. C., Oxford University Press. **39:** 227-247.

Bice, K. L. and Marotzke, J. (2001). Numerical Evidence Against Reversed Thermohaline Circulation in the Warm Paleocene/Eocene Ocean. *Journal of Geophysical Research* **106**: 11529-11542.

Bice, K. L. and Marotzke, J. (2002). Could changing ocean circulation have destabilized methane hydrate at the Paleocene/Eocene boundary? *Paleoceanography* **17**(2): 10.1029/2001PA000678.

Billups, K. and Schrag, D. P. (2003). Application of benthic Mg/Ca ratios to questions of Cenozoic climate change. *Earth and Planetary Sciences Letters* **209**: 181-195.

Birkeland, P. W. (1999). *Soils and Geomorphology*. Oxford, Oxford University Press.

Blow, W. H. (1979). *The Cainozoic Globigerinida: A Study of the Morphology, Taxonomy, Evolutionary Relationships and the Stratigraphical Distribution of Some Globigerinida (Mainly Globigerinacea)*. Leiden, E. J. Brill.

Bohaty, S. M. and Zachos, J. C. (2003). Significant Southern Ocean warming event in the late middle Eocene. *Geology* **31**(11): 1017-1020.

Bowen, G. J., Beerling, D. J., Koch, P. L., Zachos, J. C. and Quattlebaum, T. (2004). A humid climate state during the Palaeocene/Eocene thermal maximum. *Nature* **432**: 495-499.

Bown, P. R., Ed. (1998). *Calcareous Nannofossil Biostratigraphy*. British Micropalaeontological Society Publication Series. London, Chapman & Hall.

Bown, P. R., Dunkley Jones, T., Lees, J. A., Randell, R. D., Mizzi, J. A., et al. (2008). A Paleogene calcareous microfossil Konservat-Lagerstätte from the Kilwa Group of coastal Tanzenia. *GSA Bulletin* **120**(1/2): 3-13.

Boyle, E. A. and Keigwin, L. D. (1985/86). Comparison of Atlantic and Pacific paleochemical records for the last 215,000 years: changes in deep ocean circulation and chemical inventories. *Earth and Planetary Sciences Letters* **76**: 135-150.

Brinkhuis, H. (1994). Late Eocene to early Oligocene dinoflagellate cysts from the Priabonian type-area (northeast Italy); biostratigraphy and palaeoenvironmental interpretation. *Palaeogeography, Palaeoclimatology, Palaeoecology* **107**: 121-163.

Brinkhuis, H. and Biffi, U. (1993). Dinoflagellate cyst stratigraphy of the Eocene/Oligocene transition in central Italy. *Marine Micropaleontology* **22**: 131-183.

Brinkhuis, H., Schouten, S., Collinson, M. E., Sluijs, A., Sinninghe Damste, J. S., et al. (2006). Episodic fresh surface waters in the Eocene Arctic Ocean. *Nature* **441**: 606-609.

Broecker, W. S. and Clark, E. (2004). Shell weights from South Atlantic. *Geochemistry, Geophysics, Geosystems* **5**(3): 5.

Brönnimann, P. (1952). *Globigerinoita* and *Globigerinatheka*, new genera from the Tertiary of Trinidad, W. I. *Contributions from the Cushman Foundation for Foraminiferal Research* **3**: 25-29.

Brotzen, F. and Pozaryska, K. (1961). Foraminifères du Paléocène et de l'Eocène inférieur en Pologne septentrionale; remarques paléogéographiques. *Revue de Micropaléontologie* **4**: 167.

Brown, D. A. (1954). The geology of Moeraki Subdivision. *New Zealand Geological Society Bulletin - Unpublished.*

Brown, S. J. and Elderfield, H. (1996). Variations in Mg/Ca and Sr/Ca ratios of planktonic foraminifera caused by postdepositional dissolution: Evidence of shallow Mg-dependent dissolution. *Paleoceanography* **11**(5): 543-551.

Browning, J. V., Miller, K. G. and Pak, D. K. (1996). Global implications of lower to middle Eocene sequence boundaries on the New Jersey coastal plain: The icehouse cometh. *Geology* **24**(7): 639-642.

Burgess, C. E., Pearson, P. N., Lear, C. H., Morgans, H. E., Handley, L., et al. (2008). Middle Eocene climate cyclicity in the southern Pacific: Implications for global ice volume. *Geology* **in press**.

Buzas, M. A. (1990). Another look at confidence limits for species proportions. *Journal of Paleontology* **64**(5): 842-844.

Cameron, A. A. and Waghorn, D. B. (1985). *Bortonian/Kaitian Foraminifera and Calcareous Nannofossils from Hampden Beach and McCulloch's Bridge*. Hornibrook Symposium.

Carpenter, W. B., Parker, W. K. and Jones, T. R. (1862). *Introduction to the Study of the Foraminifera*. London, Ray Society Publications.

Carter, R. M. (1988). Plate boundary tectonics, global sea-level changes and the development of the eastern South Island continental margin, New Zealand, Southwest Pacific. *Marine and Petroleum Geology* **5**: 90-106.

Carter, R. M., McCave, I. N. and Carter, L. (2004). Leg 181 Synthesis: Fronts, Flows, Drifts, Volcanoes, and the Evolution of the Southwestern Gateway to the Pacific Ocean, Eastern New Zealand. *Proceedings of the Ocean Drilling Program, Scientific Results* **181**: 1-111.

Carter, R. M., McCave, I. N., Richter, C. and Carter, L. (1999). Proceedings of the Ocean Drilling Program, Initial Reports, Ocean Drilling Program. **181:** 80.

Cavalier-Smith, T. (1998). A revised six-kingdom system of life. *Biological Reviews of the Cambridge Philosophical Society* **73**: 203-266.

Cookson, I. C. and Eisenack, A. (1961). Tertiary microplankton from the Rottest Island Bore, Western Australia. *Journal of the Royal Society of Australia* **44**: 39-47.

Cookson, I. C. and Eisenack, A. (1965). Microplankton from the Browns Creek Clays, SW Victoria. *Proceedings of the Royal Society of Victoria* **79**: 119-131.

Coxall, H. K. and Pearson, P. N. (2006). Taxonomy, biostratigraphy and phylogeny of Hantkeninidae (Clavigerinella, Hantkenina and Cribrohantkenina). *Atlas of Eocene Planktonic*

Foraminifera. Pearson, P. N., Olsson, R. K., Huber, B. T., Hemleben, C. and Berggren, W. A., Cushman Foundation for Foraminiferal Research: 213-252.

Coxall, H. K., Wilson, P. A., Pälike, H., Lear, C. H. and Backman, J. (2005). Rapid stepwise onset of Antarctic glaciation and deeper calcite compensation in the Pacific Ocean. *Nature* **433**: 53-57.

Crouch, E. M. (2001). *Environmental change at the time of the Paleocene-Eocene biotic turnover*.

Crouch, E. M. and Brinkhuis, H. (2005). Environmental change across the Paleocene-Eocene transition from eastern New Zealand: A marine palynological approach. *Marine Micropaleontology* **56**: 138-160.

Crowley, T. J. (1998). Significance of Tectonic Boundary Conditions for Paleoclimate Simulations. *Tectonic Boundary Conditions for Climate Reconstructions*. Crowley, T. J. and Burke, K. C.: 3-17.

Crowley, T. J. and North, G. R. (1991). *Paleoclimatology*. Oxford, United Kingdom, Oxford University Press.

Crowley, T. J. and Zachos, J. C. (2000). Comparison of zonal temperature profiles for past warm periods. *Warm Climates in Earth History*. Huber, B. T., MacLeod, K. G. and L, W. S., Cambridge University Press: 50-77.

Curry, W. B. and Lohmann, G. P. (1983). Reduced advection into atlantic Ocean deep eastern basins during the last glaciation maximum. *Nature* **306**: 577 - 580.

Curtis, C. D. (1990). Aspects of climatic influence on the clay mineralogy and geochemistry of soils, palaeosols and clastic sedimentary rocks. *Journal of the Geological Society of London* **147**(2): 351-357.

Cushman, J. A. and Bermúdez, P. J. (1949). Some Cuban Species of *Globorotalia*. *Contributions from the Cushman Laboratory Foraminiferal Research* **25**: 26-46.

D'Hondt, S. and Arthur, M. A. (1996). Late Cretaceous oceans and the cool tropic paradox. *Science* **271**: 1838-1842.

Davey, R. J. and Williams, G. L. (1966). The genus *Hystrichosphearidium* and it's allies. *Studies on Mesozoic and Cainozoic dinoflagellate cysts*. Davey, R. J., Downie, C., Sarjeant, W. A. S. and Williams, G. L.: 53 - 106.

De La Rocha, C. L., Brzezinski, M. A., DeNiro, M. J. and Shemesh, A. (1998). Silicon-isotope composition of diatoms as an indicator of past oceanic change. *Nature* **395**: 680-683.

de Villiers, S. (2004). Optimum growth conditions as opposed to calcite saturation as a control on the calcification rate and shell-weight of marine foraminifera. *Marine Biology* **144**(1): 45-49.

de Villiers, S., Greaves, M. and Elderfield, H. (2002). An intensity ratio callibration method for the accurate determination of Mg/Ca and Sr/Ca of marine carbonates by ICP-AES. *Geochemistry, Geophysics, Geosystems* **3**: 14.

DeConto, R. M. and Pollard, D. (2003). Rapid Cenozoic glaciation of Antarctica induced by declining atmospheric CO_2. *Nature* **421**: 245-249.

Deflandre, G. and Cookson, I. C. (1955). Fossil microplankton from Australian and Late Mesozoic and Tertiary sediments. *Australian journal of marine and freshwater research* **6**: 242 - 313.

Demicco, R. V., Lowenstein, T. K. and Hardie, L. A. (2003). Atmospheric pCO_2 since 60Ma from records of seawater pH, calcium and primary carbonate mineralogy. *Geology* **31**(9): 793-796.

Dennison, J. M. and Hay, W. W. (1967). Estimating the needed sampling area for subaquatic ecologic studies. *Journal of Paleontology* **41**: 706-708.

Dickens, G. R., O'Neil, J. R., Rea, D. K. and Owen, R. M. (1995). Dissociation of oceanic methane hydrate as a cause of the carbon isotope excursion at the end of the Paleocene. *Paleoceanography* **10**(6): 965-972.

Diester-Haass, L. and Zahn, R. (1996). Eocene-Oligocene transition in the Southern Ocean: History of water mass circulation and biological productivity. *Geology* **24**: 163-166.

Dodge, J. D. and Lee, J. J. (2000). Pylum Dinoflagellata. *An Illustrated Guide to the Protozoa.* Lee, J. J., Leedale, G. F. and Bradbury, P. Lawrence, Kansas, Society of Protozoologists. **1:** 656-689.

Duplessy, J.-C., Labeyrie, L., Juillet-Leclerc, A., Maitre, F., Duprat, J. and Sarnthein, M. (1991). Surface salinity reconstruction of the North Atlantic Ocean during the last glacial maximum. *Oceanologica Acta* **14**(4): 311-324.

Edgar, K. M., Wilson, P. A., Sexton, P. F. and Suganuma, Y. (2007). No extreme bipolar glaciation during the main Eocene calcite compensation shift. *Nature* **448**: 908-911.

Ehrenberg, C. G. (1838). Über das Massenverhältniss der jezt lebenden Kiesel-Infusorien und über ein neues Infusorien-Conglomerat als Polirschiefer von Jastraba in Ungarn. *Abhandlungen der Preussischen Akademie der Wissenschaften 1838*: 109-135.

Ehrmann, W. U. and Mackensen, A. (1992). Sedimentological evidence for the formation of an East Antarctic ice sheet in Eocene/Oligocene time. *Palaeogeography, Palaeoclimatology, Palaeoecology* **93**: 85-112.

Eichwald, E. v. (1830). *Zoologica Specialis.*

Eisenack, A. (1938). Die Phosphoritknollen der Bernsteinformation als Überlieferer Tertiären Planktons. *Schriften der Physsikalischökonomischen Gesellschaft zu Königsberg* **70**: 181-188.

Eisenack, A. (1964). *Katalog der fossilen Dinoflagellaten, Hystrichosphären and verwandten Mikrofossilien: Band I Dinoflagellaten.* Stuttgart, E. Schweizerbart'sche Verlagsbuchhandlung.

El-Naggar, Z. R. (1971). On the classification, evolutionand stratigraphical distribution of the Globerinacea. *Proceedings II Planktonic Conference.* Farinacci, A. Rome, Edizioni Tecnoscienza. **1:** 421-476.

Elderfield, H. and Ganssen, G. (2000). Past temperature and $\delta^{18}O$ of surface ocean waters and inferred from foraminiferal Mg/Ca ratios. *Nature* **405**: 442-445.

Eldrett, J. S., Harding, I. C., Wilson, P. A., Butler, E. and Roberts, A. P. (2007). Continental ice in Greenland during the Eocene and Oligocene. *Nature* **446**: 176-179.

Emiliani, C. (1954). Depth habitats of some species of pelagic foraminifera as indicated by oxygen isotope ratios. *American Journal of Science* **252**: 149-158.

Emiliani, C. (1955). Pleistocene temperatures. *Journal of Geology* **63**: 538-578.

Epstein, S., Buchsbaum, R., Lowenstam, H. A. and Urey, H. C. (1951). Carbonate-water isotopic temperature scale. *Geological Society of America Bulletin* **63**: 417-426.

Erez, J. and Luz, B. (1983). Experimental paleotemperature equation for planktonic foraminifera. *Geochemica et Cosmochemica Acta* **47**: 1025-1031.

Evitt, W. R. (1985). *Sporopollenin Dinoflgellate Cysts: Their Morphology and Interpretation.* Texas, The American Association of Stratigraphic Palynologists.

Exon, N. F., Kennett, J. P. and Malone, M. J. (2004). Leg 189 synthesis: Cretaceous-Holocene history of the Tasmanian Gateway. *Proceedings of the Ocean Drilling Programme, Scientific Results 189.* Exon, N. F., Kennett, J. P. and Malone, M. J. **189:** 1-37.

Falkowski, P. G., Katz, M. E., Miligan, A. J., Fennel, K., Cramer, B. S., et al. (2005). The rise of oxygen over the last 205 million years and the evolution of large placental mammals. *Science* **30**: 2202-2204.

Fensome, R. A., Taylor, F. J. R., Norris, G., Sarjeant, W. A. S., Wharton, D. I. and Williams, G. L. (1993). *A classification of fossil and living dinoflagellates*, Micropaleontology Press.

Finlay, H. J. (1939a). New Zealand Foraminifera: Key Species in Stratigraphy - No. 2. *Transactions of the Royal Society of New Zealand* **69**(1): 89-128.

Finlay, H. J. (1939b). New Zealand Foraminifera: The Occurence of *Rzehakina*, *Hantkenina*, *Rotaliatina*, and *Zeauvigerina*. *Transactions of the Royal Society of New Zealand* **68**: 534-538.

Firth, J. V. (1996). Upper Middle Eocene to Oligocene dinoflagellate biostratigraphy and assemblage variations in hole 913B, Greenland Sea. *Proceedings of the Ocean Drilling Program, Scientific Results*. Thiede, J., Myrhe, A. M., Firth, J. V., Johnson, G. L. and Ruddiman, W. F.: 203-242.

Frakes, L. A., Francis, J. E. and Syktus, J. L. (1992). *Climate modes of the Phanerozoic*. Cambridge, United Kingdom, Cambridge University Press.

Galeotti, S., Coccioni, R. and Gersonde, R. (2002). Middle Eocene-Early Pliocene Subantarctic planktic foraminiferal biostratigraphy of Site 1090, Aghulas Ridge. *Marine Micropaleontology* **45**: 357-381.

Gersonde, R., Hodell, D. A., Blum, P. and al, e. (1999). Leg 177 Summary: Southern Ocean Paleoceanography. *Proceedings of the Ocean Crilling Program, Initial Reports*. **177**.

Gibson, T. G. (1989). Planktonic Benthonic Foraminiferal Ratios: Modern Patterns and Tertiary Applicability. *Marine Micropaleontology* **15**: 29 - 52.

Greenwood, D. R. and Wing, S. L. (1995). Eocene continental climates and latitudinal temperature gradients. *Geology* **23**: 1044-1048.

Hall, I. R., McCave, I. N., Zahn, R., Carter, L., Knutz, P. C. and Weedon, G. P. (2003). Paleocurrent reconstruction of the deep Pacific inflow during the middle Miocene: Reflections of East Antarctic Ice Sheet growth. *Paleoceanography* **18**(2).

Handley, L. (2008). Biomarkers and isotopes as means of studying Paleogene climate change. *Organic Geochemistry Unit, Bristol Biogeochemistry Research Centre, School of Chemistry*. Bristol, University of Bristol. **PhD**.

Hays, J. D., Imbrie, J. and Shackleton, N. J. (1976). Variations in the Earth's Orbit: Pacemaker of the Ice Ages. *Science* **194**(4270): 1121-1132.

Hayward, B. W., Grenfell, H. R., Carter, R. M. and Hayward, J. J. (2004). Benthic foraminiferal proxy evidence for the Neogene palaeoceanographic history of the Southwest Pacific, east of New Zealand. *Marine Geology* **205**: 147-184.

Hemleben, C. and Olsson, R. K. (2006). Wall textures of Eocene planktonic foraminifera. *The Eocene Atlas of Planktonic Foraminifera.* Pearson, P. N., Olsson, R. K., Huber, B. T., Hemleben, C. and Berggren, W. A., The Cushman Foundation: 47-66.

Hemleben, C., Spindler, M. and Anderson, O. R. (1989). *Modern Planktonic Foraminifera.* New York, Springer-Verlag.

Hemming, N. G. and Hanson, G. N. (1992). Boron isotopic composition in modern marine carbonates. *Geochimica et Cosmochimica Acta* **56**: 537-543.

Henderson, G. M. (2002). New oceanic proxies for paleoclimate. *Earth and Planetary Sciences Letters* **203**: 1-13.

Herbert, T. D. (1997). A long marine history of carbon cycle modulation by orbital-climatic changes. *Proceedings of the National Academy of Science* **94**: 8362-8369.

Hodell, D. A., Gersonde, R. and Blum, P. (2002). Leg 177 synthesis: insights into Southern Ocean paleoceanography on tectonic to millenial timescales. *Proceedings of the Ocean Drillling Program, Scientific Results*. Gersonde, R., Hodell, D. A. and Blum, P. **177:** 1-54.

Hofker, J. (1976). La famillie Turborotalitidae. *Revue de Micropaléontologie* **19**: 47-53.

Hollis, C. J., Dickens, G. R., Field, B. D., Jones, C. M. and Strong, C. P. (2005). The Paleocene-Eocene transition at Mead Stream, New Zealand: a southern Pacific record of early Cenozoic global change. *Palaeogeography, Palaeoclimatology, Palaeoecology* **215**: 313-343.

Hopmans, E. C., Weijers, J. W. H., Schefuß, E., Herfort, L., Sinninghe Damste, J. S. and Schouten, S. (2004). A novel proxy for terrestrial organic matter in sediments based on branched and isoprenoid tetraether lipids. *Earth and Planetary Sciences Letters* **224**: 107-116.

Hornibrook, N. d. B., Brazier, R. C. and Strong, C. P. (1989). *Manual of New Zealand Permian to Pleistocene Foraminiferal Biostratigraphy*, New Zealand Geological Survey.

Huber, B. T., Hodell, D. A. and Hamilton, C. P. (1995). Middle-Late Cretaceous climate of the southern high latitudes: Stable isotopic evidence for minimal equator-to-pole thermal gradients. *Geological Society of America Bulletin* **107**: 1164-1191.

Huber, B. T. and Quillévéré, F. (2005). Revised Paleogene planktonic foraminiferal biozonation for the Austral Realm. *Journal of Foraminiferal Research* **35**: 219-314.

Huber, B. T. and Quillévéré, F. (2006). A revised Paleogene planktonic foraminiferal biozonation for the Austral Realm. *Atlas of Eocene Planktonic Foraminifera*. Pearson, P. N., Olsson, R. K., Huber, B. T., Hemleben, C. and Berggren, W. A., Cushman Foundation For Foraminiferal Research. **41:** 41-46.

Huber, M., Brinkhuis, H., Stickley, C. E., Döös, K., Sluijs, A., et al. (2004). Eocene circulation of the Southern Ocean: Was Antarctica kept warm by subtropical waters? *Paleoceanography* **19**: PA4026, doi:10.1029/2004PA001014.

Huber, M. and Nof, D. (2006). The ocean circulation in the southern hemisphere and it's climatic impacts in the Eocene. *Palaeogeography, Palaeoclimatology, Palaeoecology* **231**: 9-28.

Huber, M. and Sloan, L. C. (2001). Heat transport, deep waters, and thermal gradients: Coupled simulation of an Eocene Greenhouse Climate. *Geophysical Research Letters* **28**: 3481-3484.

Hurley, J. V. and Fluegeman, R. H. (2003). Late Middle Eocene Glacioeustasy: Stable Isotopes and Foraminifera from the Gulf Coastal Plain. *From Greenhouse to Icehouse: The Marine Eocene-Oligocene Transition*. Prothero, D. R., Ivany, L. C. and Nesbitt, E. A. New York, Columbia University Press: 223-231.

Imbrie, J. and Kipp, N. J. (1971). A new micropaleontological method for quantitaive paleoclimatology: Application to a late Pleistocene Caribbean core. *The late Cenozoic glacial ages*. Turekian, K. K. New Haven, Conneticutt, Yale University Press: 71-181.

Jenkins, D. G. (1971). *New Zealand Cenozoic Planktonic Foraminifera*, New Zealand Geological Survey.

Jenkins, D. G. (1993). The Evolution of Cenozoic southern high- and mid-latitude planktonic foraminiferal faunas. *The Antarctic Paleoenvironment: A Perspective on Global Change*. Kennett, J. P. and Warnke, D. A. Washington, DC, American Geophysical Union. **60:** 175-194.

Jovane, L., Floridino, F., Coccioni, R., Dinar, S., Turell, J., et al. (2007). The middle Eocene climatic optimum event in the Contessa Highway section, Umbrian Apennines, Italy. *Geological Society of America Bulletin* **119**: 413-427.

Jovane, L., Floridino, F., Sprovieri, M. and Pälike, H. (2006). Astronomic calibration of the late Eocene/early Oligocene Massignano section (central Italy). *Geochemistry, Geophysics, Geosystems* **7**(7): 10.

Kaiho, K. (1994). Benthic foraminiferal dissolved-oxygen index and dissolved-oxygen levels in the modern ocean. *Geology* **22**: 719-722.

Katz, M. E., Katz, D. R., Wright, J. D., Miller, K. G., Pak, D. K., et al. (2003). Early Cenozoic benthic foraminiferal isotopes: Species reliability and interspecies correction factors. *Paleoceanography* **18**: 10.1029/2002PA000798.

Kennett, J. P., Houtz, R. E., Andrews, P. B., Edwards, A. R., Gostin, V. A., et al. (1975). Cenozoic paleoceanography in the southwest Pacific Ocean, Antarctic glaciation, and the development of the Circum-Antarctic Current. *Initial Reports of the Deep Sea Drilling Project* **29**: 1155-1169.

Kennett, J. P. and Stott, L. D. (1991). Abrupt deep-sea warming, palaeoceanographic changes and benthic extinctions at the end of the Palaeocene. *Nature* **353**: 225-229.

Kershaw, S. (2000). *Oceanography: An Earth Science Perspective*. Cheltenham, Stanley Thornes.

Kim, J.-H., Schouten, S., Buscali, R., Ludwig, W., Bonnin, J., et al. (2006). Origin and distribution of terrestrial organic matter in the NW Mediterranean (Gulf of Lions): Exploring the newly developed BIT index. *Geochemistry, Geophysics, Geosystems* **7**: Q117017.

Kim, J. H., Schouten, S., Hopmans, E. C., Donner, B. and Sinninghe Damste, J. S. (2008). Global sediment core-top calibration of the TEX_{86} paleothermometer in the ocean *Geochimica et Cosmochimica Acta* **72**(4): 1154-1173.

Kim, S.-T. and O'Neil, J. R. (1997). Equilibrium and nonequilibrium oxygen isotope effects in synthetic carbonates. *Geochimica et Cosmochimica Acta* **61**(16): 3461-3475.

King, P. R. (2000). Tectonic Reconstructions of New Zealand: 40Ma to the Present. *New Zealand Journal of Geology and Geophysics* **43**: 611-638.

King, P. R., Naish, T. R., Browne, G. H., Field, B. D. and Edbrooke, S. W. (1999). Cretaceous to Recent sedimentary patterns in New Zealand. *Institute of Geological & Nuclear Sciences folio series 1*. Lower Hutt, Institute of Geological & Nuclear Sciences: 35p, 1 enclosure.

Klumpp, B. (1953). Beitrag zur Kenntnis der Mikrofossilien des mittleren und oberen Eozän. *Palaeontographica Abteilung A* **103**: 377-406.

Kominz, M. A., Miller, K. G. and Browning, J. V. (1998). Long-term and short-term global Cenozoic sea-level estimates. *Geology* **26**(4): 311-314.

Kroon, D. and Zachos, J. C. (2007). Leg 208 synthesis: Cenozoic climate cycles and excursions. *Proceedings of the Ocean Drilling Program, Scientific Results* **208**: 1-55.

Kroopnick, P. M. (1985). The distribution of ^{13}C of CO 2 in the world oceans *Deep Sea Research* **32**(1): 57-84.

Kump, L. R. and Pollard, D. (2008). Amplification of Cretaceous Warmth by Biological Cloud Feedbacks. *Science* **320**: 195.

Laskar, J., Robutel, R., F, J., Gastineau, M., Correia, A. C. M. and Levrard, B. (2004). A long-term numerical solution for the insolation quantities of the Earth. *Astronomy and Astrophysics* **428**: 261-285.

Lea, D. W., Mashiotta, T. A. and Spero, H. J. (1999). Controls on magnesium and strontium uptake in planktonic foraminifera determined by live culturing. *Geochimica et Cosmochimica Acta* **63**(16): 2369-2379.

Lear, C. H. (2007). Mg/Ca palaeothermometry: a new windown into Cenozoic climate change. *Deep-Time Perspectives on Climate Change: Marrying the Signal from Computer Models and Biological Proxies*. Williams, M., Haywood, A. M., Gregory, F. J. and Schmidt, D. N. London, The Micropalaeontological Society: 313-322.

Lear, C. H., Bailey, T. R., Pearson, P. N., Coxall, H. K. and Rosenthal, Y. (2008). Cooling and ice growth across the Eocene-Oligocene transition. *Geology* **36**(3): 251-254.

Lear, C. H., Elderfield, H. and Wilson, P. A. (2000). Cenozoic Deep-SeaTemperatures and Global Ice Volumes from Mg/Ca in Benthic Foraminiferal Calcite. *Science* **287**: 269-272.

Lear, C. H., Rosenthal, Y. and Slowey, N. (2002). Benthic foraminiferal Mg/Ca-paleothermometry: A revised core-top calibration. *Geochimica et Cosmochimica Acta* **66**(19): 3375-3387.

Lee, J. J., Pawlowski, J., Debenay, J.-P., Whittaker, J., Banner, F., et al. (2000). Phylum Granuloreticulosa. *An Illustrated Guide to the Protozoa*. Lee, J. J., Leedale, G. F. and Bradbury, P. Lawrence, Kansas, Society of Protozoologists. **2:** 875-951.

Leeder, M. (1999). *Sedimentology and Sedimentary Basins: From Turbulence to Tectonics*. Oxford, Blackwell Science.

Lipps, J. H., Berger, W. H., Buzas, M. A., Douglas, R. G. and Ross, C. A., Eds. (1979). *Foraminiferal Ecology and Paleoecology*. SEPM Short Course. Houston, Society of Economic Paleontologists and Mineralogists.

Locarnini, R. A., Mishonov, A. V., Antonov, J. I., Boyer, T. P. and Garcia, H. E. (2006, 25 Sept 2007). World Ocean Atlas 2005, Volume 1: Temperature. *NOAA Atlas NESDIS 61* Retrieved 31/03/2008, 2008, from http://iridl.ldeo.columbia.edu/SOURCES/.NOAA/.NODC/.WOA05/.Grid-1x1/.Monthly/.an/.temperature/.

Loeblich, A. R. J. and Tappan, H. (1961). Suprageneric classification of the Rhizopodea. *Journal of Paleontology* **35**: 245-250.

Loeblich, A. R. J. and Tappan, H. (1964). Part C. Protista 2. Chiefly "Thecamoebians" and Foraminiferida. *Treatise on Invertebrate Palaeontology*. Moore, R. C. Lawrence, Kansas, The Geological Society of America and University of Kansas Press: 900.

Loeblich, A. R. J. and Tappan, H. (1988). *Foraminiferal genera and their classification*. New York, Van Nostrand Reinhold.

Lourens, L. J., Sluijs, A., Kroon, D., Zachos, J. C., Thomas, E., et al. (2005). Astronomical pacing of late Palaeocene to early Eocene global warming events. *Nature* **435**: 1083-1087.

Lowenstein, T. K. and Demicco, R. V. (2006). Elevated Eocene atmospheric CO_2 and its subsequent decline. *Science* **313**: 1928-1929.

Lüthi, D., Le Floch, M., Bereiter, B., Blunier, T., Barnola, J.-M., et al. (2008). High-resolution carbon dioxide concentration record 650,000–800,000 years before present. *Nature* **453**: 379-381.

Lyle, M., Barron, J., Bralower, T. J., Huber, M., Lyle, A. O., et al. (2008). Pacific Ocean and Cenozoic Evolution of Climate. *Reviews of Geophysics* **46**: 47.

Mackensen, A. and Ehrmann, W. U. (1992). Middle Eocene through Early Oligocene climate history and paleoceanography in the Southern Ocean: Stable oxygen and carbon isotopes from ODP Sites on Maud Rise and Kerguelen Plateau. *Marine Geology* **108**: 1-27.

Magurran, A. E. (2004). *Measuring Biological Diversity*, Blackwell.

Malmgren, B. A., Kucera, M., Nyberg, J. and Waelbroeck, C. (2001). Comparison of statistical and artificial neural network techniques for estimating past sea surface temperatures from planktonic foraminifer census data. *Paleoceanography* **16**: 1-11.

Martini, E. (1971). *Standard Tertiary and Quaternary calcareous nannoplankton zonation*. Proceedings II Planktonic Conference, Roma 1970, Edizioni Tecnoscienza.

Mashiotta, T. A., Lea, D. W. and Spero, H. J. (1999). Glacial-interglacial changes in Subantarctic sea surface temperature and δ^{18}O-water using foraminiferal Mg. *Earth and Planetary Sciences Letters* **170**: 417-432.

McCave, I. N., Manighetti, B. and Robinson, S. G. (1995). Sortable silt and fine sediment size/composition slicing: Parameters for palaeocurrent speed and palaeoceanography. *Paleoceanography* **10**: 593-610.

McElwain, J. C. (1998). Do fossil plants signal palaeoatmospheric CO_2 concentration in the geological past. *Philosophical Transactions of the Royal Society of London, B* **353**: 83-96.

McMillan, S. G. (1999). Geology of Northeast Otago: Hampden (J42) and Palmerston (J43). *Institute of Geological & Nuclear Sciences science report.* Dunedin, Institute of Geological & Nuclear Sciences: 2 sheets + 55 p.

McSaveney, E. and Nathan, S. (2007, 21 September 2007). Geology - overview. *Te Ara - the Encyclopedia of New Zealand* Retrieved 28 February, 2008, from http://www.TeAra.govt.nz/EarthSeaAndSky/Geology/GeologyOverview/en

Milankovitch, M. (1941). *Canon of Insolation of the Earth and its Application to the Problem of the Ice-Ages*. Belgrade, Yugoslavia, Royal Serbian Academy.

Miller, K. G., Fairbanks, R. G. and Mountain, G. S. (1987). Tertiary oxygen isotope synthesis, sea level history, and continental margin erosion. *Paleoceanography* **2**: 1-19.

Miller, K. G., Wright, J. D. and Fairbanks, R. G. (1991). Unlocking the Ice House: Oligocene-Miocene Oxygn Isotopes, Eustasy and Margin Erosion. *Journal of Geophysical Research* **96**(B4): 6829-6848.

Morgans, H. E. (2004). Paleogene (Dannevirke, Arnold and Landon Series). *The New Zealand Geological Timescale*. Cooper, R. A., Institute of Geological and Nuclear Sciences: 125-161.

Morgans, H. E. G. (2008). Late Paleocene - Middle Eocene stratigraphy, foraminiferal biostratigraphy and status of the Bortonian Stage lectostratotype at Moeraki-Hampden coastal section, eastern South Island, New Zealand. *New Zealand Journal of Geology and Geophysics* **in press**.

Mountain, G. S. and Miller, K. G. (1992). Seismic and geologic evidence for early Paleogene deepwater circulation in the western north Atlantic. *Paleoceanography* 7(4): 423-439.

Murphy, M. G. and Kennett, J. P. (1985). Development of latitudinal thermal gradients during the Oligocene: Oxygen-isotope evidence from the southwest Pacific. *Initial Reports of the Deep*

Sea Drilling Program. Kennett, J. P. and von der Borch, C. C. Washington, US Government Printing Office. **90:** 1347-1360.

Murray, J. W. (1973). *Distribution and Ecology of Living Benthic Foraminiferids*. London, Heinemann Educational Books.

Naish, T. R., Woolfe, K. J., Barrett, P. J., Wilson, G. S., Atkins, C., et al. (2001). Orbitally induced oscillations in the East Antarctic ice sheet at the Oligocene/Miocene boundary. *Nature* **413**: 719-723.

Nelson, C. S. and Cooke, P. J. (2001). History of oceanic front development in the New Zealand sector of the Southern Ocean during the Cenozoic - a synthesis. *New Zealand Journal of Geology and Geophysics* **44**: 535-553.

Nicolo, M. J., Dickens, G. R., Hollis, C. J. and Zachos, J. C. (2007). Multiple early Eocene hyperthermals: Their sedimentary expression on the New Zealand continental margin and in the deep sea. *Geology* **35**(8): 699-702.

Norris, R. D. and Wilson, P. A. (1998). Low-latitude sea-surface temperatures for the mid-Cretaceous and the evolution of planktic foraminifera. *Geology* **29**(9): 823-826.

Nürnberg, D., Buma, J. and Hemleben, C. (1996). Assessing the reliability of magnesium in foraminiferal calcite as a proxy for water mass temperatures. *Geochimica et Cosmochimica Acta* **60**(5): 803-814.

Okada, H. and Bukry, D. (1980). Supplementary modification and introduction of code numbers to the low-latitude coccolith biostratigraphic zonation (Bukry, 1973; 1975). *Marine Micropaleontology* **5**: 321-324.

Olsson, R. K., Hemleben, C., Huber, B. T. and Berggren, W. A. (2006a). Taxonomy, biostratigraphy, and phylogeny of Eocene *Globigerina, Globoturborotalita, Subbotina*, and *Turborotalita*. *Atlas of Eocene Planktonic Foraminifera*. Pearson, P. N., Olsson, R. K., Huber, B. T., Hemleben, C. and Berggren, W. A., Cushman Foundation For Foraminiferal Research. **41:** 111-168.

Olsson, R. K., Pearson, P. N. and Huber, B. T. (2006b). Taxonomy, biostratigraphy, and phylogeny of Eocene *Catapsydrax, Globorotaloides, Guembelitrioides, Paragloborotalia, Parasubbotina* and *Pseudoglobigerinella* N. Gen. *Atlas of Eocene Planktonic Foraminifera*. Pearson, P. N., Olsson, R. K., Huber, B. T., Hemleben, C. and Berggren, W. A., Cushman Foundation For Foraminiferal Research. **41:** 67-110.

Pagani, M., Zachos, J. C., Freeman, K. H., Tipple, B. and Bohaty, S. M. (2005). Marked decline in Atmospheric Carbon Dioxide Concentrations During the Paleogene. *Science* **309**: 600-603.

Pak, D. K. and Miller, K. G. (1992). Paleocene to Eocene bethic foraminiferal isotopes and assemblages: Implications for deepwater circulation. *Paleoceanography* **7**: 405-422.

Pälike, H., Norris, R. D., Herrle, J., O, Wilson, P. A., Coxall, H. K., et al. (2006). The Heartbeat of the Oligocene Climate System. *Science* **314**: 1894-1898.

Pälike, H., Spofforth, D. J. A., O'Regan, M. and Gattacceca, J. (2008). Orbital scale variations and timescales from the Arctic Ocean. *Paleoceanography* **23**: 13.

Park, J., D'Hondt, S. L., King, J. W. and Gibson, C. (1993). Late Cretaceous precessional cycles in double time: a warm-Earth Milankovitch response. *Science* **261**: 1431-1435.

Pearson, P. N. and Burgess, C. E. (2008). Foraminifer shell preservation and diagenesis: comparison of high latitude Eocene sites. *Biogeochemical Controls on Palaeoceanographic Proxies.* Austin, W. A., Geological Society of London. **(in press)**.

Pearson, P. N., Ditchfield, P. W., Singano, J., Harcourt-Brown, K. G., Nicholas, C. J., et al. (2001). Warm tropical sea surface temperatures in the Late Cretaceous and Eocene epochs. *Nature* **413**: 481-487.

Pearson, P. N., Olsson, R. K., Huber, B. T., Hemleben, C. and Berggren, W. A., Eds. (2006a). *Atlas of Eocene Planktonic Foraminifera.* Special Publication, Cushman Foundation For Foraminiferal Research.

Pearson, P. N. and Palmer, M. R. (1999). Middle Eocene Seawater pH and Atmospheric Carbon Dioxide Concentrations. *Science* **284**: 1824-1826.

Pearson, P. N. and Palmer, M. R. (2000). Atmospheric carbon dioxide concentrations over the past 60 million years. *Nature* **406**: 695-699.

Pearson, P. N., Premec-Fucek, V. and Premoli Silva, I. (2006b). Taxonomy, biostratigraphy, and phylogeny of Eocene Turborotalia. *Atlas of Eocene Planktonic Foraminifera.* Pearson, P. N., Olsson, R. K., Huber, B. T., Hemleben, C. and Berggren, W. A., Cushman Foundation For Foraminiferal Research. **41:** 433-460.

Pearson, P. N., Shackleton, N. J. and Hall, M. A. (1993). Stable isotope paleoecology of Middle Eocene planktonic Foraminifera and multi-species isotope stratigraphy, DSDP Site 523, South Atlantic. *Journal of Foraminiferal Research* **23**: 123-140.

Pearson, P. N., van Dongen, B. E., Nicholas, C. J., Pancost, R. D., Schouten, S., et al. (2007). Stable warm tropical climate through the Eocene Epoch. *Geology* **35**(3): 211-214.

Perch-Nielsen, K. (1985). Cenozoic calcareous nannofossils. *Plankton Stratigraphy*. Bolli, H. M., Saunders, J. B. and Perch-Nielsen, K. Cambridge, Cambridge University Press: 427-484.

Petit, J. R., Jouzel, J., Raynaud, D., Barkov, N. I., Barnola, J.-M., et al. (1999). Climate and atmospheric history of the past 420,000 years from the Vostok ice core, Antarctica. *Nature* **399**: 429-436.

Pfhul, H. A. and McCave, I. N. (2005). Evidence for late Oligocene establishment of the Antarctic Circumpolar Current. *Earth and Planetary Sciences Letters* **235**(3-4): 715-728.

Pospichal, J. J. and Wise, S. W. (1990). Paleocene to middle Eocene calcareous nannofossils of ODP sites 689 and 690, Maud Rise, Weddell Sea. *Proceedings of the Ocean Drilling Program, Scientific Results*. Barker, P. F. and Kennett, J. P. **113:** 613 - 638.

Premoli Silva, I., Wade, B. S. and Pearson, P. N. (2006). Taxonomy, biostratigraphy, and phylogeny of *Globigerinatheka* and *Orbulinoides*. *Atlas of Eocene Planktonic Foraminifera*. Pearson, P. N., Olsson, R. K., Huber, B. T., Hemleben, C. and Berggren, W. A., Cushman Foundation For Foraminiferal Research. **41:** 169-211.

Prentice, M. L. and Matthews, R. K. (1988). Cenozoic ice-volume history: Development of a composite oxygen isotope record. *Geology* **16**: 963-966.

Prothero, D. R., Ivany, L. C. and Nesbitt, E. A., Eds. (2003). *From greenhouse to icehouse: The marine Eocene-Oligocene transition*. New York, Columbia University Press.

Ramsey and al, e. (1994). Eocene-Quaternary Indian Ocean hiatuses. *Paleoceanography*: 857-877.

Reichart, G.-J. and Brinkhuis, H. (2003). Late Quaternary *Protoperidinium* cysts as indicators of paleoproductivity in the northern Arabian Sea. *Marine Micropaleontology* **49**(4): 303-370.

Robert, C. and Kennett, J. P. (1997). Antarctic continental weathering changes during Eocene-Oligocene cryosphere expansion: Clay mineral and oxygen isotope evidence. *Geology* **25**(7): 587-590.

Roehl, U., Brinkhuis, H., Fuller, M., Stickley, C. E., Warnaar, J. and Williams, G. L. (2002). *Cyclicity in Eocene Southern Ocean Sediments; Patterns From the Tasmanian Gateway, ODP 189, Site 1172*. American Geophysical Union, Fall Meeting 2002, American Geophysical Union.

Röhl, U., Westerhold, T., Monechi, S., Thomas, E., Zachos, J. C. and Donner, B. (2005). The third and final early Eocene thermal maximum: characteristics, timing, and mechanisms of the "X" event. *Geological Society of America Annual Meeting - Abstracts* **37**(7): 1.

Rosenthal, Y., Perron-Cashman, S., Lear, C. H., Bard, E., Barker, S., et al. (2004). Interlaboratory comparison study of Mg/Ca and Sr/Ca measurements in planktonic foraminifera for paleoceanographic research. *Geochemistry, Geophysics, Geosystems* **4**(4): 29.

Royer, D. L. (2006). CO2-forced climate thresholds during the Phanerozoic. *Geochimica et Cosmochimica Acta* **70**: 5665-5675.

Royer, D. L., Berner, R. A. and Beerling, D. J. (2001). Phanerozoic atmospheric CO_2 change: evaluating geochemical and paleobiological approaches. *Earth Science Reviews* **54**: 349-392.

Ruddiman, W. F. (2001). *Earth's Climate: Past and Future*. New York, WH Freeman and Company.

Sangiorgi, F., Brumsack, H.-J., Willard, D. A., Schouten, S., Stickley, C. E., et al. (2008a). A 26 million year gap in the central Arctic record at the greenhouse-icehouse transition: Looking for clues. *Paleoceanography* **23**(1).

Sangiorgi, F., van Soelen, E. E., Spofforth, D. J. A., Pälike, H., Stickley, C. E., et al. (2008b). Cyclicity in the middle Eocene central Arctic Ocean sediment record: Orbital forcing and evironmental response. *Paleoceanography* **23**: 14.

Schouten, S., Eldrett, J. S., Greenwood, D. R., Harding, I. C., Baas, M. and Sinninghe Damste, J. S. (2008). Onset of long-term cooling of Greenland near the Eocene-Oligocene boundary as revealed by branched tetraether lipids. *Geology* **36**(2): 147-150.

Schouten, S., Hopmans, E. C., Forster, A., Breugel, v., Kuypers, M. M. M. and Sinninghe Damste, J. S. (2003). Extremely high sea-surface temperatures at low latitudes durng the middle Cretaceous as revealed by archael membrane lipids. *Geology* **31**(12): 1069-1072.

Schouten, S., Hopmans, E. C., Schefuβ, E. and Sinninghe Damste, J. S. (2002). Distributional variations in marine crenarchaeotal membrane lipids: a new tool for reconstructing ancient sea water temperatures. *Earth and Planetary Sciences Letters* **204**: 265-274.

Schrag, D. P. (1999). Effects of diagenesis on the isotopic record of late paleogene tropical sea surface temperatures. *Chemical Geology* **161**: 215-224.

Schrag, D. P., DePaolo, D. J. and Richter, F. M. (1995). Reconstructing past sea surface temperatures: Correcting for diagenesis of bulk marine carbonate. *Geochimica et Cosmochimica Acta* **59**(11): 2265-2278.

Schröder-Adams, C. J. (1991). Middle Eocene to Holocene benthic foraminifer assemblages from the Kerguelen Plateau (Southern Indian Ocean). *Proceedings of the Ocean Drilling Program, Scientific Results*. Barron, J., Larsen, B. and al, e. **119:** 611-630.

Schulz, M. and Mudelsee, M. (2002). REDFIT: estimating red-noise spectra directly from unevenly spaced paleoclimatic time series. *Computers & Geosciences* **28**: 421-426.

Segar, D. A. (2007). *Introduction to ocean sciences*. New York, W. W. Norton & Company.

Sexton, P. F., Wilson, P. A. and Norris, R. D. (2006a). Testing the Cenozoic multisite composite $\delta^{18}O$ and $\delta^{18}C$ curves: New monospecific Eocene records from a single locality, Demerara Rise (Ocean Drilling Program Leg 207). *Paleoceanography* **21**: 17.

Sexton, P. F., Wilson, P. A. and Pearson, P. N. (2006b). Microstructural and geochemical perspectives on planktic foraminiferal preservation: "Glassy" vs "Frosty". *Geochemistry, Geophysics, Geosystems* 7(12): 1-29.

Shackleton, N. J. and Boersma, A. (1981). The climate of the Eocene ocean. *Journal of the Geological Society of London* **138**: 153-157.

Shackleton, N. J. and Kennett, J. P. (1975). Paleotemperature history of the Cenozoic and the initiation of Antarctic glaciation: oxygen and carbon isotope analyses in DSDP sites 277, 279 and 281. *Initial Reports of the Deep Sea Drilling Project* **29**: 743-755.

Sloan, L. C. and Pollard, D. (1998). Polar stratospheric clouds: A high latitude warming mechanism in an ancient greenhouse world. *Geophysical Research Letters* **25**(18): 3517-3520.

Sloan, L. C. and Rea, D. K. (1995). Atmospheric carbon dioxide and early Eocene climate: A general circulation modelling sensitivity study. *Palaeogeography, Palaeoclimatology, Palaeoecology* **119**: 275-292.

Sluijs, A., Pross, J. and Brinkhuis, H. (2004). From greenhouse to icehouse; organic-walled dinoflagellate cysts as paleoenvironmental indicators in the Paleogene. *Earth Science Reviews* **68**: 281-315.

Sluijs, A., Schouten, S., Pagani, M., Woltering, M., Brinkhuis, H., et al. (2006). Subtropical Arctic Ocean temperatures during the Palaeocene/Eocene thermal maximum. *Nature* **441**: 610-613.

Spero, H. J., Bijma, J., Lea, D. W. and Bemis, B. E. (1997). Effect of seawater carbonate concentration on foraminiferal carbon and oxygen isotopes. *Nature* **390**: 497-500.

Spivack, A. J., You, C.-F. and Smith, H. J. (1993). Foraminiferal boron isotope ratios as a proxy for surface ocean pH over the past 21 Myr. *Nature* **363**: 149-151.

Spofforth, D. J. A., Agnini, C., Pälike, H., Fornaciari, E., Giusberti, L., et al. (2008). *Evidence for the Middle Eocene Climatic Optimum ("MECO") in the Venetian Alps*. EGU General Assembly 2008, Vienna, European Geophysical Union.

Stott, L. D. and Kennett, J. P. (1990). Antarctic Paleogene Planktonic Foraminifer Biostratigraphy: ODP Leg 113, Sites 689 and 690. *Proceedings of the Ocean Drilling Program, Scientific Results* **113**: 549-569.

Stover, L. E. and Williams, G. L. (1995). A revision of the Paleogene dinoflagellate genera *Aerosphaeridium* Eaton 1971 and *Eatonicysta* Stover and Evitt 1978. *Micropaleontology* **41**(2): 97-141.

Subbotina, N. N. (1953). Isopaemye foraminifery SSSR (Globigerinidy, Khantkenininidy i Globorotaliidy). *Trudy Vsesoyznogo Nauchno-Issledovatel'skogo Geologo-razvedochnogo Instituta (VNIGRI)* **76**: 296.

Suggate, Stevens and Punga, Eds. (1978). *The Geology of New Zealand.* Wellington, Government Printer.

Thomas, D. J., Bralower, T. J. and Zachos, J. C. (1999). New evidence for subtropical warming during the late Paleocene thermal maximum: Stable isotopes from Deep Sea Drilling Project Site 527, Walvis Ridge. *Paleoceanography* **14**: 561-570.

Tripati, A., Backman, J., Elderfield, H. and Ferretti, P. (2005). Eocene bipolar glaciation associated with global carbon cycle changes. *Nature* **436**: 341-346.

Upchurch, G. R. and Wolfe, J. A. (1987). Mid-Cretaceous to Early Tertiary vegetation and climate: evidence from fossil leaves and woods. *The origins of Angiosperms and their biological consequences*. Fris, E. M. and al, e. Cambridge, Cambridge University Press: 75-106.

Urey, H. C. (1947). The thermodynamic properties of isotopic substances. *Journal of the Chemical Society*: 562-581.

Van der Zwaan, G. J., Duijnstee, I. A. P., den Dulk, M., Ernst, S. R., Jannink, N. T. and Kouwenhoven, T. J. (1999). Benthic foraminifers: proxies or problems? A review of paleocological concepts. *Earth Science Reviews* **46**: 213-236.

Wade, B. S. and Kroon, D. (2002). Middle Eocene regional climate instability: Evidence from the western North Atlantic. *Geology* **30**(11): 1011-1014.

Wade, B. S., Kroon, D. and Norris, R. D. (2001). Orbitally forced climate change in late mid-Eocene time at Blake Nose (Leg 171B): evidence from stable isotopes in foraminifera. *Western North Atlantic Palaeogene and Cretaceous Palaeoceanography*. Kroon, D., Norris, R. D. and Klaus, A. London, Geological Society of London. **183:** 273-291.

Waelbroeck, C., Labeyrie, L., Duplessy, J.-C., Guiot, J., Labracherie, M., et al. (1998). Improving past sea surface temperature estimates based on planktonic fossil faunas. *Paleoceanography* **13**: 272-283.

Warnaar, J. (2006). Climatological implications of Australian-Antarctic separation. *Laboratory of Palaeobotany and Palynology*, Utrecht University. **PhD:** 144.

Warnaar, J., Huber, M., Brinkhuis, H., Röhl, U., Sriver, R. and Visscher, H. (2006). Orbitally forced climatic changes in the Tasman sector during the middle Eocene. *Climatological implications of Australian-Antarctic separation*. Warnaar, J. Urecht, Ipskamp PrintPartners**:** 87-106.

Weedon, G. (2003). *Time Series Analysis and Cyclostratigraphy*, Cambridge University Press.

Weedon, G. P. (1986). Hemipelagic shelf sedimentation and climatic cycles: the basal Jurassic (Blue Lias) of South Britain. *Earth and Planetary Sciences Letters* **76**(3-4): 321-335.

Wei, W. (1992). Paleogene Chronology of Southern Ocean Drill Holes: An Update. *The Antarctic Paleoenvironment: A Perspective on Global Change*. Kennett, J. P. and Warnke, D. A. Washington D. C., American Geophysical Union. **1:** 75-96.

Weijers, J. W. H., Schouten, S., Sluijs, A., Brinkhuis, H. and Sinninghe Damste, J. S. (2007a). Warm arctic continents during the Palaeocene–Eocene thermal maximum. *Earth and Planetary Sciences Letters* **261**: 230-238.

Weijers, J. W. H., Schouten, S., van den Donker, J. C., Hopmans, E. C. and Sinninghe Damste, J. S. (2007b). Environmental controls on bacterial tetraether membrane lipid distribution in soils. *Geochimica et Cosmochimica Acta* **71**: 703-713.

White, R. E. (1987). *Introduction to the Principles and Practice of Soil Science*, Blackwell Scientific Publishing.

Wilkinson, B., H and Algeo, T., J (1989). Sedimentary Carbonate Record of Calcium - Magnesium Cycling. *American Journal of Science* **289**: 1158-1194.

Williams, G. L., Fensome, R. A., Brinkhuis, H. and Pross, J. (2006). The Paleobiology of Dinoflagellates. *A text revised for the Dinoflagellate Short Course in Urbino, July 2006*: 36.

Wilson, G. J. (1967a). Some new species of lower Tertiary dinoflagellates from McMurdo Sound, Antarctica. *New Zealand Journal of Botany* **5**: 57-83.

Wilson, G. J. (1967b). Some species of *Wetzeliella* Eisenack (Dinophyceae) from New Zealand Eocene and Paleocene strata. *New Zealand Journal of Botany* **5**: 469-497.

Wilson, G. J. (1988). *Paleocene and Eocene Dinoflagellate Cysts from Waipawa, Hawkes Bay, New Zealand.* Lower Hutt, New Zealand Geological Survey.

Wilson, P. A. and Norris, R. D. (2001). Warm tropical ocean surface and global anoxia during the mid-Cretaceous period. *Nature* **412**: 425-429.

Wilson, P. A., Norris, R. D. and Cooper, M. J. (2002). Testing the Cretaceous greenhouse hypothesis using glassy foraminiferal calcite from the core of the Turonian tropics on Demerara Rise. *Geology* **30**(7): 607-610.

Wise, S. W. J. (1983). Mesozoic and Cenozoic calcareous nannofossils recovered by Deep Sea Drilling Project Leg 71 in the Falkland Plateau region, Southwest Atlantic Ocean. *Initial Reports of the Deep Sea Drilling Project* **71**(2): 481-550.

Young, J. R., Bergen, J. A., Bown, P. R., Burnett, J. A., Fiorentino, A., et al. (1997). Guidelines for coccolith and calcareous nannofossil terminology. *Palaeontology* **40**(4): 875-912.

Young, J. R., Geisen, M., Cros, L., Kleijne, A., Sprengel, C., et al. (2003). A guide to extant coccolithophore taxonomy. *Journal of Nannoplankton Research* **1**(1): 1-125.

Yu, J., Elderfield, H., Greaves, M. and Day, J. (2007). Preferential dissolution of benthic foraminiferal calcite during laboratory reductive cleaning. *Geochemistry, Geophysics, Geosystems* **8**(6): 17.

Zachos, J. C., Arthur, M. A., Bralower, T. J. and Spero, H. J. (2002). Tropical temperatures in greenhouse episodes. *Nature* **419**: 897-898.

Zachos, J. C., Breza, J. R. and Wise, S. W. (1992). Early Oligocene ice-sheet expansion on Antarctica: Stable isotope and sedimentological evidence from Kergulen Plateau, Southern Ocean. *Geology* **20**: 569-573.

Zachos, J. C., Dickens, G. R. and Zeebe, R. E. (2008). An early Cenozoic perspective on greenhouse warming and carbon-cycle dynamics. *Nature* **451**: 279-283.

Zachos, J. C., Opdyke, B. N., Quinn, T. M., Jones, C. E. and Halliday, A. N. (1999). Early cenozoic glaciation, antarctic weathering, and seawater $^{87}Sr/^{86}Sr$: is there a link? *Chemical Geology* **161**: 165-180.

Zachos, J. C., Pagani, M., Sloan, L. C., Thomas, E. and Billups, K. (2001). Trends, Rhythms, and Aberrations in Global Climate 65 Ma to Present. *Science* **292**: 686-693.

Zachos, J. C., Quinn, T. M. and Salamy, K. A. (1996). High-resolution (10^4 years) deep-sea foraminiferal stable istope records of the Eocene-Oligocene climate transition. *Paleoceanography* **11**: 251-266.

Zachos, J. C., Stott, L. D. and Lohmann, K. C. (1994). Evolution of early Cenozoic marine temperatures. *Paleoceanography* **9**: 353-387.

Zeebe, R. E. and Zachos, J. C. (2007). Reversed deep-sea carbonate ion basin gradient during Paleocene-Eocene thermal maximum. *Paleoceanography* **22**: PA3201.

Appendix 1. Hampden Section sample record

New Zealand Geological Survey Fossil Record File locality numbers for Hampden Beach samples collected during 2005 field season and integrated stratigraphic column showing Hampden Beach samples curated by GNS Science.

SF	F Number	Field Number
Hugh Morgans (Hantkenina)		
J42/f436	F37359	HB09C
J42/f437	F37360	HB13A
J42/f438	F37361	HB13B
J42/f439	F37362	HB13C
J42/f440	F37363	HB13D
J42/f441	F37364	HB42F
J42/f442	F37365	HB47B
J42/f443	F37366	HB54B
J42/f444	F37367	HB55B
J42/f445	F37368	HB56B
J42/f446	F37369	HB57B
J42/f447	F37370	HB58B
J42/f448	F37371	HB59B
J42/f449	F37372	HB60B
J42/f450	F37373	HB61B
J42/f451	F37374	HB62B
J42/f452	F37375	HB63B
J42/f453	F37376	HB64B
J42/f454	F37377	HB65B
J42/f455	F37378	HB66B
J42/f456	F37379	HB67B
J42/f457	F37380	HB68B
J42/f458	F37381	HB69B
J42/f459	F37382	HB70B
J42/f460	F37383	HB71B
J42/f461	F37384	HB72B
J42/f462	F37385	HB73B
J42/f463	F37386	HB74B
J42/f464	F37387	HB75B
J42/f465	F37388	HB76B
J42/f466	F37389	HB77B
J42/f467	F37390	HB78B
J42/f468	F37391	HB79C
J42/f469	F37392	HB80B
J42/f470	F37393	HB81B
J42/f471	F37394	HB82B
J42/f472	F37395	HB84B
J42/f473	F37396	HB86B
J42/f474	F37397	HB87B
J42/f475	F37398	HB88B
J42/f476	F37399	HB89B
J42/f477	F37400	HB90B
J42/f478	F37401	HB91B
J42/f479	F37402	HB92B
J42/f480	F37403	HB93B
HEGM Kurinui/Hampden		
J42/f481	F37404	HB42G
J42/f482	F37405	HB42H
J42/f483	F37406	HB42I
J42/f484	F37407	HB42J
J42/f485	F37408	HB42K
J42/f486	F37409	HB42L
J42/f487	F37410	HB42M
J42/f488	F37411	HB42N
J42/f489	F37412	HB42O
Cat Burgess section 1 (locality 14)		
J42/f637	F37560	CB05HB450
J42/f636	F37559	CB05HB449
J42/f635	F37558	CB05HB448
J42/f634	F37557	CB05HB447
J42/f633	F37556	CB05HB446
J42/f632	F37555	CB05HB445
J42/f631	F37554	CB05HB444
J42/f630	F37553	CB05HB443
J42/f629	F37552	CB05HB442
J42/f628	F37551	CB05HB441
J42/f627	F37550	CB05HB440
J42/f626	F37549	CB05HB439
J42/f625	F37548	CB05HB438
J42/f624	F37547	CB05HB437
J42/f623	F37546	CB05HB436
J42/f622	F37545	CB05HB435
J42/f621	F37544	CB05HB434
J42/f620	F37543	CB05HB433
J42/f619	F37542	CB05HB432
J42/f618	F37541	CB05HB431
J42/f617	F37540	CB05HB430
J42/f616	F37539	CB05HB429
J42/f615	F37538	CB05HB428
Cat Burgess section 1 (locality 5)		
J42/f614	F37537	CB05HB098
J42/f613	F37536	CB05HB097
J42/f612	F37535	CB05HB096
J42/f611	F37534	CB05HB095
J42/f610	F37533	CB05HB094
J42/f609	F37532	CB05HB093
J42/f608	F37531	CB05HB092
J42/f607	F37530	CB05HB091
J42/f606	F37529	CB05HB090
J42/f605	F37528	CB05HB089
J42/f604	F37527	CB05HB088
J42/f603	F37526	CB05HB087
J42/f602	F37525	CB05HB086
J42/f601	F37524	CB05HB085
J42/f600	F37523	CB05HB084
J42/f599	F37522	CB05HB083
J42/f598	F37521	CB05HB082
J42/f597	F37520	CB05HB081
J42/f596	F37519	CB05HB080
J42/f595	F37518	CB05HB079
J42/f594	F37517	CB05HB078
J42/f593	F37516	CB05HB077
J42/f592	F37515	CB05HB076
J42/f591	F37514	CB05HB075
J42/f590	F37513	CB05HB074
J42/f589	F37512	CB05HB073
J42/f588	F37511	CB05HB072
J42/f587	F37510	CB05HB071
J42/f586	F37509	CB05HB070
J42/f585	F37508	CB05HB069
J42/f584	F37507	CB05HB068
J42/f583	F37506	CB05HB067
J42/f582	F37505	CB05HB066
J42/f581	F37504	CB05HB065
J42/f580	F37503	CB05HB064
J42/f579	F37502	CB05HB063
J42/f578	F37501	CB05HB062
J42/f577	F37500	CB05HB061
Location 4		
J42/f576	F37499	CB05HB060
J42/f575	F37498	CB05HB059
J42/f574	F37497	CB05HB058
J42/f573	F37496	CB05HB057
J42/f572	F37495	CB05HB056
J42/f571	F37494	CB05HB055
J42/f570	F37493	CB05HB054
J42/f569	F37492	CB05HB053
J42/f568	F37491	CB05HB052
J42/f567	F37490	CB05HB051
J42/f566	F37489	CB05HB050
J42/f565	F37488	CB05HB049
J42/f564	F37487	CB05HB048
J42/f563	F37486	CB05HB047
J42/f562	F37485	CB05HB046
J42/f561	F37484	CB05HB045
J42/f560	F37483	CB05HB044
J42/f559	F37482	CB05HB043
J42/f558	F37481	CB05HB042
J42/f557	F37480	CB05HB041
J42/f556	F37479	CB05HB040
J42/f555	F37478	CB05HB039
J42/f554	F37477	CB05HB038
J42/f553	F37476	CB05HB037
J42/f552	F37475	CB05HB036
J42/f551	F37474	CB05HB035
J42/f550	F37473	CB05HB034
J42/f549	F37472	CB05HB033
J42/f548	F37471	CB05HB032
J42/f547	F37470	CB05HB031
J42/f546	F37469	CB05HB030
J42/f545	F37468	CB05HB029
J42/f544	F37467	CB05HB028
J42/f543	F37466	CB05HB027
J42/f542	F37465	CB05HB026
J42/f541	F37464	CB05HB025
J42/f540	F37463	CB05HB024
J42/f539	F37462	CB05HB023
J42/f538	F37461	CB05HB022
J42/f537	F37460	CB05HB021

SF	F Number	Field Number
J42/f536	F37459	CB05HB020
J42/f535	F37458	CB05HB019
J42/f534	F37457	CB05HB018
J42/f533	F37456	CB05HB017
J42/f532	F37455	CB05HB016
J42/f531	F37454	CB05HB015
J42/f530	F37453	CB05HB014
J42/f529	F37452	CB05HB013
J42/f528	F37451	CB05HB012
J42/f527	F37450	CB05HB011
J42/f526	F37449	CB05HB010
J42/f525	F37448	CB05HB009
J42/f524	F37447	CB05HB008
J42/f523	F37446	CB05HB007
J42/f522	F37445	CB05HB006
J42/f521	F37444	CB05HB005
J42/f520	F37443	CB05HB004
J42/f519	F37442	CB05HB003
J42/f518	F37441	CB05HB002
J42/f517	F37440	CB05HB001
Cat Burgess section 1 (locality 13)		
J42/f516	F37439	CB05HB427
J42/f515	F37438	CB05HB426
J42/f514	F37437	CB05HB425
J42/f513	F37436	CB05HB424
J42/f512	F37435	CB05HB423
J42/f511	F37434	CB05HB422
J42/f510	F37433	CB05HB421
J42/f509	F37432	CB05HB420
J42/f508	F37431	CB05HB419
J42/f507	F37430	CB05HB418
J42/f506	F37429	CB05HB417
J42/f505	F37428	CB05HB416
J42/f504	F37427	CB05HB415
J42/f503	F37426	CB05HB414
J42/f502	F37425	CB05HB413
J42/f501	F37424	CB05HB412
J42/f500	F37423	CB05HB411
J42/f499	F37422	CB05HB410
J42/f498	F37421	CB05HB409
J42/f497	F37420	CB05HB408
J42/f496	F37419	CB05HB407
J42/f495	F37418	CB05HB406
J42/f494	F37417	CB05HB405
J42/f493	F37416	CB05HB404
J42/f492	F37415	CB05HB403
J42/f491	F37414	CB05HB402
J42/f490	F37413	CB05HB401
Cat Burgess section 2 (locality 7): 550m north of Kakaho Creek		
J42/f711	F37634	CB05HB172
J42/f710	F37633	CB05HB171
J42/f709	F37632	CB05HB170
J42/f708	F37631	CB05HB169
J42/f707	F37630	CB05HB168
J42/f706	F37629	CB05HB167
J42/f705	F37628	CB05HB166
J42/f704	F37627	CB05HB165
J42/f703	F37626	CB05HB164
J42/f702	F37625	CB05HB163
J42/f701	F37624	CB05HB162
J42/f700	F37623	CB05HB161
J42/f699	F37622	CB05HB160
J42/f698	F37621	CB05HB159
J42/f697	F37620	CB05HB158
J42/f696	F37619	CB05HB157
J42/f695	F37618	CB05HB156
J42/f694	F37617	CB05HB155
J42/f693	F37616	CB05HB154
J42/f692	F37615	CB05HB153
J42/f691	F37614	CB05HB152
J42/f690	F37613	CB05HB151
J42/f689	F37612	CB05HB150
J42/f688	F37611	CB05HB149
J42/f687	F37610	CB05HB148
J42/f686	F37609	CB05HB147
J42/f685	F37608	CB05HB146
J42/f684	F37607	CB05HB145
J42/f683	F37606	CB05HB144
J42/f682	F37605	CB05HB143
J42/f681	F37604	CB05HB142
J42/f680	F37603	CB05HB141
J42/f679	F37602	CB05HB140
J42/f678	F37601	CB05HB139
Cat Burgess section 2 (locality 6)		
J42/f677	F37600	CB05HB138
J42/f676	F37599	CB05HB137
J42/f675	F37598	CB05HB136
J42/f674	F37597	CB05HB135
J42/f673	F37596	CB05HB134
J42/f672	F37595	CB05HB133
J42/f671	F37594	CB05HB132
J42/f670	F37593	CB05HB131
J42/f669	F37592	CB05HB130
J42/f668	F37591	CB05HB129
J42/f667	F37590	CB05HB128
J42/f666	F37589	CB05HB127
J42/f665	F37588	CB05HB126
J42/f664	F37587	CB05HB125
J42/f663	F37586	CB05HB124
J42/f662	F37585	CB05HB123
J42/f661	F37584	CB05HB122
J42/f660	F37583	CB05HB121
J42/f659	F37582	CB05HB120
J42/f658	F37581	CB05HB119
J42/f657	F37580	CB05HB118
J42/f656	F37579	CB05HB117
J42/f655	F37578	CB05HB116
J42/f654	F37577	CB05HB115
J42/f653	F37576	CB05HB114
J42/f652	F37575	CB05HB113
J42/f651	F37574	CB05HB112
J42/f650	F37573	CB05HB111
J42/f649	F37572	CB05HB110
J42/f648	F37571	CB05HB109
J42/f647	F37570	CB05HB108
J42/f646	F37569	CB05HB107
J42/f645	F37568	CB05HB106
J42/f644	F37567	CB05HB105
J42/f643	F37566	CB05HB104
J42/f642	F37565	CB05HB103
J42/f641	F37564	CB05HB102
J42/f640	F37563	CB05HB101
J42/f639	F37562	CB05HB100
J42/f638	F37561	CB05HB99
Cat Burgess section 3 (locality 9)		
J42/f803	F37726	CB05HB342
J42/f802	F37725	CB05HB341
J42/f801	F37724	CB05HB340
J42/f800	F37723	CB05HB339
J42/f799	F37722	CB05HB338
J42/f798	F37721	CB05HB337
J42/f797	F37720	CB05HB336
J42/f796	F37719	CB05HB335
J42/f795	F37718	CB05HB334
J42/f794	F37717	CB05HB333
J42/f793	F37716	CB05HB332
J42/f792	F37715	CB05HB331
J42/f791	F37714	CB05HB330
J42/f790	F37713	CB05HB329
J42/f789	F37712	CB05HB328
J42/f788	F37711	CB05HB327
J42/f787	F37710	CB05HB326
J42/f786	F37709	CB05HB325
J42/f785	F37708	CB05HB324
J42/f784	F37707	CB05HB323
J42/f783	F37706	CB05HB322
J42/f782	F37705	CB05HB321
J42/f781	F37704	CB05HB320
J42/f780	F37703	CB05HB319
J42/f779	F37702	CB05HB318
J42/f778	F37701	CB05HB317
J42/f777	F37700	CB05HB316
J42/f776	F37699	CB05HB315
J42/f775	F37698	CB05HB314
J42/f774	F37697	CB05HB313
J42/f773	F37696	CB05HB312
J42/f772	F37695	CB05HB311
J42/f771	F37694	CB05HB310
J42/f770	F37693	CB05HB309

SF	F Number	Field Number
J42/f769	F37692	CB05HB308
J42/f768	F37691	CB05HB307
J42/f767	F37690	CB05HB306
J42/f766	F37689	CB05HB305
J42/f765	F37688	CB05HB304
J42/f764	F37687	CB05HB303
Cat Burgess section 3 (locality 8):.		
J42/f763	F37686	CB05HB302
J42/f762	F37685	CB05HB301
J42/f761	F37684	CB05HB300
J42/f760	F37683	CB05HB299
J42/f759	F37682	CB05HB298
J42/f758	F37681	CB05HB297
J42/f757	F37680	CB05HB296
J42/f756	F37679	CB05HB295
J42/f755	F37678	CB05HB294
J42/f754	F37677	CB05HB293
J42/f753	F37676	CB05HB292
J42/f752	F37675	CB05HB291
J42/f751	F37674	CB05HB290
J42/f750	F37673	CB05HB289
J42/f749	F37672	CB05HB288
J42/f748	F37671	CB05HB287
J42/f747	F37670	CB05HB286
J42/f746	F37669	CB05HB285
J42/f745	F37668	CB05HB284
J42/f744	F37667	CB05HB283
J42/f743	F37666	CB05HB282
J42/f742	F37665	CB05HB281
J42/f741	F37664	CB05HB280
J42/f740	F37663	CB05HB279
J42/f739	F37662	CB05HB278
J42/f738	F37661	CB05HB277
J42/f737	F37660	CB05HB276
J42/f736	F37659	CB05HB275
J42/f735	F37658	CB05HB274
J42/f734	F37657	CB05HB273
J42/f733	F37656	CB05HB272
J42/f732	F37655	CB05HB271
J42/f731	F37654	CB05HB270
J42/f730	F37653	CB05HB269
J42/f729	F37652	CB05HB268
J42/f728	F37651	CB05HB267
J42/f727	F37650	CB05HB266
J42/f726	F37649	CB05HB265
J42/f725	F37648	CB05HB264
J42/f724	F37647	CB05HB263
J42/f723	F37646	CB05HB262
J42/f722	F37645	CB05HB261
J42/f721	F37644	CB05HB260
J42/f720	F37643	CB05HB259
J42/f719	F37642	CB05HB258
J42/f718	F37641	CB05HB257
J42/f717	F37640	CB05HB256
J42/f716	F37639	CB05HB255
J42/f715	F37638	CB05HB254
J42/f714	F37637	CB05HB253
J42/f713	F37636	CB05HB252
J42/f712	F37635	CB05HB251
Cat Burgess section 4 (locality 12, Hantkenina).		
J42/f845	F37768	CB05HB400
J42/f844	F37767	CB05HB399
J42/f843	F37766	CB05HB398
J42/f842	F37765	CB05HB397
J42/f841	F37764	CB05HB396
J42/f840	F37763	CB05HB395
J42/f839	F37762	CB05HB394
J42/f838	F37761	CB05HB393
J42/f837	F37760	CB05HB392
J42/f836	F37759	CB05HB391
J42/f835	F37758	CB05HB390
Cat Burgess section 4 (locality 11		
J42/f834	F37757	CB05HB389
J42/f833	F37756	CB05HB388
J42/f832	F37755	CB05HB387
J42/f831	F37754	CB05HB386
J42/f830	F37753	CB05HB385
J42/f829	F37752	CB05HB384
J42/f828	F37751	CB05HB383
J42/f827	F37750	CB05HB382
J42/f826	F37749	CB05HB381
Cat Burgess section 4 (locality 10)		
J42/f825	F37748	CB05HB364
J42/f824	F37747	CB05HB363
J42/f823	F37746	CB05HB362
J42/f822	F37745	CB05HB361
J42/f821	F37744	CB05HB360
J42/f820	F37743	CB05HB359
J42/f819	F37742	CB05HB358
J42/f818	F37741	CB05HB357
J42/f817	F37740	CB05HB356
J42/f816	F37739	CB05HB355
J42/f815	F37738	CB05HB354
J42/f814	F37737	CB05HB353
J42/f813	F37736	CB05HB352
J42/f812	F37735	CB05HB351
J42/f811	F37734	CB05HB350
J42/f810	F37733	CB05HB349
J42/f809	F37732	CB05HB348
J42/f808	F37731	CB05HB347
J42/f807	F37730	CB05HB346
J42/f806	F37729	CB05HB345
J42/f805	F37728	CB05HB344
J42/f804	F37727	CB05HB343
Cat Burgess spot samples		
J42/f894	F37817	CB05HB250
J42/f893	F37816	CB05HB249
J42/f892	F37815	CB05HB248
J42/f891	F37814	CB05HB247
J42/f890	F37813	CB05HB246
J42/f889	F37812	CB05HB245
J42/f888	F37811	CB05HB244
J42/f887	F37810	CB05HB243
J42/f886	F37809	CB05HB242
J42/f885	F37808	CB05HB241
J42/f884	F37807	CB05HB240
J42/f883	F37806	CB05HB239
J42/f882	F37805	CB05HB238
J42/f881	F37804	CB05HB237
J42/f880	F37803	CB05HB236
J42/f879	F37802	CB05HB235
J42/f878	F37801	CB05HB234
J42/f877	F37800	CB05HB233
J42/f876	F37799	CB05HB232
J42/f875	F37798	CB05HB231
J42/f874	F37797	CB05HB230
J42/f873	F37796	CB05HB229
J42/f872	F37795	CB05HB228
J42/f871	F37794	CB05HB227
J42/f870	F37793	CB05HB226
J42/f869	F37792	CB05HB225
J42/f868	F37791	CB05HB224
J42/f867	F37790	CB05HB223
J42/f866	F37789	CB05HB222
J42/f865	F37788	CB05HB220
J42/f864	F37787	CB05HB219
J42/f863	F37786	CB05HB218
J42/f862	F37785	CB05HB217
J42/f861	F37784	CB05HB216
J42/f860	F37783	CB05HB215
J42/f859	F37782	CB05HB214
J42/f858	F37781	CB05HB213
J42/f857	F37780	CB05HB212
J42/f856	F37779	CB05HB211
J42/f855	F37778	CB05HB210
J42/f854	F37777	CB05HB209
J42/f853	F37776	CB05HB208
J42/f852	F37775	CB05HB207
J42/f851	F37774	CB05HB206
J42/f850	F37773	CB05HB205
J42/f849	F37772	CB05HB204
J42/f848	F37771	CB05HB203
J42/f847	F37770	CB05HB202
J42/f846	F37769	CB05HB201

Table A1.1 Table showing the Geological Society of New Zealand Fossil Record File locality numbers for samples collected by the author (Burgess) and by Morgans during the 2005 field season with their corresponding field sample number.

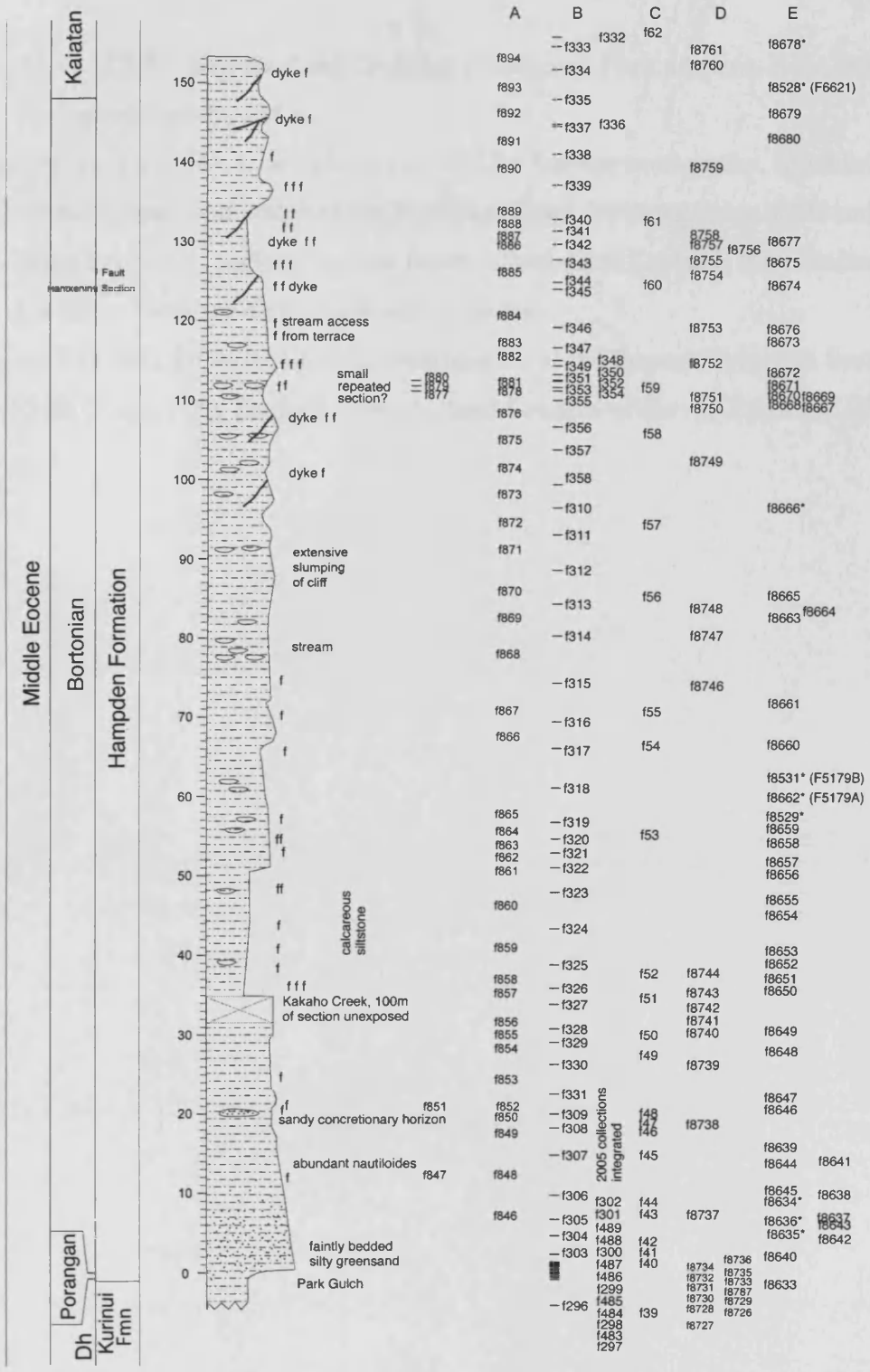

Figure A1.1 Stratigraphic column of Hampden Section adapted from Morgans (2008) using the stratigraphic thickness employed in this study. Showing locations of 2005 samples and previous sample collections. A) Burgess 2005 collection (this study); B) Morgans 1998, 2005 collections (Morgans, 2008); C) New Zealand Geological Survey 1980 collection (Wilson, 1985); D) Cameron collections 1967 to 1972; E) Early collections curated in GNS Science collected by Park, Marwick, Brown & Osbourne 1930's to 40's, * indicates sample studied by Jenkins (1971)

Jenkins, D. G. (1971). *New Zealand Cenozoic Planktonic Foraminifera*, New Zealand Geological Survey, 288 p.

Morgans, H. E. G. (2008). Late Paleocene - Middle Eocene stratigraphy, foraminiferal biostratigraphy and status of the Bortonian Stage lectostratotype at Moeraki-Hampden coastal section, eastern South Island, New Zealand. *New Zealand Journal of Geology and Geophysics* **in press**.

Wilson, G. J. (1985). Dinoflagellate Biostratigraphy of the Eocene Hampden Section, North Otago, New Zealand. *New Zealand Geological Survey Record* **8**: 93-101.

Appendix 2. Glossary of morphological terms

Glossary of terms used in the taxonomic descriptions given in Chapter 4.

2a. Foraminifera

aperture: the major opening of the test to the exterior through which the cytoplasm protrudes in life.

bulla (pl. bullae): blister-like structure partially or completely covering primary or secondary apertures.

cancellate: honeycomb-like surface.

chamber: test cavity and it's surrounding wall, formed at a single growth stage.

evolute: each whorl of an enrolled form does not embrace the previous whorls, so all whorls are visible.

globular: rounded, spherical.

high-spired: trochospiral form in which the height of the spire is greater than the breadth of the terminal face.

incised: cut-into.

intra-extra umbilical aperture: aperture that extends from the umbilicus to a position outside the umbilical region, possibly to the margin.

involute: each whorl of enrolled forms completely embraces earlier whorls so only the final whorl is visible.

lobate: having a lobed outline.

muricae: coarse pointed/conical pustules (Blow, 1979).

ovate: rounded and somewhat elongate in form.

pustule: small rounded or conical protuberance on the test surface.

quadrate: approximately square of rectangular in form.

spines: long, slender (<1 μm diameter) structures comprising a single calcite crystal.

spinose; bearing spines.

spiral side: dorsal side of trochospiral forms where all whorls are visible.

suture: line marking the join of two chambers or whorls.

test: agglutinated or secreted shell of the foraminifera.

trochospiral: chambers spirally coiled in an expanding helix.

umbilical side: side of a trochospiral form where only final whorl is visible, or is more involute.

umbilicus: centre (possibly depressed) of involute planispiral forms or umbilical (involute) side of trochospiral forms where all chambers of the last-formed whorl meet.
whorl: single turn of a coiled test through 360°.

2b. Dinoflagellates

Note: many of the morphological terms below are used in a strict sense to describe the dinoflagellate thecae, the prefix para- should be added when describing the same features of the cyst (paracingulum, paraplates, parasuture etc.). However, this makes the terminology very cumbersome so standard thecal terminology is commonly used where there is no necessity to distinguish the theca from the cyst, as in palaeontological studies where only the cyst is preserved. For further explanation of dinocyst morphology see Evitt (1985).

antapex: the posterior-most part of the cyst.
antapical: positioned at the antapex.
apex: the anterior-most part of the cyst.
apical: positioned at the apex.
archeopyle: the opening in the cyst wall through which the cell emerges during excystment.
capitate: having a distinct head.
cavate: cyst having two or more walls that are not in continuous contact. the inner endophragm and outer periphragm
cingulum: channel or depression encircling the cyst at it's equator.
curcumcavate: having a two layered wall in which the periphragm entirely encircles the endophragm.
chorate: having numerous protrusions arising from the surface.
cyst: dormant or resting cell with a wall formed of resistant organic material.
distal: position farthest from the centre of a cyst
endophragm: inner wall of a cavate cyst (that does not have protrusions that support the outer wall).
granulate: surface textured with small raised protrusions, granules.
horns: extension of the 'corners' of the cyst into horn-like projections.
intercalary: plate that does not belong to one of the encircling series of plates named under the Kofoid system.
intratabular: positioned at the centres of plates.

Kofoid system: System for naming the plates of the thecae devised by Kofoid (1907, 1909) – see Evitt (1985) for diagrams and further explanation.

membraneous: having the appearance of a thin sheet or membrane.

non-tabular: positioned with no relationship to plates

parasutural ridge: elevation of the cell wall in a line following the join between adjacent plates.

parasutural septae: thin walls arising from the line joining adjacent plates.

pennitabular: positioned at the lines and points along which plates join.

periphragm: outer wall of a cavate cyst (that is not supported by protrusions from the inner wall).

post-cingular: position posterior of the cingulum

pre-cingular: position anterior of the cingulum

reticulate: Surface ornamentation on cyst where raised straight lines or ridges cross one another creating a complex pattern resembling a network of fibres, veins or lines

sexiform tabulation pattern: tabulation pattern in which the antapical plate is in contact with six surrounding plates, giving it a hexagonal outline.

tabulation: pattern of plates on the surface of a cyst that reflects the thecal plates of the living cell.

thecal plates: cell wall plates of 'armoured' species of dinoflagellates composed of resistant organic material.

trabeculae: thread-like extensions of the distal ends of spines, cross linked to form a web-like structure.

trifurcate: branched into three.

vasiform: lace-like

Appendix 3. Benthic foraminifera species identification notes

Haplophragmoides sp. A

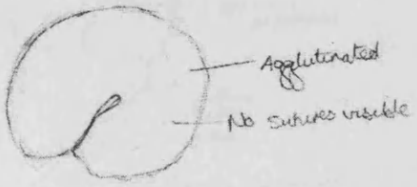

Involuted.

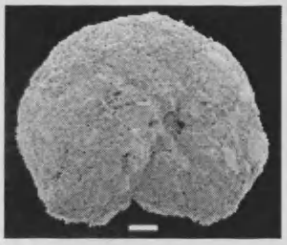

Bolivinopsis sp. A

Bolivinopsis sp. B

Angular, narrower and with less clear sutures than sp. A

Spiroplectinella sp. A

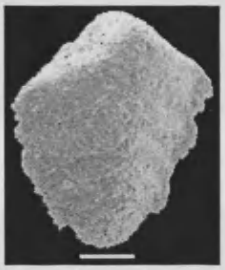

Spiroplectinealla sp. B

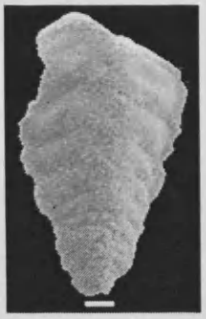

Karreriella sp. A

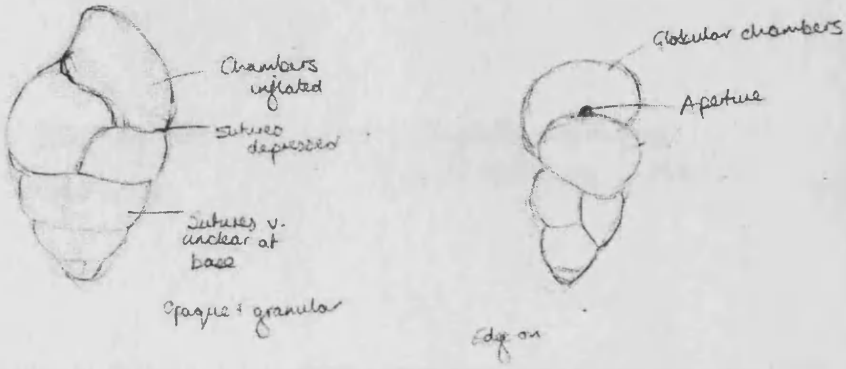

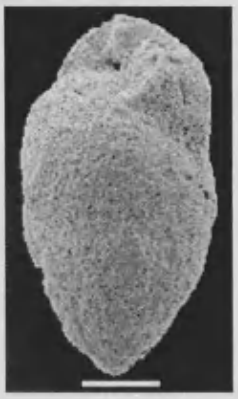

Karreriella sp. B

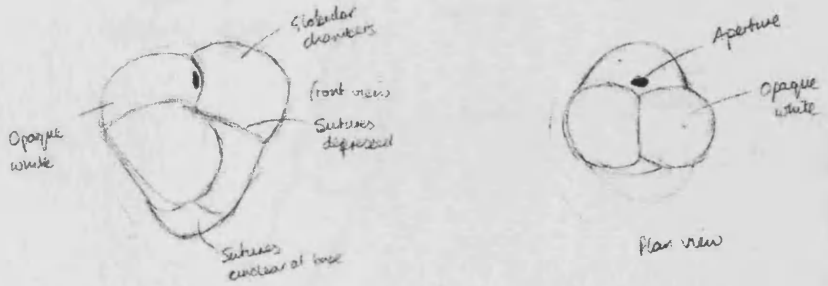

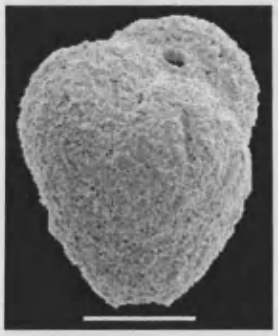

Quinqiloculina sp. A

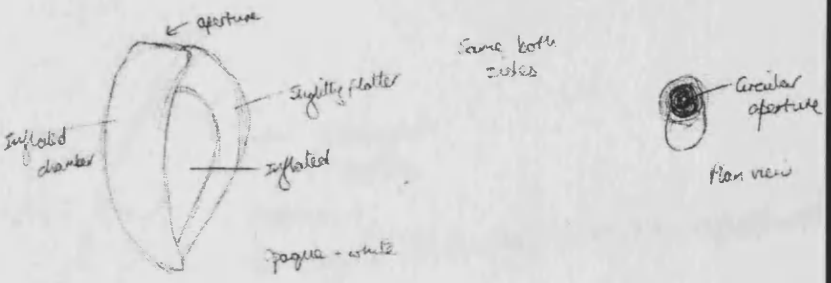

Sigmolina sp. A

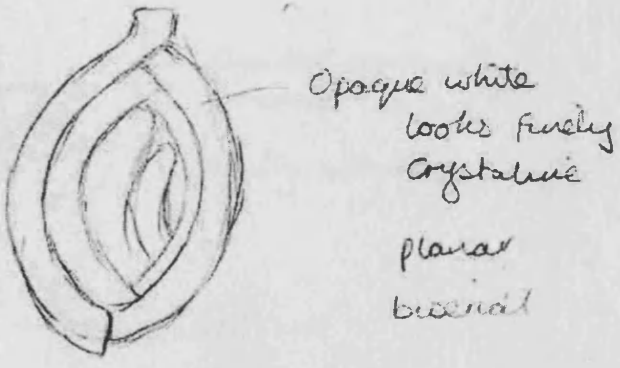

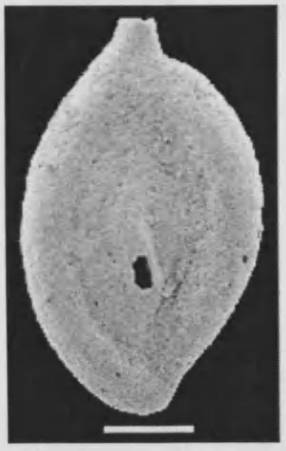

Dentalinoides sp. A

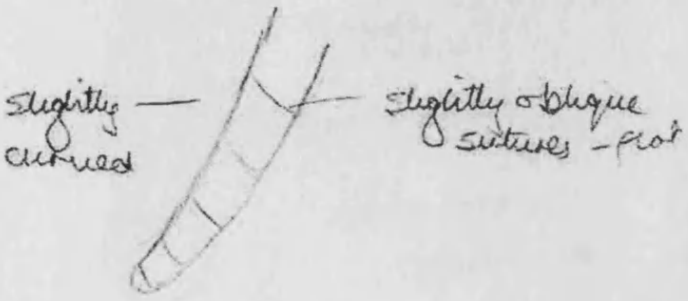

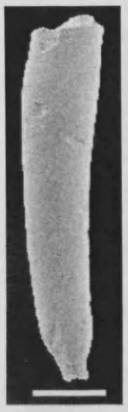

Dentalinoides sp. B

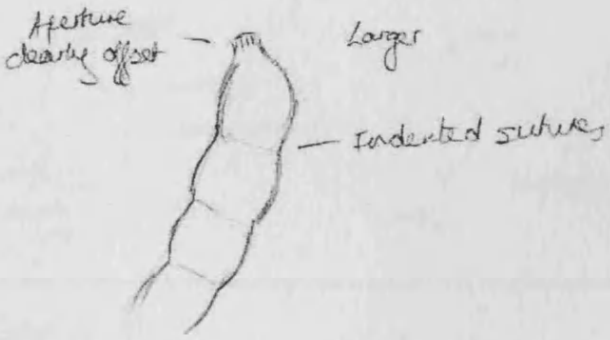

Nodosaria sp. A

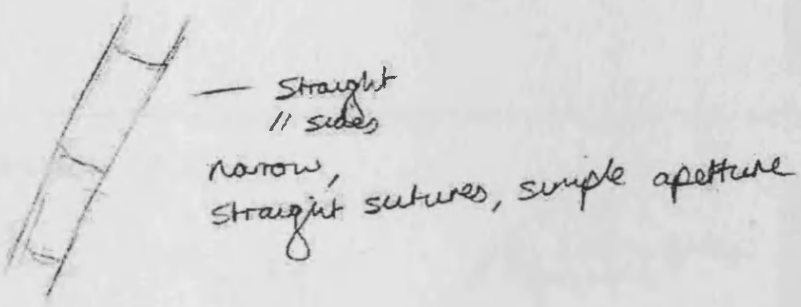

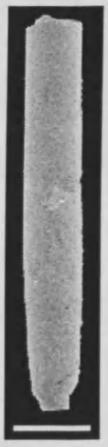

Nodosaria sp. B

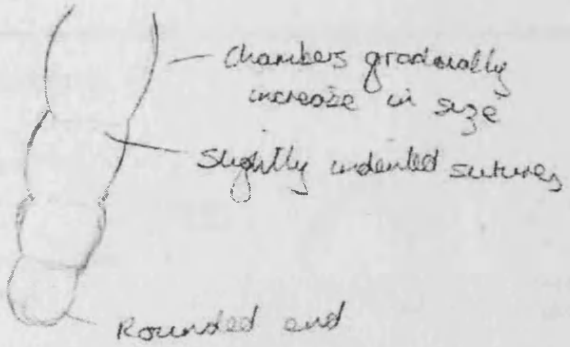

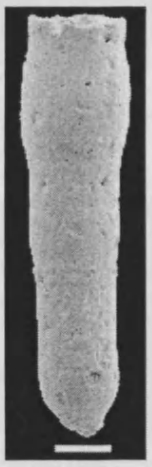

Pyramidulina sp. A

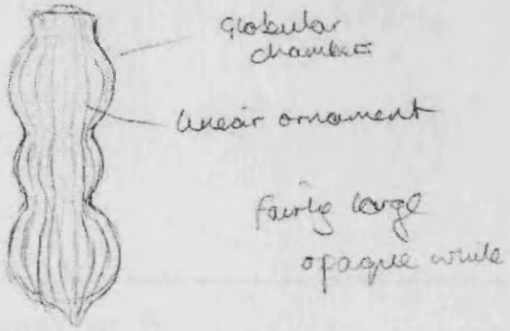

Lenticulina sp. A

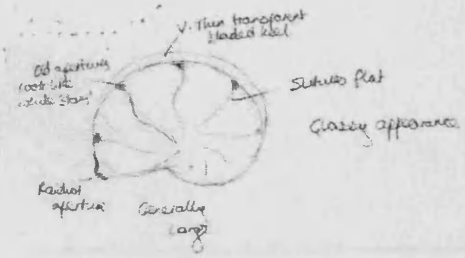

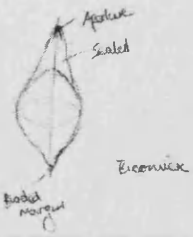

Lenticulina sp. B

) Lenticulina sp 1 - 2) A test with NO keel.

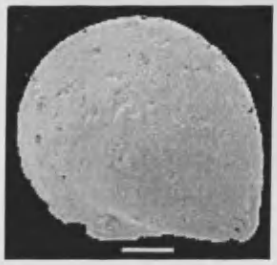

Lenticulina sp. C

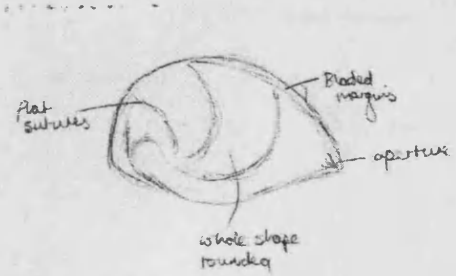

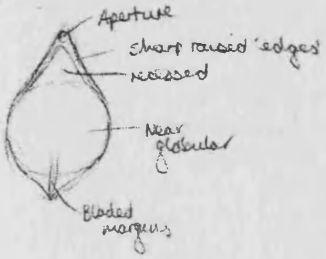

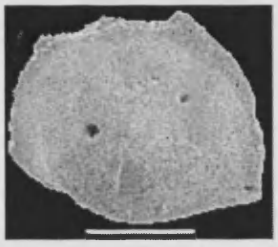

Lenticulina sp. D

Saracenaria sp. A

Saracenaria sp. B

Vaginulinopsis sp. A

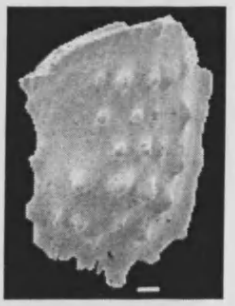

Marginulina sp. A

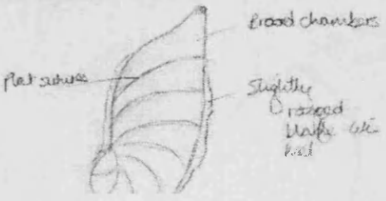

Coil slightly more
prominent on the
opposite side

Marginulina sp. B

Vaginulina sp. A

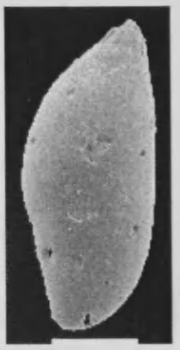

Vaginulina sp. B

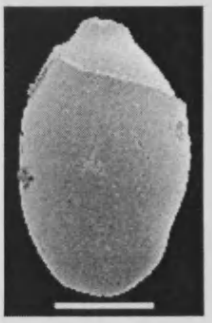

Lagena sp. A

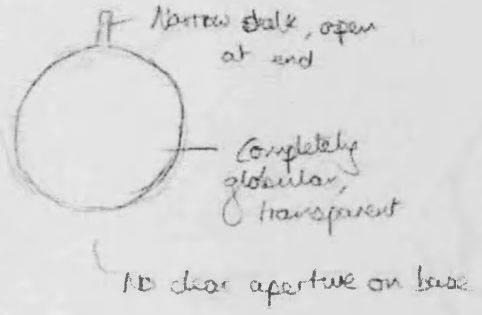

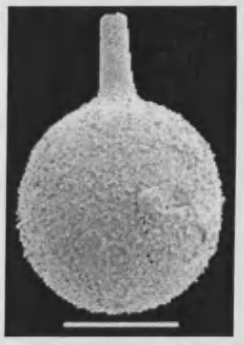

Lagena sp. B

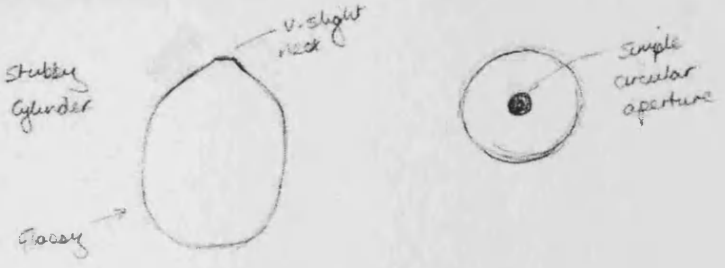

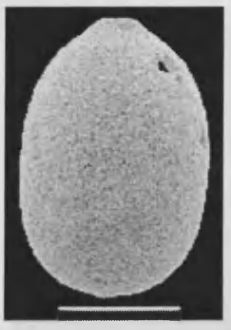

Lagena sp. C

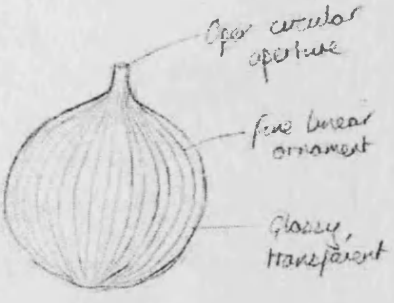

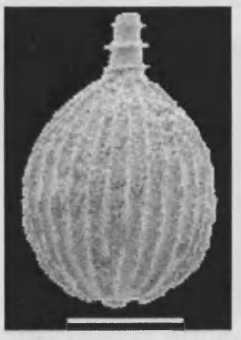

Siphoglobulina sp. A

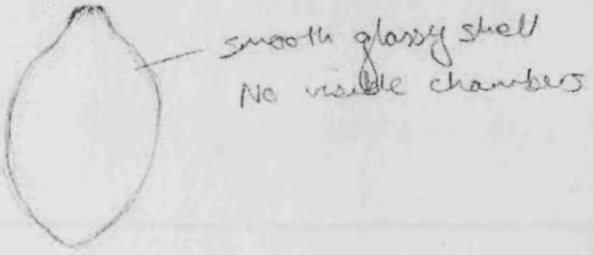

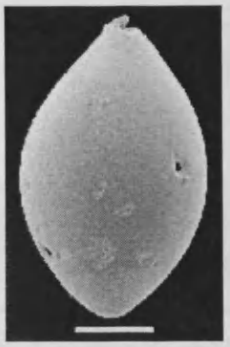

Globulina sp. A

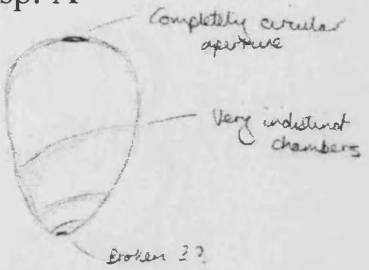

Guttalina sp. A

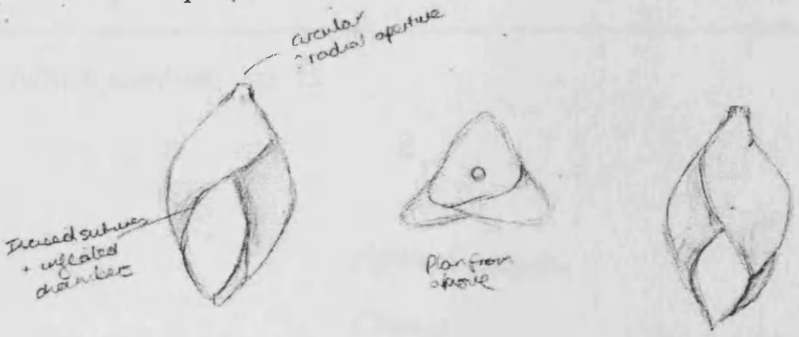

Ceratobulimina sp. A

Epistomina sp. A

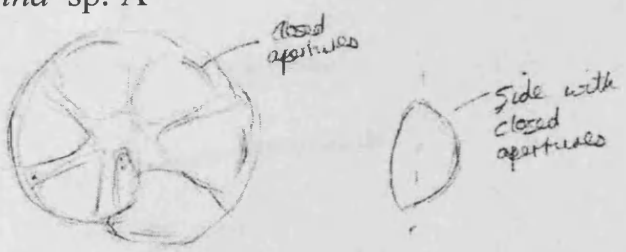

Globocassidulina sp. A

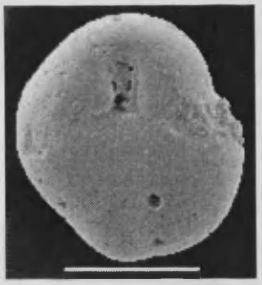

Nodogenerina sp. A

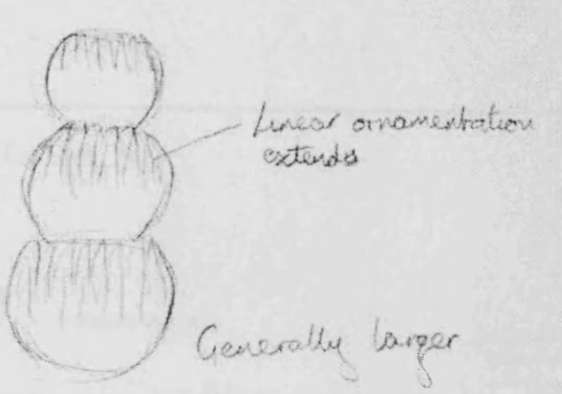

Nodogenerina sp. B

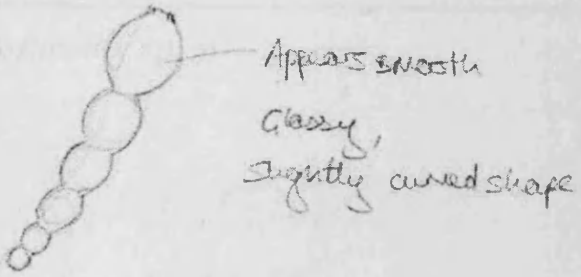

Nodogenerina sp. C

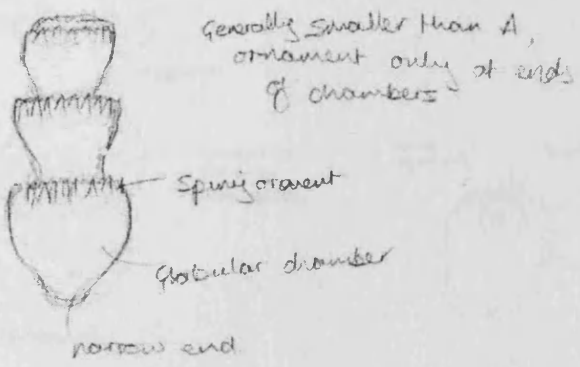

Siphonodosaria sp. A

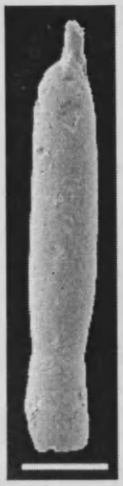

Stilostimella sp. A

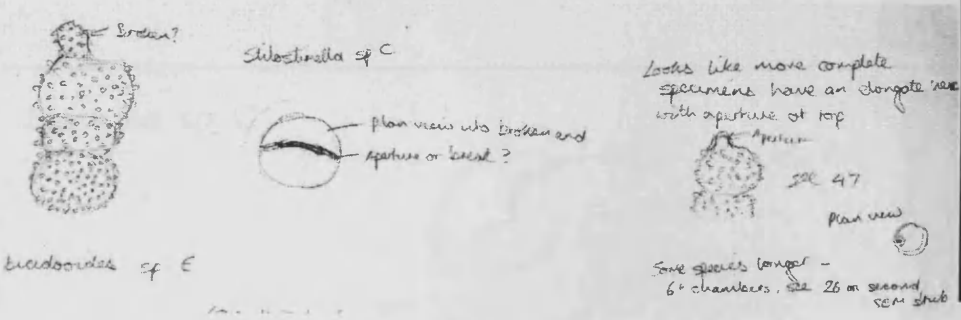

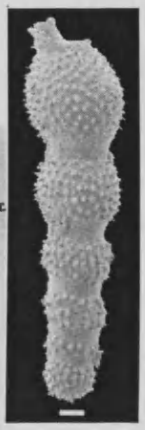

Stilostimella sp. B

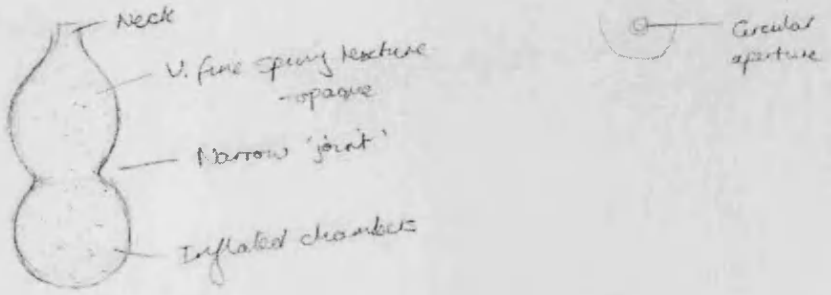

Stilostimella sp. C

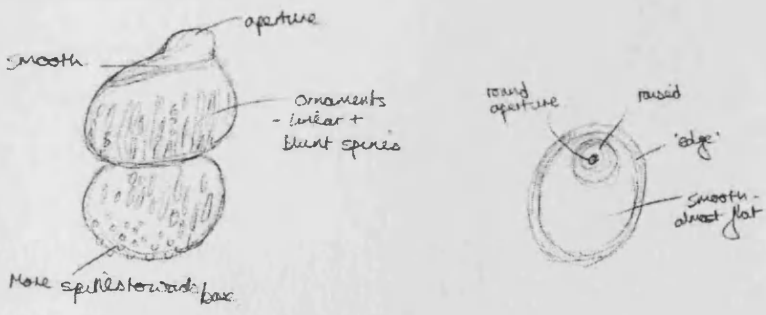

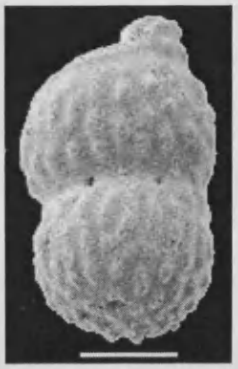

Bulimina sp. A

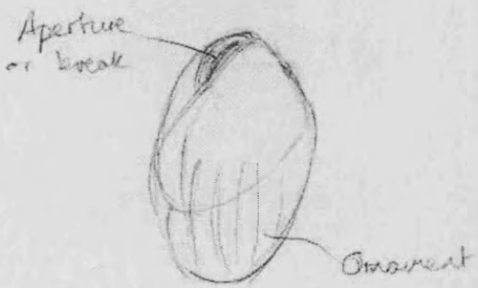

Bulimina sp. B

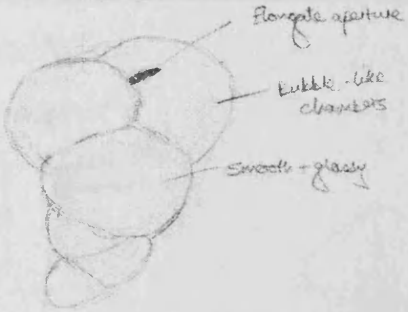

Bulimina sp. C

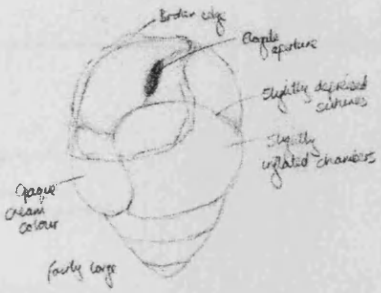

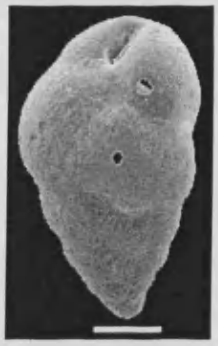

Bulimina sp. D

Globobulimina sp. A

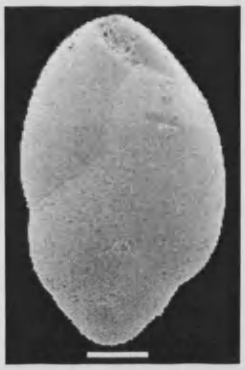

Uvigerina sp. A

Kolesnikovella sp. A

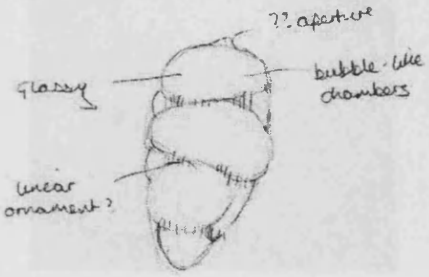

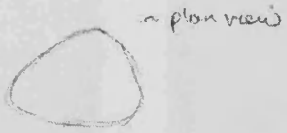

Kolesnikovella sp. B

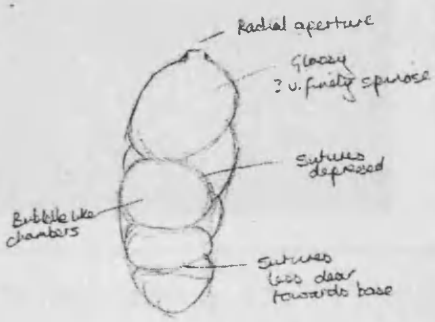

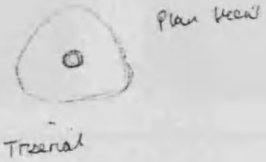

Cibicidoides sp. B

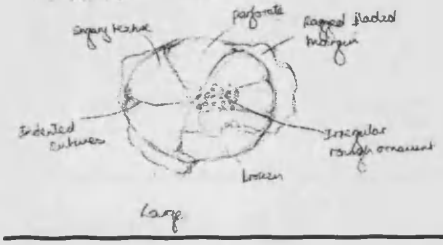

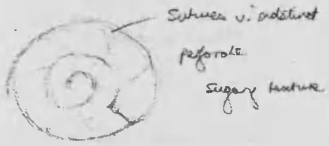

Cibicidoides sp. C

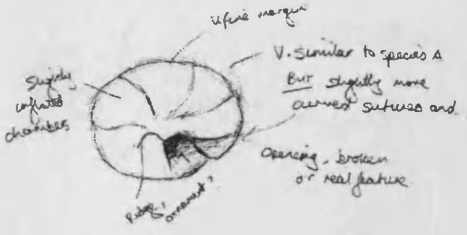

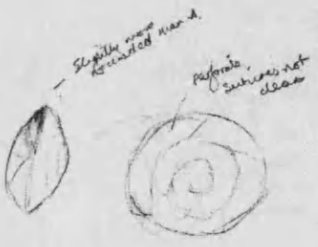

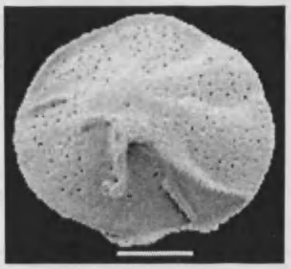

Cibicidoides sp. A

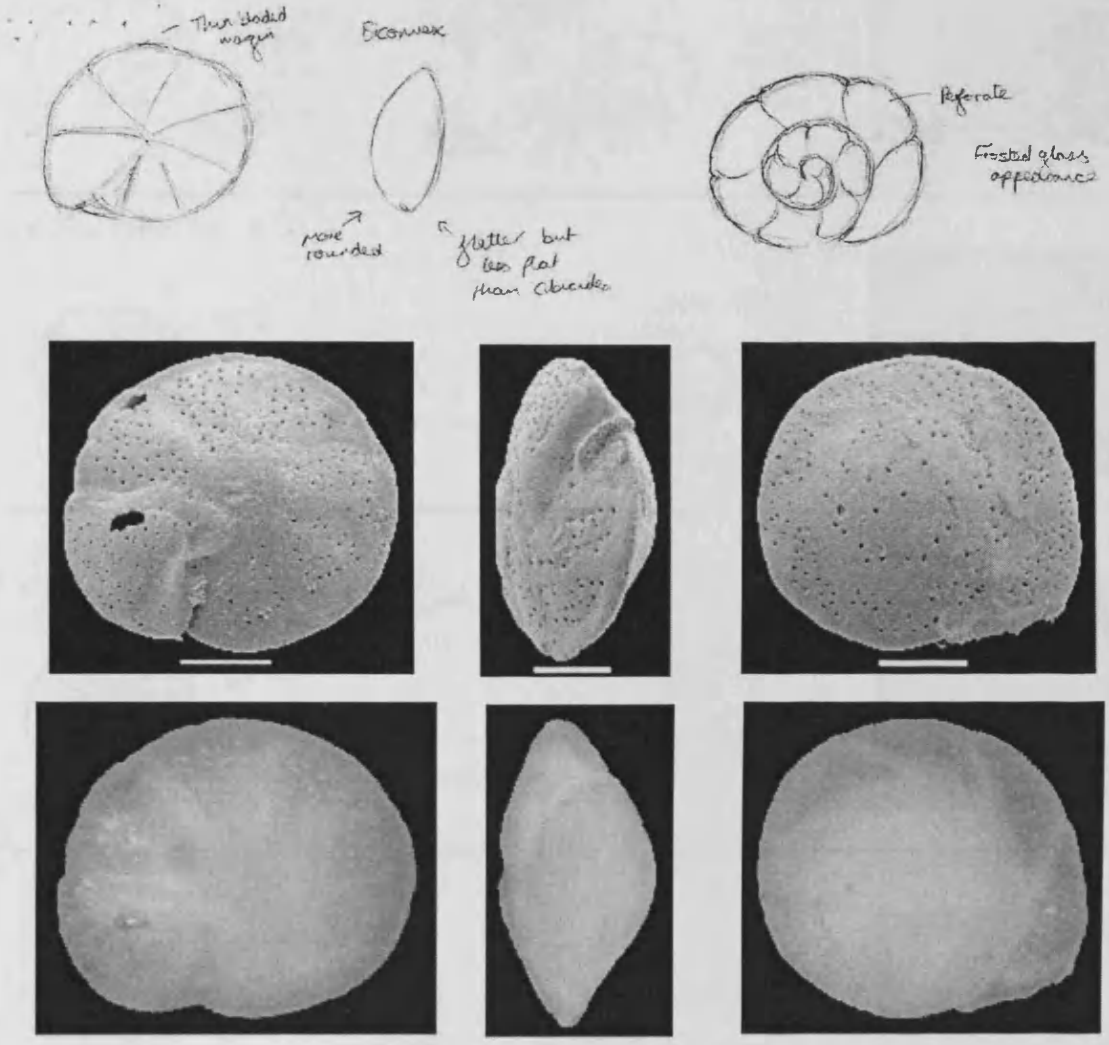

Cibicidoides sp. D

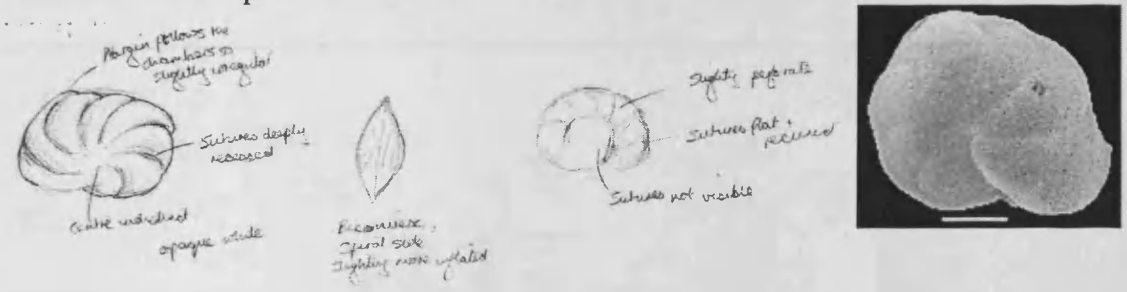

Cibicidoides sp. E

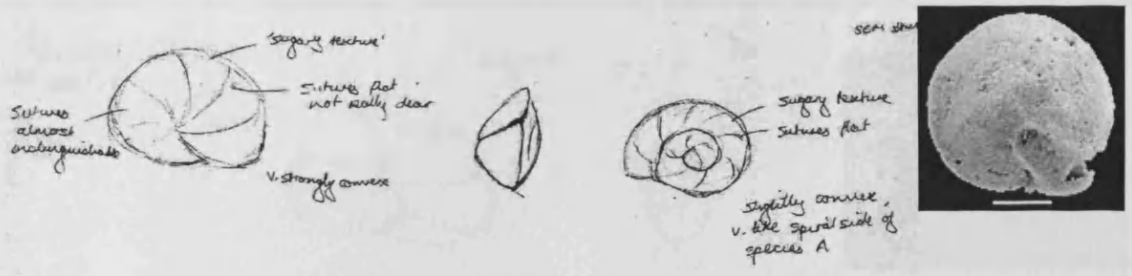

Cibicidoides sp. F

Cibicides sp. A

Cibicides sp. B

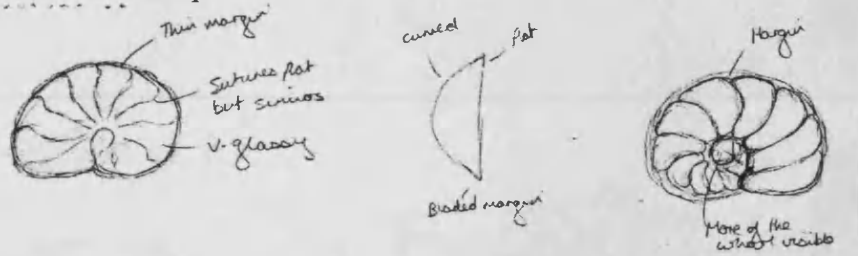

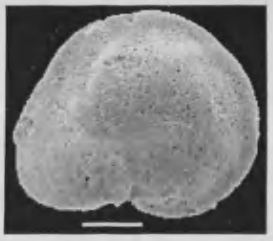

Cibicides sp. C

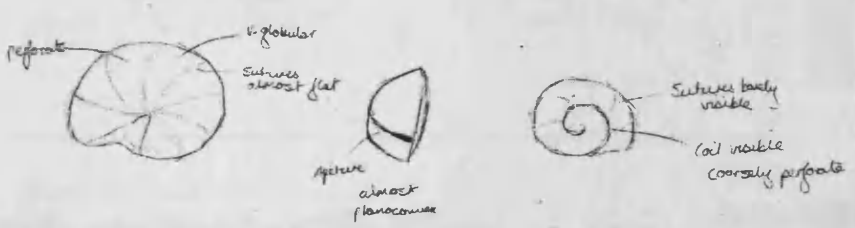

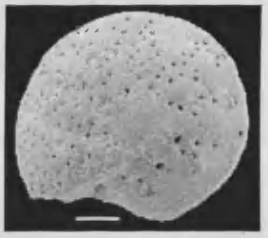

Lobatula sp. A

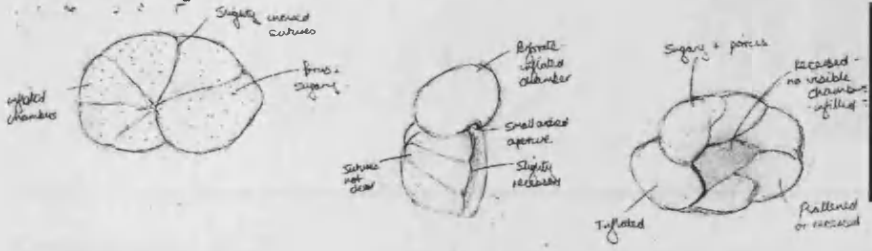

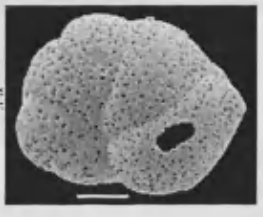

Nonionella sp. A

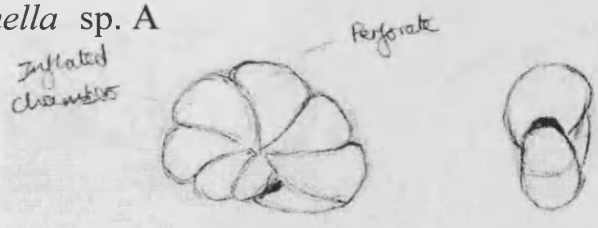

Melonis sp. A

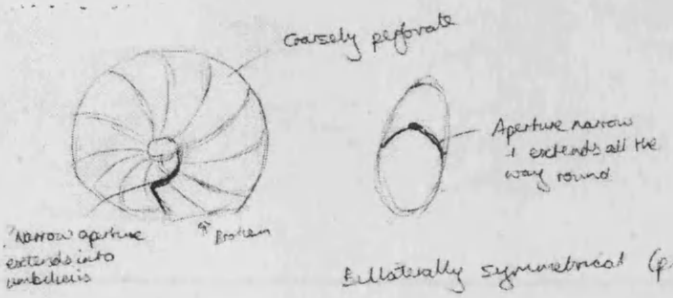

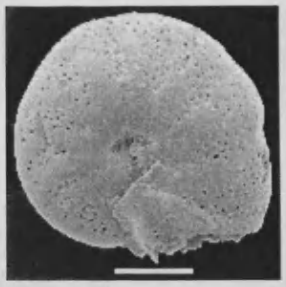

Pulinia sp. A

Pulinia sp. B

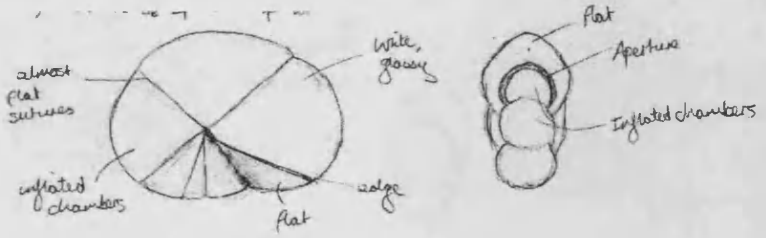

Alabamania sp. A

Oridorsalis sp. A

Anomalinoides sp. A

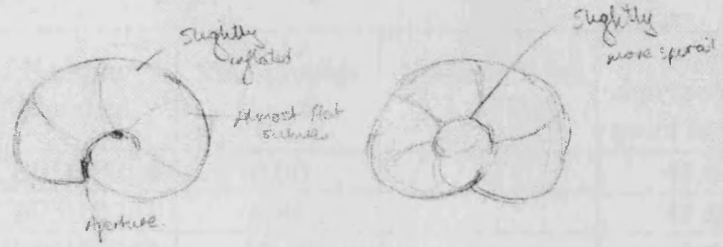

Gyroidinoides sp. A

Gavelinella sp. A

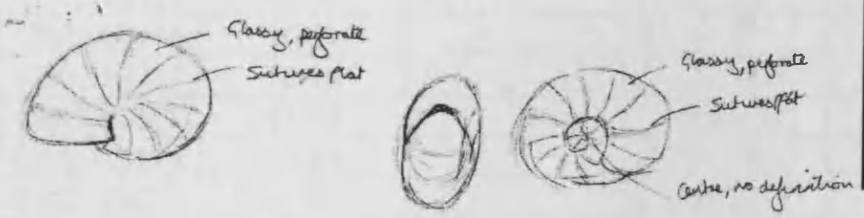

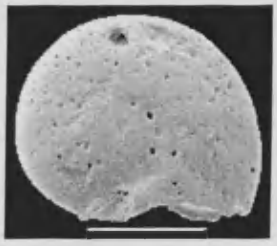

Linaresia sp. A

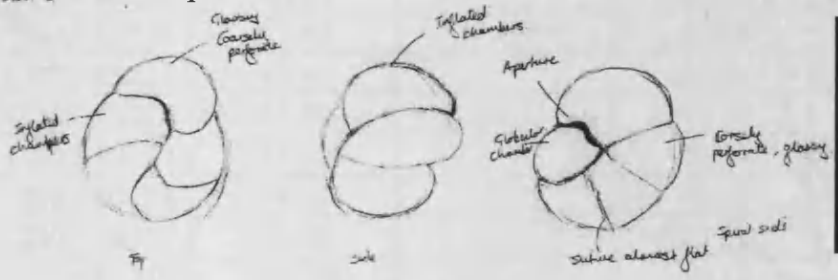

Elphidium sp. A

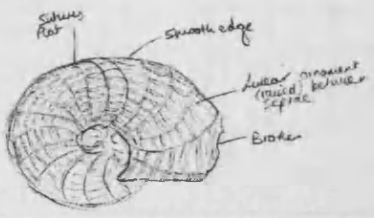

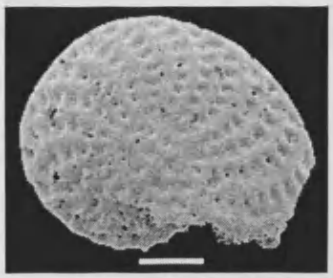

Appendix 4. Hampden Beach age model

Sample Number	Stratigraphic Height	Foraminiferal LAD (Ma)	Age interpolated point to point	Age interpolated linear
CB05HB200	0.00	43	43.00	42.95
CB05HB201	6.96		42.80	42.76
CB05HB202	12.19		42.65	42.62
CB05HB203	12.19		42.65	42.62
CB05HB204	17.41		42.49	42.48
CB05HB205	19.16		42.44	42.43
CB05HB206	20.90		42.39	42.39
CB05HB207	20.90		42.39	42.39
CB05HB208	24.39		42.29	42.29
CB05HB209	28.25		42.18	42.19
CB05HB210	29.99		42.13	42.14
CB05HB211	31.74		42.08	42.09
CB05HB212	35.22		41.97	42.00
CB05HB213	36.97		41.92	41.95
CB05HB214	40.96		41.81	41.84
CB05HB215	46.18		41.66	41.70
CB05HB216	50.41		41.53	41.59
CB05HB217	52.16		41.48	41.54
CB05HB218	53.90		41.43	41.50
CB05HB219	55.65		41.38	41.45
CB05HB220	57.89		41.32	41.39
CB05HB221	63.98		41.14	41.22
CB05HB222	67.47		41.04	41.13
CB05HB223	70.96		40.93	41.04
CB05HB224	77.92		40.73	40.85
CB05HB225	82.41		40.60	40.73
CB05HB226	85.89	40.5	40.50	40.63
CB05HB227	91.12		40.38	40.49
CB05HB228	94.61		40.30	40.40
CB05HB229	98.10		40.21	40.31
CB05HB230	101.58		40.13	40.21
CB05HB231	105.07		40.05	40.12
CB05HB232	108.56		39.97	40.02
CB05HB233	111.18		39.91	39.95
CB05HB234	111.18		39.91	39.95
CB05HB235	111.98		39.89	39.93
CB05HB236	112.46		39.88	39.92
CB05HB237	112.21		39.88	39.92
CB05HB238	115.70		39.80	39.83

Sample Number	Stratigraphic Height	Foraminiferal LAD (Ma)	Age interpolated point to point	Age interpolated linear
CB05HB240	120.67		39.68	39.70
CB05HB241	126.16		39.55	39.55
CB05HB242	129.65		39.47	39.45
CB05HB243	130.52		39.45	39.43
CB05HB244	132.27		39.41	39.38
CB05HB245	134.01		39.37	39.34
CB05HB246	139.24		39.25	39.20
CB05HB247	142.72		39.16	39.10
CB05HB248	146.21		39.08	39.01
CB05HB249	149.70	39	39.00	38.91
CB05HB250	153.19		38.92	38.82

Appendix 5. "Long section" geochemical data

Sample No.	Strat Height (m)	Age	Wt % Coarse	Planktonic foraminiferal $\delta^{13}C$ vs. PDB (‰)	Planktonic foraminiferal $\delta^{18}O$ vs. PDB (‰)	SST using Erez & Lutz with $\delta^{18}O_{SW}$ = -1.2 ‰
CB05HB201	6.96	42.91				
CB05HB202	12.19	42.77	43.44	1.811	-1.003	16.11
CB05HB203	12.19	42.77	34.70	2.072	-0.957	15.90
CB05HB204	17.41	42.62	31.00	2.208	-0.757	15.00
CB05HB205	19.16	42.57	34.68	2.036	-1.237	17.17
CB05HB206	20.90	42.52	41.96	2.150	-1.573	18.69
CB05HB207	20.90	42.52	40.68	1.925	-1.654	19.06
CB05HB208	24.39	42.43	27.92	1.761	-0.940	15.83
CB05HB209	28.25	42.32	33.62	2.482	-1.564	18.65
CB05HB210	29.99	42.27	27.36	2.419	-1.699	19.26
CB05HB211	31.74	42.22	37.76	1.975	-1.424	18.01
CB05HB212	35.22	42.12	34.42	2.041	-0.845	15.40
CB05HB213	36.97	42.07	17.72	2.187	-0.884	15.57
CB05HB214	40.96	41.96	30.32	1.997	-1.320	17.54
CB05HB215	46.18	41.81	43.64	1.611	-1.274	17.33
CB05HB216	50.41	41.70	26.10	2.180	-0.993	16.07
CB05HB217	52.16	41.65	32.06	2.447	-1.562	18.64
CB05HB218	53.90	41.60	34.58	2.054	-1.137	16.72
CB05HB219	55.65	41.55	20.20	1.713	-0.767	15.05
CB05HB220	57.89	41.49	30.02	2.197	-0.711	14.80
CB05HB221	63.98	41.32				
CB05HB222	67.47	41.22	24.90	1.423	-0.940	15.83
CB05HB223	70.96	41.12	33.06	1.967	-0.987	16.04
CB05HB224	77.92	40.92	36.70	2.390	-0.910	15.69
CB05HB225	82.41	40.80	29.60	1.959	-0.405	13.43
CB05HB226	85.89	40.70	13.28	2.030	-0.608	14.34
CB05HB227	91.12	40.55	32.48	2.152	-0.955	15.89
CB05HB228	94.61	40.46	13.64	2.124	-0.980	16.01
CB05HB229	98.10	40.36	34.10	2.027	-0.765	15.04
CB05HB230	101.58	40.26	31.92	2.409	-0.863	15.48
CB05HB231	105.07	40.16	25.24	1.889	-0.316	13.03
CB05HB232	108.56	40.07	30.56	1.784	-0.464	13.69
CB05HB233	111.18	39.99	25.54	2.205	-0.866	15.49
CB05HB234	111.18	39.99	31.46	2.459	-1.074	16.43
CB05HB235	111.98	39.97	31.38	2.320	-1.430	18.04
CB05HB236	112.46	39.96	25.48	2.276	-0.870	15.51
CB05HB237	112.21	39.96	38.04	2.715	-1.261	17.28
CB05HB238	115.70	39.87	25.44	1.976	-0.952	15.88
CB05HB239	117.18	39.82	30.42	2.405	-0.714	14.81

Sample No.	Strat Height (m)	Age	Wt % Coarse	Planktonic foraminiferal $\delta^{13}C$ vs. PDB (‰)	Planktonic foraminiferal $\delta^{18}O$ vs. PDB (‰)	SST using Erez & Lutz with $\delta^{18}O_{SW}$ = -1.2 ‰
CB05HB241	126.16	39.57	7.20	2.103	-0.911	15.69
CB05HB242	129.65	39.47	6.18	2.111	-0.872	15.52
CB05HB243	130.52	39.45	4.18	1.682	-1.191	16.96
CB05HB244	132.27	39.40	36.86	2.580	-1.056	16.35
CB05HB245	134.01	39.35	26.48	2.103	-0.560	14.12
CB05HB246	139.24	39.21	13.32	2.265	-0.316	13.03
CB05HB247	142.72	39.11	22.66	2.134	-0.666	14.60
CB05HB248	146.21	39.01	27.48	2.223	-0.602	14.31
CB05HB249	149.70	38.91	13.98	1.812	-0.316	13.03
CB05HB250	153.19	38.81	12.60	2.263	-1.103	16.56

Appendix 6. "Long section" sediment composition

Sample No.	Strat Height (m)	Wt % Coarse	% Carbonate	% Clays	% Feldspar	% Silica	% Mica	% Pyrite	Kaolinite / Montmorillonite
CB05HB201	6.96		14.28	16.78	12.92	51.17	4.85	0.00	0.95
CB05HB202	12.19	43.44							
CB05HB203	12.19	34.70							
CB05HB204	17.41	31.00							
CB05HB205	19.16	34.68	12.78	19.55	12.67	51.44	3.55	0.00	3.46
CB05HB206	20.90	41.96							
CB05HB207	20.90	40.68							
CB05HB208	24.39	27.92							
CB05HB209	28.25	33.62							
CB05HB210	29.99	27.36	6.03	25.31	16.66	47.67	4.32	0.00	2.58
CB05HB211	31.74	37.76							
CB05HB212	35.22	34.42							
CB05HB213	36.97	17.72							
CB05HB214	40.96	30.32							
CB05HB215	46.18	43.64	6.87	25.99	16.95	44.06	6.14	0.00	2.68
CB05HB216	50.41	26.10							
CB05HB217	52.16	32.06							
CB05HB218	53.90	34.58							
CB05HB219	55.65	20.20							
CB05HB220	57.89	30.02	8.27	21.32	7.89	57.05	5.47	0.00	1.95
CB05HB221	63.98								
CB05HB222	67.47	24.90							
CB05HB223	70.96	33.06							
CB05HB224	77.92	36.70							
CB05HB225	82.41	29.60	6.46	16.70	16.94	56.59	3.31	0.00	1.87
CB05HB226	85.89	13.28							
CB05HB227	91.12	32.48							
CB05HB228	94.61	13.64							
CB05HB229	98.10	34.10							
CB05HB230	101.58	31.92	4.94	16.74	26.86	48.39	3.07	0.00	1.52
CB05HB231	105.07	25.24							
CB05HB232	108.56	30.56							
CB05HB233	111.18	25.54							
CB05HB234	111.18	31.46							
CB05HB235	111.98	31.38	5.63	18.33	33.81	39.43	2.80	0.00	1.36

Sample No.	Strat Height (m)	Wt % Coarse	% Carbonate	% Clays	% Feldspar	% Silica	% Mica	% Pyrite	Kaolinite / Montmorillonite
CB05HB237	112.21	38.04							
CB05HB238	115.70	25.44							
CB05HB239	117.18	30.42							
CB05HB240	120.67	5.40	5.28	30.79	15.10	43.98	2.96	1.90	2.16
CB05HB241	126.16	7.20							
CB05HB242	129.65	6.18							
CB05HB243	130.52	4.18							
CB05HB244	132.27	36.86							
CB05HB245	134.01	26.48	10.84	26.36	12.61	45.66	4.53	0.00	2.27
CB05HB246	139.24	13.32							
CB05HB247	142.72	22.66							
CB05HB248	146.21	27.48							
CB05HB249	149.70	13.98							
CB05HB250	153.19	12.60	17.38	16.23	19.79	42.24	4.36	0.00	1.20

Appendix 7. "Long section" planktonic foraminiferal assemblages

Sample Number	*G. index*	*G. kulgeri*	*A. praetopilensis*	*A. mcgowrani*	*A. primitiva*	*A. collactea*	*A. bullbrooki*	*A. pseudosubspherica*	*C. unicavus*	*G. bassriverensis*	*G. martini*	*G. ouachitaensis*	*S. angiporoides*	*S. cf utilisindex*	*S. linaperta*	*S. senni*	*G. nuttalli*	*T. pomeroli*	*T. frontosa*	Others	Fragments	Total
HB250	37	1									9		3	1	35				2	1	15	89
HB249	120		1	6	61	1		1		3	55	1	12		91			10	5	8		375
HB248	19	1	1		1			2			15		2		49				2	4		96
HB247	15	1			4					1?	6		1		19				1			47
HB246	5				8						5				11						2	29
HB245	98		5	2	17			1			48	2	1		435			4	17	3		633
HB244	15		1	2	6						8			4	64			2	3			105
HB243	15									1	4				4			3	2	2	1	31
HB242	19			1	4						9				6			4	3	2	1	48
HB241	11										7				6				1			25
HB240	6										1				3			1	1			12
HB239	3														1							4
HB238	31				7						12				3							53
HB237	10			1	2	1		1			5	1			1					1		23
HB236	48		3		4			1			15		2	1	15			2		1		92
HB235	39				5						13		3	4	26			2	1			93
HB234	70		2		4	2		3		1	14		13	9	80			7	2	1		208
HB233	38		1		3					2	10		15	4	55			3	1			132
HB232	12		1	3	2			2			8		1		31			2	16	2		80
HB231	10		1	3	5							2	5	5	26			3	3		1	63
HB230	3		3	1	1	1		2			1		5	5	32			1	2			57
HB229	32		1		3						9		13	11	51							120
HB228	51		1		1	2		3	2		22		3	21					1	1		108
HB227	77		2	2	2			1	1	3	29		5	9	67	?		1	1	2		202
HB226	42	1	2	1	2		12	1	1	1	9	1	11	13	91			1	1			190
HB225	5		2				1				1		2	1	16							28
HB224	9			1						2	1	1	5	1	15							35
HB223	51		10	1	10		2			4	26	3	13	2	4	2		1	1	4	2	134
HB222	5		1		2		8					4			5				2	2		29
HB220	26		3		6		4			1	15	1	7		15	1		1	2	2	3	84
HB219	10		3	2	9		12			8	7	22	7	4	36			2	17	1	2	140
HB218	22		2		10		1			2	9	26	12	1	12	1		1	8	2	2	109
HB217	26			1	9	1	1			4	4	9	8	2	18	1		1	6	1	5	92
HB216	12		1	1	15	2	4				3	5	9	5	15	1				1		74
HB215	12		2	2	18					9	3	18	2	1	2	3			6			78
HB214	38		3	14	52	2				41	8	76	7	13	17		1	10	30	6		318

Sample Number	*G. index*	*G. kulgeri*	*A. praetopilensis*	*A. mcgowrani*	*A. primitiva*	*A. collactea*	*A. bullbrooki*	*A. pseudosubspherica*	*C. unicavus*	*G. bassriverensis*	*G. martini*	*G. ouachitaensis*	*S. angiporoides*	*S. cf utilisindex*	*S. linaperta*	*S. senni*	*G. nuttalli*	*T. pomeroli*	*T. frontosa*	Others	Fragments	Total
HB212	15		6	6	12					1	5	1	7		16					2		71
HB211	3		5	7	18					3		4			3					4		47
HB210	7		1	2	2					5	1	7	4		5					5		39
HB209	7		8	9	14				1?	6	2	13	3		10	1				1		74
HB208	8		8	10	31	1				4	2	5	1		6					1		77
HB207	5		3	7	17					2	1	3	2		5					1	1	46
HB206	5		3	10	23	1				9	1	10	3		5					2		72
HB205	21		2	2	10	2				9	5	9	6							4		70
HB204	7		1	4	25					4	3	6	1		6	1						58
HB203	7		2		10					2	2	1	3		3	1				1		32
HB202	6		1	1	5					1	3									2		19

	Mixed layer' dwelling foraminifera species
	Sub thermocline dwelling' foraminifera species

Appendix 8. "High-resolution" section geochemical data

Sample Number	Height (m)	Weight % >63 μm	Benthic foraminiferal $\delta^{18}O$ vs. PDB (‰)	Planktonic foraminiferal $\delta^{18}O$ vs. PDB (‰)	Benthic foraminiferal $\delta^{13}C$ vs. PDB (‰)	Planktonic foraminiferal $\delta^{13}C$ vs. PDB (‰)	Benthic Mg/Ca (mmol/mol)	Mg/Ca Eocene SW corrected (mmol/mol)	Mg/Ca Temp - Lear (°C)	Calculated $\delta^{18}O_{SW}$	Temp calc from planktonic $\delta^{18}O$ - Erez & Lutz (°C)
CB05HB021	1.45	34.4		-2.04		3.13					
CB05HB022	1.50	33.7	-0.110		0.293		2.53	3.21	12.0	-1.01	
CB05HB023	1.55	36.8	-0.053	-1.48	0.591	2.78	2.62	3.32	12.3	-0.88	18.3
CB05HB024	1.60	38.2	-0.234	-0.96	0.558	1.92					
CB05HB025	1.65	40.9	-0.193	-1.08	0.508	2.06	2.18	2.76	10.6	-1.40	16.4
CB05HB026	1.70	43.7	-0.239	-0.67	0.393	2.03	2.32	2.94	11.2	-1.32	14.6
CB05HB027	1.75	41.4	-0.165	-1.34	0.228	2.80	2.04	2.59	10.0	-1.50	17.6
CB05HB028	1.80	38.7	-0.274	-1.07	0.290	2.23	2.65	3.37	12.4	-1.07	16.4
CB05HB029	1.85	34.6	-0.228	-1.23	0.349	2.25	2.57	3.26	12.1	-1.09	17.1
CB05HB030	1.90	32.6		-1.27		2.20					
CB05HB031	1.95	27.2	-0.239	-1.31	0.325	2.37					
CB05HB032	2.00	25.4	-0.191	-1.48	0.452	2.93	2.66	3.37	12.5	-0.99	18.3
CB05HB033	2.05	24.4	-0.230	-1.09	0.442	2.33	2.44	3.09	11.7	-1.20	16.5
CB05HB034	2.10	22.5	-0.297	-1.01	0.491	2.43					
CB05HB035	2.15	23.8	-0.308	-1.36	0.650	2.50	2.47	3.14	11.8	-1.25	17.7
CB05HB036	2.20	27.1	-0.250	-0.67	0.399	2.06	2.22	2.82	10.8	-1.42	14.6
CB05HB037	2.25	31.5	-0.368	-1.12	0.393	1.85	2.60	3.29	12.2	-1.21	16.6
CB05HB038	2.30	41.2	-0.315	-1.15	0.412	2.07	2.49	3.16	11.9	-1.24	16.8
CB05HB039	2.35	44.0	-0.360	-1.39	0.283	2.18	2.54	3.22	12.0	-1.25	17.9
CB05HB040	2.40	44.7	-0.360	-1.18	0.275	2.22	2.46	3.12	11.8	-1.31	16.9
CB05HB041	2.45	42.4	-0.377	-1.22	0.098	2.05	2.57	3.26	12.1	-1.25	17.1
CB05HB042	2.50	44.5	-0.375	-1.49	0.282	1.89	2.49	3.16	11.9	-1.30	18.3
CB05HB043	2.55	45.2	-0.396	-1.56	0.261	2.23	2.54	3.23	12.1	-1.28	18.6
CB05HB043X	2.60	40.7	-0.286	-1.70	0.230	2.01	2.62	3.32	12.3	-1.11	19.3
CB05HB044	2.65	39.1	-0.408	-1.44	0.207	2.00	2.55	3.24	12.1	-1.29	18.1
CB05HB045	2.70	34.9	-0.325	-1.01	0.190	1.93	2.53	3.21	12.0	-1.22	16.1
CB05HB046	2.75	26.3	-0.296	-1.23	0.284	2.30					
CB05HB047	2.80	24.2	-0.319	-1.31	0.312	2.21	2.78	3.52	12.9	-1.03	17.5
CB05HB048	2.85	21.0	-0.361	-1.60	0.356	2.38	2.57	3.26	12.2	-1.22	18.8
CB05HB049	2.90	18.6	-0.306	-1.50	0.086	2.44	2.54	3.22	12.0	-1.19	18.4
CB05HB050	2.95	18.3	-0.179	-1.73	0.231	2.46	2.57	3.25	12.1	-1.05	19.4
CB05HB051	3.00	14.9	-0.227	-1.04	0.316	2.48	2.65	3.36	12.4	-1.03	16.3
CB05HB052	3.05	17.0	-0.211	-1.83	0.212	2.79	2.44	3.10	11.7	-1.18	19.9
CB05HB053	3.10	20.9	-0.319	-1.38	0.486	2.47	2.42	3.07	11.6	-1.31	17.8
CB05HB054	3.15	19.9	-0.314	-1.54	0.397	2.36	2.53	3.20	12.0	-1.21	18.5

CB05HB055	3.20	33.4	-0.248	-1.90	0.297	2.74	2.64	3.35	12.4	-1.06	20.2
CB05HB056	3.25	35.0	-0.263	-1.87	0.221	2.13	2.75	3.48	12.8	-0.99	20.0
CB05HB057	3.30	38.8	-0.380	-1.84	-0.113	2.18	2.72	3.46	12.7	-1.13	19.9
CB05HB058	3.35a	37.3	-0.372	-1.72	-0.267	1.73	2.66	3.38	12.5	-1.16	19.4
CB05HB059	3.40a	34.8	-0.363	-1.84	0.170	1.97	2.42	3.07	11.6	-1.35	19.9
CB05HB060	3.45a	33.9	-0.439	-1.82	-0.021	2.25	2.63	3.33	12.3	-1.26	19.8
CB05HB061	3.35b	39.5	-0.471	-1.29	0.005	1.84					
CB05HB062	3.40b	36.6	-0.329	-1.22	0.076	1.61	2.59	3.28	12.2	-1.18	17.1
CB05HB063	3.45b	34.2	-0.404	-1.68	0.170	1.68	2.66	3.37	12.5	-1.20	19.2
CB05HB064	3.50	31.9	-0.345	-1.16	-0.157	1.50	2.41	3.06	11.6	-1.34	16.8
CB05HB065	3.55	29.2	-0.317		-0.026		2.63	3.34	12.4	-1.13	
CB05HB066	3.60	31.4	-0.368		-0.145		2.80	3.55	12.9	-1.06	
CB05HB067	3.65	28.0	-0.323	-1.35	-0.077	2.18	2.41	3.06	11.6	-1.32	17.7
CB05HB068	3.70	24.2	-0.366	-1.09	-0.059	2.25	2.40	3.04	11.5	-1.37	16.5
CB05HB069	3.75	23.7	-0.322	-1.70	-0.028	2.29	2.58	3.28	12.2	-1.18	19.3
CB05HB070	3.80	22.3	-0.373	-1.15	0.116	2.08	2.47	3.13	11.8	-1.32	16.8
CB05HB071	3.85	19.1	-0.377	-1.44	0.006	2.22	2.48	3.15	11.8	-1.32	18.1
CB05HB072	3.90	18.3	-0.286	-1.32	0.287	2.19	2.63	3.33	12.4	-1.11	17.6
CB05HB073	3.95	16.1	-0.275	-1.50	0.111	3.00	2.47	3.13	11.8	-1.22	18.3
CB05HB074	4.00	17.9	-0.322	-1.60	0.169	2.09	2.52	3.19	12.0	-1.23	18.8
CB05HB075	4.05	19.1	-0.328		0.322		2.40	3.04	11.5	-1.34	
CB05HB076	4.10	22.2	-0.363	-1.61	0.436	2.30	2.45	3.11	11.7	-1.33	18.9
CB05HB077	4.15	27.6	-0.356	-1.75	0.213	2.20	2.53	3.21	12.0	-1.25	19.5
CB05HB078	4.20	35.2	-0.425	-1.75	-0.012	2.29	2.45	3.11	11.7	-1.39	19.5
CB05HB079	4.25	44.0	-0.422	-1.84	0.054	2.29	2.39	3.03	11.5	-1.44	19.9
CB05HB080	4.30	41.3	-0.350	-1.64	-0.140	2.18	2.75	3.48	12.8	-1.08	19.0
CB05HB081	4.35	41.4	-0.412		0.081		2.47	3.13	11.8	-1.36	
CB05HB082	4.40	43.2	-0.345	-1.33	0.195	2.09	2.59	3.29	12.2	-1.19	17.6
CB05HB083	4.45	38.6	-0.448	-1.23	0.294	1.86	2.53	3.21	12.0	-1.34	17.1
CB05HB084	4.50	37.4	-0.354	-1.16	0.418	2.15	2.67	3.38	12.5	-1.14	16.8
CB05HB085	4.55	36.7	-0.289	-1.48	0.166	2.30	2.50	3.17	11.9	-1.21	18.3
CB05HB086	4.60	36.7	-0.316	-1.22	0.114	2.25	2.51	3.19	11.9	-1.23	17.1
CB05HB087	4.65	30.5	-0.297	-1.37	0.330	2.17	2.57	3.26	12.2	-1.16	17.8
CB05HB088	4.70	30.6	-0.148	-1.21	0.212	2.48	2.73	3.46	12.7	-0.89	17.0
CB05HB089	4.75	26.9	-0.257	-1.42	0.458	2.61	2.70	3.43	12.6	-1.02	18.0
CB05HB090	4.80	26.9	-0.221	-0.98	0.279	2.00	2.69	3.42	12.6	-0.99	16.0
CB05HB091	4.85	22.9	-0.254	-1.31	0.299	2.61	2.43	3.08	11.6	-1.23	17.5
CB05HB092	4.90	22.3	-0.197	-1.55	0.215	2.31	2.52	3.19	12.0	-1.11	18.6
CB05HB093	4.95	25.9	-0.194	-1.59	0.453	2.84	2.48	3.15	11.8	-1.13	18.8
CB05HB094	5.00	21.7	-0.312	-1.33	0.238	2.10	2.53	3.21	12.0	-1.21	17.6
CB05HB095	5.05	23.1		-1.34		2.62	2.51	3.19	11.9		
CB05HB096	5.10	18.8	-0.194	-1.59	0.238	2.84	2.63	3.34	12.4	-1.01	18.8
CB05HB097	5.15	22.8	-0.312	-1.33	0.293	2.10	2.99	3.79	13.5	-0.87	17.6
CB05HB098	5.20	20.3		-1.34		2.62					

Appendix 9. "High-resolution" section sediment composition

Sample Number	Height (m)	Coarse Weight (%)	Carbonate (%)	Clays (%)	Feldspar (%)	Silica (%)	Mica (%)	Kaolinite / Montmorillonite
CB05HB021	1.45	34.4						
CB05HB022	1.50	33.7	8.8	29.5	9.9	46.2	5.7	1.61
CB05HB023	1.55	36.8						
CB05HB024	1.60	38.2						
CB05HB025	1.65	40.9						
CB05HB026	1.70	43.7	8.0	25.0	5.2	56.8	4.9	1.60
CB05HB027	1.75	41.4						
CB05HB028	1.80	38.7						
CB05HB029	1.85	34.6						
CB05HB030	1.90	32.6	8.7	24.6	16.7	45.0	5.0	1.79
CB05HB031	1.95	27.2						
CB05HB032	2.00	25.4						
CB05HB033	2.05	24.4						
CB05HB034	2.10	22.5	6.9	30.3	5.5	52.4	4.8	1.39
CB05HB035	2.15	23.8						
CB05HB036	2.20	27.1						
CB05HB037	2.25	31.5						
CB05HB038	2.30	41.2	6.3	23.8	21.5	43.4	5.0	1.18
CB05HB039	2.35	44.0						
CB05HB040	2.40	44.7						
CB05HB041	2.45	42.4						
CB05HB042	2.50	44.5	7.8	24.7	17.6	45.4	4.5	1.06
CB05HB043	2.55	45.2						
CB05HB043X	2.60	40.7						
CB05HB044	2.65	39.1						
CB05HB045	2.70	34.9						
CB05HB046	2.75	26.3	11.3	34.0	5.9	43.0	4.5	0.81
CB05HB047	2.80	24.2						
CB05HB048	2.85	21.0						
CB05HB049	2.90	18.6						
CB05HB050	2.95	18.3	12.7	33.3	4.0	41.2	4.2	1.08
CB05HB051	3.00	14.9						
CB05HB052	3.05	17.0						
CB05HB053	3.10	20.9						
CB05HB054	3.15	19.9	10.7	20.0	8.7	56.1	4.5	1.28
CB05HB055	3.20	33.4						
CB05HB056	3.25	35.0						
CB05HB057	3.30	38.8	8.7	18.0	6.6	61.2	4.2	0.97

Sample Number	Height (m)	Coarse Weight (%)	Carbonate (%)	Clays (%)	Feldspar (%)	Silica (%)	Mica (%)	Kaolinite / Montmorillonite
CB05HB059	3.40a	39.5						
CB05HB060	3.45a	34.8						
CB05HB061	3.35b	36.6						
CB05HB062	3.40b	34.2	11.9	22.1	19.4	41.3	5.3	0.81
CB05HB063	3.45b	33.9						
CB05HB064	3.50	31.9						
CB05HB065	3.55	29.2						
CB05HB066	3.60	31.4	11.5	20.1	8.6	54.9	4.9	0.67
CB05HB067	3.65	28.0						
CB05HB068	3.70	24.2						
CB05HB069	3.75	23.7						
CB05HB070	3.80	22.3	9.8	21.7	5.9	58.0	4.6	1.09
CB05HB071	3.85	19.1						
CB05HB072	3.90	18.3						
CB05HB073	3.95	16.1	10.7	22.2	13.9	47.1	3.4	1.02
CB05HB074	4.00	17.9						
CB05HB075	4.05	19.1						
CB05HB076	4.10	22.2						
CB05HB077	4.15	27.6						
CB05HB078	4.20	35.2	12.8	18.3	18.2	45.1	5.7	0.79
CB05HB079	4.25	44.0						
CB05HB080	4.30	41.3						
CB05HB081	4.35	41.4						
CB05HB082	4.40	43.2	8.2	15.4	18.7	53.3	4.4	0.73
CB05HB083	4.45	38.6						
CB05HB084	4.50	37.4						
CB05HB085	4.55	36.7						
CB05HB086	4.60	36.7	8.9	16.4	19.3	52.4	3.0	0.72
CB05HB087	4.65	30.5						
CB05HB088	4.70	30.6						
CB05HB089	4.75	26.9						
CB05HB090	4.80	26.9	12.0	22.6	11.2	50.4	3.8	0.80
CB05HB091	4.85	22.9						
CB05HB092	4.90	22.3						
CB05HB093	4.95	25.9						
CB05HB094	5.00	21.7	11.4	17.9	8.0	58.4	4.4	0.68
CB05HB095	5.05	23.1						
CB05HB096	5.10	18.8						
CB05HB097	5.15	22.8						
CB05HB098	5.20	20.3	9.4	18.9	9.3	55.3	4.4	0.96

Appendix 10. "High-resolution" planktonic foraminiferal assemblage data

Sample number	Sample Height (cm)	*G.index* used in isotopic analysis	*G.index* remaining	*G. bassriverensis*	*G. martini*	*G. ouchitaensis*	*A. bullbrooki*	*A. mcgowrani*	*A. primitiva*	*A. collectea*	*S. angiporoides*	*S. linaperta*	*S. semni*	*C. unicavus*	Others	Frragments	Unknown sp 1	Forams per gram	Proportion 'mixed layer' species	Proportion 'mixed layer' + 'unknown' species	95% CI 'mixed layer' species ±	95% CI 'sub-thermocline' species ±
CB05HB022	150	4	0	1	2		23	8	34	1	1	2			3			0.16	0.92	0.96	0.12	0.08
CB05HB024	160	4	3	2	1	1	13	4	11	2	4	5	1	1	5	1		0.12	0.71	0.81	0.23	0.20
CB05HB026	170	8	2	1	3	2	14	5	22		3	5		1	5			0.14	0.80	0.87	0.19	0.15
CB05HB028	180	10	9	5	2	11	17	10	20		4	5		2	5	3		0.21	0.82	0.89	0.15	0.12
CB05HB030	190	9	16	5	7	8	24	11	15	2	3	5	1	2	3	0	1	0.22	0.87	0.90	0.13	0.11
CB05HB032	200	9	6	7	9	6	14	5	18	2	7	11	1	1	8	1		0.21	0.72	0.81	0.17	0.15
CB05HB034	210	8	6	1	5	5	12	2	8	2	4	7	1	0	3	2	3	0.14	0.71	0.83	0.21	0.18
CB05HB036	220	12	19	2	2	5	12	4	12		4	2	2	1	5			0.16	0.83	0.89	0.16	0.14
CB05HB038	230	8	7	3	4	9	14	3	11	0	4	2	0	1	11	0	1	0.16	0.76	0.91	0.19	0.13
CB05HB040	240	6	7	5	3	4	7	5	12	0	4	1	1	3	5			0.13	0.78	0.86	0.21	0.17
CB05HB042	250	9	12	3	10	21	52	22	54	6	3	12	0	1	25	2	1	0.47	0.81	0.93	0.10	0.07
CB05HB044	265	8	6	2	1	4	10	4	10	0	4	4		1	4	2		0.12	0.75	0.85	0.22	0.18
CB05HB046	275	10	13	2	6	7	23	5	17	1	7	6	0	2	9	0	0	0.22	0.78	0.86	0.16	0.13
CB05HB048	285	12	26	8	23	11	38	13	30	5	6	9			10	2		0.39	0.86	0.92	0.10	0.08
CB05HB050	295	16	19	6	9	16	18	20	12	3	9	4	0	3	15	1	2	0.31	0.78	0.90	0.13	0.10
CB05HB051	300	2	8	2	4	4	17	2	16	0	6	5	1	2	5			0.15	0.74	0.81	0.20	0.18
CB05HB054	315	7	3	2	2	0	17	5	6	0	3	7	0	2	7	1	0	0.12	0.68	0.81	0.23	0.20
CB05HB056	325	16	9	11	14	13	15	10	18	1	4	9	2	4	13	1		0.28	0.76	0.86	0.14	0.11

Appendix 10. "High-resolution" planktonic foraminiferal assemblage data

Sample number	Sample Height (cm)	*G.index* used in isotopic analysis	*G.index* remaining	*G. bassriverensis*	*G. martini*	*G. ouchitaensis*	*A. bullbrooki*	*A. mcgowrani*	*A. primitiva*	*A. collectea*	*S. angiporoides*	*S. linaperta*	*S. semi*	*C. unicavus*	Others	Frragments	Unknown sp 1	Forams per gram	Proportion 'mixed layer' species	Proportion 'mixed layer' + 'unknown' species	95% CI 'mixed layer' species ±	95% CI 'sub-thermocline' species ±
CB05HB060	345	9	3	13	16	10	21	10	13		4	3			2	1		0.21	0.90	0.93	0.11	0.10
CB05HB062	340	6	7	6	4	8	18	8	8	2	3	3	1	3	9	1	1	0.18	0.76	0.89	0.18	0.13
CB05HB064	350	7	4	3	2	6	24	7	22	1	3	4	1		6	1		0.18	0.84	0.91	0.15	0.12
CB05HB066	360	9	5	3	10	5	31	3	10	0	3	6	1	2	4	1	0	0.19	0.82	0.87	0.16	0.14
CB05HB070	380	7	5	3	5	9	10	0	1	1	2	1	1	1	1	0	0	0.09	0.87	0.89	0.19	0.18
CB05HB072	390	10	5	6	8	7	7	1	1	1	4	5		0	1	1		0.11	0.81	0.84	0.20	0.19
CB05HB073	395	9		0	2	2	12	1	2	0	0	6	0	2	2	1	0	0.08	0.72	0.79	0.28	0.25
CB05HB076	410	3	3	2	1	1	7	1	3	0	0	4	0		1	0		0.05	0.81	0.85	0.30	0.28
CB05HB078	420	3		2	1	1	13	4	2	4	0	2	0	0	2	0	0	0.07	0.88	0.94	0.22	0.16
CB05HB080	430	7	1	1	4	2	7	2	10	3		3	1	1	3			0.09	0.82	0.89	0.22	0.18
CB05HB082	440	11	5	2	3	3	17	3	8	2	1	5	0	1	1	0	0	0.12	0.87	0.89	0.17	0.16
CB05HB084	450	3	2	0	4	3	2	2	1	1	1	1		1	1			0.04	0.82	0.86	0.32	0.29
CB05HB088	470	15	9	1	3	4	18	6	12	4	3	6		0	5			0.17	0.84	0.90	0.16	0.13
CB05HB090	480	13	11	2	10	9	20	2	8	1	2	4		1		1		0.17	0.90	0.92	0.13	0.12
CB05HB092	490	9	5	1	2	2	1	1	0	0	2	0		1	0			0.05	0.88	0.88	0.26	0.26
CB05HB094	500	6	6	2	2	4	14	0	1	0	1	2		0	1			0.08	0.90	0.92	0.19	0.17

Mixed layer' dwelling foraminifera species
Sub thermocline dwelling' foraminifera species

Appendix 11. "High-resolution" section total foraminiferal assemblage data

	Oxygen	CB05HB079		CB05HB074		CB05HB058		CB05HB050	
Weight of >63µm fraction (g)		220.2		89.4		197.3		91.7	
Strat Height (cm)		425		400		335		295	
		Absolute	**%**	**Absolute**	**%**	**Absolute**	**%**	**Absolute**	**%**
Acarinina bullbrooki		8	1.18	6	1.00	8	1.87	11	1.83
Acarinina collectea		5	0.74	1	0.17	4	0.94	6	1.00
Acarinina primitiva		23	3.40	16	2.67	21	4.92	18	2.99
Globigerinatheka index		9	1.33	9	1.50	10	2.34	8	1.33
Globoturborotalia martini		9	1.33	10	1.67	10	2.34	8	1.33
Globoturborotalia ouchitatensis		5	0.74	8	1.34	15	3.51	3	0.50
Guembelitroides nuttalli		0	0.00	2	0.33	2	0.47	2	0.33
Pseudohastigerina micra		1	0.15	0	0.00		0.00		0.00
Subbotina linaperta		13	1.92	17	2.84	11	2.58	28	4.65
Subbotina minima		11	1.63	7	1.17	4	0.94	9	1.50
Unknown sp. 1 - Acarinina?		2	0.30	2	0.33		0.00	2	0.33
Unknown sp. 2		1	0.15	0	0.00		0.00	1	0.17
Unknown sp. 3		2	0.30	1	0.17		0.00	1	0.17
Unknown sp. 4				3	0.50		0.00		0.00
Unknown sp. 5				2	0.33		0.00		0.00
Total Planktonics		89	13.17	84	14.02	85	19.91	97	16.11
Alabamina sp. A	*Oxic*	3	0.44	1	0.17	3	0.71	3	0.51
Anomaloides sp.A	*Oxic*	2	0.29	0	0.00		0.00		0.00
Astocolus sp. A	*Oxic*	1	0.15	1	0.17		0.00	1	0.17
Bolivenopsis sp. A		9	1.33	5	0.83	7	1.67	4	0.68
Bolivenopsis sp. B		2	0.29	2	0.33		0.00		0.00
Bullimina sp. A	*Suboxic*	84	12.37	58	9.68	61	14.52	6	1.02
Bullimina sp. B	*Dysoxic*	6	0.88	28	4.67	8	1.90	50	8.53
Bullimina sp. C	*Suboxic*		0.00	17	2.84	7	1.67	39	6.66
Bulimina alavanensis	*Suboxic*	11	1.62	23	3.84	9	2.14	47	8.02
Ceratobullimina	*Suboxic*	3	0.44	7	1.17	3	0.71	3	0.51
Ceratocancris	*Suboxic*	0	0.00	2	0.33		0.00		0.00
Cibicides sp. A	*Oxic*	27	3.98	12	2.00	9	2.14	5	0.85
Cibicides sp. B	*Oxic*	17	2.50	14	2.34	6	1.43	6	1.02
Cibicides sp. C	*Oxic*	7	1.03	3	0.50	4	0.95	5	0.85
Cibicidoides sp. A	*Oxic*	30	4.42	33	5.51	16	3.81	20	3.41
Cibicidoides sp. B	*Oxic*	13	1.91	4	0.67	8	1.90	10	1.71
Cibicidoides sp. C	*Oxic*	11	1.62	20	3.34	8	1.90	11	1.88
Cibicidoides sp.D	*Oxic*	6	0.88	2	0.33	2	0.48	1	0.17

	Oxygen	CB05HB079		CB05HB074		CB05HB058		CB05HB050	
Cibicidoides sp.E	*Oxic*	15	2.21	3	0.50	8	1.90	7	1.19
Cibicidoides sp.F	*Oxic*	5	0.74	3	0.50	1	0.24	2	0.34
Cibicidoides sp.G	*Oxic*	5	0.74	5	0.83	3	0.71	9	1.54
Cibicidoides sp.H	*Oxic*	10	1.47	14	2.34	9	2.14	12	2.05
Dentolina sp. A	*Dysoxic*	6	0.88	6	1.00	7	1.67	7	1.19
Dentolina sp. B	*Dysoxic*	4	0.59	6	1.00	3	0.71		0.00
Gavalinella sp. A	*Suboxic*	24	3.53	14	2.34	11	2.62	8	1.37
Globobullimina sp. A	*Dysoxic*	3	0.44	7	1.17	3	0.71	7	1.19
Globocassidulina	*Oxic*	3	0.44	1	0.17		0.00	1	0.17
Guttilina sp. A	*Suboxic*	1	0.15	0	0.00		0.00		0.00
Gyroidinoides	*Suboxic*	10	1.47	5	0.83	1	0.24	14	2.39
Hoeglandina	*Oxic*	21	3.09	30	5.01	6	1.43	13	2.22
Karirriella	*Suboxic*	0	0.00	0	0.00		0.00		0.00
Lenticulina sp. A	*Suboxic*	14	2.06	6	1.00	9	2.14	13	2.22
Lenticulina sp. B	*Suboxic*	15	2.21	8	1.34	7	1.67	7	1.19
Lenticulina sp. C	*Suboxic*	1	0.15	9	1.50		0.00	3	0.51
Lenticulina sp. D	*Suboxic*		0.00		0.00	1	0.24		0.00
Marginulina sp. A	*Suboxic*	6	0.88	3	0.50	1	0.24	1	0.17
Marginulina sp. B	*Suboxic*		0.00	1	0.17	1	0.24	1	0.17
Melonis sp. A	*Suboxic*	30	4.42	23	3.84	18	4.29	16	2.73
Nodosaria sp. A	*Dysoxic*	36	5.30	33	5.51	17	4.05	25	4.27
Nodosaria sp.B	*Suboxic*	6	0.88	3	0.50	2	0.48	5	0.85
Nodosaria sp.C	*Suboxic*	6	0.88	2	0.33	2	0.48	4	0.68
Oridosalis	*Suboxic*	0	0.00	0	0.00		0.00	2	0.34
Pseudonodosaria sp. A	*Suboxic*	1	0.15	0	0.00		0.00		0.00
Pullinia	*Suboxic*	25	3.68	17	2.84	11	2.62	17	2.90
Saracenaria sp. A	*Suboxic*	2	0.29	0	0.00	1	0.24	1	0.17
Saracenaria sp. B	*Suboxic*		0.00	1	0.17		0.00		0.00
Siphoglobulina sp. A	*Suboxic*	2	0.29	3	0.50	1	0.24	1	0.17
Siphonodosaria	*Dysoxic*	2	0.29	0	0.00		0.00		0.00
Spiroplectinella		7	1.03	8	1.34	1	0.24	2	0.34
Stilostemella sp. A	*Suboxic*	24	3.53	8	1.34	11	2.62	21	3.58
Stilostemella sp. B	*Suboxic*	11	1.62	3	0.50	6	1.43	3	0.51
Stilostemella sp. C	*Suboxic*	8	1.18	6	1.00	6	1.43	5	0.85
Stilostemella sp. D	*Suboxic*	11	1.62	6	1.00	10	2.38	8	1.37
Stilostemella sp. E	*Suboxic*		0.00	10	1.67	1	0.24	1	0.17
Textularia			0.00	1	0.17		0.00		0.00
Uvigerina sp. A	*Suboxic*	3	0.44	0	0.00	1	0.24	1	0.17
Uvigerina sp. B	*Suboxic*		0.00		0.00		0.00	38	6.48
Vaginulinopsis sp. A	*Suboxic*	1	0.15	0	0.00		0.00		0.00
Siphoglobulina sp. B?	*Suboxic*	2	0.29	0	0.00		0.00		0.00
Anomalinella?	*Oxic*	3	0.44	1	0.17	2	0.48	2	0.34
Lagena	*Suboxic*	1	0.15	0	0.00	1	0.24		0.00
Sigmoilina		1	0.15	0	0.00		0.00	2	0.34

	Oxygen	CB05HB079		CB05HB074		CB05HB058		CB05HB050	
Unknown sp. E - spiral	*Oxic*	8	1.18	10	1.67	2	0.48	6	1.02
Haplophragmoides		2	0.29	2	0.33	1	0.24	2	0.34
Unknown sp. G - petaloid		1	0.15	1	0.17	1	0.24		0.00
Nodosarid sp. A	*Suboxic*	1	0.15	0	0.00		0.00		0.00
Pullinia sp. B	*Oxic*	2	0.29	9	1.50	4	0.95	2	0.34
Lobatula	*Suboxic*	1	0.15	0	0.00		0.00		0.00
Kolesnikovella sp. B	*Suboxic*	6	0.88	0	0.00	5	1.19		0.00
Karíriella sp. B?		1	0.15	1	0.17		0.00	2	0.34
Nodosarid sp. A	*Suboxic*	2	0.29	0	0.00	1	0.24		0.00
Vaginulina sp.B	*Suboxic*	3	0.44	1	0.17	2	0.48		0.00
Globulina?	*Dysoxic*	1	0.15	0	0.00		0.00		0.00
Unknown sp. Q - agglutinated biserial		1	0.15	2	0.33		0.00		0.00
Quinquelloculina?		2	0.29	0	0.00		0.00	1	0.17
Karíriella sp. C		1	0.15	0	0.00	4	0.95		0.00
Unknown sp. T - spiral	*Suboxic*	1	0.15	0	0.00		0.00		0.00
Unknown sp. U - spiral	*Dysoxic*			1	0.17		0.00		0.00
Lagena sp. B	*Suboxic*			2	0.33		0.00		0.00
Zeaflorilus?	*Oxic*			2	0.33		0.00	1	0.17
Lagena sp. C	*Suboxic*			1	0.17	2	0.48	4	0.68
Ostracod!				1	0.17		0.00		0.00
Zeaflorilus?	*Oxic*			2	0.33		0.00	1	0.17
Kolesnikovella sp. C	*Suboxic*			1	0.17		0.00		0.00
Elphidium	*Oxic*			1	0.17		0.00		0.00
a						1			
b						1			
c						2			
d						2			
e						1			
f						1			
g								1	
h								1	
I								2	
j								1	
k								1	
l								2	
m								1	
n								1	
o								1	
p								1	
q								1	0

	CB05HB079		CB05HB074		CB05HB058		CB05HB050	
Total Benthics	590		515		335		489	
Total Forams	679		599		420		586	
% Planktonic specimens	13.1		14.0		20.2		16.6	
Total Oxic	189		171		91		118	
Total Suboxic	316		240		192		269	
Total Dysoxic	58		81		38		89	
Oxygen Index	76.5		67.9		70.5		57.0	
Shannon-Weaver Diversity Index	3.78		4.07		4.16		3.99	

Appendix 12. "High-resolution" section palynological counts: First 100 - all palynomorphs

Lycopodium Batch
No. 938934 No. of Lycopodium 10679 +/- 953

	CB05HB030	CB05HB034	CB05HB038	CB05HB042	CB05HB046	CB05HB050	CB05HB054	CB05HB057	CB05HB062	CB05HB066	CB05HB070	CB05HB073	CB05HB078	CB05HB082	CB05HB086	CB05HB090	CB05HB094	CB05HB098
Strat Height (m)	1.9	2.1	2.3	2.5	2.75	2.95	3.15	3.3	3.4	3.6	3.8	3.95	4.2	4.4	4.6	4.8	5	5.2
Lycopodium (exotics)	**31**	**25**	**44**	**27**	**27**	**27**	**21**	**42**	**30**	**30**	**20**	**24**	**35**	**57**	**31**	**30**	**31**	**24**
Dry weight of sample	9.69	9.68	9.75	9.74	9.73	9.66	9.73	9.75	9.72	9.79	9.76	9.74	9.78	9.79	9.82	9.80	9.80	9.84
Pollen (simple)	16	20	25	20	29	26	25	23	29	32	26	27	24	34	24	33	35	39
Pollen (bisaccate)							2	1	1	1	2	1	2	2	1	1	1	
Pollen (Notophagus)	2	2	4	6		1	3	1	1		1	3	2	1	2	1		2
Spores	21	23	11	13	16	15	14	14	17	13	13	17	13	22	19	16	19	18
Pollen / Spore (undetermined)	1																	
Subtotal Terrestrial	**40**	**45**	**40**	**39**	**45**	**42**	**44**	**39**	**48**	**46**	**42**	**48**	**41**	**59**	**46**	**51**	**55**	**59**
Acritarchs (simple)	6	17	12	9	11	8	7	11	5	6	4	4	5	3	3	3	6	9
Acritarchs ('T' ends)	1	1	5	2	2	2	4	1	5	2	3	6	4	2	6	3	3	4
Acritarchs (complex webs)			2	2	2	2		1	1	2		3	2			1	1	1
Acritarchs (others)						1	1		3	3		1				1		
Foram linings	6	1	6	6	2	5	8	13	9	6	10	6	7	11	10	7	11	9
Dinocyst Fragments		1	1								1	1						
Palynomorph Indet	2										1		1					
Subtotal 'Others'	**15**	**20**	**26**	**19**	**17**	**18**	**20**	**26**	**23**	**19**	**19**	**21**	**19**	**16**	**19**	**15**	**21**	**23**
Skolacochorate Dinos		1	1					1	2		1		1	2			1	1
Spiniferites ramosus spp.	19	15	16	21	17	22	14	14	16	15	10	13	12	11	19	15	9	6
Spiniferites pseudofurcatus	2	4	1	1			1	1			1	1	2		1	1	2	
Cribroperidinium spp.																		
Impagidium dispertitum																		
Impagidium maculatum	2		2						1			1	2	2			1	
I. maculatum - long ridges			1															
Impagidium crassimuratum	4	4	2	1	8	1	5	2	2	7		1	2	1				2
I. Crassimuratum - long ridges				1		2	2			2						1		
Areosphaeridium partridgei						1		2	1				1	1				
Chordosphaeridium fibrospinities			2	3	1	2	1	3			6	2	2		1		1	
Hystrichtosphearidium tuberiferum			1		2		1	1	2	3			1		2	1	2	1
Hystrichtokolpoma rigaudiae	1							2		1	11	6	2	1				
Deflandrea antarctica													1			1	1	1
Aliocysta																		
Dapsilidinium spp.	1	1	1		1	1	1	1			1	3	4	1	4	4		1
Diphyes colligerum											1							
Corrundinium incompositum																		
Lejeuneysta																		
Wilsonium echinosuratum																		
Cleistosphaeridium ancyrea	2	1											1			2		
Pyxinodopsis	3			1				2			2	1	1		2			

Tritonites sp.	3	5	3	10	1	4	4	4	2	3	2	1	5	4	4	5	5	5
Hystrictosphearidium sp. With plates			2	1			2			3					1	3	2	1
D. elipticum - ?acritarch	1	2				2	1		1									
Unknown 1 - Acritarch	1																	
Unknown 2 - Lingulodinium ?	1	1														1		
Unknown 3 - spore	1																	
Unknown 4 - Acritarch	1																	
Unknown 5	1																	
Unknown 6					4	5	2	1			2		1					
Unknown 7 - Aritarch	1																	
Unknown 8 - Acritarch	1																	
Unknown 9		1																
Unknown 10																		
Unknown 11			2		1		1		1									
Unknown 12					1													
Unknown 13				1														
Unknown 14				2			1						2					
Unknown 15									1	1		1		1				
Unknown 16					1													
Unknown 17					1									1				
Unknown 18																		
Unknown 19															1			
Unknown 20								1			1	1						
Unknown 21											2							
Unknown 22												1						
Unknown 23																		
Unknown 24														1				
Unknown 25																		
Subtotal Dinos	**45**	**35**	**34**	**42**	**38**	**40**	**36**	**35**	**29**	**35**	**38**	**31**	**40**	**25**	**35**	**34**	**24**	**18**
Total	**100**	**100**	**100**	**100**	**100**	**100**	**100**	**100**	**100**	**100**	**99**	**100**	**100**	**100**	**100**	**100**	**100**	**100**
Proportion of spores (vs pollen)	0.46	0.49	0.73	0.67	0.64	0.64	0.68	0.64	0.65	0.72	0.69	0.65	0.68	0.63	0.59	0.69	0.65	0.69
Proportion of of marine palynomorphs	0.58	0.55	0.60	0.61	0.55	0.58	0.56	0.61	0.52	0.54	0.57	0.52	0.58	0.41	0.54	0.49	0.45	0.41
Dinos / g	1599	1544	846	1705	1545	1638	1881	912	1062	1273	2078	1416	1248	478	1227	1234	844	814
Pollen / g	640	970	722	1055	1179	1105	1568	652	1135	1200	1586	1416	873	708	947	1271	1266	1855
Spores / g	746	1014	274	528	651	614	732	365	623	473	711	777	405	421	666	581	668	814
Unknown / g	533	882	647	771	691	737	1045	678	842	691	1039	959	593	306	666	545	738	1041
Total Palynomorphs / g	3519	4411	2489	4059	4066	4094	5226	2607	3663	3637	5414	4568	3119	1914	3506	3631	3517	4524

Appendix 13. "High-resolution" section palynological counts: Count of 100 dinoflagellates

		CB05HB030	CB05HB034	CB05HB038	CB05HB042	CB05HB046	CB05HB050	CB05HB054	CB05HB057	CB05HB062	CB05HB066	CB05HB070	CB05HB073	CB05HB078	CB05HB082	CB05HB086	CB05HB090	CB05HB094	CB05HB098
	Stratigraphic Height (cm)	190	210	230	250	275	295	315	330	340	360	380	395	420	440	460	480	500	520
	Lycopodium (exotics)	75	76	96	81	77	57	54	121	107	84	39	70	82	161	104	96	105	101
	Dry weight of sample (g)	9.69	9.68	9.75	9.74	9.73	9.66	9.73	9.75	9.72	9.79	9.76	9.74	9.78	9.79	9.82	9.80	9.80	9.84
Gonyacaloid	*Glaphyrocysta*												1						
Gonyacaloid	*Chordosphaeridium fibrospinities*	1	2	5	4	2	5	1	4	2	2	15	6	5	5	1		3	1
Gonyacaloid	*Cribroperidinium*					1						3		1	2				
Gonyacaloid	*Diphyes colligerum*											1							
Gonyacaloid	*Hystrichtokolpoma rigaudiae*	1				1			4	1	5	24	13	6	3	1	1		
Gonyacaloid	*Lingulodinium ?*	1	1	2	2				1	1				3	3	4	2	3	1
Gonyacaloid	*Impagidium maculatum*	4	2	4		2				2	1		2	3	2		1	1	
Gonyacaloid	*I. cf. maculatum*			3			1					1		1					
Gonyacaloid	*Impagidium dispertitum*	8	16	3	2	11	10	14	6	4	14	3	2	5	2	1	1		5
Gonyacaloid	*I. cf. dispertitum*				4	4	2	4	1	1	3	1	1		2		1		
Gonyacaloid	*Spiniferites pseudofurcatus*	11	9	4	2		1	3	1	1	3	1	3	4		3	4	6	
Gonyacaloid	*Spiniferites ramosus* spp.	45	43	41	44	39	52	38	49	48	42	27	46	33	46	43	52	45	39
Gonyacaloid	*Spiniferites*					1						1			1				1
Gonyacaloid	*Areosphaeridium partridgei*				3		1		4	2	1	2		2	3	2			
Gonyacaloid	*Pyxinodopsis*	4	1		2			1	5		3	3	4	4		3	2	1	
Gonyacaloid	*Hystrichtosphearidium tuberiferum*		1	2	2	5	2	3	3	5	4		1	4	3	2	1	6	7
Gonyacaloid	*Hystrictosphearidium truswelliae*			5	1			2		2	4		1			4	5	7	3
Gonyacaloid	*Cleistosphaeridium ancyrea*	4	5	2	4				1	3	1		1	1			2		1
Gonyacaloid	*Dapsilidinium* spp.	4	2	8		4	4	2	1		5	5	7	6	4	9	7	2	4
Gonyacaloid	*Skolacochorate Dinos*		1	1	1		1	3	2	3	2	3	1	2	4		3	3	3
Peridinioid	*Deflandrea antarctica*			1	1				1					3		3	3	1	3
Peridinioid	*Wilsondinium echinosuratum*								1			3	3						
Acritarchs and Unknown Dinoflagellates	*Tritonites* sp.	6	12	8	20	12	6	13	8	11	5	4	3	9	11	17	11	16	26
Acritarchs and Unknown Dinoflagellates	Unknown 1 - Acritarch	1		1															
Acritarchs and Unknown Dinoflagellates	Unknown 3 - spore	1																	
Acritarchs and Unknown Dinoflagellates	Unknown 4 - Acritarch	2								1									
Acritarchs and Unknown Dinoflagellates	Unknown 5	1																	
Acritarchs and Unknown Dinoflagellates	Unknown 6	1	2	2		12	11	8	1	1	2	3	3	3			2	1	3
Acritarchs and Unknown Dinoflagellates	Unknown 7 - Aritarch	1																	
Acritarchs and Unknown Dinoflagellates	Unknown 8 - Acritarch	1		1															
Acritarchs and Unknown Dinoflagellates	Unknown 9		1																
Acritarchs and Unknown Dinoflagellates	Unknown 11 - Acritarch			3		1		3	1	2									
Acritarchs and Unknown Dinoflagellates	Unknown 12 - Acritarch			2		2													
Acritarchs and Unknown Dinoflagellates	Unknown 13 - Acritarch				1														
Acritarchs and Unknown Dinoflagellates	Unknown 14 - Acritarch				5	2		2	3	6	1			2		2		3	
Acritarchs and Unknown Dinoflagellates	Unknown 15 - Acritarch				1				2	2	1		1	1	1		1		

	CB05HB030	CB05HB034	CB05HB038	CB05HB042	CB05HB046	CB05HB050	CB05HB054	CB05HB057	CB05HB062	CB05HB066	CB05HB070	CB05HB073	CB05HB078	CB05HB082	CB05HB086	CB05HB090	CB05HB094	CB05HB098
Unknown 16 - Acritarch				1	1		2							1				
Unknown 19						1				1				3	3	1		1
Unknown 23													2					
Unknown 24														4			1	1
Unknown 25															1		1	
D. elipticum - ?acritarch	3	2	2			3	1	1	2			1			1			1
Dinoflagellates Total	100	100	100	100	100	100	100	100	100	100	100	100	100	100	100	100	100	100
Dinoflagellates / g	1469	1451	1141	1353	1426	1939	2032	905	1027	1299	2804	1566	1331	678	1045	1135	1038	1075
Shannon Index	2.09	1.90	2.30	1.99	2.07	1.75	2.11	2.08	2.08	2.17	2.20	2.05	2.52	2.11	2.02	1.89	1.95	1.93
% P-Cysts	0.00	0.00	1.20	1.39	0.00	0.00	0.00	2.35	0.00	0.00	3.23	3.23	3.61	0.00	3.90	3.53	1.28	4.35
Subtotal 'Transantarctic' Cysts	0	0	6	5	0	1	2	5	4	5	2	1	5	3	9	8	8	6
Proportion 'transantarctic'	0.00	0.00	0.06	0.05	0.00	0.01	0.02	0.05	0.04	0.05	0.02	0.01	0.05	0.03	0.09	0.08	0.08	0.06
95% CI ±	0.00	0.00	0.09	0.09	0.00	0.04	0.05	0.09	0.08	0.09	0.05	0.04	0.09	0.07	0.11	0.11	0.11	0.09
Subtotal 'Low-latitude' Cysts	18	22	17	14	25	20	23	23	15	32	47	30	28	17	8	7	11	13
Proportion 'Low-Latitude' Cysts	0.18	0.22	0.17	0.14	0.25	0.20	0.23	0.23	0.15	0.32	0.47	0.30	0.28	0.17	0.08	0.07	0.11	0.13
95% CI ±	0.15	0.16	0.15	0.14	0.17	0.16	0.16	0.16	0.14	0.18	0.20	0.18	0.18	0.15	0.11	0.10	0.12	0.13